

**Magma Degassing and Wall Rock Alteration  
in the Rare Metal-Rich Peralkaline Granite at Strange Lake,  
Quebec/Labrador**

by  
Stefano Salvi

December, 1994

A thesis submitted to the Faculty of Graduate Studies and Research  
in partial fulfilment of the requirements of the degree of  
Doctor of Philosophy

*Department of Earth and Planetary Sciences  
McGill University  
Montreal, Quebec  
Canada*

## Abstract

Two characteristics of igneous rocks that are poorly understood and appear to be restricted to peralkaline bodies, are extreme enrichment in HFSE, notably Zr, Nb, Y and REE, and the occurrence of fluid inclusions dominated by methane and higher hydrocarbons. Although HFSE enrichment can be partly explained by magmatic processes, the common coincidence of hydrothermal alteration with parts of intrusions most enriched in these elements suggests that hydrothermal processes may also play an important role in HFSE concentration. However, the conditions under which a hydrothermal fluid might remobilise these elements and the extent to which this could occur, have not been established. Likewise, although the presence of methane in the fluid inclusions can be satisfactorily explained by low temperature magma degassing under reducing conditions, it has not been demonstrated that this degassing can account for the higher hydrocarbons.

This thesis investigates the problems of HFSE enrichment and hydrocarbon formation using the Strange Lake pluton, a small, middle-Proterozoic intrusion of peralkaline granite, which contains some of the highest concentrations of Zr, REE, and Y ever reported in an igneous body, and is characterised by abundant hydrocarbon-dominated fluid inclusions. Field observations, petrographic and fluid inclusion studies, and analyses of whole-rock chemical data have permitted reconstruction of the post-magmatic history. The data indicate that a saline orthomagmatic fluid circulated in the pluton with an immiscible CH<sub>4</sub>-dominated fluid containing significant proportions of higher hydrocarbons soon after intrusion. A case is made that a carbonic fluid exsolved from the magma, but that the hydrocarbons were produced by Fischer-Tropsch hydrogenation during hydrothermal alteration of primary arfvedsonite by the orthomagmatic brine. Evidence is presented that Zr, Y and REE were concentrated in the apical parts of the pluton (a >20% enrichment) during a metasomatic event in which alkali HFSE-minerals were replaced by calcic equivalents. A model is presented in which the orthomagmatic brine transported these elements upwards as fluoride complexes, encountered the Ca-metasomatising fluid, which was drawn into the intrusion from the country rocks, and deposited the HFSE-minerals as a result of a sharp reduction in ligand concentration (due to fluorite saturation) and/or increase in pH which accompanied mixing.

## Résumé

Un enrichissement extrême en éléments à champ de force élevé (ECFE), notamment le Zr, le Nb, l'Y et les T.R., et la présence d'inclusions fluides dans lesquelles prédominent le méthane et des hydrocarbures plus lourds sont deux caractéristiques des corps ignés hyperalcalins qui demeurent peu comprises. Bien que l'enrichissement en ECFE puisse être partiellement expliqué par des processus magmatiques, la coïncidence fréquente des altérations hydrothermales avec les parties les plus enrichies en ces éléments des intrusifs hyperalcalins suggère que des processus hydrothermaux jouent un rôle important dans la concentration des ECFE. Cependant, les conditions sous lesquelles un fluide hydrothermal pourrait remobiliser ces éléments et l'étendu avec lequel le procédé de remobilisation pourrait se produire ne sont pas établis. De plus, quoique la présence de méthane dans les inclusions fluides puisse être expliquée de façon satisfaisante par un procédé de dégazage magmatique à basse température et sous des conditions réductrices, il n'a pas été démontré que ce dégazage soit responsable de la formation d'hydrocarbures plus lourds.

Le but de cette thèse est d'apporter un éclaircissement aux problèmes qui ont trait à l'enrichissement en ECFE et à la formation d'hydrocarbures en utilisant le pluton de Strange Lake; une petite intrusion de granite hyperalcalin datée du Protérozoïque moyen, qui contient quelques-unes des concentrations les plus élevées en Zr, T.R. et Y jamais rapportées dans un corps igné, et qui est caractérisée par des inclusions fluides dont le contenu est dominé par des hydrocarbures.

Les observations de terrain, l'examen pétrographique et l'étude des inclusions fluides, ainsi que l'analyse des données chimiques de roche totale ont permis de reconstruire l'histoire post-magmatique du pluton. L'ensemble des informations indique qu'un fluide orthomagmatique salin a circulé dans le pluton peu après son intrusion, avec un fluide immiscible dont le contenu était dominé par le méthane avec des proportions significatives en hydrocarbures plus lourds. Une hypothèse est avancée qui suggère qu'un fluide carbonique s'est séparé du magma hyperalcalin, mais que les hydrocarbures se sont formés par un procédé d'hydrogénation du type Fischer-Tropsch durant l'altération hydrothermale de l'arfvedsonite primaire par le fluide orthomagmatique. Il ressort d'un nombre d'évidences que le Zr, l'Y et les T.R. ont été concentrés dans la partie apicale du pluton (un

enrichissement de plus de 20%) au cours d'une période de métasomatose durant laquelle les minéraux sodiques porteurs d'ECFE ont été remplacés par des équivalents calciques. Un modèle en deux étapes est présenté pour la formation des minéraux porteurs des ECFE et de Ca: 1) le fluide orthomagmatique a transporté les ECFE dans un mouvement ascendant sous forme de complexes fluorés, et 2) les ECFE et le Ca ont précipité sous forme de minéraux exotiques suite au mélange du fluide orthomagmatique avec le fluide responsable de la métasomatose calcique par décroissance abrupte de la concentration en ligands (due à la saturation en fluorine) et/ou par accroissement du pH.

## Riassunto

Un estremo arricchimento in elementi ad elevata forza di campo (EEFC), in particolare Zr, Nb, Y e terre rare, e la presenza di inclusioni fluide caratterizzate da metano e idrocarburi pesanti, rappresentano due aspetti peculiari delle intrusioni peralcaline il cui significato non è ancora ben conosciuto. Nonostante che l'arricchimento in EEFC può essere attribuito a processi di natura puramente magmatica, il fatto che le zone di arricchimento in questi elementi siano tipicamente associate ad una alterazione pervasiva, suggerisce che i processi idrotermali possono giocare un ruolo importante nella loro concentrazione. Le condizioni alle quali un fluido idrotermale può mobilitare gli EEFC, e l'intensità che questo processo può raggiungere, rappresentano tuttavia aspetti non ancora stabiliti nè quantificati. Infatti, benchè la presenza di metano nelle inclusioni fluide può essere spiegata da un degassamento del magma a bassa temperatura in condizioni riducenti, non è ancora stato dimostrato che la genesi degli idrocarburi pesanti sia attribuibile allo stesso fenomeno.

Questo lavoro di tesi ha affrontato la tematica dell'arricchimento in EEFC e della formazione degli idrocarburi nei complessi alcalini nel contesto del plutone di Strange Lake situato al confine Labrador-Quebec (Canada). Questo plutone è rappresentato da una piccola intrusione di granito peralcalino di età Proterozoica (1189 Ma) ed è caratterizzato dalle concentrazioni più elevate in Zr, terre rare e Y mai osservate in un corpo intrusivo a scala mondiale.

La ricostruzione della evoluzione post-magmatica del granito peralcalino di Strange Lake è stata effettuata sulla base delle osservazioni di terreno, dello studio mineralogico-petrografico, della analisi delle inclusioni fluide e della composizione chimica delle rocce.

L'insieme dei dati indica che negli stadi precoci della evoluzione in sub-solidus, il sistema idrotermale era dominato da un fluido di origine magmatica caratterizzato da elevate salinità e circolante in condizioni di immiscibilità con un fluido ricco in metano e in idrocarburi pesanti. Il fluido carbonico è interpretato essere direttamente essolto dal magma in via di cristallizzazione ma la formazione degli idrocarburi pesanti è attribuita ad un processo di idrogenazione per mezzo di una reazione tipo Fischer-Tropsch durante l'alterazione idrotermale della arfvedsonite primaria da parte del fluido salino.

Lo zirconio, l'ittrio e le terre rare, sono state concentrate nelle parti apicali della intrusione nel corso di un evento metasomatico che ha prodotto in concomitanza la sostituzione dei minerali esotici ad elementi alcalini e ad elevata forza di campo, da parte di minerali equivalenti ricchi in calcio.

Il modello che è stato elaborato prevede il trasporto di Zr, Y e terre rare da parte del fluido salino di origine magmatica per mezzo di complessi fluorurici. Il successivo incontro ed il mescolamento di questo fluido con acque ricche in calcio, fluite all'interno della intrusione dalle rocce incassanti, avrebbe causato la precipitazione dei minerali esotici contenenti Ca e EEFC in seguito alla drastica riduzione della concentrazione del legante causata dalla raggiunta saturazione in fluorite, e/o dall'aumento del pH che ha accompagnato il mescolamento dei due fluidi.

## Acknowledgements

I wish to thank my supervisor, Prof. A.E. Williams-Jones, for his constant enthusiasm, encouragement and support during my permanence at McGill. *Grazie Willy.*

Thanks are extended to the many who have provided stimulating discussion, inspiration and constructive criticism, J. Clark, F. Dudas, J. Fein, D. Francis, J. Gittins, R. Linnen, A. Mariano, R. Marr, R. Martin, B. Moine, B. Mountain, T. Mulja, J. Mungall, G. Nassif, C. Normand, J. Roelofsen, J. Seitz, T. Skulski, B. Stefanini, R. Wares, S. Wood, and any others who I may be forgetting. Technical assistance provided by several individuals is also appreciated: G. Poirier (electron microprobe); J. Mungall and E. Campbell (scanning electron microscope); R. Rossi (Raman Microscopy); C. Colassin (mechanical workshop); A. Fournier (darkroom skills); G. Panagiotidis (rock preparation workshop). S. "Uncley" McCauley, the computer wizard, saved several computers from being thrown out of a window, and the undersigned from subsequently being made to follow. I thank C. Normand, not just for translating the abstract into French, but doing it with such a passion. *Merci chum.*

I am indebted to G. Gauthier (Hewlett-Packard<sup>®</sup> Ltd., Kirkland, QC) and C. Bray (University of Toronto). Their enormous patience and confidence was of utmost importance in the successful completion of the gas chromatographic system.

The author is grateful to the Iron Ore Company of Canada, and in particular to B. Chanda, for allowing access to the deposit and to their drill core library. Field work was particularly gratifying also because of the good company and spirit of the expedition party.

Financial support to the author was provided through doctoral scholarships from the National Science and Engineering Research Council of Canada (NSERC) and from *les Fonds pour la Formation de Chercheurs et l'Aide à la Recherche* (FCAR). Additional financial support for this research was provided by NSERC operating, strategic and Lithoprobe grants, and by a FCAR team grant, to A.E.W.-J.

Finally, you will have to excuse me for this, but I cannot thank my parents in English, therefore... *ringrazio i miei genitori, che sono riusciti a essermi vicini nei momenti difficili anche se da un oceano di distanza.*

Saturday, January 14th, 1995. Now that this thesis has been evaluated, I feel that I can try expressing what my feelings are towards my supervisor, without the risk of sounding phony.

I met Professor A.E. Williams-Jones in the early summer of 1987. Close to finishing my B.Sc. at Carleton University, I had applied to various schools for post-graduate studies. These were U.B.C. (Professor Greenwood), Memorial (Professor Wilton), and McGill (Professor Williams-Jones). A few months later, on a field trip in Newfoundland (lead by Prof. Wilton among others), I got a phone call in my hotel room in Nowhere, Nfld, from Willy — ... “My name is Anthony, which is too combersome, and I don't look like a Tony; call me Willy”... — telling me that he had received my application and was very keen on having me in his group... How he got a hold of me remains a mystery. As I had not made up my mind yet between the three offers, he insisted that we met, to talk things over. I told him it would be impossible, as I was to leave for Italy soon after I returned to Ottawa. He saw no obstacle in that. He arranged to pick me up at the Dorval bus station on my way to the Mirabel airport, offer me lunch at his house, talk about science and the project he had in mind for me, and drive me back to Mirabel two hours later to catch (literally) my plane. I was impressed.

Willy supervises a relatively large number of students, and has been able to make this an advantage for us rather than an impediment based on antagonism. One of the qualities that I value most in him is an extraordinary ability of making the students feel at ease, a state of mind of utmost importance as there is nothing that inhibits learning more than fear of expressing doubts.

After doing a M.Sc. and a Ph.D. with him, my main regret when I leave Montreal will be that the odds of finding another scientist of his talent, enthusiasm and drive, who can also treat you as a friend, will be very slim.

To she who is responsible for this thesis to exist,  
by simply having being there – all of the time.

# Table of Contents

<b>ABSTRACT</b>	<b>ii</b>
<b>RESUME</b>	<b>iii</b>
<b>RIASSUNTO</b>	<b>v</b>
<b>ACKNOWLEDGEMENTS</b>	<b>vii</b>
<b>PREFACE</b>	<b>xiv</b>
<b>CHAPTER I</b>	<b>1</b>
GENERAL INTRODUCTION	
<b>INTRODUCTION</b>	<b>2</b>
REDUCED GASES IN ALKALIC IGNEOUS ROCKS	
HFSE IN ALKALIC IGNEOUS ROCKS	4
THE STRANGE LAKE PLUTON	6
<b>THESIS ORGANISATION</b>	<b>8</b>
<b>REFERENCES</b>	<b>11</b>
<b>CHAPTER II</b>	<b>18</b>
MANUSCRIPT: "REDUCED ORTHOMAGMATIC C-O-H-N-NaCl FLUIDS IN THE STRANGE LAKE RARE-METAL GRANITIC COMPLEX, QUEBEC/LABRADOR, CANADA"	
<b>ABSTRACT</b>	<b>19</b>
<b>INTRODUCTION</b>	<b>21</b>
<b>GEOLOGICAL SETTING</b>	<b>22</b>
REGIONAL GEOLOGY	22
LOCAL GEOLOGY	22
<b>FLUID INCLUSION PETROGRAPHY</b>	<b>25</b>
SAMPLE DESCRIPTION	25
TYPES OF FLUID INCLUSIONS	26
<b>MICROTHERMOMETRY</b>	<b>28</b>
LOW-TEMPERATURE PHASE RELATIONS	30
HIGH-TEMPERATURE PHASE RELATIONS	39
<b>SEM DECREPITATE ANALYSES</b>	<b>41</b>
<b>RAMAN SPECTROSCOPY</b>	<b>44</b>
<b>FOURIER TRANSFORM INFRARED SPECTROSCOPY</b>	<b>47</b>
<b>DISCUSSION</b>	<b>49</b>
PRESSURE-TEMPERATURE CONDITIONS	49
SOURCE OF AQUEOUS FLUID	50

SOURCE OF HYDROCARBON FLUIDS _____	53
FLUID EVOLUTION _____	54
SUMMARY AND CONCLUSIONS _____	57
REFERENCES _____	58
<b>CHAPTER III</b> _____	<b>65</b>
CHARACTERISATION OF THE CARBONIC INCLUSIONS	
PROLOGUE _____	66
REFERENCES _____	68
MANUSCRIPT: "FLUID-INCLUSION VOLATILE ANALYSIS BY GAS CHROMATOGRAPHY: APPLICATION OF A WIDE-BORE POROUS-POLYMER CAPILLARY COLUMN TO THE SEPARATION OF ORGANIC AND INORGANIC COMPOUNDS" _____	70
ABSTRACT _____	71
INTRODUCTION _____	72
EXPERIMENTAL PROCEDURE _____	74
INTRODUCTION _____	74
THE GAS CHROMATOGRAPH _____	75
FLUID-INCLUSION VOLATILE EXTRACTION SYSTEM _____	77
CHOICE OF COLUMN _____	79
CHOICE OF DETECTOR _____	83
PRINCIPLES OF DETECTION _____	85
Micro-Thermal Conductivity Detector _____	85
Photoionisation Detector _____	87
DATA COLLECTING AND PROCESSING _____	87
APPARATUS SET-UP _____	88
RESULTS _____	92
PACKED COLUMN _____	92
CAPILLARY COLUMN _____	101
ANALYSIS OF HYDROGEN _____	112
REPRODUCIBILITY OF GAS CHROMATOGRAPHIC ANALYSIS _____	116
CONCLUSIONS _____	116
REFERENCES _____	119
<b>CHAPTER IV</b> _____	<b>122</b>
MANUSCRIPT: "MAGMATIC HYDROCARBONS AND THEIR ALTERATION IN THE STRANGE LAKE PERALKALINE GRANITE, QUEBEC/LABRADOR: EVIDENCE FROM FLUID INCLUSIONS"	
ABSTRACT _____	123

<b>INTRODUCTION</b>	<b>125</b>
<b>GEOLOGICAL SETTING</b>	<b>126</b>
<b>FLUID INCLUSION CHARACTERISTICS</b>	<b>129</b>
“FRESH” PEGMATITES	129
ALTERED PEGMATITES	131
<b>GAS CHROMATOGRAPHY</b>	<b>131</b>
ANALYTICAL PROCEDURE	132
SAMPLE PREPARATION	134
STANDARDISATION AND IDENTIFICATION OF SPECIES	135
<b>RESULTS</b>	<b>137</b>
“FRESH” PEGMATITES	137
ALTERED PEGMATITES	140
<b>DISCUSSION</b>	<b>142</b>
SOURCE OF HYDROCARBONS	142
Equilibrium Models	148
HYDROCARBON FORMATION BY FISCHER-TROPSCH SYNTHESIS	150
ALTERATION OF GAS COMPOSITION	157
<b>CONCLUSIONS</b>	<b>158</b>
<b>REFERENCES</b>	<b>159</b>
<b>CHAPTER V</b>	<b>165</b>
MANUSCRIPT: “ZIRCONOSILICATE PHASE RELATIONS IN THE STRANGE LAKE (LAC BRISSON) PLUTON, QUEBEC-LABRADOR, CANADA”	
<b>ABSTRACT</b>	<b>166</b>
<b>INTRODUCTION</b>	<b>167</b>
<b>GEOLOGICAL SETTING</b>	<b>168</b>
<b>GEOLOGY OF DDH SL-182</b>	<b>172</b>
<b>DISTRIBUTION OF ZIRCONOSILICATE MINERALS IN DDH SL-182</b>	<b>175</b>
<b>GEOCHEMISTRY</b>	<b>179</b>
<b>CATHODOLUMINESCENCE</b>	<b>179</b>
<b>DISCUSSION</b>	<b>184</b>
<b>CONCLUSIONS</b>	<b>189</b>
<b>REFERENCES</b>	<b>190</b>
<b>CHAPTER VI</b>	<b>194</b>
MANUSCRIPT: “THE ROLE OF HYDROTHERMAL PROCESSES IN CONCENTRATING HFSE IN THE STRANGE LAKE PERALKALINE COMPLEX, NORTHEASTERN CANADA”	
<b>ABSTRACT</b>	<b>195</b>

<b>INTRODUCTION</b>	<b>197</b>
<b>GEOLOGICAL SETTING</b>	<b>198</b>
<b>ALTERATION</b>	<b>202</b>
<b>CHEMICAL CHANGES DURING ALTERATION</b>	<b>204</b>
INTRODUCTION	204
DESCRIPTION OF LITHOLOGIES	205
CHEMICAL COMPOSITIONS OF UNALTERED ROCKS	208
METASOMATIC CHANGES IN COMPOSITION	211
NORMATIVE CALCULATIONS AND MINERALOGICAL VARIATIONS	216
<b>DISCUSSION</b>	<b>220</b>
INTRODUCTION	220
EARLY ALTERATION	222
LATE ALTERATION	223
<b>CONCLUSIONS</b>	<b>228</b>
<b>REFERENCES</b>	<b>230</b>
<b>CHAPTER VII</b>	<b>234</b>
CONCLUSIONS	
GENERAL CONCLUSIONS	236
CONTRIBUTIONS TO KNOWLEDGE	238
RECOMMENDATION FOR FUTURE WORK	239
REFERENCES	241
<b>APPENDICES</b>	<b>242</b>
<b>APPENDIX 1</b>	<b>242</b>
FLUID-INCLUSION MICROTHERMOMETRIC DATA	
<b>APPENDIX 2</b>	<b>247</b>
THERMODYNAMIC CALCULATIONS TO DETERMINE THE EQUILIBRIUM COMPOSITION OF AN ORTHOMAGMATIC CARBON-BEARING FLUID, FOR THE SYSTEM C-O-H.	
<b>APPENDIX 3</b>	<b>253</b>
ELECTRON MICROPROBE ANALYSES OF THE ZIRCONOSILICATE MINERALS ELPIDITE, ARMSTRONGITE AND GITTINSITE.	
<b>APPENDIX 4</b>	<b>257</b>
ELECTRON MICROPROBE ANALYSES OF SELECTED MINERALS, USED FOR CALCULATING NORMATIVE MINERAL ABUNDANCES.	
<b>APPENDIX 5</b>	<b>261</b>
WHOLE-ROCK ANALYSES OF HAND SAMPLES OF DRILL HOLE SL-182.	

## Preface

The research presented in this thesis builds on an investigation of low temperature hydrothermal activity in the rare metal-enriched Strange Lake pluton, Quebec/Labrador, which was carried out by the author, and formed the basis of his M.Sc. thesis at McGill University. Much of the work was subsequently published as an article in *Geochimica et Cosmochimica Acta*, 1990, vol. 54, pp. 2403-2418. The current thesis is composed of seven chapters, five of which are presented in manuscript format, and the remaining two are a general introduction and conclusions. Chapter 2 was published in the *European Journal of Mineralogy*, 1992, vol. 4, pp. 1155-1174, chapter 5 has been accepted for publication in *American Mineralogist*, and chapters 3, 4 and 6 have yet to be submitted. In each these manuscripts Prof. A.E. Williams-Jones, the author's advisor, appears as second author. He proposed the thesis topic, provided advice on research methodology, assisted in some of the early data collection, contributed to the interpretations presented in the thesis, and critically reviewed the text. Field work, including mapping and sample collection, was carried out in the summer of 1989 with the assistance of Prof. Williams-Jones and G. Nassif. A large part of the available diamond drill core was logged, also with the assistance of Prof. Williams-Jones, in the summer of 1990. Petrographic studies, fluid inclusion microthermometry, SEM analyses of fluid inclusion residues, and Raman and FTIR spectroscopic analyses of fluid inclusion gas species, were conducted by the author. Electron microprobe analyses of mineral compositions, except where noted, were made by the author with the assistance of G. Poirier. Bulk rock compositions were analysed by T. Ahmedali at the Department of Earth and Planetary Sciences, McGill University and by Acme<sup>®</sup> Analytical Laboratories Ltd., Vancouver, B.C. Analyses of fluid inclusion gas compositions in bulk samples were made using a system built by the author (described in Chapter 3), incorporating a gas chromatograph purchased from Hewlett-Packard<sup>®</sup> of Canada Ltd. and stainless steel crushers manufactured in the workshop of the Geology Department at the University of Toronto.

As required by the Faculty of Graduate Studies and Research at McGill University, the following excerpt from the “Guidelines Concerning Thesis Preparation” is reported below:

Candidates have the option of including, as part of the thesis, the text of a paper(s) submitted or to be submitted for publication, or the clearly-duplicated text of a published paper(s). These texts must be bound as an integral part of the thesis.

If this option is chosen, connecting texts that provide logical bridges between the different papers are mandatory. The thesis must be written in such a way that it is more than a mere collection of manuscripts; in other words, results of a series of papers must be integrated.

The thesis must still conform to all other requirements of the “Guidelines for Thesis Preparation”. The thesis must include: A Table of Contents, an abstract in English and French, an introduction which clearly states the rationale and objectives of the study, a comprehensive review of the literature, a final conclusion and summary, and a thorough bibliography or reference list.

Additional material must be provided where appropriate (e.g., in appendices) and in sufficient detail to allow a clear and precise judgement to be made of the importance and originality of the research reported in the thesis.

In the case of manuscripts co-authored by the candidate and others, the candidate is required to make an explicit statement in the thesis as to who contributed to such work and to what extent. Supervisors must attest to the accuracy of such statements at the doctoral oral defence. Since the task of the examiners is made more difficult in these cases, it is in the candidate’s best interest to make perfectly clear the responsibilities of all the authors of the co-authored papers. Under no circumstances can a co-author of any component of such a thesis serve as an examiner for that thesis.

# **CHAPTER I**

## **GENERAL INTRODUCTION**

---

## Introduction

**A**LTHOUGH peralkaline intrusive magmatism is responsible for only a small proportion of the total volume of igneous rocks in the Earth's crust, a comparatively large proportion of the petrological literature has been devoted to its study. Two major reasons for this interest are an unusual enrichment in the high-field strength elements Zr, Nb, Y, and REE, (cf. Sørensen, 1974; Bonin, 1982; Bowden, 1985; Fitton and Upton, 1987; Wooley, 1987), and the reduced nature of the gases contained as fluid inclusions in these rocks (*e.g.*, Petersilie and Sørensen, 1970; Konnerup-Madsen and Rose-Hansen, 1982; Kogarko *et al.*, 1986). Recently, the elevated contents of the HFSE have also stirred significant interest for economic reasons, as a result of technological developments during the past decade which have sharply increased demand for these elements (*e.g.*, Drysdall *et al.*, 1984; Kogarko, 1990; and Sinclair *et al.*, 1992).

The purpose of this thesis is to report on an investigation of the nature and origin of hydrocarbon-bearing fluid inclusions, and the role of hydrothermal processes in the enrichment of Zr, Y, and REE, in the peralkaline granite pluton at Strange Lake, Quebec/Labrador.

### Reduced Gases in Alkalic Igneous Rocks

The reduced nature of carbonic fluids in silica-undersaturated alkalic igneous rocks was first clearly documented as a result of a 10-year investigation (1955-1965) of the gases released, sometimes explosively, in apatite mines in the Khibina Mountains of the Kola Peninsula, northwest Russia (Petersilie, 1958, 1963; Ikorskii and Romanikhin, 1964; Ikorskii, 1967; Petersilie *et al.*, 1967). This investigation showed that the gases consist primarily of the hydrocarbons, CH<sub>4</sub>, C<sub>2</sub>H<sub>6</sub>, C<sub>3</sub>H<sub>8</sub> and C<sub>4</sub>H<sub>10</sub>, as well as H<sub>2</sub>, and reported the presence of solid bituminous substances (oil, alcohol-benzol resins and asphaltenes). Given the lack of hydrocarbons in the immediate country rocks, it was suggested that these gases originated from the nepheline syenites which host the apatite deposits and eudyalite cumulates. This conclusion was challenged by a number of

authors, including Florovskaya and Melkov (1962), who noted that bituminous inclusions are found only in altered rocks, and Lyutkevich (1967), who proposed that the gases may have migrated into the intrusives from sedimentary rocks in the region. Since the early discoveries in the Khibina Mountains, the list of occurrences of hydrocarbon gases in alkalic igneous rocks has expanded to include, the McClure Mountain, Colorado (Heinrich and Anderson, 1965), the Lovozero massif, Kola Peninsula (Petersilie and Sørensen, 1970), intrusives of the Gardar peralkaline igneous province (cf. Upton and Emeleus, 1987), including the Ilímaussaq intrusion, in southwest Greenland (Petersilie and Sørensen, 1970; Sobolev *et al.*, 1970, 1974; Konnerup-Madsen *et al.*, 1979, 1985; Konnerup-Madsen, 1984) and the Strange Lake granite pluton, Quebec/Labrador (Salvi and Williams-Jones, 1990 and 1992).

Support for the magmatic theory for the origin of the hydrocarbons has grown with the discovery of the juvenile signature of the isotopes of carbon in gases from the Khibina, Lovozero and Ilímaussaq complexes (Petersilie and Sørensen, 1970), although Konnerup-Madsen *et al.* (1988), have cautioned that the possibility cannot be excluded by these data, that the gases were derived from assimilation of sedimentary or metamorphic carbonate minerals. Most authors, proposing an igneous source for the carbonic fluids, envisage separation of a high temperature (>400°C, and possibly >600°C) CO<sub>2</sub>-bearing fluid from the magma, which transforms to methane on cooling along a path buffered by the rock to QFM redox conditions (Gerlach, 1980; Kogarko *et al.*, 1986; Kogarko, 1992). This theory satisfactorily explains the production of methane, as it has been shown by French (1966) and Eugster and Skippen (1967) that around ~500°C (depending on pressure), the composition of a C-O-H gas in equilibrium with a fluid buffered by QFM will change, with a small decrease in temperature, from CO<sub>2</sub>-dominated to CH<sub>4</sub>-dominated. However, this theory does not explain how hydrocarbons heavier than methane form in this environment (CH<sub>4</sub> is very much more stable than the other reduced carbon species), nor, to my knowledge has the problem of the origin of the higher hydrocarbon species ever been systematically addressed. It has been tacitly assumed that the higher hydrocarbons derive from methane by condensation on cooling, without

showing whether this is possible or how it might occur (*e.g.* Konnerup-Madsen *et al.*, 1988). Another observation that has not been explained is that of Konnerup-Madsen and Rose-Hansen (1982) who noted that, whereas the fluids of silica-undersaturated intrusions in the Gardar Province are dominated by methane and higher hydrocarbons, those trapped by silica-saturated magmas tend to be CO<sub>2</sub> -rich.

### **HFSE in Alkalic Igneous Rocks**

The high contents of the HFSE in alkaline rocks may be partly attributed to a much higher proportion of non-bridging oxygens in peralkaline melts than in metaluminous or peraluminous melts, which permits correspondingly higher proportions of these highly charged cations to be accommodated (*e.g.*, Scarfe, 1977). The elevated contents of alkalis and fluorine in peralkaline magmas also increase the solubility of HFSE by promoting the formation of polymeric alkali-silicate complexes and/or alkali-fluoride complexes with these metals (*e.g.*, Watson, 1979; Collins *et al.*, 1982; Collerson 1982). However, some complexes contain such extraordinarily high concentrations of HFSE that it must be questioned whether or not igneous processes alone are sufficient to account for the enrichment.

Examples of deposits in alkaline igneous rocks with HFSE contents high enough to constitute economic or potentially economic resources of these elements include: eudyalite cumulates containing Zr, REE and Nb in the Lovozero massif (*e.g.*, Kogarko, 1990); apatite REE deposits at Khibina (Vlasov *et al.*, 1966); Zr in elpidite at Ilímaussaq and Narsarsuk in Greenland (Lindström, 1894; Gerasimovsky, 1969; Karup-Møller, 1978); Nb, Zr, REE, U and Th mineralisation in peralkaline granites of the Arabian Shield (Drysdall *et al.*, 1984; Jackson *et al.*, 1985); Nb, Ta, U mineralisation in the Nigerian peralkaline granites (Bowden, 1985; Kinnaird *et al.*, 1985); Zr, Y, REE, Nb, Be in the Strange Lake pluton (Miller, 1986; 1990; Zajac, 1992); Be, Zr, Nb, REE in the Thor Lake syenite and granite (NWT) (Trueman *et al.*, 1988); and the Y, Zr prospect in the Kipawa peralkaline complex (Quebec) (Allan, 1992).

Many alkaline igneous complexes, particularly those that are unusually enriched in HFSE, or the more enriched parts of complexes that have typical enrichment in these elements, display evidence of hydrothermal alteration. For example, Florovskaya and Melkov (1962) reported that the nepheline syenites of the Khibina Massif, which host the apatite REE deposits, have been extensively altered. Bonin (1988) presented evidence for the alteration of arfvedsonite to aegirine plus iron oxides in the apical parts of peralkaline granites in Corsica, particularly the Evisa massif, which he attributed to post-magmatic circulation of oxidising fluids. Many of the Nigerian granites contain Nb-U mineralisation apparently related to sodic metasomatism (Kinnaird, 1985). The Kipawa peralkaline complex displays significant evidence of alteration, including hematisation with which elevated contents of Y are associated (cf. Allan, 1992). Finally, Trueman *et al.* (1988) have shown that the main mineralization zone of the Thor lake deposit has undergone extensive albitisation. In view of the above, it seems likely that hydrothermal fluids play a significant role in the enrichment of HFSE in these environments.

The fact that at least some HFSE can be mobilised by hydrothermal fluids is now well established for a variety of geological environments. For example, REE enrichment has been shown to occur during fenitisation (Martin *et al.*, 1978), carbonitisation of alkaline rocks (Mitchell and Brunfeldt), and formation of porphyry Cu (Palacios *et al.*, 1986), and massive sulphide deposits (*e.g.*, MacLean, 1988; Shandl and Gordon, 1991). Moreover, there are several examples of hydrothermal deposits which have been exploited primarily for their REE, *e.g.* the Mary Kathleen U-REE skarn, Australia (Kwak and Abeyasinghe, 1987), the epithermal Gallinas Mountains Cu-REE deposits, New Mexico (Perhac and Heinrich, 1964), and the carbonatite-related vein deposits at Karonge, Burundi (van Wambeke, 1977). There is also direct evidence of hydrothermal REE transport in the form of REE-bearing daughter minerals in fluid inclusions (Kwak and Abeyasinghe, 1987; Heinritzi *et al.*, 1989; Salvi and Williams-Jones, 1990) and the measurement of elevated REE concentrations in fluid inclusion leachates (Banks *et al.*, 1994). The probable mode of transport of the REE in hydrothermal fluids is likewise, reasonably well understood, primarily through theoretical studies of aqueous REE speciation by Wood (1990). This

study shows that REE form their most stable complexes with F, although strong complexes can also be formed with carbonate and sulphate ligands. There is much less information on the factors controlling REE-mineral deposition; most of this comes from theoretical studies by Burt (1989) and Williams-Jones and Wood (1992).

The extent to which other HFSE, in particular Zr, can be mobilised in hydrothermal fluids is much more poorly known. Nonetheless, there is accumulating evidence that, under some circumstances, even this element can be transported in significant concentrations. Some of the best evidence for hydrothermal Zr mobility is the presence of Zr-daughter minerals in fluid inclusions, *e.g.*, baddeleyite ( $\text{ZrO}_2$ ) (Philippot and Selverstone, 1991; Belkin, 1992), and weloganite ( $\text{Sr}_5\text{Zr}_2(\text{CO}_3)_9 \cdot 4\text{H}_2\text{O}$ ) (Vard and Williams-Jones, 1993), and the occurrence of zirconium minerals in rocks which are clearly metasomatic or hydrothermal, *e.g.*, zirconolite ( $\text{CaZrTi}_2\text{O}_7$ ) in skarn (Gi re, 1986) and carbonate veins (Gi re and Williams, 1992) and zircon in limestone-hosted fluorite replacement bodies (Rubin *et al.*, 1989, 1993). Unfortunately, our knowledge of the speciation of Zr in geologic aqueous media is extremely scanty and, to the writer's knowledge, the only high temperature data are those of Aja *et al.* (1995) who reported formation constants for hydroxy and fluoride species, based on the solubility of zirconosilicate minerals and weloganite. Their data suggest that appreciable Zr can be transported in fluorine-rich solutions. The only data on the stability of zirconosilicate bearing mineral assemblages are an experimental study by Lazutkina *et al.* (1980) on the melting behaviour of some alkali zirconosilicate minerals, reversed experiments by Currie and Zaleski (1985) on the breakdown of elpidite to vlasovite plus quartz, and a theoretical study by Marr and Wood (1992) of alkali zirconosilicate phase relations.

### **The Strange Lake Pluton**

The Strange Lake pluton is a peralkaline granite intrusion, which outcrops over area of about 36 km<sup>2</sup> on the border between the provinces of Quebec and Newfoundland at latitude 56°18' N and longitude 64°07' W, and was discovered by the Iron Ore Company of Canada while exploring for uranium mineralization in 1979. The discovery followed report

of a Pb and F anomaly in waters and sediments of Strange Lake, some 30 km northeast of the pluton, by the Canada-Newfoundland Uranium Reconnaissance Program, (Geological Survey of Canada, 1979), and was made by re-tracing the path of a glacially transported boulder train (cf. Zajac *et al.*, 1984). However, instead of finding important concentrations of uranium, the exploration led to delineation of a potential orebody with reserves comprising approximately 30 million tons grading 3.25% ZrO<sub>2</sub>, 0.66% Y<sub>2</sub>O<sub>3</sub>, 0.12% BeO, 0.56% Nb<sub>2</sub>O<sub>5</sub> and 1.3% REE oxides (Zajac *et al.*, 1984; Currie, 1985; Miller, 1986). The mineralisation consists of a large number of unusual minerals, of which the most important are; gittinsite (CaZrSi<sub>2</sub>O<sub>7</sub>), pyrochlore ((Ca,Na)<sub>2</sub>(Nb,Ta)<sub>2</sub>O<sub>6</sub>(O,OH,F)), bastnäsite ((La,Ce,Nd,Y)CO<sub>3</sub>F), monazite ((Ce,La,Th)PO<sub>4</sub>), kainosite (Ca<sub>2</sub>(Ce,Y)<sub>2</sub>Si<sub>4</sub>O<sub>12</sub>(CO<sub>3</sub>)·H<sub>2</sub>O + HREE), elpidite (Na<sub>2</sub>ZrSi<sub>6</sub>O<sub>15</sub>·3H<sub>2</sub>O), thorite (ThSiO<sub>4</sub>) and titanite (CaTiSiO<sub>5</sub>).

The first published map of the pluton was by Currie (1985), who recognised its peralkaline character and reported the first determination of its age, 1.24 Ga., from K-Ar geochronology. He also suggested, on the basis of this age and its peralkaline character, that the pluton might represent an extension of the Gardar peralkaline province of Greenland into Canada. Miller (1986) subsequently divided the pluton into exotic-rich, exotic and exotic-poor facies of granite, from the distribution of HFSE minerals, and further subdivided the exotic-poor facies, which makes up the bulk of the intrusion, into inclusion-bearing and inclusion absent facies. Nassif and Martin (1991) renamed the inclusion-bearing and inclusion-absent facies, subsolvus and hypersolvus granites, based on the occurrence of two or one alkali feldspar minerals, respectively, and also identified a unit of transsolvus granite transitional between the two facies of granite. The exotic and exotic-rich granites of Miller (1986) were shown to represent progressively more altered varieties of subsolvus granite (Salvi and Williams-Jones, 1990). Other studies of the Strange Lake pluton, in addition to those presented in this thesis, include; a geochronological study by Pillet *et al.*, (1989), an investigation of the zirconosilicate mineralogy by Birkett *et al.* (1992), and petrological studies by Miller (1990), Pillet *et al.*, (1992) and Boily and Williams-Jones (1994).

## Thesis Organisation

In his M.Sc. thesis at McGill University, the author carried out an investigation of low temperature hydrothermal activity in the rare metal-enriched Strange Lake pluton, Quebec/Labrador. He recognised that the rocks had been subjected to hydrothermal alteration, and that the potential ore zone was characterised by the pseudomorphic replacement of sodic HFSE minerals, notably elpidite, by calcic equivalents. On the basis of fluid inclusion data, it was proposed that a low temperature (<200°C) Ca-rich brine, probably of meteoric origin, had entered the pluton, and was responsible for the pseudomorphism observed in the mineralised zone. It was also suggested that this hydrothermal activity may have played a role in HFSE mineralisation. However, the author recognised that, due to its elevated Ca content and the probability that the HFSE had been dissolved as fluoride complexes, the Ca-rich brine could not have transported the HFSE, because the low solubility of fluorite would have ensured that F<sup>-</sup> concentrations were maintained at unreasonably low values. Accompanying the Ca-rich fluid inclusions, were methane-rich fluid inclusions which were assumed to have been introduced from the country rock.

Chapter 2 of the present thesis investigates the possibility, using quartz in pegmatites, that some hydrothermal fluid may have been derived from the Strange Lake magma. Fluid inclusions discovered in this investigation are described, and the case is made that the magma exsolved a NaCl brine essentially devoid of Ca and an immiscible methane-rich gas. It is proposed that the orthomagmatic brine caused replacement of arfvedsonite by aegirine in a separate higher temperature episode of alteration than that responsible for the pseudomorphism of primary HFSE minerals. It is also speculated that this brine might have had an elevated concentration of fluorine, and therefore been able to transport the HFSE. The methane-rich inclusions are shown from their strong fluorescence under UV illumination, and FTIR spectroscopic analyses, to contain higher hydrocarbons. However, it was not possible to identify the higher hydrocarbon species using the techniques available to the author at the time that this stage of the research was completed.

In order to identify the hydrocarbon species referred to in Chapter 2, the author built a gas chromatographic system for the analysis of fluid inclusion volatiles in bulk samples. This system is described in Chapter 3, and incorporates several improvements over systems currently in use in other laboratories. In particular, as discussed in this chapter, it is able to analyse hydrocarbons up to carbon number six, separate nitrogen, hydrogen and argon, and detect most gases at up to an order of magnitude lower concentrations than is possible with other gas chromatographic fluid inclusion systems.

Chapter 4 compares results of gas chromatographic analyses of the bulk compositions of the carbonic inclusions in quartz from pegmatites that had undergone early alteration with those in which primary HFSE minerals had been pseudomorphed by calcic equivalents. These data indicate that both sets of samples contain inclusions with aliphatic hydrocarbons up to carbon number six but that samples representing late alteration have higher proportions of CO<sub>2</sub>. Thermodynamic calculations are reported which show that the various gas species could not have been in equilibrium, at any condition between those of magma degassing and entrapment, or post-entrapment. Instead it is proposed that the hydrocarbon species formed via a Fischer-Tropsch reaction involving magnetite-catalysed hydrogenation of CO<sub>2</sub> and CO. It is suggested that the required hydrogen and the catalyst were produced by reaction between the orthomagmatic brine and arfvedsonite, during alteration of the latter mineral to aegirine. The higher CO<sub>2</sub> content of the inclusions associated with late alteration is attributed to oxidation by the meteoric fluid.

The replacement textures involving zirconsilicate minerals, which were first reported in the author's M.Sc. thesis, are further investigated in Chapter 5. Additional textures are reported from drill cores below the potential ore zone which were not available to the author at the time of his M.Sc. thesis. These textures show that, whereas, in the potential ore zone, pseudomorphism of elpidite involved replacement by gittinsite and quartz, in the underlying zone this pseudomorphism involved the creation of pore space without quartz. Moreover, some elpidite was replaced by armstrongite. The creation of pore space is explained by the much smaller molar volume of gittinsite compared to elpidite and the lack of quartz, to silica undersaturation of the Ca-rich meteoric fluid. Schematic phase

diagrams are presented to show that pseudomorphism of elpidite by armstrongite instead of gittinsite, reflects locally higher silica activities due to lower water/rock ratios. The presence of quartz in the gittinsite pseudomorphs in the potential ore zone is attributed to saturation with quartz, possibly due to a decrease in temperature or evolution of the fluid to higher  $\text{SiO}_{2(\text{aq})}$ .

Chapter 6 makes use of whole-rock chemical analyses and data presented in the preceding chapters, to investigate mass changes that might have accompanied the two episodes of alteration which affected the pluton. It is shown that the early alteration involving arfvedsonite was isochemical, whereas later alteration involving pseudomorphism of alkali-HFSE minerals was accompanied by addition of Ca and Mg, and removal of Na. It is also shown that Zr, Y and REE were added to the potential ore zone and depleted in the porous zone immediately below it. These observations are combined with available data on the solubility of Zr in hydrothermal solutions to develop a model in which Zr and the other ore elements were transported as fluoride complexes by the orthomagmatic brine and deposited when this fluid mixed with the Ca-rich meteoric fluid in the apical parts of the intrusion.

## References

- Aja, S.U., Wood, S.A. and Williams-Jones, A.E., 1995.** The aqueous geochemistry of Zr and the solubility of some zirconium-bearing minerals. *Applied Geochemistry* (submitted).
- Allan, J.F., 1992.** Geology and mineralization of the Kipawa yttrium-zirconium prospect, Quebec. *Explor. Mining Geol.*, 1, 283-292.
- Banks, D.A., Yardley, B.W.D., Campbell, A.R. and Jarvis, K.E., 1994.** REE composition of an aqueous magmatic fluid: A fluid inclusion study from the Capitan Pluton, New Mexico, U.S.A. *Chem. Geol.*, 113, 259-272.
- Belkin, H.E., 1992.** Baddeleyite (ZrO<sub>2</sub>), a hydrothermal mineral in Mesozoic mafic intrusive rocks, eastern North America: Implications for aqueous transport and solubility of zirconium [abs]. *Program with abstract, V.M. Goldschmidt Conference*, A-7.
- Birkett, T.C., Miller, R.R., Roberts, A.C. and Mariano, A.N., 1992.** Zirconium-bearing minerals of the Strange Lake intrusive complex, Quebec-Labrador. *Can. Mineral.*, 30, 191-205.
- Boily, M. and Williams-Jones, A.E., 1994.** The role of magmatic and hydrothermal processes in the chemical evolution of the Strange Lake plutonic complex (Quebec-Labrador). *Contrib. Mineral. Petrol.*, 118, 33-47.
- Bonin, B., 1982.** *Les Granites des Complexes Annulaires*. Bureau de Recherches Géologiques et Minières. Manuels et Méthodes, 4. BRGM publ. 176 p.
- Bonin, B., 1988.** Peralkaline granites in Corsica: Some petrological and geochemical constraints. *Rendiconti della Società Italiana di Mineralogia e Petrologia*, 73, 1191-1194.
- Bowden, P., 1985.** The geochemistry and mineralization of alkaline ring complexes in Africa (a review). *J. African Earth Sci.*, 3, 17-39.
- Burt, D.M., 1989.** Compositional and phase relationships among rare earth element minerals. In B.R. Lipin and G.A. McKay (eds). *Geochemistry and Mineralogy of Rare Earth Elements. Mineral. Soc. Am. Rev. Mineral.*, 21, 259-308.

- Collerson, K.D., 1982.** Geochemistry and Rb-Sr Geochronology of associated proterozoic peralkaline and subalkaline anorogenic granites from Labrador. *Contrib. Mineral. Petrol.*, 81, 126-147.
- Collins, W.J., Beams, S.D., White, A.J.R. and Chappell, B.W., 1982.** Nature and origin of A-type granites with particular reference to southeastern Australia. *Contrib. Mineral. Petrol.*, 80, 189-200.
- Currie, K.L., 1985.** An unusual peralkaline granite near Lac Brisson, Quebec-Labrador: *Geol. Surv. Can. Paper 85-1A*, p. 73-90.
- Currie, K.L. and Zaleski, E., 1985.** The relative stability of elpidite and vlasovite: A P-T indicator for peralkaline rocks: *Can. Mineral.*, 23, 577-582.
- Drysdall, A.R., Jackson, N.J., Ramsay, C.R., Douch, C.J. and Hackett, D., 1984.** Rare element mineralization related to Precambrian alkali granites in the Arabian Shield: *Econ. Geol.*, 79, 1366-1377.
- Eugster, H.P. and Skippen, G.B., 1967.** Igneous and metamorphic reactions involving gas equilibria. In *Researches in Geochemistry*, P.H. Abelson ed., 2, Wiley, New York, 492-520.
- Fitton, J.G. and Upton, B.G.J., (eds), 1987.** *Alkaline Igneous Rocks*. Geological Society Special Publication No. 30, 568 p.
- Florovskaya, U.N. and Melkov, V.G., 1962.** Bitumen in igneous rocks. *Min. Syr'e, Vses. Nauk. Issled. Inst. Mineral. Syr'ya*, 5, 83-86. *Chem. Abs.* 59, 11126.
- French, B.M., 1966.** Some geologic implications of equilibrium between graphite and a C-O-H gas phase at high temperatures and pressures. *Rev. Geophys.*, 4, 223-253.
- Geological Survey of Canada, 1979.** Regional lake sediment and water geochemical reconnaissance data, Labrador. *Geol. Surv. Can.*, Open file 559.
- Gerasimovsky, V.I., 1969.** *Geochemistry of the Ilímaussaq Alkaline Massif (South-West Greenland)*. Nauka, Moskow, 174 pp. (in Russian).
- Gerlach, T.M., 1980.** Chemical characteristics of the volcanic gases from Nyiragongo lava Lake and the generation of CH<sub>4</sub>-rich fluid inclusions in alkaline rocks. *J. Volcanol. Geotherm. Res.*, 8, 177-189.
- Gieré, R., 1986.** Zirconolite, allanite and hoegbomite in a marble skarn from the Bergell contact aureole: Implication for mobility of Ti, Zr and REE. *Contrib. Mineral. Petrol.* 65, 459-470.

- Gieré, R. and Williams, C.T., 1992.** REE-bearing minerals in a Ti-rich vein from the Adamello contact aureole (Italy). *Contrib. Mineral. Petrol.* 112, 83-100.
- Heinrich, E. Wm. and Anderson, R.J., 1965.** Carbonatites and alkalic rocks of the Arkansas River area, Fremont County, Colorado. 2. Fetid gas from carbonatite and related rocks. *Am. Mineral.*, 50, 1915-1916.
- Heinritzi, F., Williams-Jones, A.E. and Wood, S.A., 1989.** Fluid inclusions in calcite and dolomite of the REE-zone in the St. Honore carbonatite complex, Quebec [abs]. In *Program with Abstracts, GAC-MAC-CSPG joint annual meeting*, 14, A20-21.
- Ikorskii, S.V., 1967.** *The Organic Substances in the Minerals of Igneous Rocks* (in Russian). Nauka, Leningrad. 131 p.
- Ikorskii, S.V. and Romanikhin, A.M., 1964.** The mode of occurrence of hydrocarbon gases in nepheline of the Khibina alkalic massif. *Geokhimiya*, 3, 276-281.
- Jackson, N.J., Drysdall, A.R. and Stoesser, D.B., 1985.** Alkali granite-related Nb-Zr-REE-U-Th mineralization in the Arabian Shield. In *High Heat Production (HHP) Granites, Hydrothermal Circulation and Ore Genesis*: Institute of Mining and Metallurgy, London, p. 479-487.
- Karup-Møller, S., 1978.** The ore minerals in the Ilímaussaq intrusion: Their mode of occurrence and their conditions of formation. *Bull. Grøn. Geol. Unders.*, 127, 1-51.
- Kinnaid, J.A., 1985.** Hydrothermal alteration and mineralization of the alkaline anorogenic ring complexes of Nigeria. *J. of African Earth Sci.*, 3, 229-251.
- Kinnaid, J.A., Bowden, P, Ixen, R.A. and Odling, N.W.A., 1985.** Mineralogy, geochemistry and mineralization of the Ririwai complex, northern Nigeria. *J. of African Earth Sci.*, 3, 229-251.
- Kogarko, L.N., Kosztolanyi, Ch. and Ryabchikov, I.D., 1986.** Geochemistry of the reduced fluid in alkali magmas. *Geokhimiya*, 12, 1688-1986. Translated in *Geochem. Int.* 24, (7), 1987, 20-27.
- Kogarko, L.N., 1980.** Ore-forming potential of alkaline magmas. *Lithos*, 26, 167-175.
- Konnerup-Madsen, J., 1984.** Compositions of fluid inclusions in granites and quartz syenites from the gardar continental rift province (South Greenland). *Bull. Minéral.*, 107, 327-340.

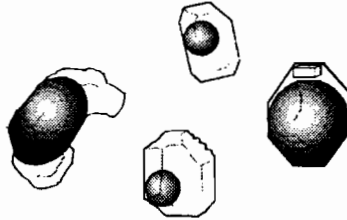
- Konnerup-Madsen, J. and Rose-Hansen, J., 1982.** Volatiles associated with alkaline igneous rift activity: Fluid inclusions in the Ilímaussaq intrusion and the gardar granitic complexes (South Greenland). *Chem. Geol.*, 37, 79-93.
- Konnerup-Madsen, J., Larsen, E. and Rose-Hansen, J., 1979.** Hydrocarbon-rich inclusions in minerals from the alkaline Ilímaussaq intrusion, South Greenland. *Bull. Minéral.*, 102, 642-653.
- Konnerup-Madsen, J., Dubessy, J. and Rose-Hansen, J., 1985.** Combined Raman microprobe spectrometry and microthermometry of fluid inclusions in minerals from igneous rocks of the Gardar province (South Greenland). *Lithos*, 18, 271-280.
- Konnerup-Madsen, J., Kreulen, R. and Rose-Hansen, J., 1988.** Stable isotope characteristics of hydrocarbon gases in the alkaline Ilímaussaq complex, south Greenland. *Bull. Minéral.*, 111, 567-576.
- Kwak, T.A.P. and Abeysinghe, P.B., 1987.** Rare earth and uranium minerals present as daughter crystals in fluid inclusions, Mary Kathleen U-REE skarn, Queensland, Australia. *Mineral. Mag.*, 51, 665-670.
- Lazutkina, L.N., Kogarko, L.N., and Krigman, L.D., 1980.** Stability of zirconium minerals in alkali agpaitic magmas. *Geochemistry International*, 17 (4), 83-86.
- Lindström, G., 1894.** Mineral analyser. Elpidit, ett nytt mineral fran Igaliko. *G.F.F.*, Stockholm, 16, 330-335.
- Lytkevich, Ye.M., 1967.** On bitumen and gas shows of Kola Peninsula and nature of original matter. In *Genesis Nefti i Gaza* (Genesis of oil and gas), Moskcow, Izd. Nedra, 255-261 (in Russian).
- MacLean, W.H., 1988.** Rare earth mobility at constant inter-REE ratios in the alteration zone at the Phelps Dodge Massive Sulfide Deposit, Mattagami, Quebec. *Mineral. Deposita*, 23, 231-238.
- Marr, R.A., Wood, S.A., 1992.** Preliminary petrogenetic grids for sodium and calcium zirconosilicate minerals in felsic peralkaline rocks: The  $\text{SiO}_2\text{-Na}_2\text{ZrO}_3$  and  $\text{SiO}_2\text{-CaZrO}_3$  pseudobinary system. *Am. Mineral.*, 77, 810-820.
- Martin, R.F., Whitley, J.E. and Woolley, A.R., 1978.** An investigation of rare-earth mobility: fenitized quartzites, Borralan Complex, N.W. Scotland. *Contrib. Mineral. Petrol.*, 66, 69-73.

- Miller, R.R., 1986.** Geology of the Strange Lake Alkalic Complex and the associated Zr-Y-Be-REE mineralization. *Newfoundland Department of Mines and Energy, Mineral Development Division, Report 86-1*, 11-19.
- Miller, R.R., 1990.** The Strange Lake pegmatite-aplite hosted rare metal deposit, Labrador. *Newfoundland Department of Mines and Energy, Geological Survey Branch, Report 90-1*, 171-182.
- Mitchell, R.H. and Burnfelt, A.O., 1975.** Rare earth element geochemistry of the Fen alkaline complex, Norway. *Contrib. Mineral. Petrol.*, 52, 247-259.
- Nassif, G.J. and Martin, R.F., 1991.** The hypersolvus granite-subsolvus granite transition at Strange Lake, Quebec-Labrador. In *Abstracts with Program, Geol. Ass. of Canada*, A89.
- Palacios, C.M., Hein, U.F. and Dulski, P., 1989.** Behavior of rare earth elements during hydrothermal alteration at the Buena Esperanza copper-silver deposit, Northern Chile. *Earth Planet. Sci. Lett.*, 80, 208-216.
- Perhac, R.M., and Heinrich, E.W., 1964.** Fluorite-bastnaesite deposits of the Gallinas Mountains, New Mexico and bastnaesite paragenesis. *Econ. Geol.*, 59, 226-239.
- Petersilie, I.A., 1958.** Hydrocarbon gases in the intrusive massifs of the central part of the Kola Peninsula. *Dokl. Akad. Nauk SSSR*, 122, 1086-1089 (in Russian).
- Petersilie, I.A., 1963.** Organic matter in igneous and metamorphic rocks of the Kola peninsula, in A.P. Vinogradov, ed., *Chemistry of the Earth's Crust*, 1, 178-184.
- Petersilie, I.A. and Sørensen, H., 1970.** Hydrocarbon gases and bituminous substances in rocks from the Ilímaussaq alkaline intrusion, south Greenland. *Lithos*, 3, 59-76.
- Petersilie, I.A., Pavlova, M.A., Malashkina, V.T. and Petersilie, M.D., 1967.** The organic substances in igneous and metamorphic rocks. In *Genezis Nefti i Gaza* (Genesis of oil and gas), Moskow, Izd. Nedra, 342-350 (in Russian).
- Philippot, P. and Selverstone, J., 1991.** Trace-element-rich brines in eclogitic veins: Implications for fluid composition and transport during subduction. *Contrib. Mineral. Petrol.*, 106, 417-430.
- Pillet, D., Bonhomme, M.G., Duthou, J.L. and Chenevoy, M., 1989.** Chronologie Rb/Sr et K/Ar du granite peralkalin du lac Brisson, Labrador central, Nouveau-Québec: *Can. J. Earth Sci.*, 26, 328-332.

- Pillet, D., Chenevoy, M. and Bélanger, M., 1992.** Pétrologie du granite peralcalin du lac Brisson, Labrador central, Nouveau-Québec. 1. Mode de mise en place et évolution chimique. *Can. J. Earth Sci.*, 29, 353-372.
- Rubin, J.N., Henry, C.D. and Price, J.G., 1989.** Hydrothermal zircons and zircon overgrowths, Sierra Blanca Peaks, Texas. *Am. Mineral.*, 74, 865-869.
- Rubin, J.N., Henry, C.D. and Price, J.G., 1993.** The mobility of zirconium and other "immobile" elements during hydrothermal alteration. *Chem. Geol.*, 110, 29-47.
- Salvi, S. and Williams Jones, A.E., 1990.** The role of hydrothermal processes in the granite hosted Zr, Y, REE deposit at Strange Lake, Quebec/Labrador: Evidence from fluid inclusions. *Geochim. Cosmochim. Acta*, 54, 2403-2418.
- Salvi, S. and Williams-Jones A.E., 1992.** Reduced orthomagmatic C-O-H-NaCl fluids in the Strange Lake rare-metal granitic complex, Quebec/Labrador, Canada. *Eur. J. Mineral.*, 4, 1155-1174.
- Scarfe, C.M., 1977.** Viscosity of a pantellerite melt at one atmosphere. *Can. Mineral.*, 15, 185-189.
- Schandl, E.S. and Gordon, M.P., 1991.** Postore mobilization of rare earth elements at Kidd Creek and other Archean massive sulfide deposits. *Econ. Geol.*, 86, 49-63.
- Sinclair, W.D., Jambor, J.L. and Birkett, T.C., 1992.** Rare earths and the potential for rare-earth deposits in Canada. *Explor. Mining Geol.*, 1, 265-281.
- Sobolev, V.S., Bazarova, T.Y., Shugurova, N.A., Bazarov, L.Sh., Dolgov, Yu.A., Sørensen, H., 1970.** A preliminary examination of fluid inclusions in nepheline, sorensonite, tugtupite and chkalovite from the Ilímaussaq alkaline intrusion, South Greenland, *Medd. Grønl.*, 181, 1-32.
- Sobolev, V.S., Bazarova, T.Yu. and Kostyuk, V.P., 1974.** Inclusions in the minerals of some types of alkaline rocks. In *The Alkaline Rocks*, H. Sørensen ed., John Wiley & Sons, London, 389-401.
- Sørensen, H. (ed), 1974.** *The Alkaline Rocks*: Wiley Interscience. New York, 622 p.
- Trueman, D.L., Pedersen, J.C., de St. Jorre, L., and Smith, D.G.W., 1988.** The Thor Lake, N.W.T., rare-metal deposits. In Taylor, R.P. and Strong, D.F. (eds), *Recent Advances in the Geology of Granite-related mineral deposits: Geology, petrogenesis and tectonic setting*. Canadian Institute of Mining and Metallurgy, Special Volume 39, 280-290.

- Upton, B.G.J. and Emeleus C.H., 1987.** Mid-Proterozoic alkaline magmatism in southern Greenland: The Gardar province. In Fitton, J.G. and Upton, B.G.J. (eds). *Alkaline Igneous Rocks*. Geological Society Special Publication No. 30, 449-471.
- Vard, E. and Williams-Jones, A.E., 1993.** A fluid inclusion study of vug minerals in dawsonite-altered phonolite sills, Montreal, Quebec: Implications for HFSE mobility. *Contrib. Mineral. Petrol.*, 113, 410-423.
- Vlasov, K.A., Kuz'menko, M.Z. and Es'kova, E.M., 1966.** *The Lovozero Alkali Massif*, translated by D.G. Fry and K. Syers. S.I. Tomkeiff, M.H. Battey, eds. Hafner Pub. Co., New York, 627 p.
- Wambeke, van, L., 1977.** The Karonge rare earth deposit, Republic of Burundi: New mineralogical-geochemical data and origin of the mineralization. *Miner. Deposita*, 12, 373-380.
- Watson, E.B., 1979.** Zircon saturation in felsic liquids: Experimental results and applications to trace elements geochemistry. *Contrib. Mineral. Petrol.*, 70, 407-419.
- Williams-Jones, A.E. and Wood, S.A., 1992.** A preliminary petrogenetic grid for REE fluorocarbonates and associated minerals. *Geochim. Cosmochim. Acta.*, 56, 725-738.
- Wood, S.A., 1990.** The aqueous geochemistry of the rare-earth elements and yttrium 2. Theoretical predictions of speciation in hydrothermal solutions to 350°C at saturation water vapor pressure. *Chem. Geol.*, 88, 99-125.
- Woolley, A.R. (ed), 1987.** *Alkaline Rocks and Carbonatites of the World. Part 1: North and South America*. British Museum (Natural History), London, 216 p.
- Zajac, I.S., 1992.** The Strange Lake Complex and its yttrium and zirconium mineralization [abs]. *Society for Mining Metallurgy and Exploration Abstracts with Program*, 69.
- Zajac, I.S., Miller, R.R., Birkett, T., Nantel, S., 1984.** Le gîte de Zr, Y, Nb, et Be du complexe alcalin de Strange Lake, Québec-Labrador. *Ministère de l'Énergie et des Ressources, Québec*, DV 84-18, 127-142.

## CHAPTER II



# REDUCED ORTHOMAGMATIC C-O-H-N-NaCl FLUIDS IN THE STRANGE LAKE RARE-METAL GRANITIC COMPLEX, QUEBEC/LABRADOR, CANADA

---

STEFANO SALVI

AND

ANTHONY E. WILLIAMS-JONES

*Department of Earth & Planetary Sciences  
McGill University  
Montreal, QC  
Canada*

## Abstract

The Strange Lake complex is a small, middle-Proterozoic pluton containing F-enriched hypersolvus and subsolvus peralkaline granites with unusually high concentrations of Y, Zr, REE, Nb, Be. The subsolvus granite hosts abundant pegmatites and displays extensive evidence of hydrothermal alteration.

Quartz in the pegmatites contains primary inclusions concentrated along growth zones, and pseudosecondary inclusions in the cores of crystals. Four types of fluid inclusions have been recognised: aqueous, liquid-rich (type I); CH<sub>4</sub>, vapour-only (type II); aqueous-CH<sub>4</sub> (type III) and higher hydrocarbon-bearing (fluoresce under UV light; type IV). Coexisting type-III inclusions show highly variable aqueous/carbonic phase ratios, suggesting that the system comprised separate aqueous and carbonic fluids. Type-I inclusions are accurately modelled by the system H<sub>2</sub>O-NaCl, and mainly have salinities close to the eutectic. A small proportion of type-I inclusions have lower salinities. The aqueous phase in most type-III and type-IV inclusions also has a salinity close to the H<sub>2</sub>O-NaCl eutectic. The salinities of type-III inclusions that appear to condense a hydrocarbon liquid which does not fluoresce under UV light are similar to those of the lower-salinity type-I inclusions. Both type-I and type-III inclusions homogenise mainly at temperatures above 300°C. The CH<sub>4</sub> phase displays critical homogenisation. Raman analyses failed to detect CO<sub>2</sub> in the CH<sub>4</sub>-bearing inclusions. Significant N<sub>2</sub> is, however, present, with X<sub>CH<sub>4</sub></sub> as low as 0.2 in N<sub>2</sub>-rich inclusions. The latter belong to the low-salinity type-III inclusion group.

The trapping temperature of the inclusions was estimated to be approximately 340°C, *i.e.*, the modal homogenisation temperature of the aqueous inclusions; the trapping pressure was estimated to be 700 bar, from the intersection of this isotherm with the critical isochore of CH<sub>4</sub>.

Both aqueous and hydrocarbon fluids are interpreted to have originated from the magma, possibly in two stages of aqueous-carbonic fluid exsolution marked by changes in the salinity and N<sub>2</sub> contents of the exsolved fluids. The presence of CH<sub>4</sub> in the absence of

CO<sub>2</sub> is unusual, and to our knowledge, has not been previously reported from silica-saturated igneous rocks, but is consistent with the low  $fO_2$  estimated for the subsolvus granite.

## Geological Setting

### Regional Geology

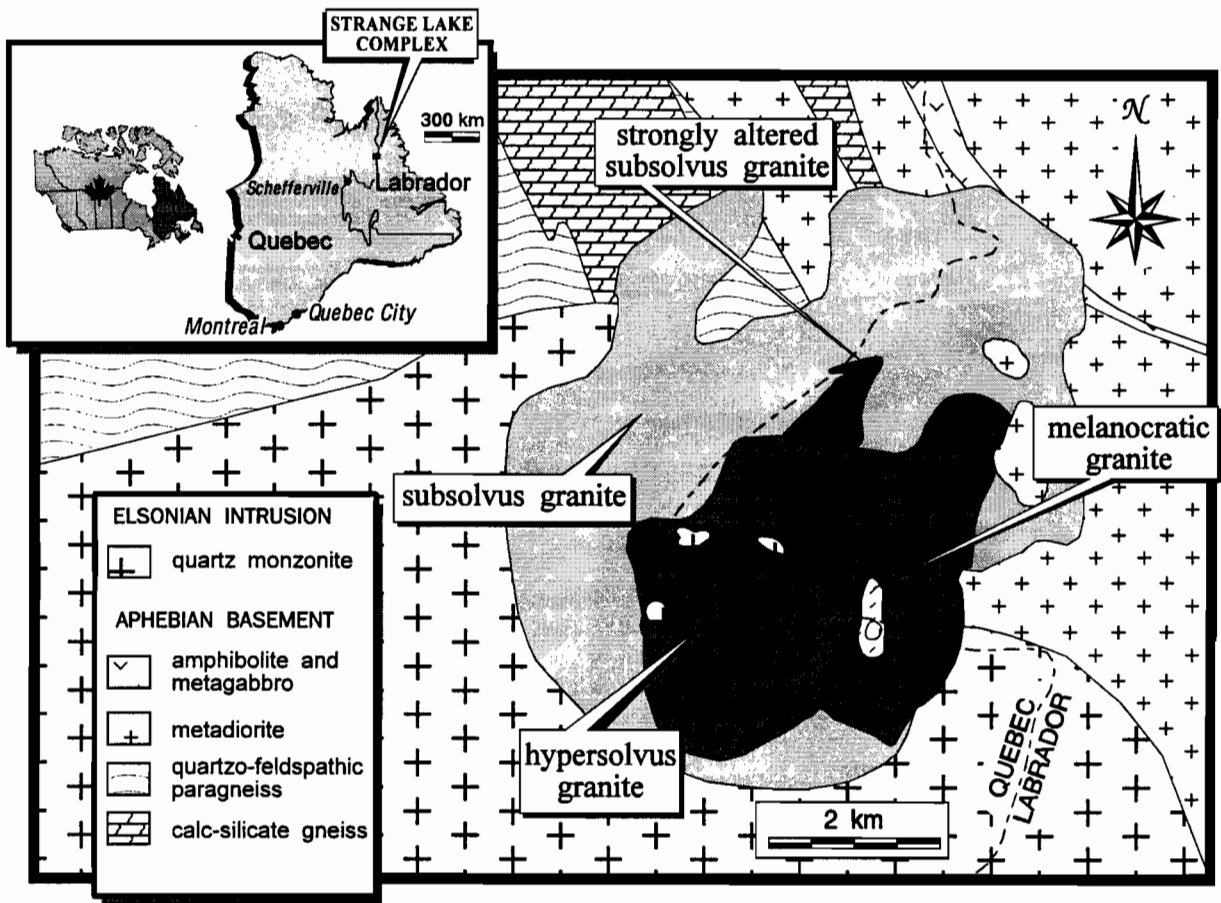
The Strange Lake pluton is a peralkaline complex of Proterozoic age ( $1189 \pm 32$  Ma, whole-rock Rb/Sr age, Pillet *et al.*, 1989), emplaced in Aphebian and Elsonian rocks of the eastern Rae province of the Canadian Shield, immediately west of the Labrador Trough (Hoffman, 1988). Together with the alkaline complexes of Flower Lake and Red Wine to the south, the Strange Lake granites are believed to represent the Labrador counterpart of the Gardar anorogenic event (Upton, 1974) in Greenland (Currie, 1985; Pillet *et al.*, 1989). This interpretation is consistent with the local tectonic model outlined by van der Leeden *et al.* (1987; see also Bélanger and van der Leeden, 1987), according to which Strange Lake is emplaced in the plateau region of the Labrador Trough (Dimroth, 1981) continental-plate collisional orogen.

The main rock types to the north of the Strange Lake pluton are Aphebian gneisses and migmatites, metamorphosed to amphibolite and granulite grade, and strongly foliated about a north-northwest south-southeast trending axis during the Hudsonian orogeny (1750 - 1800 Ma, Taylor, 1975). To the south, the Strange Lake granites intrude an Elsonian quartz monzonite, one of a number of isolated magmatic bodies believed to constitute satellite intrusions of the large, post-orogenic, 1.4-Ga-old Mistastin Batholith (Bélanger, 1984; Currie, 1985). The unfoliated nature of the Strange Lake pluton indicates that it did not undergo deformation during the Grenville orogeny (*ca.* 1100 Ma).

### Local Geology

The pluton is composed of fluorine-enriched peralkaline granites that can be subdivided, on the basis of feldspar mineralogy, into hypersolvus granite and more evolved, volatile-saturated subsolvus granites (Nassif and Martin, 1991) (Fig. 1). These rocks are mainly leucocratic, fine- to medium-grained and silica-saturated. The hypersolvus granite consists mostly of perthite, interstitial quartz and late arfvedsonite, whereas the subsolvus granite is characterised by idiomorphic quartz, arfvedsonite and alkali feldspars.

**FIGURE 1**  
Location and geological map of the Strange Lake pluton (modified after Salvi and Williams-Jones, 1990).



The granites contain abundant accessory rare-metal bearing minerals, which include aenigmatite, apatite, armstrongite, astrophyllite, dalyite, elpidite, fluorite, kainosite, yttrian milarite (Cerný *et. al.*, 1991), monazite, narsarsukite, polyolithionite, pyrochlore, thorite, titanite, vlasovite, willemite, zircon.

The quartz monzonite, which hosts the Strange Lake pluton to the south, is pink to reddish in colour, massive, and homogeneous. It is coarse-grained and contains feldspars in a rapakivi texture, quartz, hornblende, commonly replaced by biotite, and minor accessory fluorite. Rare gneiss xenoliths can be found within the quartz monzonite. The metamorphic rocks to the north of the pluton consist of quartzofeldspathic gneisses, calc-silicate gneisses, metamphibolites, metagabbros, and metadiorites. Graphitic paragneisses have also been reported by Bélanger (1984). Several large enclaves or roof pendants of both quartz monzonite and basement gneiss occur in the complex. This feature, together with the roughly circular shape and the small diameter of the pluton, suggests a shallow level of emplacement.

The subsolvus granites generally display hematite alteration, particularly at the centre of the complex (Fig. 1), where they host a potential orebody (up to 3.25% ZrO<sub>2</sub>, 1.3% REE oxides, 0.66% Y<sub>2</sub>O<sub>3</sub>, 0.56% Nb<sub>2</sub>O<sub>5</sub> and 0.12% BeO). The principal ore minerals are kainosite (Ca<sub>2</sub>[Ce,Y,HREE]<sub>2</sub>Si<sub>4</sub>O<sub>12</sub>[CO<sub>3</sub>]<sub>x</sub>H<sub>2</sub>O), gadolinite (Y<sub>2</sub>FeBe<sub>2</sub>Si<sub>2</sub>O<sub>10</sub>), gittinsite (CaZrSi<sub>2</sub>O<sub>7</sub>), gagarinite (Na[Y,Ca,Na,REE]<sub>2</sub>F<sub>6</sub>), bastnäsite ([La,Ce,Nd]CO<sub>3</sub>F), monazite ([Ce,La]PO<sub>4</sub>), and pyrochlore ([Ca,Na]<sub>2</sub>[Nb,Ta,HREE]<sub>2</sub>O<sub>6</sub>[O,OH,F]). These hematite-rich granites have lower alkali contents, higher Fe<sup>3+</sup>/Fe<sup>2+</sup>, and much higher Ca contents than the fresh subsolvus rocks. The ore zone has been the subject of a detailed fluid-inclusion study by Salvi and Williams-Jones (1990), who showed that many of the ore minerals are secondary and were precipitated by a calcium-rich aqueous fluid at a temperature of less than 200°C. This fluid was associated with a coexisting methane-rich fluid which, it was suggested, may have been derived from graphitic gneisses that occur in the area.

Salvi and Williams-Jones (1990) also described an earlier, more widely distributed episode of alteration manifested chiefly by the transformation of arfvedsonite to aegirine, and suggested that it may represent an oxidising sodium metasomatic event. This alteration

polished plates from such crystals, fluid inclusions were found along the growth zones, and along planes truncated by inclusion-free overgrowths. These inclusions are therefore interpreted to be of primary or pseudosecondary origin, respectively. Inclusions were also found in anhedral quartz concentrated in the cores of grains and aligned along short planes that parallel each other. These inclusions are also interpreted to be primary or pseudosecondary.

### Types of Fluid Inclusions

The primary and pseudosecondary fluid inclusions are classified on the basis of 1) their appearance at room temperature and 2) microthermometric data, as follows:

I) two-phase aqueous;

II) one-phase CH<sub>4</sub>;

and

III) two-phase aqueous-CH<sub>4</sub> (Fig. 2).

In addition to these, there is a group of primary and pseudosecondary inclusions that fluoresce under ultraviolet light (type-IV inclusions).

Most inclusions range from a few  $\mu\text{m}$  up to several tens of  $\mu\text{m}$  in diameter. A few exceptionally large inclusions, up to 250  $\mu\text{m}$  in diameter, were found. The morphology of the fluid inclusions is highly variable; their habit ranges from negative crystal shapes (of  $\alpha$ -quartz) to anhedral, irregularly shaped cavities. This variable habit does not seem to reflect any difference in composition or homogenisation temperature.

The aqueous inclusions (type I) are liquid-rich and generally show consistent phase ratios (the vapour occupies about 30% of the volume of the inclusions). The aqueous-CH<sub>4</sub> inclusions (type III), on the other hand, have quite variable proportions of liquid and vapour (the vapour occupies from 30% to 100% of the inclusions by volume). The variable L/V phase ratio in type-III inclusions, together with the fact that type-I, type-II and type-III inclusions can all be found in the same area, growth zone, or plane, suggest that type-III inclusions trapped variable amounts of immiscible aqueous and hydrocarbon fluids.

FIGURE 2

Sketches of typical primary and/or pseudosecondary aqueous, aqueous-carbonic and carbonic fluid inclusions.

**AQUEOUS**

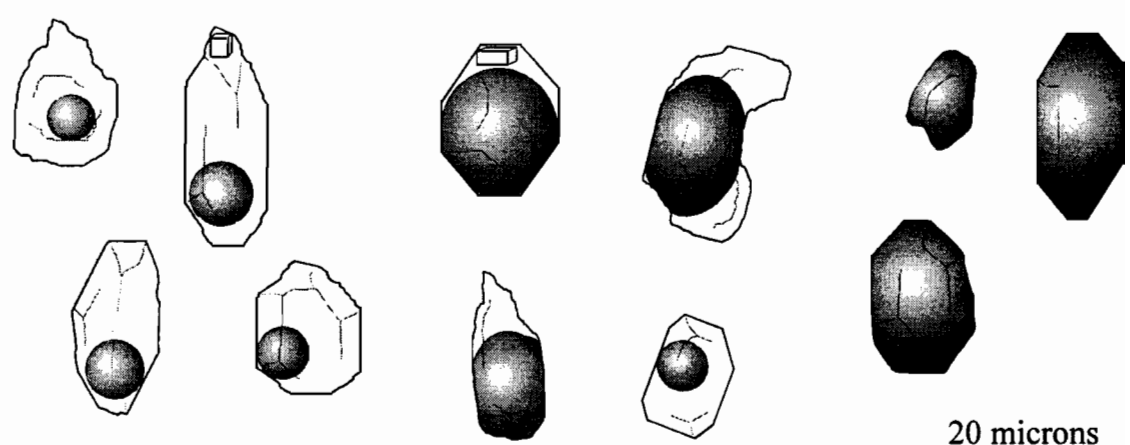
**AQUEOUS-CARBONIC**

**CARBONIC**

**(type I)**

**(type III)**

**(type II)**



20 microns

In most samples, we were able to identify type-IV inclusions. The fluorescent phase generally occurs as a meniscus around the vapour bubble in three-phase inclusions (Fig. 3) or, less commonly, occupies all of the liquid in a two-phase inclusion. Several inclusions that had been classified as type-II inclusions, *i.e.*, they only appeared to contain a vapour phase in transmitted light, were found to also contain a film of fluorescing liquid when viewed under UV illumination (Fig. 3). These inclusions were therefore reclassified as type IV. The light emitted by the fluorescing liquid ranges from aquamarine to yellow to orange, *i.e.*, wavelengths between about 500 and 620 nm of the electromagnetic spectrum, and is interpreted to be caused by the presence of aromatic or unsaturated aliphatic (or both) hydrocarbons (Rao, 1975). The fact that more than one colour of fluorescence was observed suggests that the hydrocarbon phase is composed of several compounds; furthermore, in a few cases we could observe at least two rings of different colour in the same inclusion, indicating the presence of immiscible hydrocarbons. Although by no means rare, type-IV inclusions are less abundant than type-I, type-II and type-III inclusions; they may be isolated, occur in association with other types of inclusions, or form small groups or trains.

A halite cube is present in some type-I and type-III inclusions, especially in vapour-rich ones. Generally the volume ratio of the different phases is constant, which suggests that halite is a daughter mineral. Some inclusions, however, display quite varied ratios of salt to liquid, indicating that halite crystals were locally trapped by the inclusions. On the basis of microthermometric observations (see below), the halite-bearing inclusions were not classified as a separate fluid inclusion type.

## Microthermometry

Microthermometric analyses were performed using a Fluid Inc.-adapted U.S.G.S. gas-flow heating-freezing stage (Werre *et al.*, 1979; Reynolds, 1988). Liquid N<sub>2</sub> was used as the cooling medium. The thermocouple was calibrated to  $\pm 0.2^{\circ}\text{C}$  for subzero temperatures and to  $\pm 2.0^{\circ}\text{C}$  for higher temperatures, using synthetic CO<sub>2</sub> and aqueous

**FIGURE 3**

(A) Photomicrograph showing apparent one-phase type-II and two-phase type-III fluid inclusions viewed in normal transmitted light and (B) the same inclusions viewed under ultraviolet light. Both inclusions contain fluorescing hydrocarbons and in the case of the apparent type-III inclusion the fluorescing hydrocarbons clearly surround the vapour bubble. These inclusions were therefore classified as type-IV inclusions. Scale bar = 25  $\mu\text{m}$ .

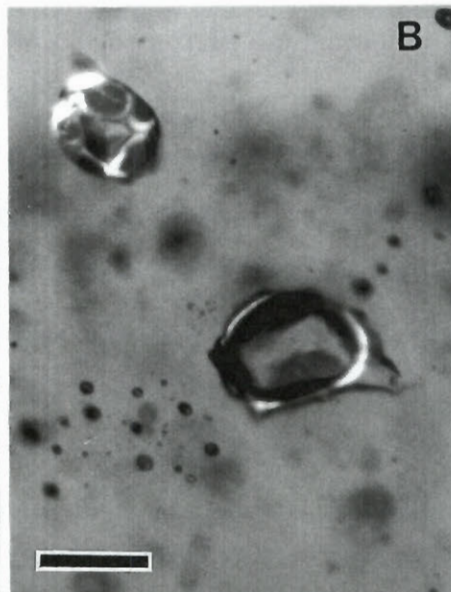
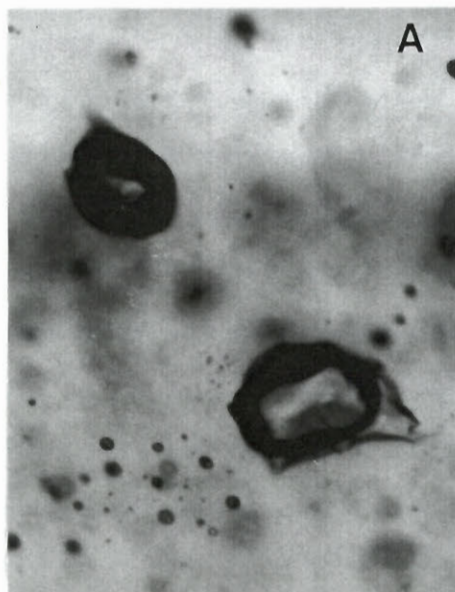


FIGURE 4

Histograms showing the distribution of initial ice melting temperatures ( $T_e$ ), final ice melting temperatures ( $T_m(\text{ice})$ ), and hydrohalite dissolution temperatures ( $T_m(\text{hyd})$ ), (A) in aqueous (type-I) fluid inclusions and (B) in the aqueous phase in aqueous-carbonic (type-III and type-IV) fluid inclusions.

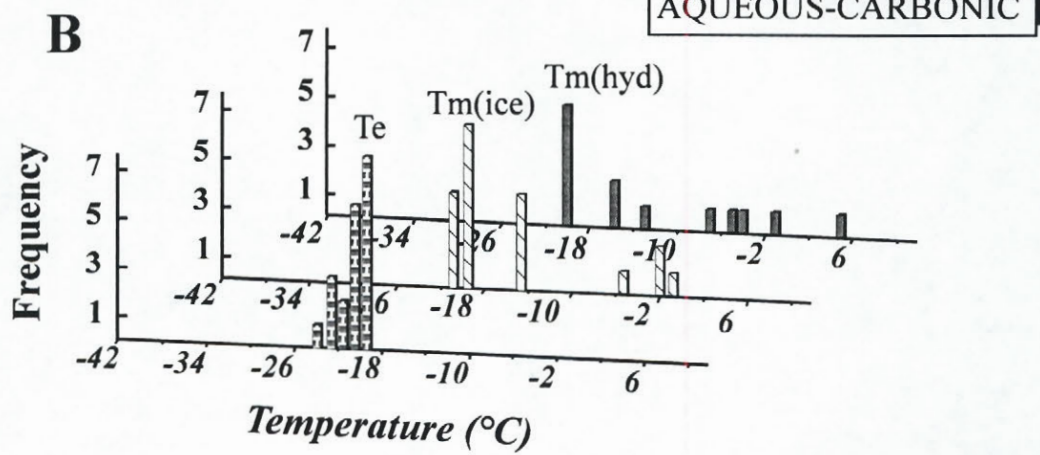
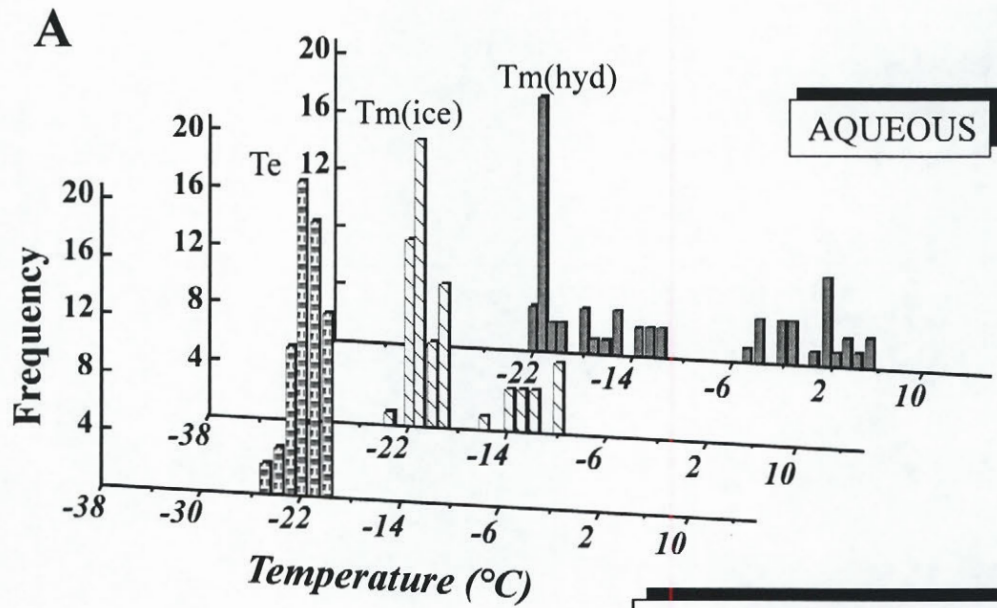
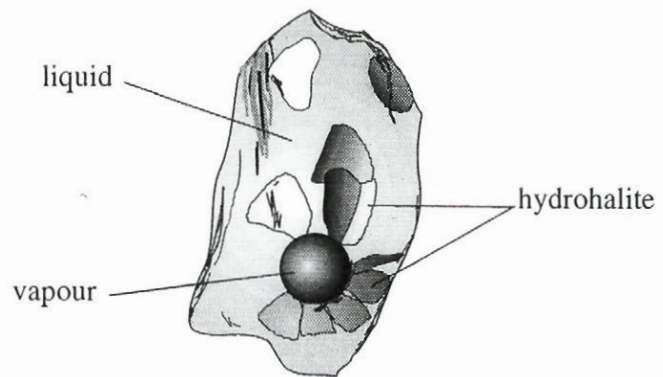


FIGURE 5

Photomicrograph under cross polars showing a type I fluid inclusion at  $-15^{\circ}\text{C}$ , containing a liquid plus several birefringent crystals of hydrohalite. Scale bar =  $25\ \mu\text{m}$ .



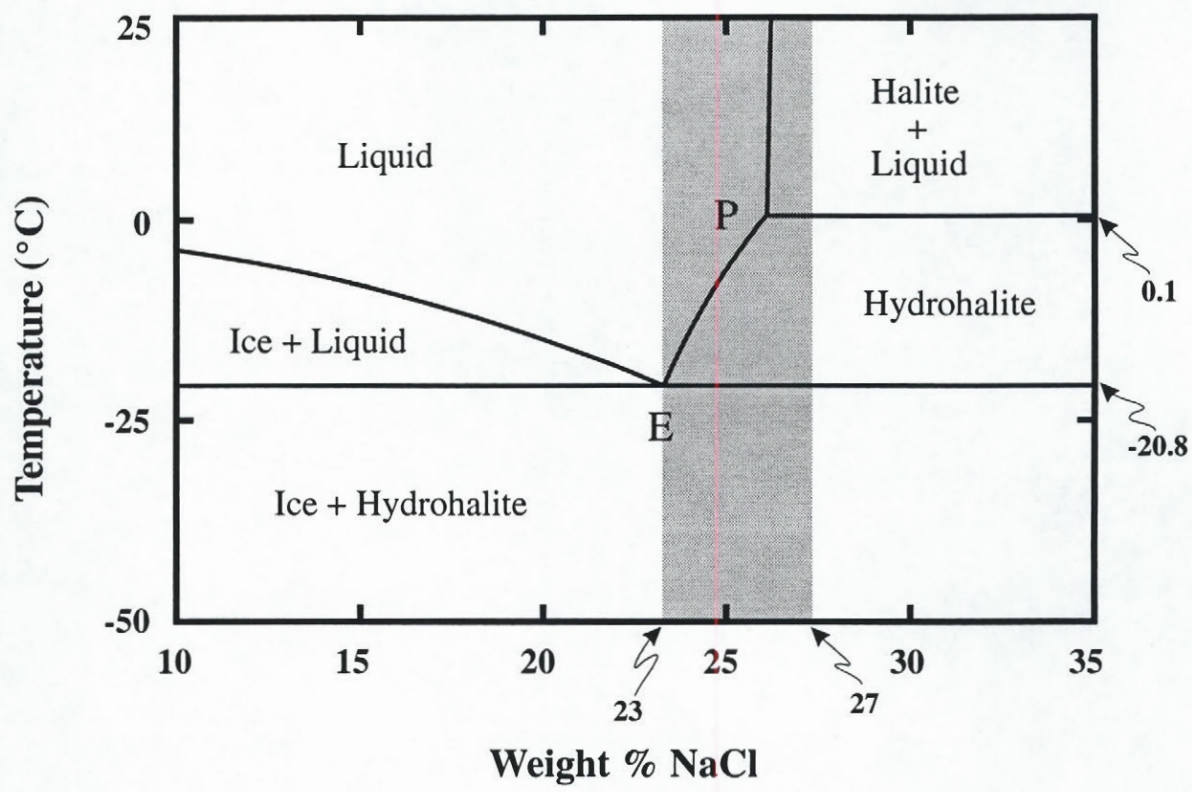
system H<sub>2</sub>O-NaCl (Fig. 6). The dissolution of hydrohalite in a few inclusions at temperatures above 0°C is attributed to metastability (Vanko *et al.*, 1988). In a small population of type-I inclusions hydrohalite does not form and the final melting of the ice occurs at higher temperature, between -16 and -10°C (Fig. 4A), corresponding to salinities between 14 wt.% and 20 wt.% NaCl (calculated using the equation of Potter *et al.*, 1978). These inclusions are typically isolated, occurring in the central parts of crystals and are not spatially associated with the higher salinity aqueous inclusions.

The aqueous solids in most type-III and type-IV inclusions display essentially identical melting characteristics to that in type-I inclusions (Fig. 4B). The ice begins to melt between -24 and -20°C, and melting is completed between -22 and -20°C; hydrohalite dissolution occurs at temperatures between -20 and +5°C. This suggests that the type-I inclusions and the aqueous phase in most type-III and type-IV inclusions represent the same fluid, and is further evidence that these latter inclusions trapped mixtures of immiscible aqueous and hydrocarbon fluids.

In a small proportion of type-III inclusions, typically liquid rich, final melting of ice occurs at temperatures between -14 and -0.2°C, and hydrohalite is not observed, indicating that these inclusions have much lower salinities than the other type-III inclusions described above. These fluid inclusions display a rather peculiar low-temperature phase behaviour (Fig. 7): at the onset of ice melting, typically at about -20°C, small bubbles or droplets appear to form with liquid along cracks that develop in the ice. These increase in number and size as melting proceeds and then, at somewhat higher temperature, usually after ~40% ice melting, dissolve in the liquid. This phenomenon is only observed on rewarming after first freezing. If the ice is allowed to recrystallise by lowering the temperature before final melting, subsequent warming is not accompanied by the appearance of the small bubbles or droplets. In most of these inclusions, a second droplet nucleates on the inner surface of the vapour bubble as the aqueous liquid freezes. The new bubble occupies about 1% to 6% of the inclusion volume. After being cooled to the temperature of liquid nitrogen and subsequently warmed, the smaller bubble undergoes a phase change at about -184°C,

FIGURE 6

Phase relations for the system H<sub>2</sub>O-NaCl (after Crawford, 1981). The hatched region indicates the range of compositions observed in the aqueous inclusions. E and P label the eutectic and peritectic points, respectively.



interpreted to represent melting; no other change can be detected on further warming, despite numerous trials. The larger bubble does not show any phase change whatsoever. The smaller bubble dissolves in the liquid as soon as the ice crystals break, generally between  $-14$  to  $-7^{\circ}\text{C}$ .

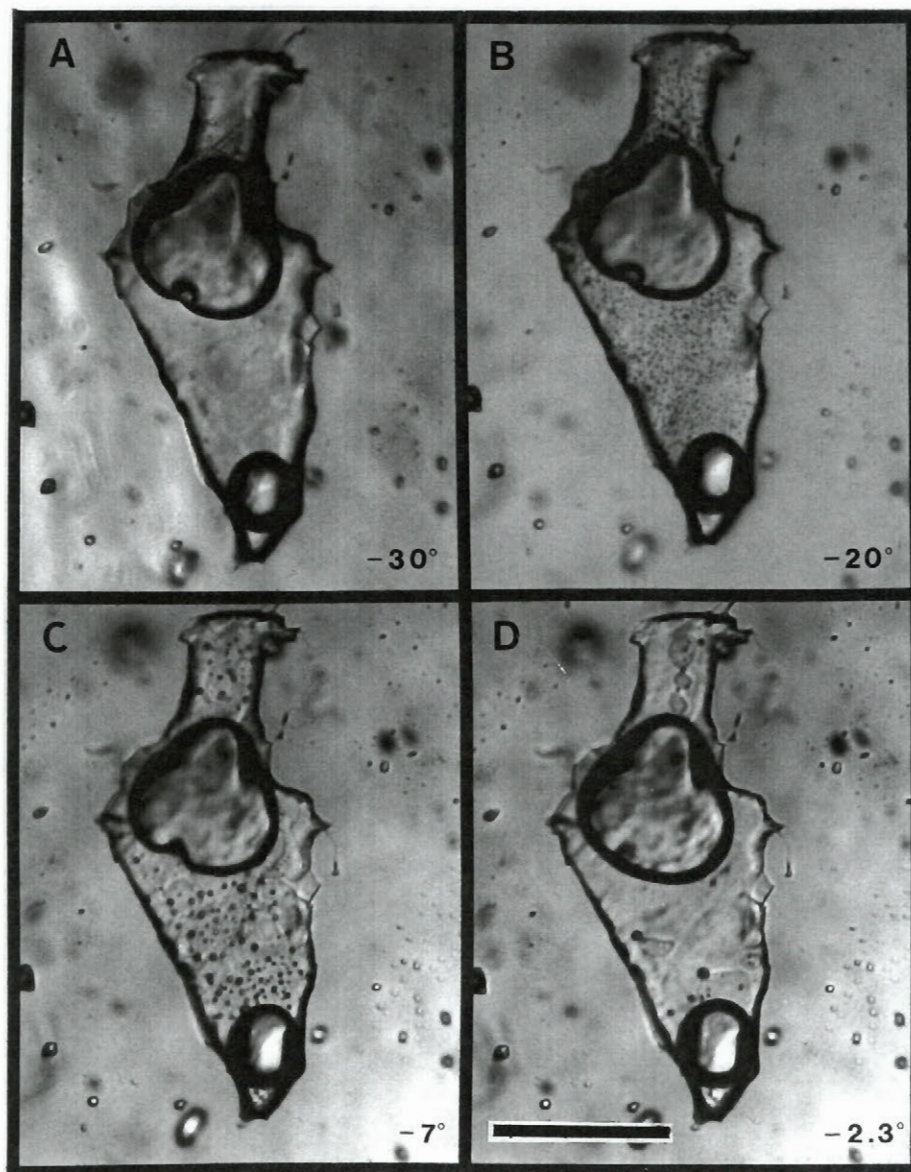
The two phenomena that have been described above are interpreted to be related to the presence of very small quantities of a hydrocarbon liquid that is miscible in the aqueous fluid at room temperature, but could not be accommodated in the ice structure. When the inclusions are frozen, most of the oil is concentrated in the second droplet, and small amounts are dispersed amongst the ice crystals. Upon warming, the oil droplets coalesce into larger, visible droplets before eventually dissolving in the aqueous liquid.

Halite-bearing type-I and type-III inclusions show essentially coincident onset and completion of ice melting, which take place in the temperature interval from  $-23$  to  $-20^{\circ}\text{C}$ . This further suggests that NaCl is the only electrolyte in the fluid. During ice melting, the halite crystal reacts with the liquid to form hydrohalite, which melts incongruently to halite +  $\text{H}_2\text{O}$  at temperatures between  $+3$  and  $+8^{\circ}\text{C}$ . In several cases, typically after an inclusion had been frozen several times, halite failed to renucleate. By contrast, several frozen two-phase inclusions nucleated a halite cube upon rewarming. These phenomena are interpreted to reflect metastable behaviour of the trapped fluid due to the fact that its composition is close to that of the  $\text{H}_2\text{O}$ -NaCl peritectic.

The majority of type-II inclusions and the  $\text{CH}_4$  phase in type-III inclusions show no phase transitions on being cooled to the temperature of liquid  $\text{N}_2$  ( $-196^{\circ}\text{C}$ ). In some cases, we were able to observe a phase change on warming the inclusions to temperatures between  $-196$  and  $-185^{\circ}\text{C}$ , but only after several attempts. This phase change probably represents liquid-vapour homogenization. Such behaviour cannot be accounted for by  $\text{CH}_4$  alone, which has its triple point at  $-182.5^{\circ}\text{C}$ , and indicates that a component that could lower the melting temperature, *e.g.*,  $\text{N}_2$ , must be present in the gas. Alternatively, the observed phase-change could represent melting, with later homogenization (to vapour) not being detectable because of the small proportion of liquid present. A less likely possibility is that it

FIGURE 7

A large type-III fluid inclusion displaying anomalous low-temperature phase behaviour. At room temperature the inclusion contains an aqueous liquid plus a carbonic vapour. Upon freezing, a small bubble nucleates along the vapour-aqueous phase interface (A). As the inclusion is warmed, small droplets appear coincident with the first ice melting (B). These droplets increase in size and number as the ice starts to break up (C), until they eventually dissolve in the liquid, after more than ~ 40% of the ice has melted (D). Scale bar = 75  $\mu\text{m}$ .



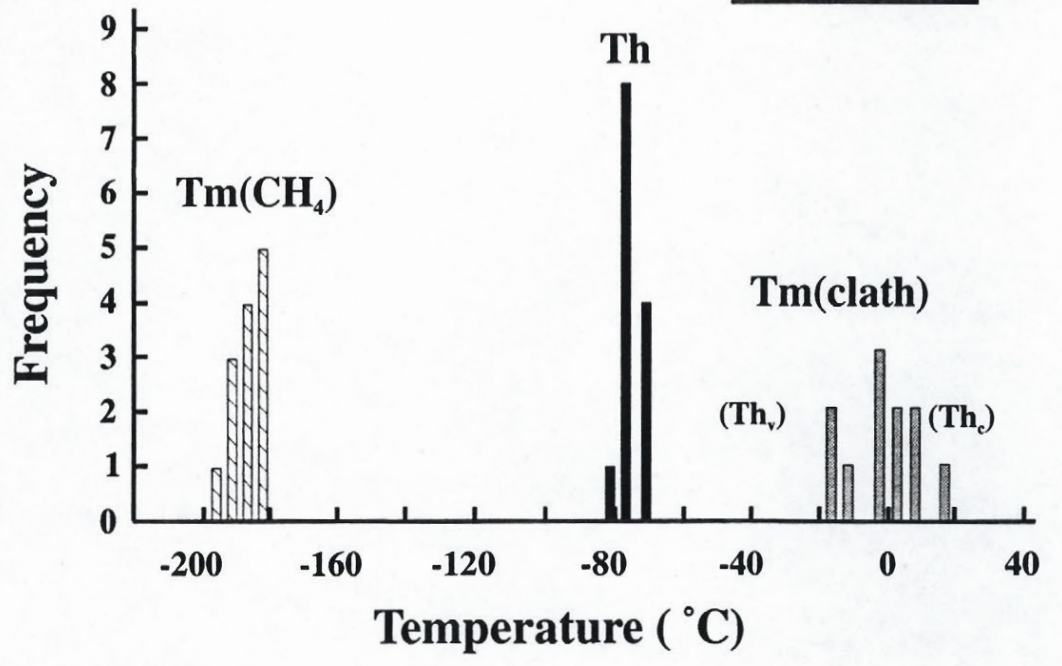
represents sublimation of the solid. When viewed under UV illumination, these inclusions do not fluoresce. Although lack of fluorescence excludes the presence of aromatic or cyclic hydrocarbons, the possibility that these inclusions contain non-fluorescing hydrocarbons, such as saturated aliphatic compounds or simple olefins (Rao, 1975), cannot be ruled out.

Some type-II inclusions, as well as the carbonic phase in some type-III and type-IV inclusions, nucleate a carbonic liquid when the temperature is lowered to about  $-100^{\circ}\text{C}$ . A solid forms when the inclusion is cooled to liquid nitrogen temperature, and melts rapidly between  $-196$  and  $-182^{\circ}\text{C}$ . Homogenization temperatures range from  $-82$  to  $-70^{\circ}\text{C}$ ; many of the inclusions homogenize critically or near critically, at temperatures between  $-78$  and  $-73^{\circ}\text{C}$  (Fig. 8). These data indicate that the carbonic phase in these inclusions, in contrast to those described above, consists dominantly of  $\text{CH}_4$  and does not contain significant  $\text{N}_2$ , but may contain minor  $\text{CO}_2$  ( $X_{\text{CO}_2}$  less than 0.1; cf. van der Kerkhof, 1988). Homogenization temperatures higher than  $-82.6^{\circ}\text{C}$  ( $T_{\text{critical}}$  of  $\text{CH}_4$ ), may alternatively be due to the presence of higher alkanes, but also in very small amounts (cf. Fig. 7 of Konnerup-Madsen *et al.*, 1979). A clathrate formed in the carbonic phase of such type-III inclusions; its melting was detected by a sudden jerk of the bubble at temperatures between  $-20$  and  $+18^{\circ}\text{C}$ , with the higher temperatures corresponding to inclusions in which homogenization of the  $\text{CH}_4$  liquid and vapour occurred near the critical temperature. The high clathrate-decomposition temperatures are consistent with recent data of Seitz and Pasteris (1990), which show that the critical isochore for  $\text{CH}_4$  intersects the decomposition boundary for  $\text{CH}_4$  clathrate at  $+19^{\circ}\text{C}$ . The lower clathrate-melting temperatures were obtained in inclusions where the  $\text{CH}_4$  phase homogenised to vapour and likewise are consistent with the data of Seitz and Pasteris (1990), which show that the temperature of clathrate melting decreases sharply with decreasing pressure, *i.e.*, decreasing density. It should be cautioned, however, that the data of Seitz and Pasteris (1990) refer to the system  $\text{CH}_4\text{-H}_2\text{O}$ , whereas the inclusions discussed here typically contain  $\geq 20$  wt.% NaCl. Unfortunately, there are no data for this system. However, by analogy with the  $\text{CO}_2\text{-H}_2\text{O}$  system, the addition of NaCl will displace the  $\text{CH}_4$ -clathrate stability field to lower temperatures (by as much as  $17^{\circ}\text{C}$  for the salinities

FIGURE 8

Histogram showing low-temperature phase relationships of the carbonic phases in type-II, type-III and type-IV fluid inclusions.  $T_m(\text{CH}_4)$  refers to the melting temperatures of the carbonic ice,  $T_h$  to the homogenization temperatures of the carbonic liquid and vapour, and  $T_m(\text{clath})$  to the decomposition of clathrate. The subscripts V and C indicate homogenization of the carbonic phase to vapour and critically, respectively.

**CARBONIC**



interpreted above; Collins, 1979). It is thus possible that the very low clathrate-melting temperatures partly reflect the effect of NaCl in the system.

Phase changes in the UV-fluorescing hydrocarbon phase in type-IV inclusions were very difficult to observe because of its small volume (Fig. 9). A few measurements indicate freezing temperatures lower than  $-100^{\circ}\text{C}$  and final melting at about  $-65^{\circ}\text{C}$ . The presence of a clathrate was inferred by a deformation of the vapour bubble, which took place after all the ice had melted. At around  $-5^{\circ}\text{C}$ , the bubble resumes its sphericity, presumably indicating clathrate melting.

### **High-Temperature Phase relations**

At temperatures above about  $350^{\circ}\text{C}$ , many inclusions decrepitated or leaked. This was particularly true of the halite-bearing inclusions. To minimise this problem, the heating rate was kept at  $1 - 2^{\circ}\text{C}/\text{min}$  above  $300^{\circ}\text{C}$ , and about  $0.5^{\circ}\text{C}/\text{min}$  near the anticipated temperature of phase changes.

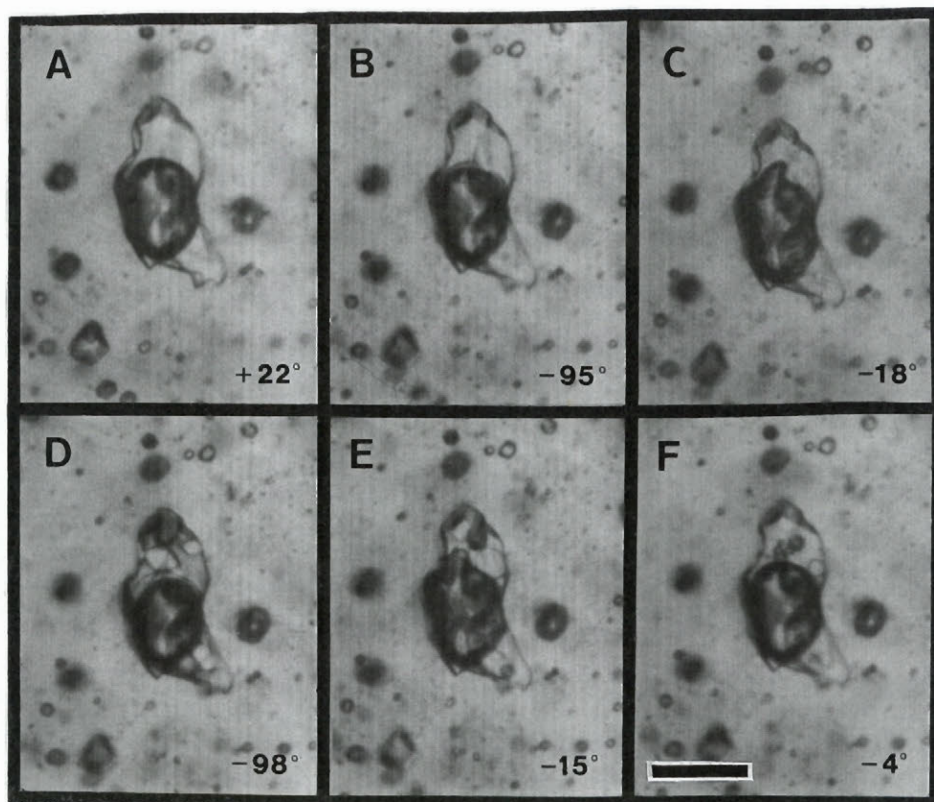
Type-I inclusions homogenize to liquid between  $100$  and  $480^{\circ}\text{C}$ , but mostly between  $300$  and  $360^{\circ}\text{C}$ ; the mode of the homogenization data is  $340^{\circ}\text{C}$  (Fig. 10). The inclusions with homogenization temperatures at either end of the scale are interpreted to reflect necking down. Leaking also took place upon heating, but inclusions that did so could be recognised because the data were not reproducible.

Type-III and type-IV inclusions homogenize to both liquid and vapour at temperatures that range from  $130^{\circ}\text{C}$  to greater than  $600^{\circ}\text{C}$ , but concentrate mainly between  $310^{\circ}\text{C}$  and  $430^{\circ}\text{C}$  (Fig. 10). This wide range of temperatures is consistent with the entrapment of mixed fluids. Liquid-rich type-III inclusions generally homogenize at temperatures between  $300$  and  $350^{\circ}\text{C}$ , whereas vapour-rich type-III inclusions homogenize at temperatures higher than  $350^{\circ}\text{C}$ , and in some cases as high as  $600^{\circ}\text{C}$  or even above the limit of the equipment ( $\geq 700^{\circ}\text{C}$ ).

The halite in halite-bearing type-I and type-III inclusions, where it was interpreted to be a daughter mineral, and in inclusions that nucleate a salt crystal during freezing (see

FIGURE 9

Low-temperature phase changes in a type-IV fluid inclusion. At room temperature the inclusion shows only two phases (A); below  $-90^{\circ}\text{C}$  the hydrocarbon ring around the vapour phase freezes, becoming visible (B); in (C) the ice has melted, leaving fine-grained hydrohalite plus a clathrate which deforms the vapour bubble. In (D) the inclusion is cooled again, before  $T_m(\text{hyd})$ , allowing growth of only a few hydrohalite crystals; the hydrocarbon ring is frozen. In (E) all the ice has melted, hydrohalite is still present and the bubble is deformed by a clathrate which melts, producing a few bubbles, at  $\sim -4^{\circ}\text{C}$  (F). Scale bar = 25  $\mu\text{m}$ .



above), generally dissolved at temperatures below 150°. These data limit the salinity of the aqueous fluid to  $\leq 27$  wt.% NaCl eq. (Fig. 6).

## SEM Decrepitate Analyses

In order to evaluate the major element composition of the aqueous fluid, we carried out SEM-EDS analyses on salt residues left by evaporation of the fluid liberated from thermally decrepitated primary fluid inclusions (Haynes and Kesler, 1987; Haynes *et al.*, 1988; Heinrich and Cousens, 1989). The instrument used was a JEM<sup>®</sup> 840 scanning electron microscope (SEM), equipped with a Tracor Northern<sup>®</sup> TN5400 energy dispersion X-ray spectrometer (EDS).

Doubly polished wafers containing primary inclusions were selected. The chips were cleaned with acetone and in an ultrasonic bath with distilled water. The samples were heated on the microthermometric stage and observed during the process. Decrepitation was achieved by holding the temperature around 400°C for a few minutes. Following the recommendation of Haynes *et al.* (1988), the temperature was kept below 450°C to avoid chloride volatilisation. The chips were allowed to cool inside the chamber and were subsequently glued onto glass slides, and carbon coated. Between the stages of sample preparation, the samples were stored in closed containers.

The morphology of the decrepitate varies from toothpaste-like twirls to hemispherical mounds to atoll- or ring-shaped masses, ranging from 5 to 20  $\mu\text{m}$  across. Euhedral salt crystals also were observed. Analyses were carried out over a rastered area covering most of the decrepitate to avoid bias from potential compositional heterogeneities, as well as differential element volatility (cf. Haynes *et al.*, 1988). The acceleration voltage was kept between 15 and 20 kV, electron beam current at 6 nA, and count time 60 s. Beam-current densities were maintained well below 0.5 nA/ $\mu\text{m}^2$ , the threshold value for light element volatility (Haynes *et al.*, 1988). Figure 11 shows an atoll-like decrepitate, with its energy-dispersion spectrum. After matrix subtraction, the only elements detected in most

FIGURE 10

Histograms showing the distribution of the homogenisation temperature of aqueous (type-I) and aqueous-carbonic (type-III and -IV) fluid inclusions.

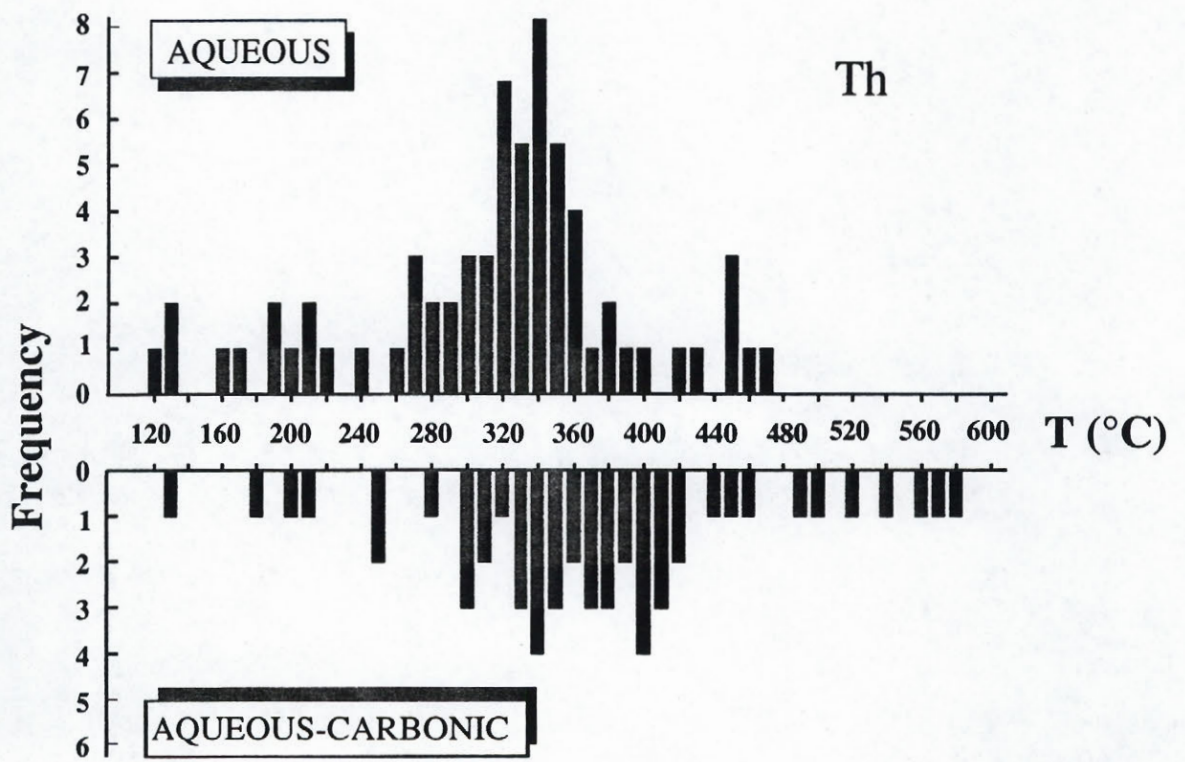
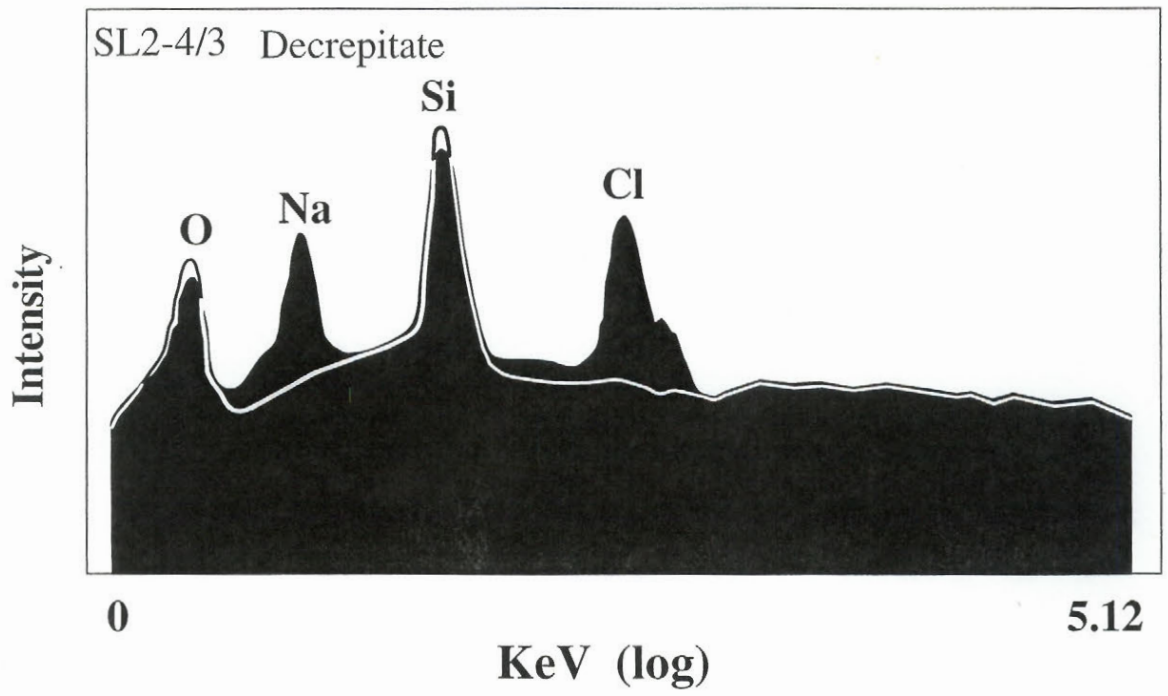
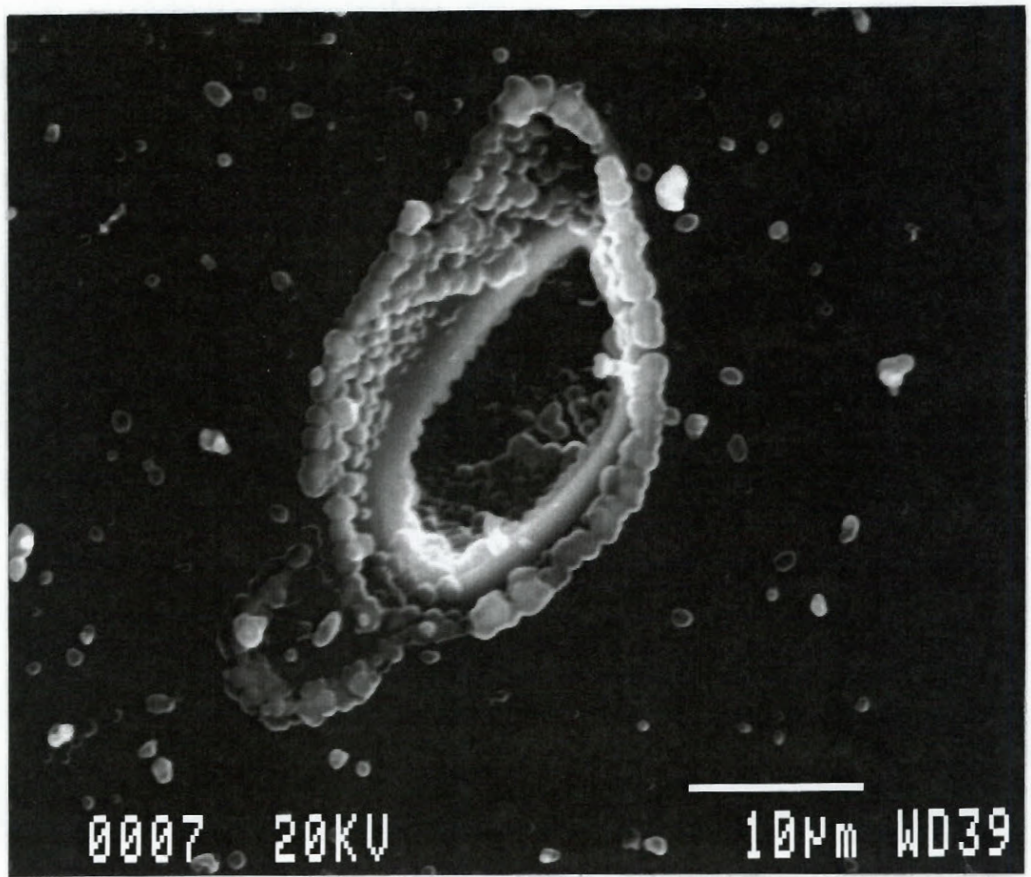


FIGURE 11

An SEM photomicrograph showing precipitates about a decrepitated primary aqueous fluid inclusion and the corresponding EDS spectrum (logarithmic scale). The white outline shows the spectrum for background quartz. The only elements detected in the precipitate are Na and Cl.



evaporite mounds were Na and Cl. Trace amounts of K were detected in a few mounds. These results confirm the microthermometric observation that NaCl is by far the most abundant salt dissolved in the aqueous fluid.

## Raman Spectroscopy

Volatile species in type-II and type-III fluid inclusions were analysed by Raman spectroscopy (Rosasco *et al.*, 1975; Delhaye and Dhamelincourt, 1975). Several type-II and type-III inclusions were sufficiently large to yield reliable results (carbonic phase >10 µm). The same doubly-polished wafers prepared for microthermometry were used for Raman analyses. Spectra were collected before performing heating runs, because of the possibility of decrepitation. Analyses were carried out on an Jobin-Yvon® Raman spectrometer, equipped with an Ionpure-Innova-100®, ionised, 6-watt argon laser source. The laser operated with a 514.5 nm exciting frequency at a laser beam power of 300 mW. Slits were set at 300 µm, and the beam was focused through a x80 objective. The monochromator was calibrated against the 918.55 cm<sup>-1</sup> peak of a neon emission lamp. Spectra were collected from co-adding 5 to 8 scans, using a counting time of 5 to 10 s and spectral increments of 0.5 cm<sup>-1</sup>. Relative concentrations (in mol%) of the gases were calculated using the equation:

$$M_a/M_b = (A_a/A_b)(F_b/F_a) = c \quad 1)$$

(Wopenka and Pasteris, 1987),

and related to mole fraction (X<sub>i</sub>) by:

$$X_a = c/(c+1) \quad 2)$$

and

$$X_b = 1/(c+1) \quad 3)$$

where

$$M_i = \text{Mol\% of species } i$$

$A_i$  = Raman peak area of species  $i$

$F_i$  = An instrument-dependent Raman quantification-factor of species  $i$  ( $\sigma_i \times \eta_h$ ) (relative to  $N_2$ ),

and

$\sigma_i$  = Raman scattering cross-section for species  $i$

$\eta_h$  = Instrumental efficiency relative to species  $i$ .

The instrument at McGill University was calibrated by analysing samples previously analysed on a similar instrument at the University of Windsor (cf. Samson and Williams-Jones, 1991); virtually identical results were obtained. These authors have calibrated the instrument at the University of Windsor using standards supplied by J.D. Pasteris of Washington University and obtained  $n$  values within 1 to 3 mol% of those determined by Pasteris and co-workers for the Washington University instrument. The  $F$  values employed in the present study are thus the same as those published by Wopenka and Pasteris (1987). Analytical precision is on the order of  $\pm 3$  mol%.

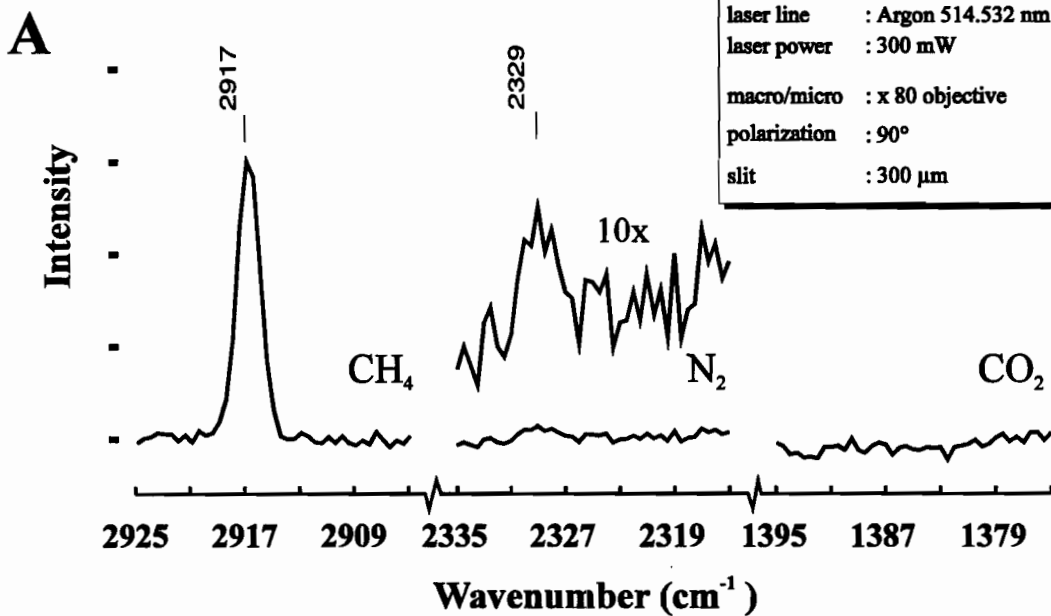
Initially, the inclusions were analysed for  $CO_2$ ,  $CH_4$ ,  $N_2$ ,  $CO$ ,  $H_2S$ ,  $C_2H_6$ ,  $NH_3$  and  $H_2$ , and only  $CH_4$  and  $N_2$  were detected. Subsequently, most inclusions were analysed only for  $CO_2$ ,  $CH_4$  and  $N_2$ , using the following spectral windows (in relative wavenumber,  $cm^{-1}$ ): 1375-1395 for  $CO_2$ , 2320-2340 for  $N_2$ , 2905-2925 for  $CH_4$ . Calculated  $X_{CH_4}$  [eq. (2),  $F_{CH_4}/F_{N_2} = 6.7$ ] was found to vary from 0.2 to 1.0, with a mode around 0.8 (Fig. 12A). The highest nitrogen contents were detected in the type-III inclusions that display the anomalously low-temperature phase behaviour described above, *i.e.* nucleation of a possible hydrocarbon liquid inside the vapour bubble on freezing. The  $X_{CH_4}$  of these inclusions ranges from 0.2 to 0.8 (Fig. 12B).

The vapour phase of fluid inclusions that were later recognised to contain a hydrocarbon phase (type-IV inclusions), fluoresces strongly (hundreds of thousands of counts/s), making it impossible to obtain Raman spectra for these inclusions.

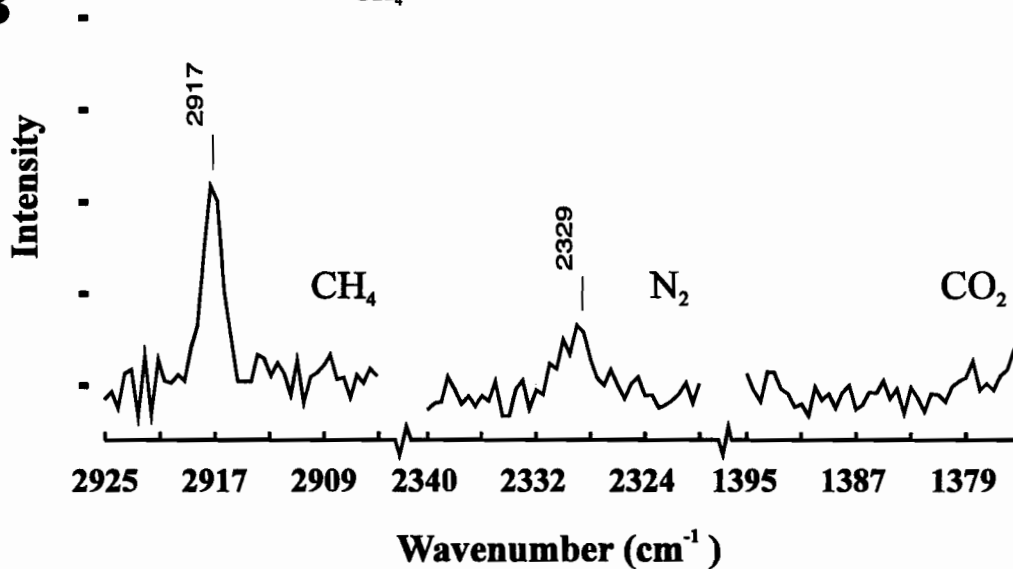
FIGURE 12

Raman spectra of the carbonic phase in aqueous-carbonic (type-III) fluid inclusions. The spectrum in (A) (low N<sub>2</sub>) is typical of a type-III fluid inclusion showing "normal" low-temperature phase relationships, whereas the spectrum in (B), in which N<sub>2</sub> is the major gas component, is of a type-III inclusion in which the aqueous phase has low salinity and in which a possible non-fluorescent hydrocarbon liquid nucleates on freezing (cf. Fig. 7).

SL4-14/6A incl. 5 ( $X_{CH_4} = 0.81$ )



**B** SL4-14/3 incl. 7 ( $X_{CH_4} = 0.18$ )



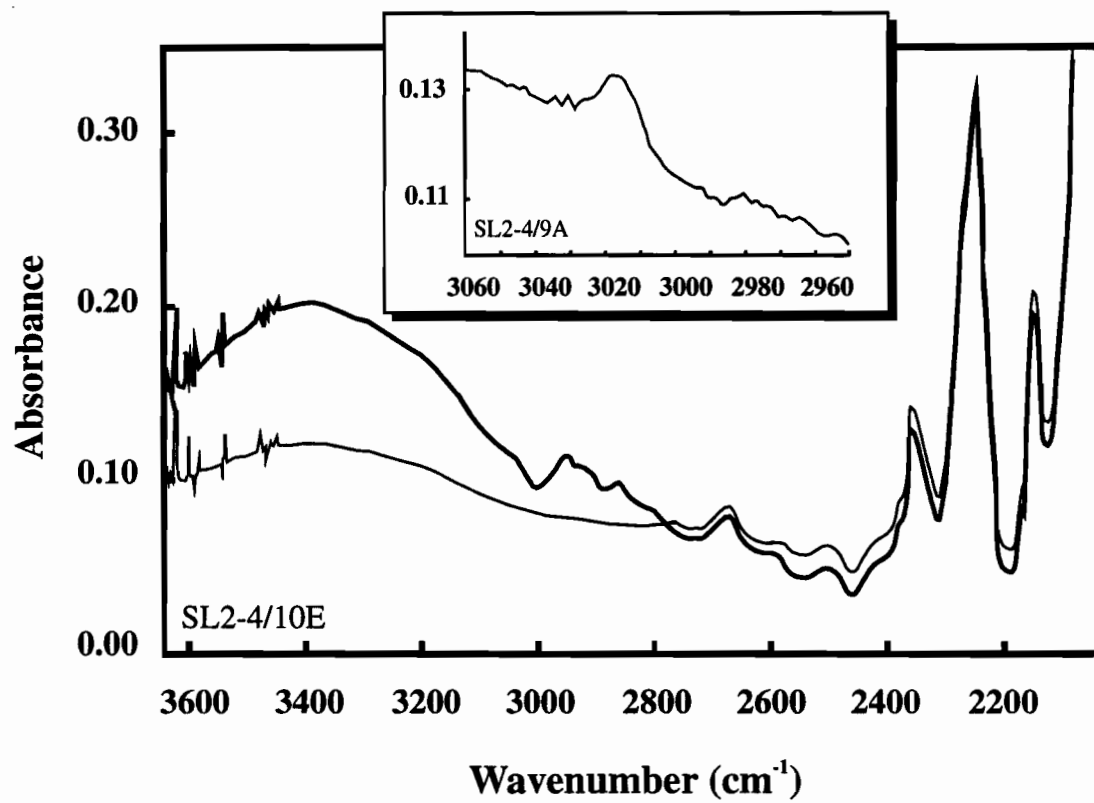
## Fourier Transform Infrared Spectroscopy

In order to identify the hydrocarbon phase contained in type-IV inclusions, and to investigate the nature of the vapour in such inclusions, which, because of fluorescence, cannot be analysed by Raman spectroscopy, Fourier transform infrared (FTIR) microspectroscopy was performed on individual inclusions (Barres *et al.*, 1987; O'Grady *et al.*, 1989; Guilhaumou *et al.*, 1990; Pironon and Barres, 1990). We also attempted to analyse type-III inclusions in which we had interpreted the presence of non-fluorescing hydrocarbons from microthermometric data. Analyses were carried out using a Perkin Elmer 16 PC FTIR spectrometer, equipped with a Perkin Elmer binocular microscope mounted with x15 objectives. Spectra were collected in transmission mode in air, co-adding 512 scans, with a spectral resolution of  $4\text{ cm}^{-1}$ , through a liquid-nitrogen cooled mercury-cadmium-telluride (MCT) detector. A blank spectrum was subtracted from each analysis to account for the effects of ambient  $\text{CO}_2$  and  $\text{H}_2\text{O}$  vapour. The doubly polished wafers containing the inclusions were placed on a petrographic slide on which a hole 2 to 3 mm in diameter had been drilled, to avoid signal interference from the glass. Spectra were collected on a transmittance scale (subsequently converted to absorbance by the instrument software) and plotted versus wavenumber (in  $\text{cm}^{-1}$ ), in the spectral range from 4400 to 2000  $\text{cm}^{-1}$  only, because quartz allows practically no transmittance at wavenumbers lower than 2000  $\text{cm}^{-1}$ .

The type-IV inclusions analysed by FTIR range from 30 to 50  $\mu\text{m}$  in diameter. When compared to the quartz matrix, the spectra for these inclusions show a broad absorbance band centred at about  $3400\text{ cm}^{-1}$ , commonly a small but well defined band at  $3018\text{ cm}^{-1}$ , and a poorly defined hump from about 3000 to  $2800\text{ cm}^{-1}$  (Fig. 13). The band at  $3400\text{ cm}^{-1}$  reflects O-H stretching of liquid water and the band at  $3018\text{ cm}^{-1}$  can probably be attributed to the  $\nu_3$  C-H stretching frequency of  $\text{CH}_4$  ( $3019\text{ cm}^{-1}$ ; Wopenka *et al.*, 1990). Although we consider it unlikely, it is possible that the  $3018\text{ cm}^{-1}$  band represents one of the C-H stretching vibrations of an aromatic hydrocarbon; these are concentrated in the 3000 to

FIGURE 13

FTIR spectra of the hydrocarbon-bearing fluid inclusion shown in Figure 9. The thin line is the quartz matrix, away from the inclusion, and the thick line is the spectrum of the inclusion. The broad band centred at  $\sim 3400\text{ cm}^{-1}$  represents the O-H stretching of water, whereas the bands below  $2700\text{ cm}^{-1}$  are due to quartz. The bands in the interval  $3000$  to  $2800\text{ cm}^{-1}$  represent symmetric and asymmetric C-H stretching of aliphatic hydrocarbons other than  $\text{CH}_4$ . The inset is a close-up of a region of the spectrum for another type-IV inclusion and shows a band at  $3018\text{ cm}^{-1}$ . This band probably represents the  $\nu_3$  C-H stretching frequency of  $\text{CH}_4$ .



3200  $\text{cm}^{-1}$  region (Guilhaumou *et al.*, 1990). The hump between 3000 and 2800  $\text{cm}^{-1}$  corresponds to C-H stretching vibrations of aliphatic hydrocarbons other than  $\text{CH}_4$ , which does not have an IR band in this region (Wopenka *et al.*, 1990). Unfortunately, the poor quality of the spectrum precludes identification of these higher hydrocarbon species.

Attempts to analyse the few type-III inclusions, interpreted to contain higher hydrocarbons (see discussion of low-temperature phase relationships), were unsuccessful, because these inclusions were either too small or too deep in the wafers.

## Discussion

### Pressure-Temperature Conditions

The coexistence of aqueous inclusions (type I), aqueous-carbonic inclusions (type III) and carbonic inclusions (type II), suggests contemporaneous entrapment of immiscible aqueous and carbonic fluids. If these fluids were in equilibrium, the compositions of the aqueous and carbonic end-members would be represented on opposite sides of a solvus and these inclusions would homogenise at the temperature of entrapment. Fluid inclusions with intermediate compositions would reflect heterogeneous entrapment of the end-member fluids and their homogenisation temperatures would be anomalously high. As will be discussed later, the data suggest that the field of immiscibility for the system  $\text{CH}_4\text{-H}_2\text{O-NaCl}_{25 \text{ wt.}\%}$  is extremely large and asymmetrical, in the sense that the aqueous phase dissolves considerably less of the  $\text{CH}_4$  component than the  $\text{CH}_4$  phase does of the aqueous component. For the purpose of estimating pressure and temperature, we have therefore assumed that the type-I inclusions could represent the aqueous fluid and the type-II inclusions (low  $\text{N}_2$ ) the carbonic fluid in this immiscible system. The small amount of  $\text{CH}_4$  (probably  $\ll 1 \text{ wt.}\%$ ) in the type-I inclusions would be easily overlooked. Although there could be as much as 10 wt.% aqueous component in the type-II inclusions, this would be in the form of a film of liquid ( $< 1\%$  of the diameter of the inclusion) and could likewise be overlooked. For obvious reasons we would have been unable to detect the final homogenisation temperature of this type-II inclusion. However, the type-I inclusions

homogenization temperature of this type-II inclusion. However, the type-I inclusions homogenize at a modal temperature of 340°C. If, as discussed above, the fluids were immiscible and trapped under equilibrium conditions, then this temperature represents the temperature of trapping. An estimate of the corresponding pressure can be obtained from the fact that the CH<sub>4</sub> phases in the type-II (low-N<sub>2</sub>) inclusions, for the most part, homogenize critically. This pressure will be given by the critical isochore of CH<sub>4</sub> at the estimated trapping temperature, 340°C, and was calculated using the equation of state of Jacobs and Kerrick (1981), to be 666 bar<sup>1</sup> (Fig. 14). If the inclusion is assumed to also contain 10 wt.% of the aqueous phase, the above estimate of pressure would increase by about 50 bar. Thus, in summary, our best estimates of the P-T conditions of fluid entrapment are approximately 700 bar and 340°C.

#### Source of Aqueous Fluid

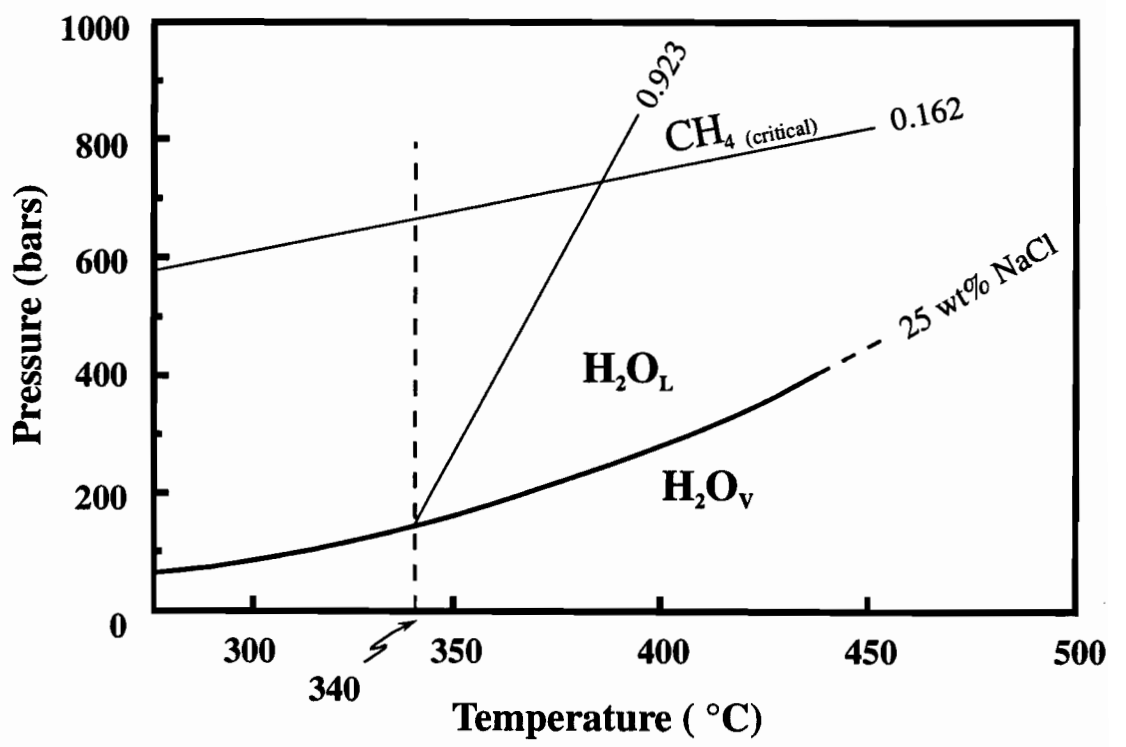
Given the concentration of many of the aqueous fluid inclusions along primary growth-zones in quartz in unaltered pegmatites and their moderately high homogenization temperatures and salinities, it is reasonable to propose that they represent an aqueous phase that separated from the crystallizing magma. The interpreted entrapment temperatures are, however, approximately 400°C below the solidus of the normal water-saturated haplogranite system (~750°C, Luth, 1976). On the other hand, there is good reason to believe that the solidus in question may have been considerably lower than 750°C. As has already been noted, the Strange Lake granites are unusually enriched in fluorine; they contain up to 2 wt.% F, which probably represents a minimum estimate for the magma, as much of the fluorine would have been lost to the vapour phase or leached during subsequent alteration. The effect of this F will have been to considerably lower the solidus temperature of the magma (Manning and Pichavant, 1985). Although there are no reports for solidus

---

<sup>1</sup> 1 bar = 100 kPa

FIGURE 14

A P-T diagram showing the bubble-point curve for the system H<sub>2</sub>O-NaCl, the modal isochore for aqueous inclusions (type I) and the critical isochore for CH<sub>4</sub>. The isochores were calculated using the computer program FLINCOR (P. Brown), with data for the aqueous system from Brown and Lamb (1989) and for CH<sub>4</sub> from Jacobs and Kerrick (1981).



temperatures of magmas comparable to those that formed the Strange Lake intrusion, it is interesting to note that a solidus temperature of 440 to 450°C at 2 kbar was reported by London *et al.* (1989) for "macusanite", a rare-element-rich volcanic glass of granitic composition containing 1.3% F. Also of interest is the solidus of 470°C at 1 kbar reported for a nepheline syenite from the rare-metal-rich Ilímaussaq complex in Greenland (Piotrowski and Edgar, 1970) which, as noted earlier, is believed to have formed during the same event of alkaline magmatism that produced the Strange Lake complex.

Thus, in summary, the above discussion suggests that the solidus temperatures of the pegmatites may have been unusually low. It is therefore reasonable to postulate that the aqueous fluids are orthomagmatic and cooled to the interpreted fluid entrapment temperatures as a result of emplacement of the pegmatite dykes into partially cooled granite and/or decompression following vapour separation. Further support for a magmatic origin for the aqueous fluids is provided by the exceptionally high proportion of Na relative to other cations in fluid inclusion decrepitates. This is consistent with predictions that low-temperature orthomagmatic fluids in equilibrium with F-enriched granites will have Na/(Na+K) ratios approaching unity (at 1 kbar and 500°C,  $Na/[Na+K] = 0.96$ ; Pichavant, 1983).

Although the bulk of the aqueous fluid inclusions are of restricted salinity, close to that of the eutectic in the system H<sub>2</sub>O-NaCl, a small proportion forms a second population with salinities ranging between 14 wt.% and 20 wt.% NaCl, and homogenisation temperatures similar to those of the other aqueous inclusions. As noted earlier, these inclusions are spatially separate from the higher-salinity type-I inclusions and occur in the central parts of crystals. According to Candela (1989; see also Bodnar and Cline, 1991), granitic magmas that become saturated with vapour at pressures below 1.3 kbar exsolve progressively more saline fluids as crystallisation proceeds. It is therefore possible that the lower-salinity inclusions represent an earlier exsolved fluid.

#### Source of Hydrocarbon Fluids

In a previous paper describing aqueous fluid inclusions associated with low-temperature (<200°C) calcic alteration of the mineralised zone at Strange Lake, Salvi and

Williams-Jones (1990) also noted the presence of coexisting CH<sub>4</sub>-vapour inclusions and concluded that these probably represented an external fluid derived from graphitic paragneisses in the surrounding Aphebian metasediments. The discovery of similar inclusions coexisting with aqueous fluid inclusions in the fresh pegmatites places this explanation in doubt. If our interpretation that the aqueous fluid inclusions are orthomagmatic is correct, then it follows that the hydrocarbon fluids also must be of magmatic origin, as inclusions containing the latter coexist with primary aqueous inclusions.

Although, to our knowledge, hydrocarbon fluid inclusions have not previously been reported from granites, they are known to occur in silica undersaturated alkaline rocks, notably in the intrusive complexes of the Gardar province in Greenland where they are interpreted to be of magmatic origin (Konnerup-Madsen, *et al.*, 1979 and 1985; Konnerup-Madsen and Rose-Hansen, 1984), and also in a number of alkaline complexes in the Soviet Union (Ikorskii, 1967; Kogarko *et al.*, 1986). Interestingly, some of these complexes contain granites but carbonic inclusions are either absent or dominated by CO<sub>2</sub> (Konnerup-Madsen and Rose-Hansen, 1982) apparently supporting the observation by Roedder (1984) that hydrocarbon fluid inclusions are restricted to silica-undersaturated alkaline igneous systems.

Many previous authors have encountered difficulty in explaining the origin of hydrocarbon fluid inclusions through magmatic processes because of the high solidus temperatures (rarely less than 700°C) of the silica-undersaturated magmas (see discussion in Roedder, 1984). At such high temperatures, significant CO<sub>2</sub> would be expected in C-O-H fluids at even the lowest geologically reasonable oxygen fugacities (cf. Holloway, 1984). In the case of Strange Lake, this problem is potentially not serious, because of the much lower inferred solidus temperatures, possibly in the range of 400 to 550°C. At 400°C and 1 kbar CH<sub>4</sub> is the only carbonic species present in the C-O-H system at  $fO_2$  less than the QFM buffer, and at 550°C and 1 kbar the same is true at  $fO_2$  2 log units below QFM (Holloway, 1984).

The presence of late, near-end-member arfvedsonite in the Strange Lake granites (Pillet, 1985; Salvi and Williams-Jones, 1990) indicates that  $fO_2$  of the magma was comparatively low. The riebeckite-arfvedsonite solid solution is characterised by variable  $Fe^{2+}/Fe^{3+}$  ratios and according to experimental data by Ernst (1962) end-member arfvedsonite reflects oxygen fugacities 2 and 5 log units lower than the QFM buffer at 400°C and 550°C, respectively. The interpreted solidus conditions are thus consistent with methane being the only species in the C-O-H system in equilibrium with the magma, amongst the species  $CH_4$ ,  $CO_2$  and  $CO$ .

If our interpretation of the origin of the  $CH_4$  is correct, then it also follows that the  $N_2$  present in some type-II and type-III fluid inclusions must be of magmatic origin. We have only been able to find one report of  $N_2$  in fluid inclusions that are interpreted to be magmatic (Chepurov *et al.*, 1975). Significantly, these inclusions were found in silica-undersaturated alkaline igneous rocks; they contain up to 20 mol%  $N_2$ .

The available data therefore support our interpretation that the  $CH_4$ , higher hydrocarbons and  $N_2$  contained in types-II, -III and -IV inclusions are of orthomagmatic origin. It is also possible that the  $CH_4$ -vapour inclusions associated with the low-temperature subsolidus alteration had the same source; our interpretation (Salvi and Williams-Jones, 1990) that they were derived from the graphitic country rocks may have been in error.

### Fluid Evolution

As noted earlier, the primary aqueous and hydrocarbon inclusions show variable ratios of hydrocarbon and aqueous phases, ranging from pure aqueous to pure hydrocarbon. This indicates that at the time of quartz growth, aqueous and hydrocarbon species were present as separate phases in the hydrothermal system and were trapped heterogeneously. It is, however, not clear whether or not separate aqueous and hydrocarbon phases were exsolved from the magma or whether a single homogeneous vapour exsolved which subsequently separated into aqueous and hydrocarbon parts. This question can, in principle, be resolved by examining phase relations in the system  $H_2O-CH_4-NaCl$ . According to the data of Krader (1985), the two-phase field increases with increasing salinity, but

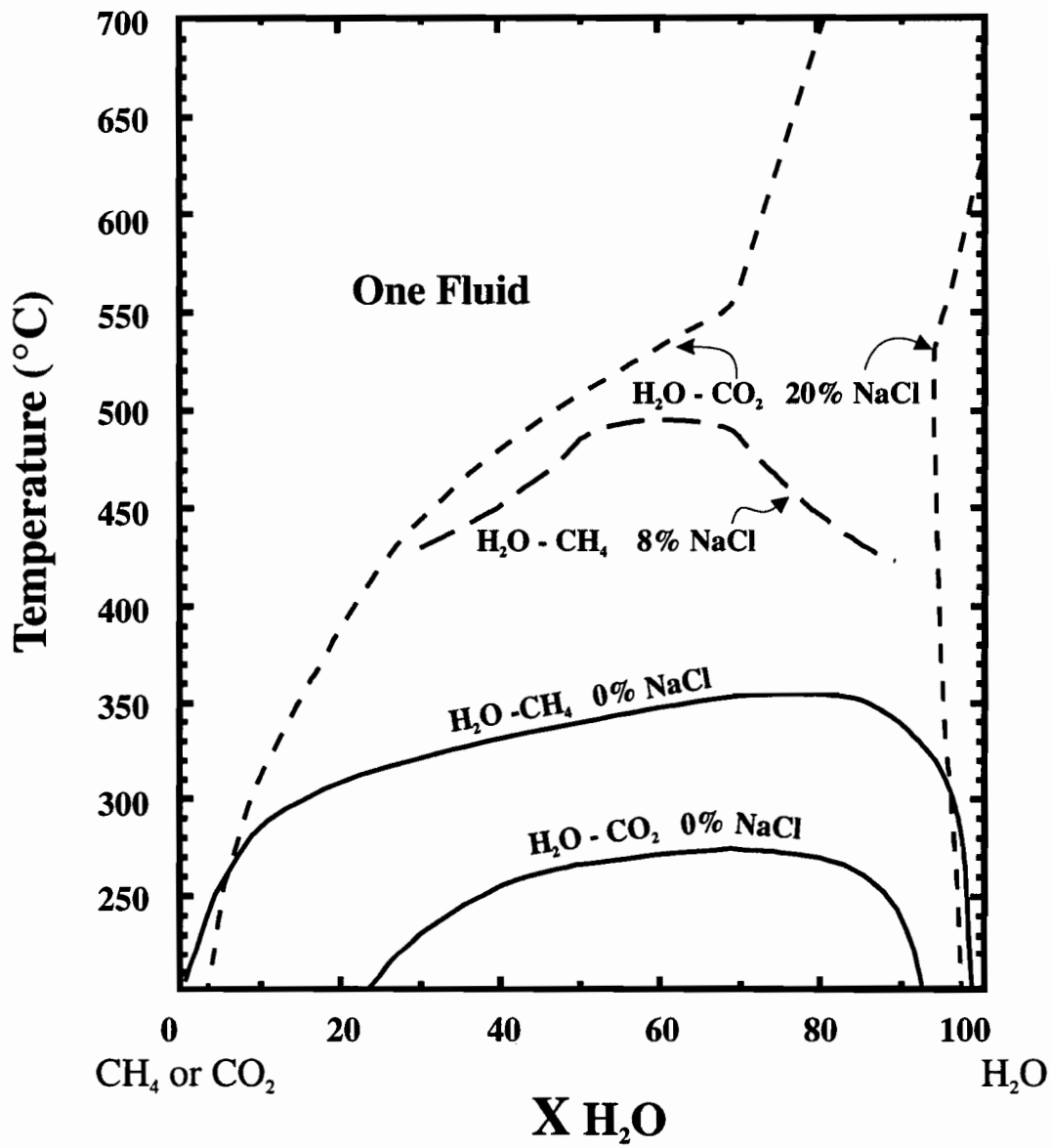
unfortunately the maximum salinity used in his experiments was 8 wt.% NaCl, whereas the aqueous fluid in the pegmatites typically contains in the order of 25 wt.% NaCl. For a fluid with 8 wt.% NaCl, the data of Krader (1985) show that there is a single homogeneous fluid for all compositions in the system H<sub>2</sub>O-CH<sub>4</sub> at temperatures above 500°C at 1 kbar (Fig. 15). If the system H<sub>2</sub>O-CO<sub>2</sub>-NaCl, for which the data of Bowers and Helgeson (1983) extend to much higher salinities, is used as an analogue, the solvus at 25 wt.% NaCl will extend to approximately 600°C. However, this undoubtedly represents a minimum temperature because, as has been shown by Holloway (1984) for the salt-free systems, the solvus for the system H<sub>2</sub>O-CH<sub>4</sub> is located at temperatures approximately 100°C higher than those of the H<sub>2</sub>O-CO<sub>2</sub> system. In view of the above discussion and the low solidus temperatures inferred for the magma, it seems likely that separate aqueous and hydrocarbon fluids were exsolved. We cannot, however, rule out the possibility that vapour saturation occurred at temperatures considerably above the solidus and that a single aqueous-hydrocarbon phase was exsolved.

Whether or not the hydrocarbon fluid exsolved separately from the aqueous fluid, it seems clear from the consistent ratios amongst hydrocarbon liquid (which fluoresces in UV light) and vapour that the hydrocarbon liquid, which contains the bulk of the higher hydrocarbons (aromatic and aliphatic), condensed after entrapment. This is consistent with the observation that virtually all hydrocarbons that are liquid at room temperature have boiling points below 300°C and more typically below 200°C, *i.e.*, well below the inferred temperature of entrapment.

The aqueous phase in a small proportion of aqueous-carbonic inclusions has final ice-melting temperatures (and salinities) considerably lower than the other aqueous-hydrocarbon inclusions described above. Moreover, the vapour phase in these inclusions is highly enriched in N<sub>2</sub>, and the higher-hydrocarbon liquid that is interpreted to occur does not fluoresce. Given the existence of a small population of lower-salinity aqueous

FIGURE 15

T-XH<sub>2</sub>O phase relations for the systems H<sub>2</sub>O-CH<sub>4</sub> and H<sub>2</sub>O-CO<sub>2</sub> at various concentrations of NaCl and 1 kbar. The solvus for 0 wt.% NaCl for the system H<sub>2</sub>O-CH<sub>4</sub> is from Holloway (1984), that for H<sub>2</sub>O-CO<sub>2</sub> is from Takenouchi and Kennedy (1964), and those for 8 wt.% and 20 wt.% NaCl are from Krader (1985) and Bowers and Helgeson (1983), respectively.



inclusions that may represent an earlier exsolved fluid, we suggest that the aqueous-carbonic inclusions discussed here represent the heterogeneously entrapped parts of the earlier exsolved fluid(s). A possible explanation for the fact that the higher hydrocarbons do not fluoresce is that ammine ( $\text{NH}_3$ ) groups eliminate fluorescence in aromatic hydrocarbons (Rao, 1975).

## Summary and Conclusions

The data indicate that the subsolvus granites and pegmatites at Strange Lake crystallized from a vapour-saturated magma that exsolved a reduced C-O-H-N-NaCl fluid(s) trapped as immiscible aqueous and hydrocarbon inclusions at temperatures and pressures of approximately 340°C and 700 kbar, respectively. There is also evidence that some of the fluids (possibly earlier) had lower salinity and were enriched in  $\text{N}_2$ . The existence of these reduced orthomagmatic fluids is consistent with the very low  $f\text{O}_2$  conditions (2 to 5 log units below the QFM buffer) interpreted for the magma from the occurrence of end-member arfvedsonite. Although similar fluids have previously been described from silica-undersaturated alkaline rocks, the pegmatites at Strange Lake provide the first example of hydrocarbon inclusions in a granitic system.

## References

- Barres, O., Burneau, A., Dubessy, J. and Pagel, M., 1987. Application of micro-FT-IR spectroscopy to individual hydrocarbon fluid inclusions analysis. *Appl. Spectrosc.*, 41, 1000-1008.
- Bélanger, M., 1984. Région du lac Brisson. *Ministère de l'Énergie et des Ressources, Québec*, DP 84-20 (carte annotée, échelle 1:50,000).
- Bélanger, M. and van der Leeden, J., 1987. Le projet Rivière George: Une première évaluation métallogénique. Exploration au Québec, études géoscientifiques récentes, Séminaire d'information, DV 87-25, 95-100.
- Bergman, S.C. and Dubessy, J., 1984. CO<sub>2</sub>-CO fluid inclusions in a composite peridotite xenolith: Implication for upper mantle oxygen fugacity. *Contrib. Mineral. Petrol.*, 85, 1-13.
- Bodnar, R.J. and Cline, J.S., 1991. Fluid inclusion petrology of porphyry copper deposits revisited: Re-interpretation of observed characteristics based on recent experimental and theoretical data [abs]. *Plinius*, 5, 24-25.
- Bowers, T. S. and Helgeson, H. C., 1983. Calculation of thermodynamic and geochemical consequences of non ideal mixing in the system H<sub>2</sub>O-CO<sub>2</sub>-NaCl on phase relations in geological systems: Equation of state for H<sub>2</sub>O-CO<sub>2</sub>-NaCl fluids at high pressures and temperatures. *Geochim. Cosmochim. Acta*, 47, 1247-1275.
- Brown, P.E. and Lamb, W.M., 1989. P-V-T properties of fluids in the system H<sub>2</sub>O±CO<sub>2</sub>±NaCl: New graphical presentations and implications for fluid inclusion studies. *Geochim. Cosmochim. Acta*, 53, 1209-1221.
- Candela, P.A., 1989. Calculation of magmatic fluid contributions to porphyry-type ore systems: Predicting fluid inclusion chemistries. *Geochem. Jour.*, 23, 295-305.
- Cerný, P., Hawthorne, F.C., Jambor, J.L. and Grice, J.D., 1991. Yttrian milarite. *Can. Mineral.*, 29, 533-541.
- Chepurov, A.I., Shatskiy, V.S., Pokachalova, O.S. and Lavrent'yev, Yu.G., 1975. Evidence from melt inclusions on the chemistry and crystallization of theralites in some Kuznetsk Alatau intrusions. *Geokhimiya*, 4, 595-602. Translated in *Geochem. Int.*, 12, 1975, 242-250.

- Chou, I-M., Pasteris, J.D. and Seitz., J.C., 1990.** High-density volatiles in the system C-O-H-N for the calibration of a laser Raman microprobe. *Geochim. Cosmochim. Acta*, 54, 535-543.
- Collins, P.L.F., 1979.** Gas hydrates in CO<sub>2</sub>-bearing fluid inclusions and the use of freezing data for estimation of salinity. *Econ. Geol.*, 74, 1435-1444.
- Crawford, M.L., 1981.** Phase equilibria in aqueous fluid inclusions. In *Fluid Inclusions: Application To Petrology.*, *Mineral. Ass. of Canada, Short course Handbook*, L.S. Hollister and M.L. Crawford, eds. 6, 39-74.
- Currie, K.L., 1985.** An unusual peralkaline granite near Lac Brisson, Quebec-Labrador. *Geological Survey of Canada, Paper 85-1A*, 73-90.
- Davis, D.W., Lowenstein, T.K. and Spencer, R.J., 1990.** Melting behaviour of fluid inclusions in laboratory-grown halite crystals in the systems NaCl-H<sub>2</sub>O, NaCl-KCl-H<sub>2</sub>O, NaCl-MgCl<sub>2</sub>-H<sub>2</sub>O and NaCl-CaCl<sub>2</sub>-H<sub>2</sub>O. *Geochim. Cosmochim. Acta*, 54, 591-602.
- Delhaye, M. and Dhamelincourt, P., 1975.** Raman microprobe and microscope with laser excitation. *J. Raman Spectr.*, 3, 33.
- Dimroth, E., 1981.** Labrador geosyncline: Type example of early Proterozoic cratonic reactivation. In *Developments in Precambrian Geology*, A. Kroner, ed., Elsevier, Amsterdam, 4, 331-352.
- Ernst, W.G., 1962.** Synthesis, stability relations, and occurrence of riebeckite and riebeckite-arfvedsonite solid solution. *J. Geol.*, 70, 689-736.
- Gerlach, T.M., 1980.** Evaluation of volcanic gas analyses from Kilauea Volcano. *J. Volcanol. Geoth. Res.*, 7, 295-317.
- Gerlach, T.M., 1982.** Interpretation of volcanic gas data from tholeiitic and alkaline mafic lavas. *Bull. Volcanol.*, 45, 235-244.
- Guilhaumou, N., Szydłowski, N. and Pradier, B., 1990.** Characterization of hydrocarbon fluid inclusions by infra-red and fluorescence microspectrometry. *Mineral. Magazine*, 54, 311-324.
- Haynes, F.M., 1985.** Determination of fluid inclusion compositions by sequential freezing. *Econ. Geol.*, 80, 1436-1439.

- Haynes, F.M. and Kesler, S.E., 1987. Chemical evolution of brines during Mississippi Valley-Type mineralization: Evidence from East Tennessee and Pine Point. *Econ. Geol.* 82, 53-71.
- Haynes, F.M., Sterner, S.M. and Bodnar, R.J., 1988. Synthetic fluid inclusions in natural quartz. IV. Chemical analyses of fluid inclusions by SEM/EDA: Evaluation of method. *Geochim. Cosmochim. Acta*, 52, 969-977.
- Heinrich, C.A. and Cousens, D.R., 1989. Semi-quantitative electron microprobe analysis of fluid inclusion salts from the Mount Isa copper deposit (Queensland, Australia). *Geochim. Cosmochim. Acta*, 53, 21-28.
- Hoffman, P.F., 1988. United plates of America, the birth of a craton: early Proterozoic assembly and growth of Proto-Laurentia. *Annual Reviews of Earth and Planetary Sciences*, 16, 71 p.
- Holloway, J.R., 1976. Fluids in the evolution of granitic magmas: Consequences of finite CO<sub>2</sub> solubility. *Geol. Soc. Am. Bull.*, 87, 1513-1518.
- Holloway, J.R., 1984. Graphite-CH<sub>4</sub>-H<sub>2</sub>O-CO<sub>2</sub> equilibria at low-grade metamorphic conditions. *Geology*, 12, 455-458.
- Ikorskii, S.V., 1967. *The Organic Substances in the Minerals of Igneous Rocks* (in Russian). Nauka, Leningrad.
- Jacobs, G.K. and Kerrick, D.M., 1981. Methane: An equation of state with application to the ternary system H<sub>2</sub>O-CO<sub>2</sub>-CH<sub>4</sub>. *Geochim. Cosmochim. Acta*, 45, 607-614
- Kerkhof, van der, A.M., 1988. *The System CO<sub>2</sub>-CH<sub>4</sub>-N<sub>2</sub> in Fluid Inclusions: Theoretical Modelling and Geological Applications*. Ph.D. Thesis, Vrije Universiteit, Amsterdam, NL, 206 p.
- Kogarko, L.N., Kosztolanyi, Ch. and Ryabchikov, I.D., 1986. Geochemistry of the reduced fluid in alkali magmas. *Geokhimiya*, 12, 1688-1986. Translated in *Geochem. Int.*, 24, 1987, 20-27.
- Konnerup-Madsen, J. and Rose-Hansen, J., 1982. Volatiles associated with alkaline igneous rift activity: fluid inclusions in the Ilímaussaq intrusion and the Gardar granitic complexes (South Greenland). *Chem. Geol.*, 37, 79-93.
- Konnerup-Madsen, J. and Rose-Hansen, J., 1984. Composition and significance of fluid inclusions in the Ilímaussaq peralkaline granite, South Greenland. *Bull. Minéral.*, 107, 317-326.

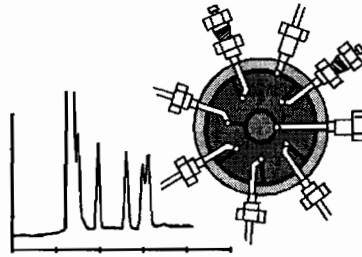
- Konnerup-Madsen, J., J. Larsen, E. and Rose-Hansen, J., 1979. Hydrocarbon-rich inclusions in minerals from the alkaline Ilímaussaq intrusion, South Greenland. *Bull. Minéral.*, 102, 642-653.
- Konnerup-Madsen, J., Dubessy, J. and Rose-Hansen, J., 1985. Combined Raman microprobe spectrometry and microthermometry of fluid inclusions in minerals from igneous rocks of the Gardar province (south Greenland). *Lithos*, 18, 271-280.
- Krader, T., 1985. *Phasengleichgewichte und Kritische Kurven des Ternären Systems H<sub>2</sub>O-CH<sub>4</sub>-NaCl bis 250 MPa und 800K*. Ph.D. Thesis, Universität Fridericiana, Karlsruhe, FRG, 109 p.
- Leeden, van der, J., Bélanger, M., Danis, D. and Girard, R., 1987. Lithotectonic domains in the high-grade terrain east of the Labrador Trough (Québec) [abs]. In *program with abstracts, GAC-MAC-CSPG joint annual meeting*, Saskatoon, 98.
- London, D., Morgan, G.B. and Hervig, R.L., 1989. Vapor-undersaturated experiments with marcusani glass plus H<sub>2</sub>O at 200 MPa, and the internal differentiation of granitic pegmatites. *Contrib. Mineral. Petrol.*, 102, 1-17.
- Luth, W.C., 1976. Granitic rocks. In *The Evolution of the Crystalline Rocks*, D.K. Bailey and R. MacDonald, eds. Academic Press, London, 335-417.
- Manning, D.A.C. and Pichavant, M., 1985. Volatiles and their bearing on the behaviour of metals in granitic systems. In *Recent Advances in the Geology of Granite-Related Mineral Deposits*, R.P. Taylor and D.F. Strong eds. CIM spec. vol., 39, 291-302.
- Miller, R.R., 1986. Geology of the Strange Lake Alkalic Complex and the associated Zr-Y-Be-REE mineralization. *Current Research, Newfoundland Dept. of Mines and Energy*, Report 86-1, 11-19.
- Nassif, G.J. and Martin R.F., 1991. The hypersolvus granite-subsolvus granite transition at Strange Lake, Québec-Labrador [abs]. In *Program with Abstracts, GAC-MAC-CSPG joint annual meeting*, Toronto, A89.
- O'Grady, M.R., Bodnar, R.J., Hellgeth, J.W., Conroy, C.M., Taylor, L.T. and Knight, C.L., 1989. Fourier-transform infrared (FTIR) microspectrometry of individual petroleum fluid inclusions in geological samples. In *Microbeam Analysis-1989*, P.E. Russell, ed., San Francisco Press Inc. 579-582.

- Pasteris, J.D. and Wanamaker, B.J., 1988. Laser Raman microprobe analyses of experimentally re-equilibrated fluid inclusions in olivine: Some implications for mantle fluids. *Am. Mineral.*, 73, 1074-1088.
- Petersilie, I.A., 1962. Origin of hydrocarbon gases and dispersed bitumens of the Khibina alkalic massif. *Geokhimiya*, 1, 15-29. Translated in *Geochem. Int.*, 1, 1962, 14-30.
- Petersilie, I.A., 1963. Organic matter in igneous and metamorphic rocks of the Kola peninsula. In *Chemistry of the Earth's Crust*, A.P. Vinogradov, ed., 1, 178-184.
- Petersilie, I.A. and Sørensen, H., 1970. Hydrocarbon gases and bituminous substances in rocks from the Ilímaussaq alkaline intrusion, south Greenland. *Lithos*, 3, 59-76.
- Pichavant, M., 1983. (Na, K) exchange between alkali feldspars and aqueous solutions containing borate and fluoride anions; experimental results at P = 1 kbar. 3<sup>rd</sup> NATO Advanced Study Institute on Feldspars, Feldspathoids and their Paragenesis, Rennes, France, 102 p.
- Pillet, D., 1985. Le granite peralkalin du lac Brisson, Territoire du Nouveau-Québec: Résultats préliminaires. *Ministère de l'Énergie et des Ressources, Québec*, MB 85-87, 51 p.
- Pillet, D., Bonhomme, M.G., Duthou, J.L. and Chenevoy, M., 1989. Chronologie Rb/Sr et K/Ar du granite peralkalin du lac Brisson, Labrador central, Nouveau-Québec. *Can. J. Earth Sci.*, 26, 328-332.
- Piotrowski, J.M. and Edgar, A.D., 1970. Melting relations of undersaturated alkaline rocks from South Greenland compared to those of Africa and Canada. *Medd. Grønland*, 181, 1-62.
- Pironon, J. and Barres, O., 1990. Semiquantitative FT-IR microanalysis limits: Evidence from synthetic hydrocarbon fluid inclusions in sylvite. *Geochim. Cosmochim. Acta*, 54, 509-518.
- Potter, R.W., Clynne, M.A. and Brown, D.L., 1978. Freezing point depression of aqueous sodium chloride solutions: *Econ. Geol.*, 73, 284-285.
- Rao, C.N.R., 1975. *Ultra-Violet and Visible Spectroscopy*. 3<sup>rd</sup> edition, Butterworths and Co., London, 242 p.
- Reynolds, T.J., 1988. *Shor*

- Roedder, E. and Coombs, D.S., 1967.** Immiscibility in granitic melts, indicated by fluid inclusions in ejected granitic blocks from Ascension Island. *J. Petrol.*, 8, 417-451.
- Rosasco, G.J., Roedder, E. and Simmons, J.H., 1975.** Laser activated Raman spectroscopy for nondestructive partial analysis of individual phases in fluid inclusions in minerals. *Science*, 190, 557-560.
- Salvi, S. and Williams-Jones, A.E., 1990.** The role of hydrothermal processes in the granite-hosted Zr, Y, REE deposit at Strange Lake, Quebec/Labrador: Evidence from fluid inclusions. *Geochim. Cosmochim. Acta*, 54, 2403-2418.
- Samson, I. and Williams-Jones, A.E., 1991.** C-O-H-N-salt fluids associated with contact metamorphism, McGerrigle Mountains, Quebec: A Raman spectroscopic study. *Geochim. Cosmochim. Acta*, 55, 169-177.
- Seitz, J.C. and Pasteris, J.D., 1990.** Theoretical and practical aspects of differential partitioning of gases by clathrate hydrates in fluid inclusions. *Geochim. Cosmochim. Acta*, 54, 631-639.
- Sobolev, V.S., Bazarova, T.Y., Shugurova, N.A., Bazarov, L.Sh., Dolgov, Yu.A. and Sørensen, H., 1970.** A preliminary examination of fluid inclusions in nepheline, sorensenite, tugtupite and chkalovite from the Ilímaussaq alkaline intrusion, South Greenland, *Medd. Grønland*, 181, 11, 1-32.
- Sommer, M.A., 1977.** Volatiles H<sub>2</sub>O, CO<sub>2</sub>, and CO in silicate melt inclusions in quartz phenocrysts from the rhyolitic Bandelier air-fall and ashflow tuff, New Mexico. *J. Geol.*, 85, 423-432.
- Takenouchi, S. and Kennedy, G.C., 1964.** The binary system H<sub>2</sub>O-CO<sub>2</sub> at high temperatures and pressures. *Am. J. Sci.*, 262, 1055-1074.
- Taylor, F.C., 1975.** Lac Brisson, Quebec-Newfoundland. *Geological Survey of Canada*, Map 1439A, scale 1:250,000.
- Upton, B.G.J., 1974.** The alkaline province of southwest Greenland. In *The Alkaline Rocks*, H. Sørensen, ed. Wiley Interscience, New York, 221-238.
- Vanko, D.A., Bodnar, R.J. and Sterner, S.M., 1988.** Synthetic fluid inclusions. VIII. Vapour-saturated halite solubility in part of the system NaCl-CaCl<sub>2</sub>-H<sub>2</sub>O, with application to fluid inclusions from oceanic hydrothermal system. *Geochim. Cosmochim. Acta*, 52, 2451-2456.

- Werre, R.W., Jr., Bodnar, R.J., Bethke, P.M. and Barton, P.B., Jr., 1979. A novel gas-flow fluid inclusion heating/freezing stage [abs.] In *Abstracts with programs, Geol. Soc. Am.*, 11, 539.
- Wopenka, B. and Pasteris, J.D., 1987. Raman intensities and detection limits of geochemically relevant gas mixtures for a laser Raman microprobe. *Anal. Chem.*, 59, 2165-2170.
- Wopenka, B., Pasteris, J.D. and Freeman, J.J., 1990. Analysis of individual fluid inclusions by Fourier transform infrared and Raman microspectroscopy. *Geochim. Cosmochim. Acta*, 54, 519-533.
- Zajac, I.S., Miller, R.R., Birkett, T. and Nantel, S., 1984. Le gîte de Zr, Y, Nb et Be du complexe alcalin de Strange Lake, Québec-Labrador. *Ministère de l'Énergie et des Ressources, Québec*, DV 84-18, 127-142.

## CHAPTER III



### CHARACTERISATION OF THE CARBONIC INCLUSIONS

---

## Prologue

ANALYSIS of the volatile content of fluid inclusions can be carried out using either destructive or non-destructive techniques (cf. Roedder, 1990 for summary). The only established quantitative non-destructive methods are laser Raman spectroscopy (*e.g.*, Rosasko *et al.*, 1975; Delhaye and Dhameincourt, 1975; Pasteris *et al.*, 1986; Chou *et al.*, 1990) and micro-Fourier transform infrared spectroscopy (FTIR) (*e.g.*, Barres *et al.*, 1987; Brown and Vry, 1990; Guilhaumou *et al.*, 1990; Pironon and Barres, 1990). In addition to the obvious advantages of sparing the sample, these techniques also overcome the problem of ensuring that only one fluid inclusion population is sampled, by permitting single inclusions to be analysed. Raman spectroscopy can also provide valuable information on the pressure of the gases in the inclusion, based on displacements of the diagnostic peaks from their standard positions (*e.g.*, Seitz *et al.*, 1993). Important limitations are high detection limits (~1 mol % for the Raman and higher for FTIR; *e.g.*, Wopenka and Pasteris, 1987) of both these techniques, the large inclusion diameter (>20  $\mu\text{m}$ ) required by FTIR (Wopenka *et al.*, 1990), and the inability of Raman spectroscopy to analyse cyclic and aromatic hydrocarbons, because of strong interference due to fluorescence of these compounds when bombarded by the laser beam (514.5 and 488.5 nm wavelength).

The destructive techniques that have been developed for the analysis of fluid inclusion volatiles make use of mass spectrometry (*e.g.*, Shepherd *et al.*, 1985; Barker and Smith, 1986; Norman and Sawkins, 1987; Guha *et al.*, 1990) and/or gas chromatography (*e.g.*, Cuney *et al.*, 1976; Andrawes and Gibson, 1979; Bray and Spooner, 1989). Mass spectrometry is generally a bulk technique, although some authors have been successful in analysing the major volatiles in individual inclusions by using laser ablation to release the inclusion content (Sommers and Gibson 1986). Detection limits using mass spectrometry are extremely low, on the order of  $10^{-9}$   $\mu\text{moles}$  (Shepherd *et al.*, 1985), allowing detection of components that are only minor constituents of fluid inclusions. On the other hand, species identification is commonly difficult because substances which produce fragments with the same molecular-weight/charge ratios cannot be resolved (*e.g.*,  $\text{N}_2$ , CO,  $\text{CO}_2$  and  $\text{C}_2\text{H}_4$  all contribute to the 28 peak) (cf. Norman and Sawkins, 1987; Landis and Rye, 1989).

Furthermore, the elevated temperature at which the instrument operates can cause cracking of hydrocarbons thereby changing the composition of the fluid by producing lighter hydrocarbons and even hydrogen. The latter gas can also be produced by the filament (cf. Bray and Spooner, 1991). Finally, substantial amounts of H<sub>2</sub>O cannot be accurately be measured by mass spectrometry, unless special techniques are employed (cf. Norman and Sawkins, 1987).

Gas chromatography applied to the study of fluid inclusions is a powerful technique for analysis of the major and trace volatile constituents of bulk samples. The technique is very versatile, allowing one to choose among a wide variety of detectors and columns so as to customise analyses to particular applications. Advantages of this over other techniques are the fact that the detectors are generally non-destructive thus permitting further analyses of the eluted gas species (*e.g.*, light stable isotope analysis), that peak overlap is typically not a problem (in most cases it can be solved by varying the temperature program of the column oven), that if an appropriate column is selected, H<sub>2</sub>O can be analysed during standard runs, and that the cost of analysis is relatively low. Gas chromatographic analyses are generally carried out at <200-250°C and never higher than 450°C, thereby avoiding the danger of cracking of hydrocarbons/H<sub>2</sub>O, which is a serious limitation of mass spectrometric methods. Its sensitivity is not as good as mass spectrometry, with the best reported detection limits being on the order of 10<sup>-6</sup> μmoles with a helium ionisation detector (Andrawes and Gibson, 1979). This restricts the application of gas chromatography to the bulk analysis of large numbers of inclusions.

## References

- Andrawes, F.F. and Gibson, E.K. Jr., 1979.** Release and analysis of gases from geological samples. *Am. Mineral.*, 64, 453-463.
- Barker, C. and Smith, M.P., 1986.** Mass spectrometric determinations of gases in individual fluid inclusions in natural minerals. *Anal. Chem.*, 58, 1330-1333.
- Barres, O., Burneau, A., Dubessy, J. and Pagel, M., 1987.** Application of micro-FT-IR spectroscopy to individual hydrocarbon fluid inclusions analysis. *Appl. Spectr.*, 41, 1000-1008.
- Bray, C.J. and Spooner, E.T.C., 1989.** Fluid inclusion volatile analysis using heated crushing (~105°C)/gas chromatography with in-series photoionization/thermal conductivity detectors and digital peak processing [abs.]. *2<sup>nd</sup> Biennial Pan-Am. Conf. Res. Fluid Inclusions*, 2, 12-13.
- Bray, C.J., Spooner, E.T.C. and Thomas, A.V., 1991.** Fluid inclusion volatile analysis by heated crushing, on-line gas chromatography; applications to Archean fluids. *J. Geochem. Exploration*, 42, 167-193.
- Brown, P.E. and Vry, J.K., 1990.** Applications of micro-FTIR spectroscopy to fluid inclusions [abs.]. *3<sup>rd</sup> Biennial Pan-Am. Conf. Res. Fluid Inclusions*, 3, 23-24.
- Chou, I-M., Pasteris, J.D. and Seitz, J.C., 1990.** High-density volatiles in the system C-O-H-N for the calibration of a laser Raman microprobe. *Geochim. Cosmochim. Acta*, 54, 535-543.
- Cuney, M., Pagel, M. and Touret, J., 1976.** L'analyse des gaz des inclusions fluides par chromatographie en phase gazeuse. *Bull. Coc. Fr. Minéral. Crystallogr.*, 99, 169-177.
- Delhaye, M. and Dhamelincourt, P., 1975.** Raman microprobe and microscope with laser excitation. *J. Raman Spectr.*, 3, 33.
- Guha, J., Lu, H-Z. and Gagnon, M., 1990.** Gas composition of fluid inclusions using solid probe mass spectrometry and its application to study of mineralizing processes. *Geochim. Cosmochim. Acta*, 54, 553-558.
- Guilhaumon, N., Szydłowski, N. and Pradier, B., 1990.** Characterization of hydrocarbon fluid inclusions by infra-red and fluorescence microspectrometry. *Mineral. Magazine*, 54, 311-324.

- Landis, G.P. and Rye, R.O., 1989.** Reconnaissance gas chemistry of the Creede, Colorado, hydrothermal system. *US Geol. Survey Open-file*, Report 89-84.
- Norman, D.I., and Sawkins, F.J., 1987.** Analysis of volatiles in fluid inclusions by mass spectrometry. *Chem. Geol.*, 61, 1-10.
- Pasteris, J.D., Kuehn, C.A. and Bodnar, R.J., 1986.** Applications of the laser Raman microprobe RAMANOR U-1000 to hydrothermal ore deposits: Carlin as an example. *Econ. Geol.*, 81, 915-930.
- Pironon, J. and Barres, O., 1990.** Semiquantitative FT-IR microanalysis limits: Evidence from synthetic hydrocarbon fluid inclusions in sylvite. *Geochim. Cosmochim. Acta*, 54, 509-518.
- Roedder, E., 1990.** Fluid inclusion analysis-prologue and epilogue. *Geochim. Cosmochim. Acta*, 54, 495-507.
- Rosasco, G.J., Roedder, E. and Simmons, J.H., 1975.** Laser activated Raman spectroscopy for nondestructive partial analysis of individual phases in fluid inclusions in minerals. *Science*, 190, 557-560.
- Seitz, J.C., Pasteris, J.D. and Chou, I.-M., 1993.** Raman spectroscopic characterization of gas mixtures. I. Quantitative composition and pressure determination of CH<sub>4</sub>, N<sub>2</sub> and their mixtures. *Amer. J. Sci.*, 293, 297-321.
- Shepherd, T.J., Rankin, A.H. and Alderton, D.H.M., 1985.** *A Practical Guide to Fluid Inclusion Studies*, Blakie, 239 p.
- Sommer, M.A. and Gibson, E.K. Jr., 1986.** Volatile determinations of individual fluid inclusions within the 3.4 b.y. North Pole barites from the Warrawoona group, Northwestern Australia [abs.]. *Lunar Planet. Sci.*, 17, 815-816.
- Wopenka, B. and Pasteris, J.D., 1987.** Raman intensities and detection limits of geochemically relevant gas mixtures for a laser Raman microprobe. *Anal. Chem.*, 59, 2165-2170.
- Wopenka, B., Pasteris, J.D. and Freeman, J.J., 1990.** Analysis of individual fluid inclusions by Fourier transform infrared and Raman microspectroscopy. *Geochim. Cosmochim. Acta*, 54, 519-533.

**FLUID-INCLUSION VOLATILE ANALYSIS BY GAS  
CHROMATOGRAPHY: APPLICATION OF A WIDE-BORE  
POROUS-POLYMER CAPILLARY COLUMN TO THE  
SEPARATION OF ORGANIC AND INORGANIC  
COMPOUNDS**

---

**STEFANO SALVI  
AND  
ANTHONY E. WILLIAMS-JONES**

*Department of Geological Sciences  
McGill University  
Montreal, QC  
Canada*

## Abstract

Gas chromatographic analyses of the volatile content of fluid inclusions were carried out using a recently developed PoraPLOT<sup>®</sup> Q mega-bore capillary column (25 m x 0.53 mm, 20  $\mu$ m film thickness, fused silica) and heated on-line crushing techniques (Andrawes and Gibson, 1979; Bray and Spooner, 1989). For comparison, the same samples were also analysed using a HayeSep<sup>®</sup> R packed column (10' x 1/8" 120 mesh, Ni alloy tubing), the most widely used column for the analysis of inclusion gases (Bray and Spooner, 1992). The wide-bore PoraPLOT<sup>®</sup> Q capillary column is ideally suited to the relatively high flow rates necessary with on-line analysis of fluid inclusions, and proved superior to the packed column in that it reduced retention times by at least half, allowed clean separation of N<sub>2</sub>, CO<sub>2</sub>, CH<sub>4</sub>, and higher hydrocarbons up to at least C<sub>6</sub> paraffins, and greatly improved detection and accuracy of water analyses. Furthermore, using N<sub>2</sub> as a carrier gas, we were able to analyse Ar and H<sub>2</sub> to  $\sim 10^{-4}$   $\mu$ moles and  $\sim 10^{-5}$   $\mu$ moles, respectively. The latter gas could not be analysed with the packed column. Optimum conditions were found to be a carrier gas flow of 20 ml/min, and an oven temperature programmed to start at -20°C, subsequently raised (10°C/min) to 35°C and held for 10 min, then again raised (5°C/min) to 115°C. Runs lasted  $\sim 80$  min.

*"...a specimen of the Goldie aplite...was split in vacuo. The liberated gas was conducted to a ... mass spectrometer, which unfortunately showed nothing. Rechecking of the specimen by subsequent splitting in air yielded the characteristic odor, which led us to conclude that the nose is more sensitive than the machine." <sup>1</sup>*

---

<sup>1</sup> Heinrich, E. Wm. and Anderson, R.J., 1965. Carbonatites and alkalic rocks of the Arkansas River area, Fremont County, Colorado. 2. Fetid gas from carbonatite and related rocks. Am. Mineral., vol. 50, pp. 1915-1916.

## Introduction

**G**AS chromatography has been employed for the analysis of major and trace volatile constituents of bulk samples of fluid inclusions for over thirty years (*e.g.*, Goguel, 1963; Petersilie and Sørensen, 1970; Mironova *et al.*, 1972; Ypma, 1974; Cuney *et al.*, 1976). However, until recently, a major limitation of the technique has been the poor detection limits, restricting analysis to only the major volatile components of fluid inclusions. With recent advances in technology, the sensitivity of gas chromatography has improved greatly, and detection limits now range from  $10^{-4}$  to  $10^{-6}$   $\mu$ moles, depending on the detector used. This makes it possible to extend the analyses to include components comprising  $<0.01$  ppm of the fluid.

Traditionally, gas chromatographic analysis of fluid inclusions has proceeded in two steps, *i.e.*, the gases were first released and collected, and then an aliquot of the captured gases was introduced into the chromatograph. Typical extraction techniques consisted of stepwise decrepitation by heating (*e.g.*, Piperon and Penchev, 1973), grinding the sample in a stainless-steel or ceramic ball mill under vacuum (*e.g.*, Abell *et al.*, 1970; Petersilie and Sørensen, 1970; Roedder, 1972), or decrepitation under vacuum followed by gas separation (Behar and Pineau, 1979; Welhan, 1988). Among these, the decrepitation/extraction method has proven the most problematic as a result of thermal decomposition and heat-induced chemical reactions, which produce unreasonably high blank concentrations of the common inclusion components, CO<sub>2</sub>, CH<sub>4</sub> and N<sub>2</sub>. However, all these extraction techniques share another major weakness, namely that only a small proportion of the released volatiles can be collected for analysis. This significantly decreases the accuracy of the analysis and the ability to detect trace components.

Andrawes and Gibson (1979) designed an on-line crushing technique that greatly improved the quality of volatile extraction. The device consists of a piston/cylinder crusher operated by a hydraulic press, in which the sample chamber is heated to  $\leq 300^{\circ}\text{C}$  (*cf.* also Andrawes *et al.*, 1984). Their technique allows direct insertion of all the released gases into the gas chromatograph as the crusher is attached to the column. Also, moderate heating of

the sample chamber induces immediate release and dilution of volatiles in the carrier gas, reducing gas adsorption while at the same time avoiding cracking of hydrocarbons/H<sub>2</sub>O.

An important limitation of early gas chromatography was an inability to quantitatively analyse water. Because of its polarity, H<sub>2</sub>O was adsorbed onto the stationary phase contained in the packed columns available at that time. This problem was solved when, in 1966, the Water Association Society developed the Porapak<sup>®</sup> series of stationary phases, a type of apolar porous polymer consisting of divinyl benzene and diethyl benzene (Hollis, 1966; Hollis and Hayes, 1966; Merle d'Aubigné and Guiochon, 1970; Gough and Simpson, 1972), which allows elution of the strongly polar H<sub>2</sub>O molecule. Since then, most gas chromatographic analyses of rock gases have been carried out on these or similar columns. Separation of H<sub>2</sub>O, CO<sub>2</sub> and light hydrocarbons up to C<sub>3</sub> has been typically carried out with Porapak<sup>®</sup> Q (*e.g.*, Cuney *et al.*, 1976; Behar and Pineau, 1979; Andrawes and Gibson, 1979; Kreulen and Schuiling, 1982; Kesler *et al.*, 1986) or Chromosorb<sup>®</sup> 102 (*e.g.*, Smith *et al.*, 1984; Kesler *et al.*, 1986), whereas columns packed with molecular sieve 5Å have been employed to separate the ±N<sub>2</sub> ±Ar ±O<sub>2</sub> ±CO ±H<sub>2</sub> composite peak (*e.g.*, Andrawes and Gibson, 1979; Andrawes *et al.*, 1984; Bray *et al.*, 1991).

Bray and Spooner (1989; see also Bray *et al.* 1991; Bray and Spooner, 1992) have taken the technique one step further by separating fluid inclusion volatiles using a single column, albeit in two separate runs with different temperature programs. They used a 10' x 1/8" (3.05 m x 3.2 mm) outside diameter (OD) Ni alloy column, packed with HayeSep<sup>®</sup> R (100/120 mesh), a material similar to Porapak<sup>®</sup>, but with higher efficiency and inertness (*cf.* Pollock *et al.*, 1984). Their system allows routine analysis of up to three samples a day for N<sub>2</sub>, Ar, CO, CH<sub>4</sub>, CO<sub>2</sub>, C<sub>2</sub>H<sub>4</sub>, C<sub>2</sub>H<sub>6</sub>, C<sub>2</sub>H<sub>2</sub>, C<sub>3</sub>H<sub>6</sub>, C<sub>3</sub>H<sub>8</sub>, C<sub>3</sub>H<sub>4</sub>, C<sub>4</sub>H<sub>8</sub> (isobutylene), COS, and H<sub>2</sub>O, with a detection limit of less than 10<sup>-4</sup> μmoles for major components (CO<sub>2</sub>, CH<sub>4</sub>, N<sub>2</sub>) and down to less than 10<sup>-5</sup> μmoles for unsaturated hydrocarbons (*cf.* Bray *et al.*, 1991). In addition to these species, they report separation of O<sub>2</sub> from standards, an unquantifiable peak for SO<sub>2</sub>, and a few unresolved composite peaks of other C<sub>4</sub> species.

We have constructed a gas chromatographic system for on-line fluid inclusion analysis at the Department of Earth and Planetary Sciences of McGill University, Montreal,

QC, based largely on the design of the system in the fluid inclusion laboratory at the University of Toronto. Unlike Bray and Spooner (1989), we have elected to use a wide bore capillary column (25 m x 0.53 mm inside diameter fused silica) coated with PoraPLOT<sup>®</sup> Q (film thickness = 20 µm). This column proves to be an ideal choice for the analysis of fluid inclusion volatiles. It allows separation of permanent gases as well as light hydrocarbons up to at least C<sub>6</sub>, and even some aromatic species, in a single run; it improves peak resolution (enhancing separation and potentially leading to lower detection limits); and it greatly improves the quality of the H<sub>2</sub>O peak thereby increasing the accuracy of analyses. Furthermore, by using N<sub>2</sub> as carrier gas, we were able to resolve H<sub>2</sub> (not possible with HayeSep<sup>®</sup> R) and can analyse this gas in fluid inclusions to levels of ~10<sup>-5</sup> µmoles. In this paper we report the results of experiments using standard mixtures of gases as well as natural samples, and compare these to the results for the same samples using a packed column identical to that employed by Bray and Spooner (1989).

## Experimental Procedure

### Introduction

Any substance that can be introduced in its gaseous state into a gas chromatographic column can be potentially analysed by this technique. The sample (generally consisting of a mixture of components) is introduced into a gas chromatograph through a heated injector which causes its vaporisation (if not already a gas, *i.e.*, permanent gases and light hydrocarbons) and is immediately fluxed in a stream of pressurised gas. Helium, H<sub>2</sub>, Ar, N<sub>2</sub>, can all be used as carrier gases, but He is best for the majority of applications. The gas stream then passes through a column (two parallel columns are also used) where the different species are retarded to differing degrees, causing their separation and subsequent sequential emergence from the column (the time from injection to elution of a species is referred to as its retention time). One or more detectors (connected in series or in parallel)

analyse the components as they exit the column and send the data to a chart recorder or computer data handling unit (Fig. 1) (*e.g.*, Jennings, 1987).

Columns are any length of coiled tubing coated with a polar or non-polar stationary phase, which interacts with the species in solution, causing their separation. In columns coated with a non-polar phase, the extent to which compounds are retarded depends on their volatility, whereas polar columns rely almost entirely on the interaction between functional groups of sample components, and those contained in the stationary phase, to cause retention of the gas. Factors influencing retention times are the length and internal diameter of the column, the thickness of coating, the oven temperature, and carrier-gas flow rate (*e.g.*, Kaliszan, 1987).

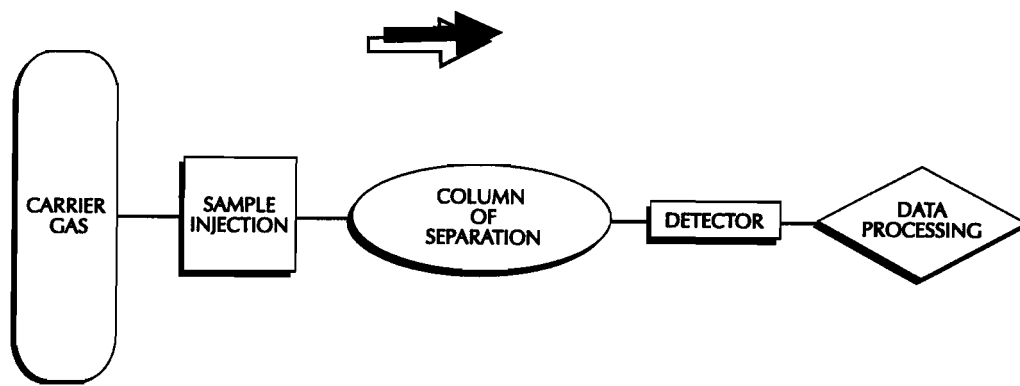
### **The Gas Chromatograph**

The instrument used in our analyses is a HP<sup>®</sup> 5890 SERIES II gas chromatograph manufactured by Hewlett-Packard<sup>®</sup>. It is reliable, easy to operate, and has the capability of being able to host a wide variety of columns, detectors and injectors. A particular advantage of the unit over other models is that it is equipped with a recently developed micro-thermal conductivity detector which offers much greater sensitivity than conventional thermal conductivity detectors (see below). The column oven of the HP<sup>®</sup> 5890 can be cooled to -80°C (using liquid nitrogen) or heated to 450°C at temperature increments as low as 0.1°C/min. Without cryogenic cooling the temperature can be maintained as low as 4°C above ambient temperature. Control of the oven temperature is precise to within  $\pm 0.01^\circ\text{C}$  of a setpoint.

Cryogenic oven control is required to permit separation of species with very low boiling points; temperature must subsequently be increased to permit elution of less volatile compounds. At present, our gas chromatograph is configured to operate cryogenically down to temperatures of -40°C using liquid CO<sub>2</sub> as a coolant, (lower temperatures are possible with this coolant but risk damage to the gas chromatograph). Cooling is achieved by

FIGURE 1

Flow chart depicting the principal steps involved in gas chromatographic analysis.



allowing high pressure liquid CO<sub>2</sub> (5000 kPa<sup>2</sup> at 25°C) to enter the oven by means of an electronically controlled solenoid valve. Expansion of the CO<sub>2</sub> to ambient pressure and subsequent sublimation of dry ice causes the cooling.

Of the several inlets available, we have chosen the split/splitless injector instead of the commonly used packed injector (*e.g.*, Bray *et al.*, 1991), as it can be used with all types of capillary columns and can be easily modified to function as an inlet for packed columns. In its present configuration, the injector is in the latter operational mode (Fig. 2), as wide bore columns (see below) require the high flow rates typical of packed columns.

### **Fluid-Inclusion Volatile Extraction System**

The apparatus employed for volatile extraction allows immediate release of the contents of the fluid inclusions to the carrier gas and their direct insertion into the HP<sup>®</sup> 5890. It consists of a heat-treated stainless-steel crusher (modified by Bray and Spooner, 1989, from an original design of Andrawes and Gibson, 1979), operated by a hydraulic ram (Fig. 3).

The basal block, where the lower portion of the crusher containing the sample chamber is hosted, is heated by two cartridge heaters inserted in cylindrical cavities located symmetrical to and below the chamber. The cartridge heaters are powered by a Powerstat variable-transformer. The temperature is set to ~120°C and is monitored with a portable thermocouple through two holes located on either side of the block.

The upper portion of the crusher contains a cylindrical piston (*cf.* Fig. 3 for dimensions) and attaches to the lower portion via a threaded connection. A seal, where the two parts join, is provided by a silicon-rubber O-ring at the base of the upper block and one at the lower end of the piston. An additional O-ring is placed near the top of the piston to create a further seal from the external atmosphere. Andrawes *et al.* (1984) used vacuum

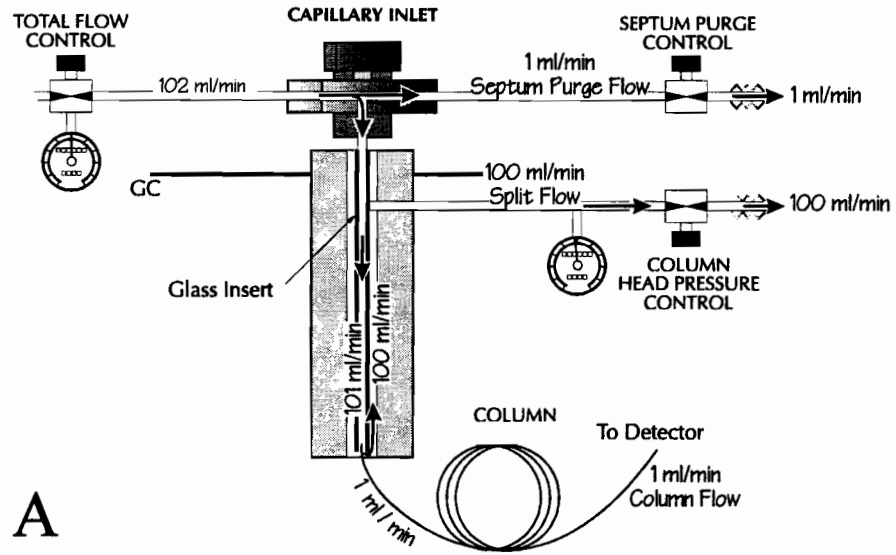
---

<sup>2</sup> 1 bar = 100 kPa

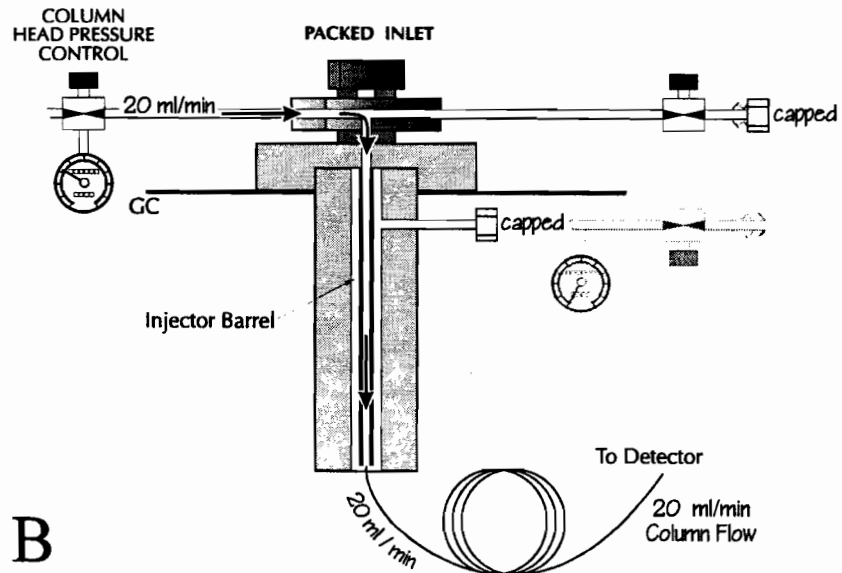
FIGURE 2

Schematic cross-section of the split/splitless gas chromatograph inlet depicting the gas flows in (A) the split configuration typically used with capillary columns and (B) in the splitless mode, compatible with packed columns.

## SPLIT FLOW



## SPLITLESS FLOW



grease to lubricate the O-rings, but we did not attempt this, for fear of contaminating the column. The dead volume between the two O-rings on the piston (Fig. 3) is pressurised with ultra-high-purity zero grade He (99.9999%), the same gas (but from a different tank) used as the carrier; this provides added protection in case the sample chamber should leak, especially when the piston is lowered during crushing (cf. also Andrawes *et al.*, 1984). Helium inlet/outlet to the sample chamber and to the upper portion of the crusher is provided via two pairs of  $1/16$ " (1.6 mm) OD Ni-alloy tube segments.

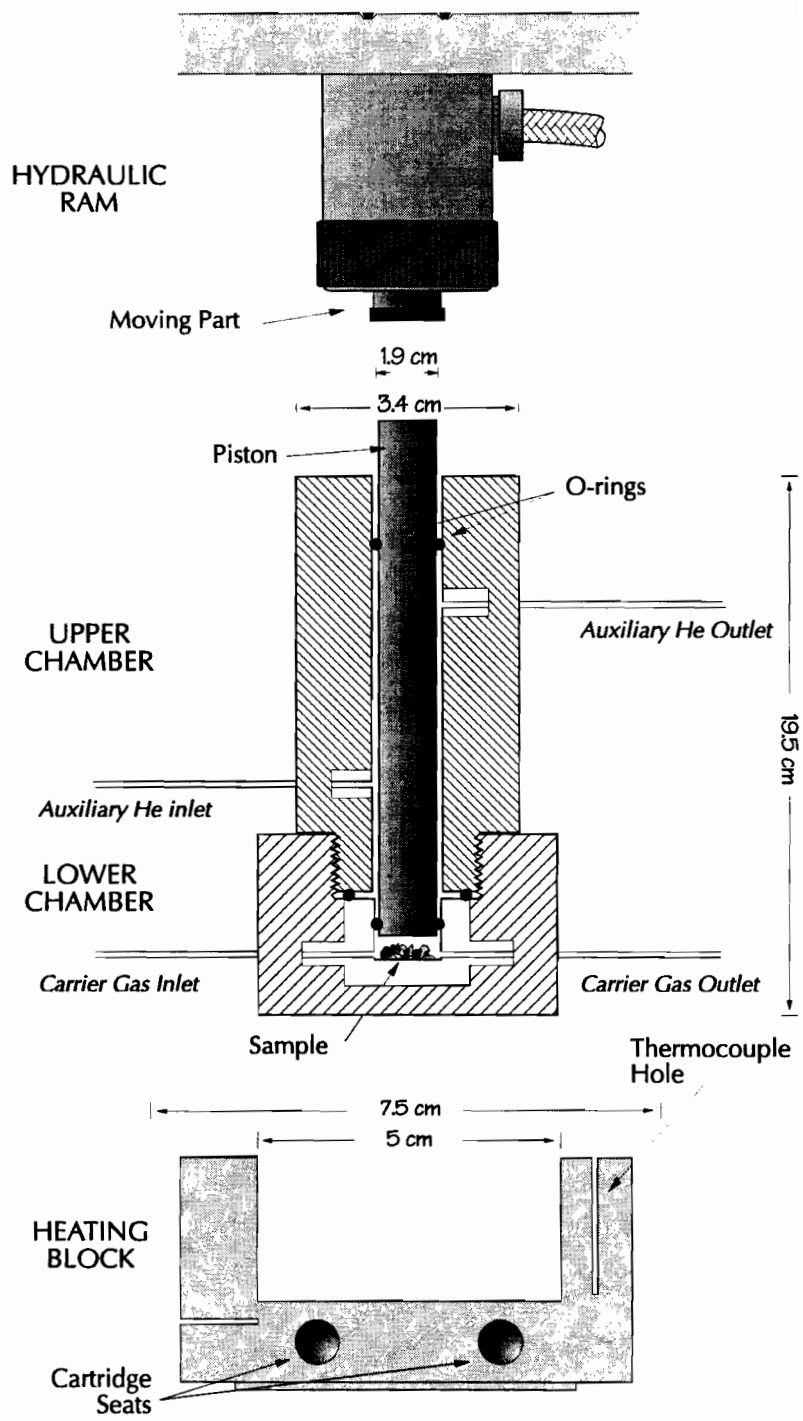
The sample to be analysed, usually quartz, is fragmented to pieces between 0.75 mm and 2 mm in diameter, and is hand-picked. Sample cleaning, as recommended by Bray *et al.* (1991), is performed using doubly distilled H<sub>2</sub>O (~ 8 MΩ-cm) to avoid any possibility of contamination from acids and/or organic solvents. Samples are then dried in an oven (~80°C) or on a hot plate (~50°C) under a fumehood to keep dust from entering the sample. Between ~0.5 g to 2 g of clean, dry material are loaded into the crusher, and the piston is lowered to just touch the grains. The cartridge heaters are switched on, and both sample and confining chambers are pressurised with a low flux of He (≤1 ml/min), for a duration of at least 12 hours (overnight). Flushing in He at temperatures above the boiling of water removes all air and H<sub>2</sub>O that may be absorbed onto the sample.

A stainless-steel frame accommodates three crushers and guides the hydraulic ram on top of each of them. Heating of the sample chambers is controlled by independent heating switches. Up to three crushers can therefore be loaded and set to purge simultaneously. An oil pump is connected to the ram by a on-off valve. Just prior to analysis, this valve is in the "off" position and the pump is loaded to about 30 to 35 MPa. Releasing this pressure by switching the valve "on" causes a sharp and sudden stroke of the ram on the piston which crushes the sample. The gas chromatograph run is started synchronously. After analysis, the sample chamber is cleaned with compressed air and clean tissues. Again, organic solvents are avoided.

### Choice of Column

The ability of a chromatographic system to separate complex mixtures depends almost entirely on the choice of column. A packed column consists typically of 0.5 m to 3

FIGURE 3  
Schematic cross-section of the crushing apparatus.



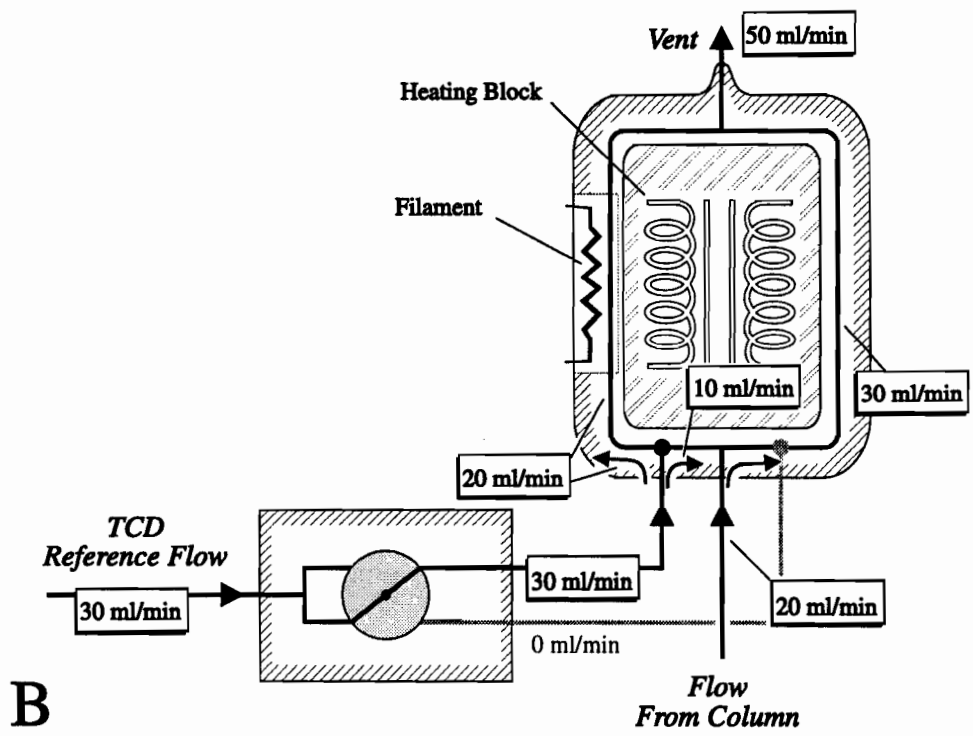
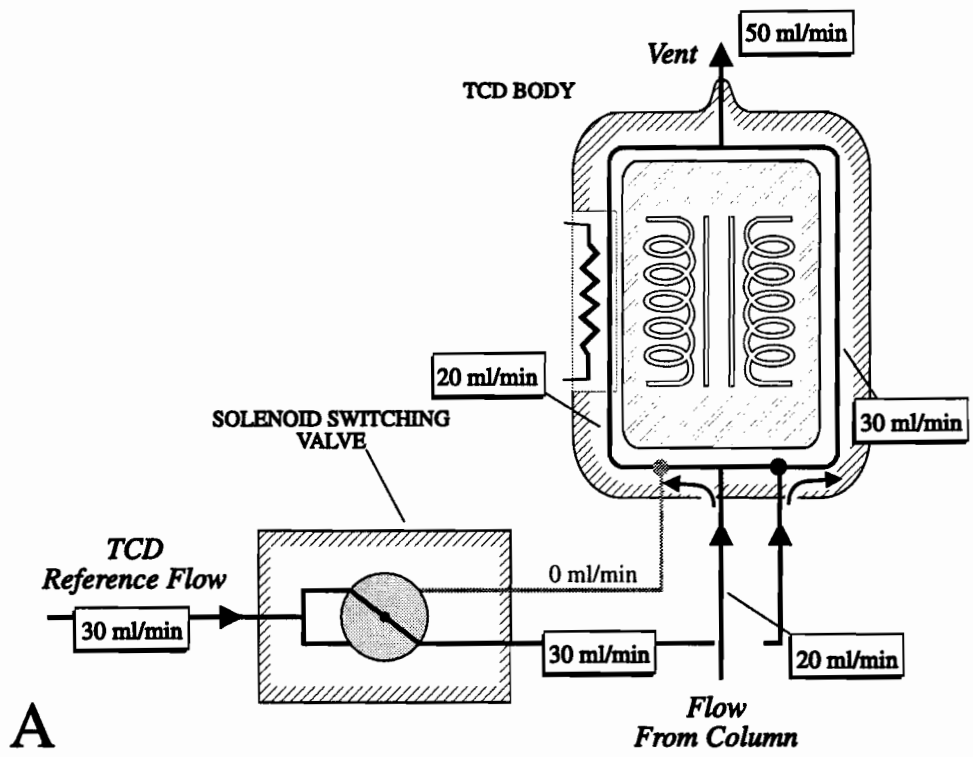
m of metal (stainless-steel, Ni alloy) or glass tubing, generally has an internal diameter (ID) between ~2 mm and ~5 mm, and is loaded with stationary phases, porous polymers, or molecular sieves. Capillary columns usually comprise between 12 m and 100 m of coiled stainless-steel or fused silica tubing of very small ID (the usual range is from 0.18 mm to 0.53 mm), and are coated with a  $\mu\text{m}$ -scale thickness of stationary phases or porous polymers (recently developed), molecular sieves, aluminium oxide or carbon. There are probably over a thousand different columns on the market today.

We initially installed a packed column identical to that used by Bray and Spooner (1989), *i.e.*, 10' x  $\frac{1}{8}$ " OD HayeSep<sup>®</sup> R (Ni Alloy tubing, 100/120 mesh). Although, as discussed by Bray *et al.* (1991) and Bray and Spooner (1992), the column allows separation of the lighter inclusion volatiles, we found that the large width of the H<sub>2</sub>O peak masked part of the region that could be occupied by C<sub>3</sub> peaks, and that resolution of hydrocarbon species eluting after about 20 minutes of running time was very poor (see below). Varying the temperature program did not improve the quality of the analysis, as gains on some aspects represented losses in others, supporting the conclusion of Bray *et al.* (1991) that the 80°C isothermal run is the best compromise for this column. We therefore investigated alternative columns.

Analytical constraints quickly focused our attention on mega-bore capillary columns (0.53 mm ID), as they have the high capacity needed to separate volatile compounds as well as to deal with the introduction of the wide range of sample volumes, which characterises fluid inclusion volatile analysis. Furthermore, their wide bore allows operation with fast flow rates (needed because of the large dead volumes inherent in the extraction system) thereby obviating the need to split the flow (*cf.* Fig. 2A), which would have proved very difficult with a crusher on line. The principal draw-back of mega-bore capillary columns was that they could not be used in the presence of H<sub>2</sub>O. However, this limitation has recently been overcome with the development of the PLOT (porous layer open tubular) series of columns by Chrompack International. We have selected a 25 m x 0.53 mm inside diameter (ID), fused-silica PoraPLOT<sup>®</sup> Q column, which features a 20- $\mu\text{m}$ -thick uniform

FIGURE 4

Schematic cross-section of the micro-thermal conductivity detector and its external components. A solenoid switching valve allows the detector to analyse alternately (every 200 msec) (A) the column effluent gas and (B) a flow of carrier gas alone.



layer of particles immobilised on the inner wall. This layer allows the separation of both polar and non-polar volatile compounds, hydrocarbons and H<sub>2</sub>O.

### Choice of Detector

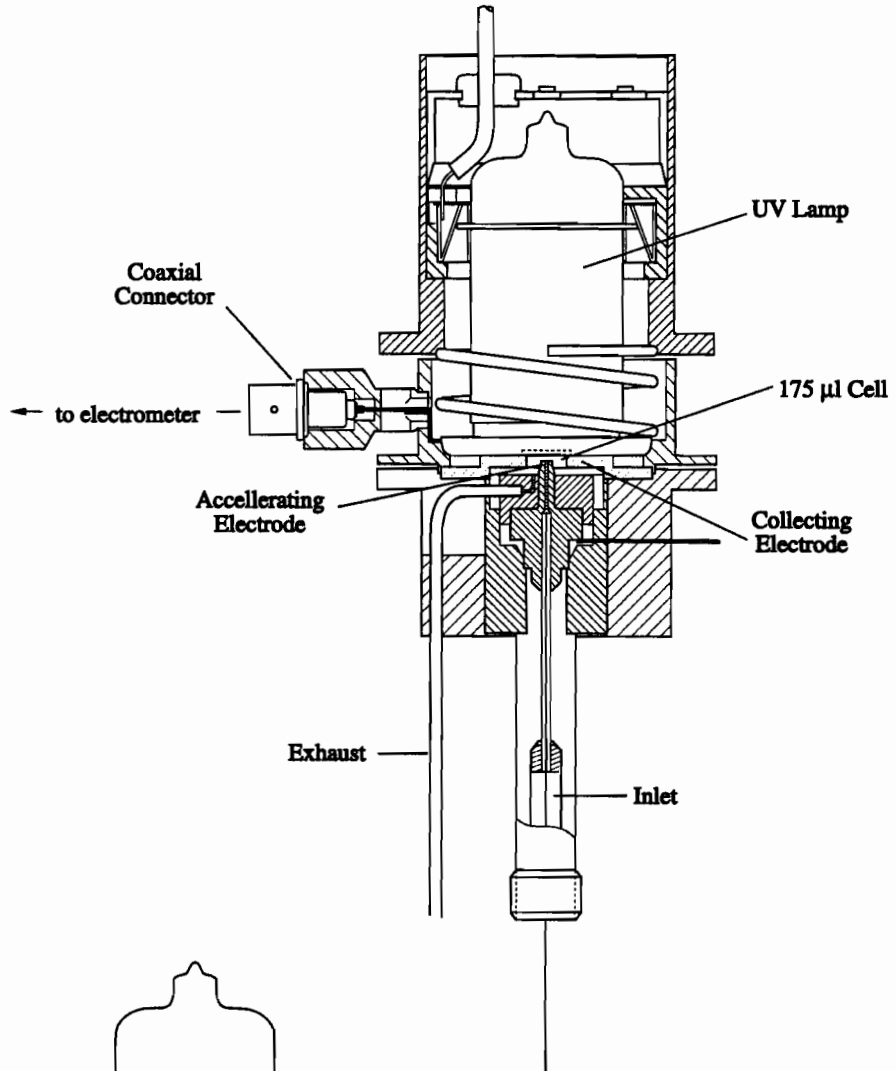
Detectors that have been used for fluid inclusion volatile analysis include the thermal conductivity detector (TCD) (*e.g.*, Behar and Pineau, 1979; Shephard *et al.*, 1985; Smith *et al.*, 1984; Bray and Spooner, 1989), flame ionisation detector (FID) (*e.g.*, Behar and Pineau, 1979; Shephard *et al.*, 1985; Smith *et al.*, 1984), helium ionisation detector (HID) (*e.g.*, Andrawes and Gibson, 1979), photoionisation detector (PID) (Bray and Spooner, 1989) and flame photometric detector (FPD) (*e.g.*, Andrawes and Gibson, 1979). Of these, TCD's are the most widely used for detection of inorganic gases such as H<sub>2</sub>, O<sub>2</sub>, CO, N<sub>2</sub>, Ar, CO<sub>2</sub>, and H<sub>2</sub>O; FPD's are the detector of choice for sulphur- and phosphorus-bearing compounds, but their application is limited to these species; FID's owe their popularity to their wide dynamic range (ability to deal with a wide range of concentrations), universal response to organics, and simple design, but have relatively high detection levels; HID's have greater sensitivity than other detectors ( $1 \times 10^{-6}$   $\mu$ moles for most compounds), but are difficult to use (*e.g.*, Andrawes and Gibson, 1979, had to add H<sub>2</sub> to the carrier gas to provide positive responses from their HID), cannot analyse H<sub>2</sub>O, and are very costly; PID's have a dynamic range similar to FID's (Driscoll and Duffy, 1987), lower detection limits (*cf.* Table 2 in Bray *et al.*, 1991), and respond to all compounds with ionisation potential  $\leq 12$  eV.

The gas chromatograph used in this study is equipped with a micro-TCD designed around a 3.5- $\mu$ l cell, which improves detection limits by a factor of at least 50 with respect to conventional TCD's (Bray *et al.*, 1991). Use of the micro-TCD also eliminates the need to pass the reference gas through a second column (*e.g.*, Behar and Pineau, 1979) by using a solenoid valve which switches continuously between the carrier and the reference gas (Fig. 4).

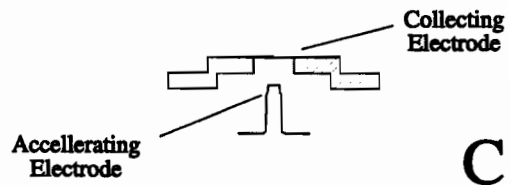
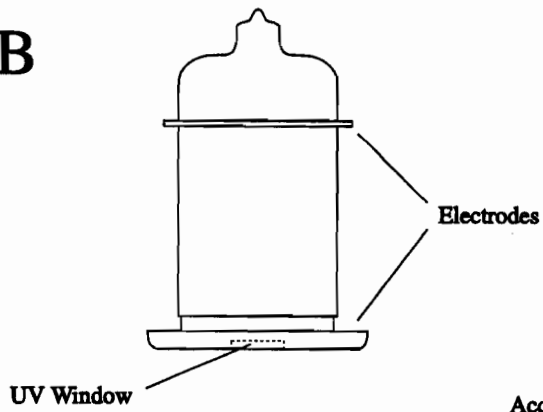
To analyse for hydrocarbons, we have selected a PID over FID's for the reasons outlined above, and also because the PID analysis is non-destructive, and this detector can

FIGURE 5  
(A) Schematic cross-section of the photoionisation detector, and exploded views of (B) the lamp assembly and (C) the ionisation chamber.

**A**



**B**



**C**

be connected in series with the TCD. The PID fitted to our system is the PI-52-02A model of HNU<sup>®</sup> Systems (Fig. 5), which has a low-volume chamber (175  $\mu$ l), and can be used with a series of ultraviolet lamps, with energies ranging from 8.3 eV to 11.7 eV. The 10.2 eV lamp has the greatest sensitivity of the available light sources (cf. Driscoll and Duffy, 1987), but cannot detect low-molecular-weight compounds such as CH<sub>4</sub>, C<sub>2</sub>H<sub>2</sub>, C<sub>2</sub>H<sub>4</sub> and C<sub>2</sub>H<sub>6</sub>, which are more tightly bonded and hence have higher ionisation potentials. The 11.7 eV lamp, having the highest ionising energy, is able to detect the widest range of molecular weights, but has an expected lifetime of only ~500 hrs and should not be operated at temperatures greater than ~100°C. This is because, in order to be transparent to the low-wavelength emission lines of argon in the 11.7 eV lamp, the window has to be made of lithium fluoride which undergoes solarisation (colour centre formation) with time, and more so at higher temperatures (cf. Driscoll and Duffy, 1987). Because the C<sub>2</sub> hydrocarbons are only poorly resolved by the TCD, but give excellent response on the 11.7 eV lamp, we fitted the PID with a 11.7 eV ultraviolet source. Methane ionises at  $\geq 12.98$  eV and therefore does not produce a linear response even on this lamp, however, it can be detected on the TCD at better than  $10^{-4}$   $\mu$ moles. Many inorganic gases of interest ionise at  $>12$  eV (N<sub>2</sub>, CO, CO<sub>2</sub>, CH<sub>4</sub>, SO<sub>2</sub> and H<sub>2</sub>O) and also cannot be detected with the PID. These are analysed with the TCD.

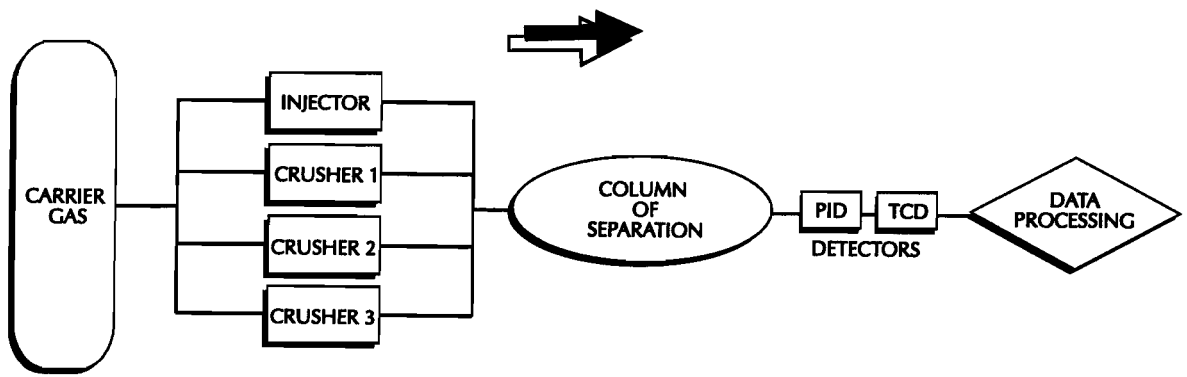
### **Principles of Detection**

#### *Micro-Thermal Conductivity Detector*

The TCD detects the difference in thermal conductivity between the effluent flow from the column (carrier gas + sample components) and a reference flow of carrier gas alone. A voltage is produced which is proportional to this difference, *i.e.*, to concentration, and it generates the output signal. Because the HP<sup>®</sup> 5890 TCD uses a single filament, it examines alternately the reference and column effluent gas streams (switching every 200 msec) (Fig. 4), which causes sample dilution of 50%. We have therefore connected the TCD to the exhaust port of the PID.

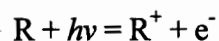
FIGURE 6

Flow chart depicting the principal steps involved in the gas chromatographic analysis of fluid-inclusion volatiles.



### *Photoionisation Detector*

The schematics of the PID are shown in Figure 5. It consists of a lamp (Fig. 5B) and an ionisation chamber (Fig. 5C). The lamp is filled with a low pressure gas (Ar in the 11.7 eV lamp) which produces an emission line of specific wavelength in the far UV region of the spectrum when excited by electrical discharge. The gas flow is exposed to the UV light in the ionisation chamber and is ionised by absorption of the UV radiation according to the expression:



where R is the species to be ionised, and  $h\nu$  (Planck's constant times frequency) describes a photon with energy greater than the ionisation potential of R. The ions become part of an electric field and the resulting current, which is proportional to concentration, is measured by an electrometer and sent to the interface.

### **Data Collecting and Processing**

The analogue signals that constitute the output of the detectors are converted to digital data by a HP® 35900C dual-channel interface; this device accepts a signal voltage in the range -18mV to +1V. The data are subsequently transmitted to an HP® 3365 Chromatographic ChemStation®, a PC Microsoft® Windows™ operated computer code designed to manipulate and integrate chromatographic spectra.

Computer-based manipulation of spectra represents a major advance over traditional chart recorders. There is no scale limitation on enlargements of specific segments of a signal trace, which allows recognition of very tiny peaks that previously would have gone undetected. Computer-manipulation also eliminates the danger of off-scaling: Bray *et al.* (1991) reported that they have to switch the TCD to low sensitivity before elution of CO<sub>2</sub> and H<sub>2</sub>O to prevent loss of data by peak truncation. As long as the signal is not stronger than 1 V, which is highly unlikely for the range of concentrations encountered with fluid inclusion analysis, the entire spectrum is stored by the software.

## Apparatus Set-Up

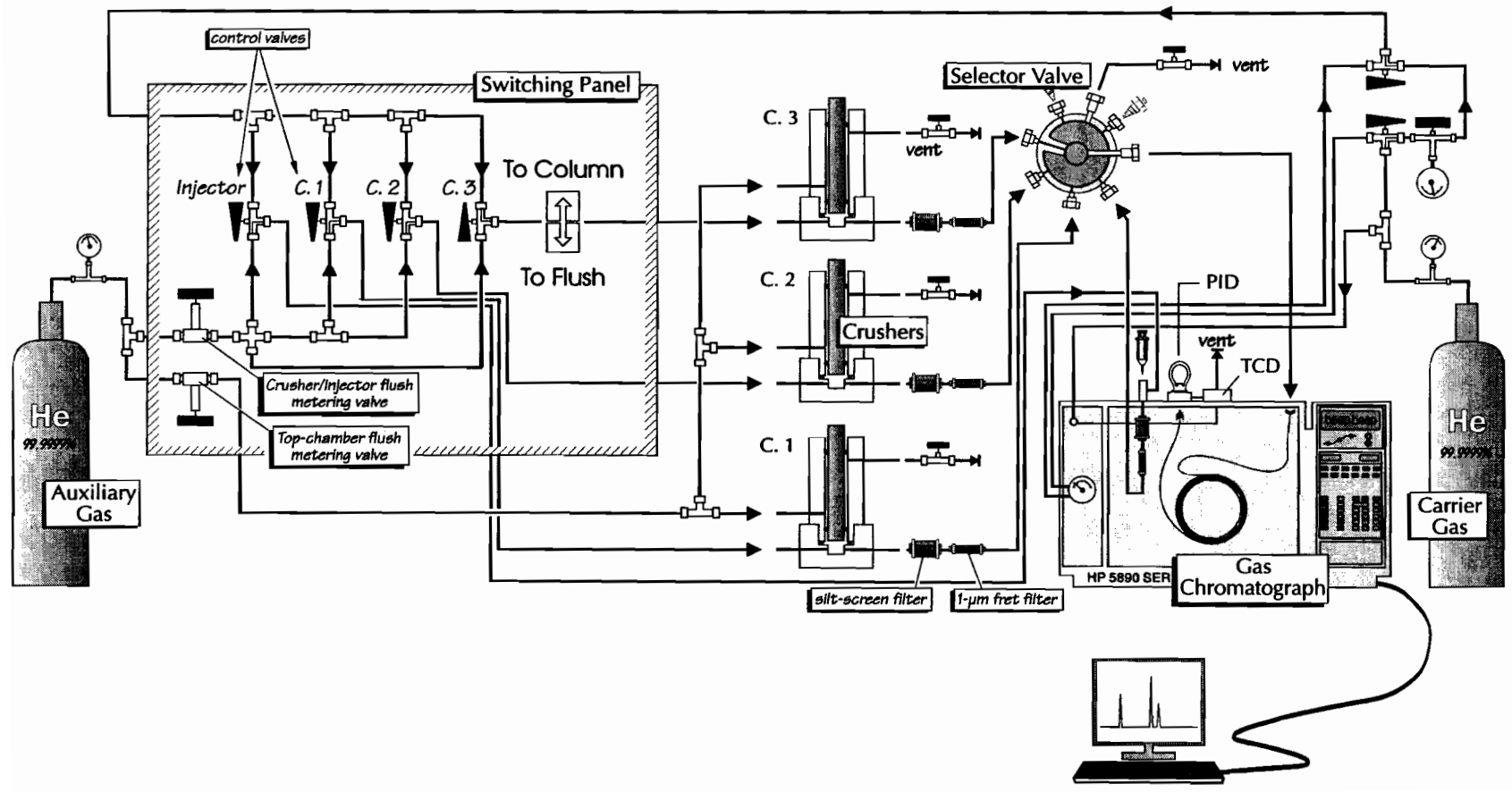
Figure 1 shows a flow chart for a regular gas chromatographic system. A similar diagram in Figure 6 illustrates schematically how the system used in this study departs from a standard gas chromatographic system. The principal modification originates from the need for four different sample introduction ports, *i.e.*, three crushers plus the regular injector. The system must allow for quick and efficient switching between any of the crushers and the injector. The latter is still needed for the introduction of standard mixtures used for calibration.

In a regular gas chromatograph, the carrier gas goes to a flow controller, which regulates the gas pressure and hence its flow through the column, and from this directly to the injector, where the sample is collected, before finally passing into the column. In this system (Fig. 7), the carrier gas (ultra-high purity He) is routed (by  $\frac{1}{8}$ " (3.2 mm) OD Cu tubing) to a three-way valve (Whitey® W1288 ball valve) (Fig. 8) which directs it either to the internal flow controller of the gas chromatograph, for capillary operation requiring split flow mode (injector configured as in Fig. 2A), or to an external regulator (0 to 400 kPa), which mimics the packed flow controller (injector configured as in Fig. 2B). Both flow controllers are connected to a second three-way valve, which directs the selected flow to a switching panel where it is split towards four three-way valves (control valves) (Fig. 7). From here the carrier gas can be directed to any of the 3 crushers or to the injector, by opening the appropriate control valve to carrier gas flow. All four injection ports are routed to a 6-port valve (zero-dead-volume Valco® SC6P-M-HC), which selects one of the entry ports while venting all others at a common exit (Fig. 8). The selected outlet is directed to the gas chromatograph and into the oven, where it is attached to the column.

Because one of the crushers or the injector can be the point where the sample is introduced into the gas chromatograph, and hence an analytical run is started, the tubing connecting each these devices to the 6-port switching valve has to be exactly the same length in order to produce comparable retention times; the tube segment from the valve to the gas chromatograph is common, and therefore its length is not relevant. To prevent absorption of sample components on their way to the column, all connections down flow

FIGURE 7

A schematic diagram showing the gas chromatographic system for analysis of fluid-inclusion volatiles.



from the crushers and the injector are made with Ni alloy tubing and Swagelok<sup>®</sup> stainless-steel fittings; the 6-port selector valve was constructed with Hastelloy<sup>®</sup> C (a highly inert material). This valve and the tubing connecting it to the gas chromatograph are heated to ~120°C to minimise condensation of higher boiling-point species.

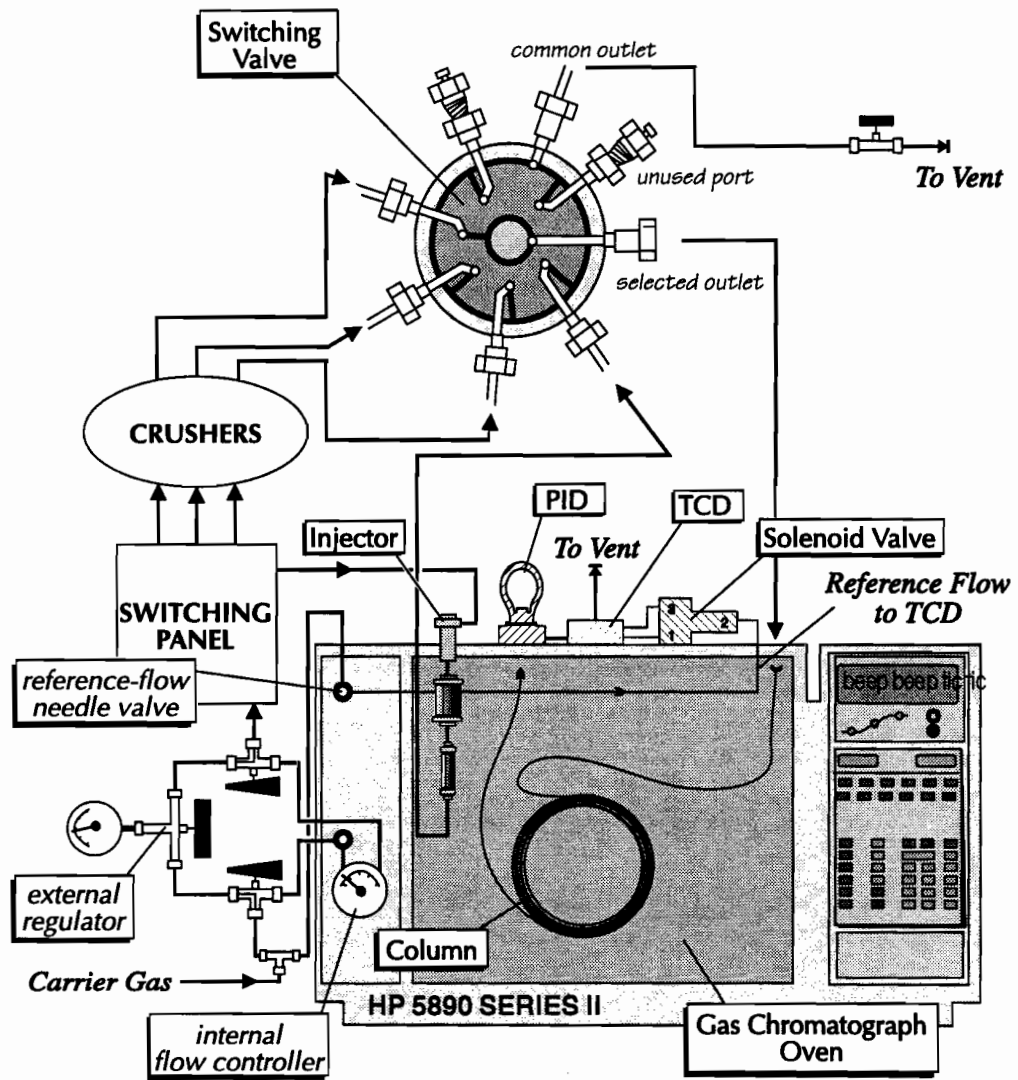
To prevent rock particles and dust from damaging the selector valve and the column, a silk-screen particle filter (~200 µm pores) and a 1-µm frit filter are connected in series to the sample chamber outlets of the crushers. A similar pair of filters are fitted on the injector line, to keep flows equal (Fig. 7). Additional protection for the column is provided by a 2.5 m x 0.53 mm ID particle trap, connected at the start of the column.

Reference gas flow to the TCD is provided via a Swagelok<sup>®</sup> T-junction off the main He line, up stream from the first three-way valve. A needle valve mounted on the HP<sup>®</sup> 5890 is used to control the flow to the TCD solenoid switching valve (Fig. 8). Because of this added gas bleed, the regulator on the main He cylinder should read at least 200 kPa greater than the pressure needed for the carrier gas flow.

A second tank of ultra-high purity He (labelled 'auxiliary gas' in Fig. 7) is used to provide the confining pressure in the upper portion of the crushers, and to supply He for flushing the crushing chamber in preparation for analysis (Fig. 7). The cylinder is connected to a Swagelok<sup>®</sup> T-union which splits the flow of gas to two metering valves (Whitey<sup>®</sup> 21RS2 needle valves) mounted on the switching panel. Downstream from the first metering valve, a Swagelok<sup>®</sup> cross- and a T-union fitting direct the gas to the other end of the four control valves. This allows crushers (and/or injector) that are not on-line with the column to be flushed, at a flow rate regulated by the metering valve, with a stream of He identical to, but independent from the carrier gas, which vents at the common exit of the 6-port selector valve. A shut-off valve fitted on this exit allows the plumbing system to be closed and the pressure to build up as needed. The second metering valve adjusts the flow to the top chambers of the crushers, where shut-off valves on the chamber outlets allow the system to be pressurised.

FIGURE 8

A schematic diagram illustrating the operation of the 6-port valve used to direct one of the sample inlets to the gas chromatographic column. As one port is selected to allow gas flow to the column, all others continue purging to a common exit.



## Results

To evaluate the performance of the gas chromatographic system, we first carried out several runs without loading the sample chamber, then crushed material with physical properties similar to those of the samples that would be analysed (usually quartz), but devoid of inclusions. Ideal candidates for such blanks are inclusion-free Brazilian quartz crystals, and pure-silica laboratory glassware. These materials were fragmented, sieved, and cleaned exactly as would be regular samples (see above), and prior to analysis they were flushed overnight with He.

Experiments involving rock material were conducted using pegmatitic quartz from the Strange Lake peralkaline complex, Quebec/Labrador (Zajac *et al.*, 1984; Miller, 1986). These pegmatites were shown to contain methane- and higher hydrocarbon-bearing fluid inclusions (Salvi and Williams-Jones, 1992). Based on their fluorescence under ultraviolet illumination, the hydrocarbons may be unsaturated aliphatic and/or aromatic compounds (Salvi and Williams-Jones, 1992).

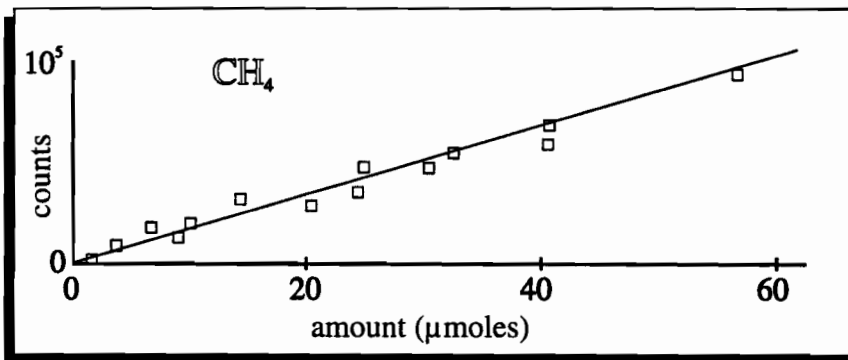
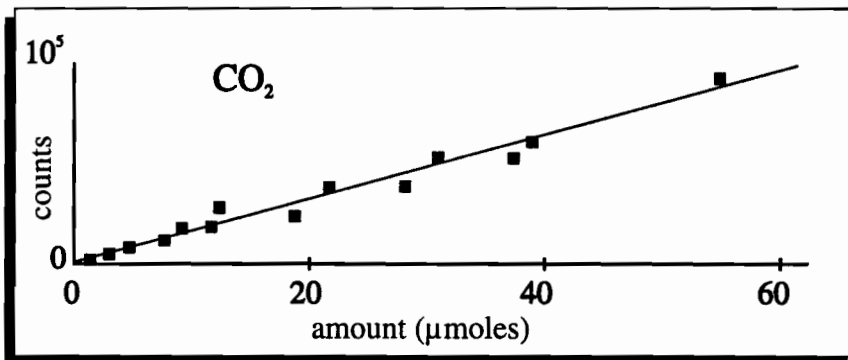
Identification of peaks and standardisation was achieved by injecting different amounts of known gas mixtures available commercially (Scott Specialty Gases Co., Plumsteadville, PA), except for water, which was injected as saturated vapour at known temperatures and pressures. Identification of species was accomplished by comparing retention times. Calibration curves (Fig. 9), constructed by plotting the integrated peak areas against the injected amounts of a species (known), were used to determine the amounts of the eluted gases.

### Packed Column

Initially, experiments were carried out using a 10' x 1/8" OD Ni-alloy column packed with HayeSep<sup>®</sup> R (100/120 mesh). The injector was set up for the packed configuration (Fig. 2A) and heated to 120°C. The PID was set at ~105°C, hot enough to keep H<sub>2</sub>O in the vapour state, yet below the recommended maximum operating temperature; the TCD was

FIGURE 9

Examples of calibration curves for volatile species created by analysing several gas mixtures of known composition.



heated to 150°C. Although the latter detector could have been set to much higher temperature, Hewlett-Packard (1991) report that greater TCD sensitivity is achieved if the detector body is maintained at low temperature. A convenient carrier gas flow rate was determined to be 20 ml/min at 80°C, measured at the vent port of the TCD (cf. Fig. 4). For this flow rate, the optimal reference gas flow to the TCD was of 30 ml/min, again as recommended by Hewlett-Packard (1991) for optimum detector performance. As mentioned above, for the purpose of volatile analysis of fluid inclusions, a constant oven temperature of 80°C during runs proved to be the best compromise. Retention times (Tables 1 and 2) were found to be slightly longer than those reported by Bray *et al.* (1991), probably due to the greater lengths of tubing connecting the crushers/injector to the column in our system.

Blanks run to simulate crush action with an empty sample chamber, *i.e.*, by just moving the piston, gave a flat signal for both TCD and PID detectors. Blanks using inclusion-free Brazilian quartz and fragmented pure-silica tubing also gave flat signals, except for a small unidentified hump at ~65 min in both quartz and Si tube runs. Bray *et al.* (1991) reported a similar unknown peak for their blank.

When analysing mixtures of the lighter gases (Table 1), the first species to exit the column are  $N_2 \pm CO \pm Ar \pm O_2$ , which produce a composite peak at 2.7 min (Fig. 10). This peak, albeit much smaller, was also observed on runs of Strange Lake quartz (Fig. 11). Bray *et al.* (1991) report the presence of the same peak in their 80°C runs, and used an oven temperature of -70°C to resolve it. They found that in all natural samples analysed the only species present was  $N_2$ . This is predicted by the extremely low fugacities of  $O_2$ , CO and Ar in nature (CO only attains significant fugacities at high temperatures – >600°C – and low  $fO_2$ ; Eugster and Skippen, 1967).

Methane elutes at 3.0 min, and  $CO_2$  is detected at 4.0 min (Figs. 10A and 11A). As mentioned above, both gases give a negative response on the PID but are well resolved by the TCD. The  $C_2$  hydrocarbons elute next, and although the PID is much more sensitive to these species than the TCD, if present in large amounts, they are also detected by the latter detector. Interestingly, while the PID generates a peak for  $C_2H_4$  (at 5.2 min) and a

**Table 1**

*Retention times and other integration results from running a standard gas mixture using the packed column (cf. Fig. 10).*

Sample Name: Mix 216; <sup>†</sup> Injected: 25 $\mu$ l						
Column: HayeSep R						
Peak #	R. T. <sup>‡</sup> (min)	Area (counts)	Height (counts)	Width (min)	Area % <sup>§</sup>	Species
<b>TCD</b>						
1	2.7	2036542	244657	0.13	94.05	N <sub>2</sub> + CO
2	3.0	36266	2894	0.18	1.67	CH <sub>4</sub> methane
3	4.0	24166	2559	0.15	1.12	CO <sub>2</sub> C dioxide
4	5.2	22967	2100	0.17	1.06	C <sub>2</sub> H <sub>4</sub> ethylene
5	6.0	19416	1700	0.17	0.90	C <sub>2</sub> H <sub>2</sub> acetylene
6	6.2	25994	2030	0.19	1.20	C <sub>2</sub> H <sub>6</sub> ethane
Total area = 2165351						
<b>PID</b>						
1	2.7	10967	1177	0.16	0.91	N <sub>2</sub> + CO
2	5.2	279968	25514	0.18	23.34	C <sub>2</sub> H <sub>4</sub> ethylene
3	5.9	908758	69339	0.22	75.75	C <sub>2</sub> H <sub>2</sub> + C <sub>2</sub> H <sub>6</sub>
Total area = 1199694						

<sup>†</sup> 1% each of CO, CO<sub>2</sub>, CH<sub>4</sub>, C<sub>2</sub>H<sub>2</sub>, C<sub>2</sub>H<sub>4</sub>, C<sub>2</sub>H<sub>6</sub> in N<sub>2</sub>

<sup>‡</sup> Retention times (R.T.) can vary up to  $\sim\pm 5\%$  due to flow rate fluctuations

<sup>§</sup> Percentages calculated for each detector

**Table 2**

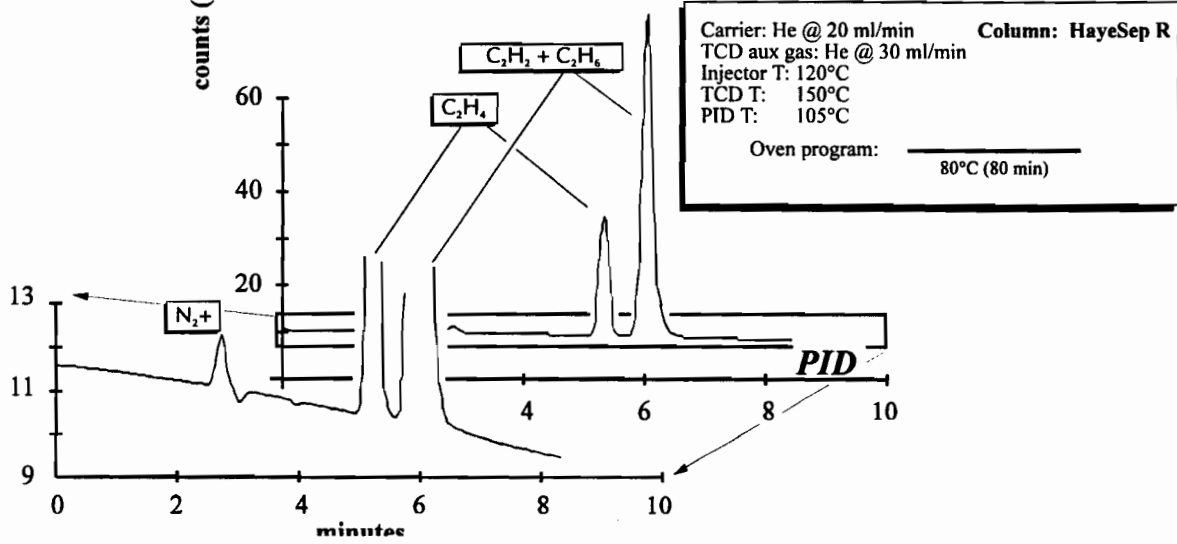
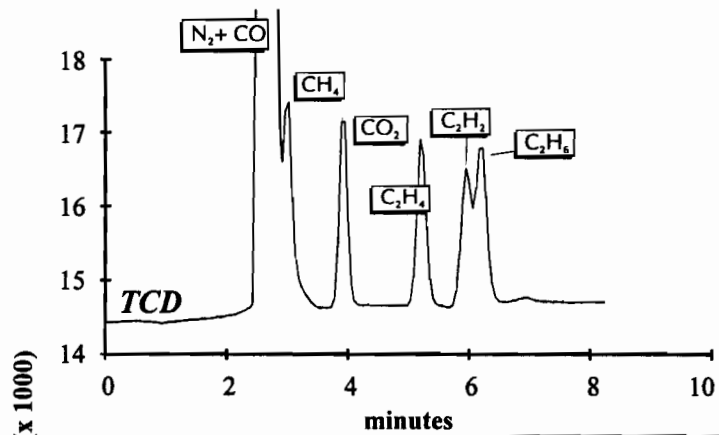
*Retention times and other integration results from analysis of quartz from Strange Lake using the packed column (cf. Fig. 11).*

Sample Name: 56-A-1; 1.3g. Crusher 1							
Column: HayeSep R							
Peak #	R. T. <sup>†</sup> (min)	Area (counts)	Height (counts)	Width (min)	Area % <sup>‡</sup>	Species	
<b>TCD</b>							
1	2.6	14321	1764	0.12	0.12	N <sub>2</sub>	nitrogen
2	3.0	332592	40392	0.13	2.69	CH <sub>4</sub>	methane
3	3.9	97981	10610	0.14	0.79	CO <sub>2</sub>	C dioxide
4	6.2	70708	5564	0.20	0.57	C <sub>2</sub> H <sub>4</sub>	ethane
5	24.5	11841600	77735	4.79	95.73	H <sub>2</sub> O	water
Total area = 12357202							
<b>PID</b>							
1	2.7	2590	332	0.13	0.32	N <sub>2</sub>	nitrogen
2	5.2	1203	117	0.17	0.15	C <sub>2</sub> H <sub>4</sub>	ethylane
3	6.2	182065	13821	0.21	22.78	(C <sub>2</sub> H <sub>2</sub> ?+)	C <sub>2</sub> H <sub>6</sub>
4	19.7	561831	11692	0.72	70.30	C <sub>3</sub> H <sub>8</sub>	propane
5	43.9	3156	31	1.72	0.39	C <sub>4</sub> H <sub>10</sub>	butane
Total area = 799168							
† Retention times (R.T.) can vary up to ~±5% due to flow rate fluctuations							
‡ Percentages calculated for each detector							

FIGURE 10

Chromatograms showing the signals from the micro-thermal conductivity (TCD) and photoionisation (PID) detectors for injection of 25  $\mu$ l of standard mixture #216, into the HayeSep<sup>®</sup>-R packed column.

Sample: STD mix # 216  
Amount: 25  $\mu$ l (1%/ea. in N<sub>2</sub>)  
Insertion: Injector



composite  $C_2H_2 \pm C_2H_6$  peak at 6 min from running the standard mix 216 (Fig. 10), the composite peak is split by the TCD into peaks at 5.9 min and 6.2 min representing  $C_2H_2$  and  $C_2H_6$ , respectively. On the other hand, concentrations of these species in natural samples are rarely high enough to produce a signal on the TCD. Bray *et al.* (1991, see also Bray and Spooner, 1992) do not report splitting of the  $C_2H_2 \pm C_2H_6$  peak. This is possibly due to slight differences in the sensitivities of the detectors.

The next peak to appear on the TCD trace is  $H_2O$  at ~25 min (Fig. 11A). Water produces a tailed peak, at least one order of magnitude wider than the earlier peaks. The skewness of the water signal most likely reflects absorption, followed by slow desorption, of  $H_2O$  onto the column phase. Chromatograms published in Bray and Spooner (1992) and in Thomas *et al.* (1990) obtained with the same packed column, show very similar shapes for the  $H_2O$  peak. The PID has a non-linear response to  $H_2O$  and, depending on the  $H_2O$  concentration, may give a negative peak of the same width as the equivalent positive peak from the TCD, or an even wider positive signal.

Most samples produced a n-propane ( $C_3H_8$ ) peak on the front shoulder of the water disturbance on the PID trace, centred at 19.5 min (Fig. 11B). Integration of this peak is problematic, firstly because at low concentrations it can be partly masked by the large  $H_2O$  peak, and secondly because the associated background is quite variable. Bray and Spooner (1992) reported detection of COS on the PID, at a retention time between that of  $C_2$  and  $C_3$  hydrocarbons, in samples from the Tanco granitic pegmatite (Manitoba), and the Boss Mountain molybdenite deposit (British Columbia). They also interpreted an  $SO_2$  peak on the negative disturbance created by  $H_2O$  on the PID trace, but could not quantify it. We have not encountered these gases in the samples analysed to date, and therefore did not run standards for them. However, it is reasonable to assume that these species can also be detected on our packed column.

After elution of water, the TCD signal is completely flat, whereas the PID inconsistently shows a small poorly shaped hump at ~45 min, tentatively assigned to a  $C_4$  species, plus the unknown hump produced by the blanks at ~65 min (Fig. 11B). It is evident from Figure 11 and Table 2 that the widths of the peaks increase rapidly with increasing

**Table 3**

*Retention times and other integration results from running a standard gas mixture using the capillary column (cf. Fig. 14).*

Sample Name: Mix 216;† Injected: 3 µl						
Column: PoraPLOT Q						
Peak #	R. T.‡ (min)	Area (counts)	Height (counts)	Width (min)	Area %§	Species
<b>TCD</b>						
1	2.4	253990	40312	0.10	94.45	N <sub>2</sub> + CO
2	2.9	2598	360	0.10	0.97	CH <sub>4</sub> methane
3	5.5	3129	391	0.10	1.16	CO <sub>2</sub> C dioxide
4	9.8	2983	449	0.11	1.11	C <sub>2</sub> H <sub>4</sub> ethylene
5	10.2	2869	487	0.10	1.07	C <sub>2</sub> H <sub>2</sub> acetylene
6	11.5	3353	547	0.10	1.25	C <sub>2</sub> H <sub>6</sub> ethane
Total area = 268922						
<b>PID</b>						
1	2.3	458	66	0.12	0.80	N <sub>2</sub> + CO
2	9.7	13214	1826	0.11	23.00	C <sub>2</sub> H <sub>4</sub> ethylene
3	10.1	41957	6463	0.10	73.04	C <sub>2</sub> H <sub>2</sub> acetylene
4	11.4	1815	276	0.10	3.16	C <sub>2</sub> H <sub>6</sub> ethane
Total area = 57444						

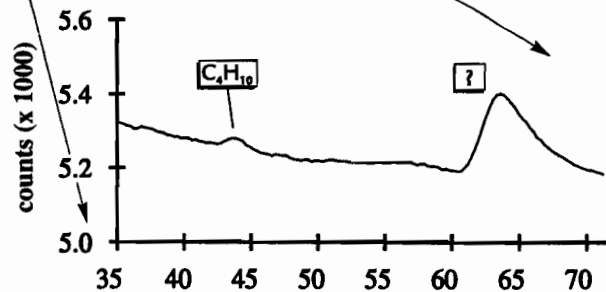
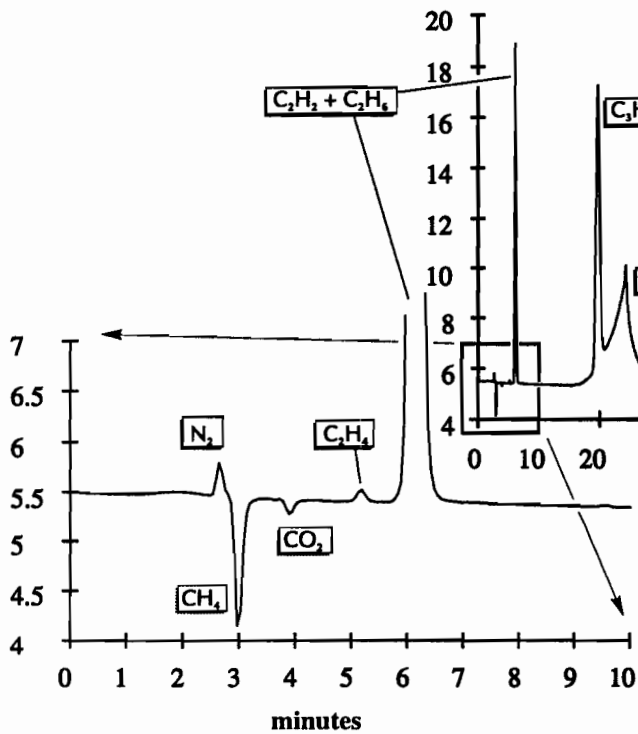
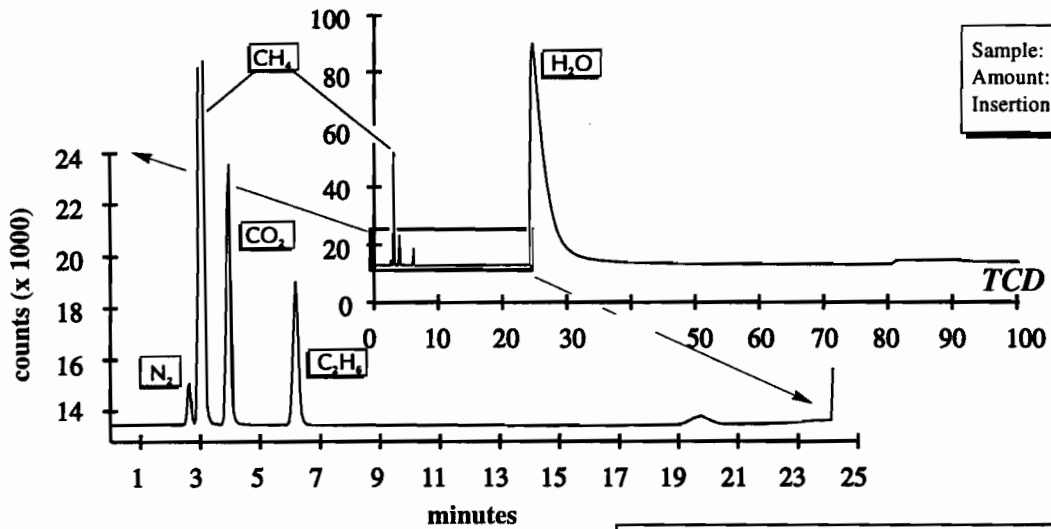
† 1% each of CO, CO<sub>2</sub>, CH<sub>4</sub>, C<sub>2</sub>H<sub>2</sub>, C<sub>2</sub>H<sub>4</sub>, C<sub>2</sub>H<sub>6</sub> in N<sub>2</sub>

‡ Retention times (R.T.) can vary up to ~±5% due to flow rate fluctuations

§ Percentages calculated for each detector

FIGURE 11

Chromatograms showing the signals from the micro-thermal conductivity (TCD) and photoionisation (PID) detectors of fluid-inclusion volatiles released by crushing 1.3 g of pegmatite quartz from the Strange Lake peralkaline complex. The analysis was carried out using the HayeSep<sup>®</sup>-R packed column.



retention times, and that species eluting after H<sub>2</sub>O have very low aspect ratios, raising detection limits and drastically reducing the precision of their quantitative analysis.

After completion of an analysis (~80 min), the oven temperature is increased to 115°C (higher carrier gas temperatures could damage the PID lamp) and held for about 30 min, to speed up elution of any possible phase still remaining in the column. Next, the column temperature is returned to 80°C, and after thermal equilibration (~20 min) another run can be started.

### Capillary Column

Because of its high capacity, the 25 m x 0.53 mm ID PoraPLOT<sup>®</sup> Q column operates best at high flow rates, which are compatible with the injector set-up in splitless mode (*i.e.*, as for packed columns, cf. Fig 2). Carrier gas flow was 20 ml/min at 35°C, and reference gas flow to the TCD was 30 ml/min, *i.e.*, the flow rates were similar to those used for the packed column. Detector body and injector temperatures were also the same as with the packed column (see above). At an oven temperature of 80°C, *i.e.*, the setting used with the packed column, elution of the lighter gases was too fast, causing them to be insufficiently separated. After several runs, we adopted a temperature program which enabled separation of the light gases with relatively short total run times; longer retention times result in inferior peak definition. With this program, the oven is cooled to -20°C before the analysis is started, and 6.5 min into the run, after elution of CO<sub>2</sub> on the TCD, the oven temperature is ramped at 10°C/min to 35°C where it is held for 10 min to allow H<sub>2</sub>O elution on a flat background (the TCD is much more sensitive to temperature fluctuations than the PID, Fig. 12). The temperature is then increased at 5°C/min to 115°C and left unchanged for ~40 min, when the run is stopped, after the C<sub>6</sub> gases are detected by the PID. Total running time is about 80 min.

Generally, the order of elution of species corresponds to the order of elution with the packed column, but retention times differ significantly (Tables 3 and 4). The most striking improvement, using the capillary column, was the appearance of a number of peaks which had not been observed when the same samples were run on the packed column. Peak

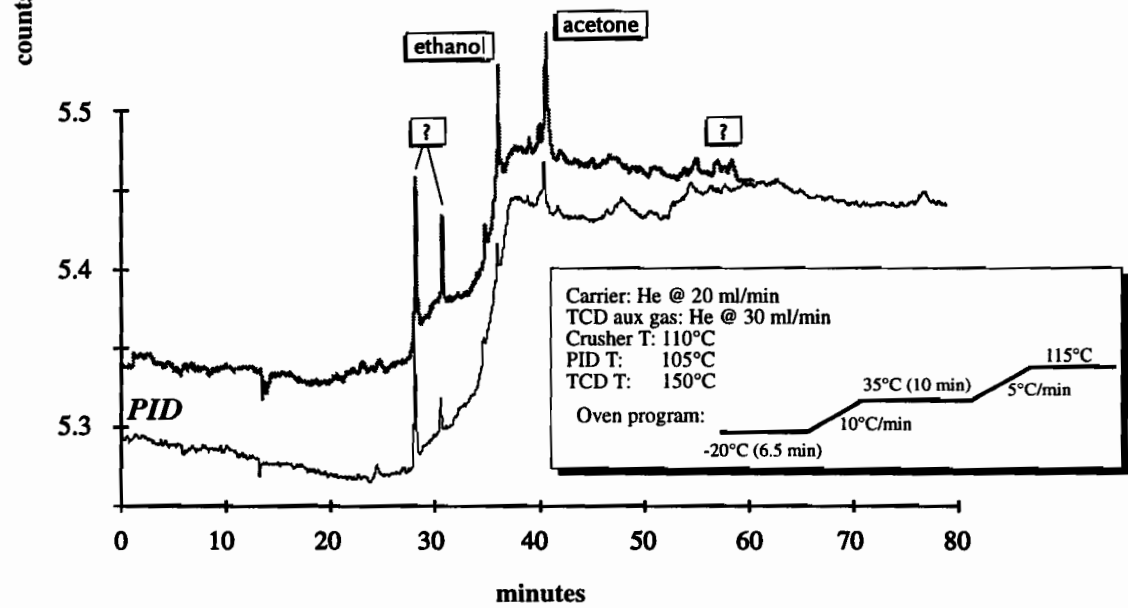
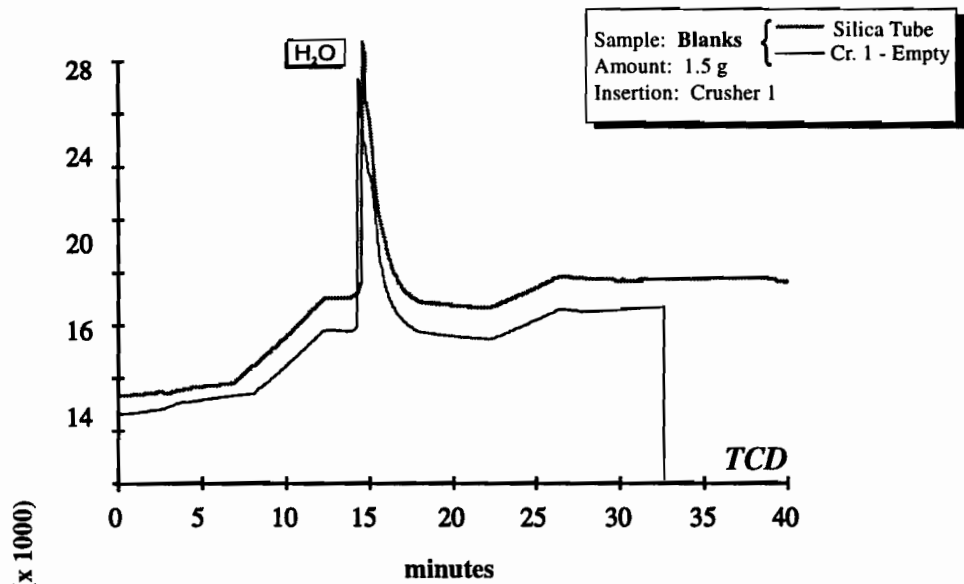
**Table 4**

*Retention times and other integration results from analysis of quartz from Strange Lake using the capillary column (cf. Fig. 15).*

Sample Name: 56-A-1; 1.5g. Crusher 2							
Column: PoraPLOT Q							
Peak #	R. T. <sup>†</sup> (min)	Area (counts)	Height (counts)	Width (min)	Area % <sup>‡</sup>	Species	
<b>TCD</b>							
1	2.4	13539	2156	0.11	0.06	N <sub>2</sub>	nitrogen
2	2.9	595860	92404	0.11	2.83	CH <sub>4</sub>	methane
3	5.6	81876	9876	0.14	0.39	CO <sub>2</sub>	C dioxide
4	11.5	133592	16843	0.13	0.63	C <sub>2</sub> H <sub>4</sub>	ethane
5	17.2	20265800	133116	1.84	96.09	H <sub>2</sub> O	water
Total area = 21091500							
<b>PID</b>							
1	2.4	485	64	0.13	0.03	N <sub>2</sub>	nitrogen
2	9.9	584	84	0.12	0.04	C <sub>2</sub> H <sub>4</sub>	ethylane
3	10.3	467	77	0.10	0.03	C <sub>2</sub> H <sub>2</sub>	acetylane
4	11.5	126552	13999	0.15	8.45	C <sub>2</sub> H <sub>6</sub>	ethane
5	24.5	407463	19071	0.36	27.21	C <sub>3</sub> H <sub>8</sub>	propane
6	34.5	38102	2228	0.29	2.54	C <sub>4</sub> H <sub>10</sub>	isobutane
7	36.3	437011	34458	0.21	29.19	C <sub>4</sub> H <sub>10</sub>	n-butane
8	44.4	151682	6125	0.41	10.13	C <sub>5</sub> H <sub>12</sub>	isopentane
9	46.8	164342	7842	0.32	10.98	C <sub>5</sub> H <sub>12</sub>	n-pentane
10	66.8	48934	876	0.93	3.27	C <sub>6</sub> H <sub>14</sub>	isohexane
11	69.2	62979	967	1.09	4.21	C <sub>6</sub> H <sub>14</sub>	neo-hexane
12	75.0	58745	969	1.01	3.92	C <sub>6</sub> H <sub>14</sub>	n-hexane
Total area = 1504082							
† Retention times (R.T.) can vary up to ~±5% due to flow rate fluctuations							
‡ Percentages calculated for each detector							

FIGURE 12

Chromatograms showing the signals from the micro-thermal conductivity (TCD) and photoionisation (PID) detectors, on running Brazilian quartz and pure-silica tubing blanks with the PorapLOT<sup>®</sup>-Q capillary column.



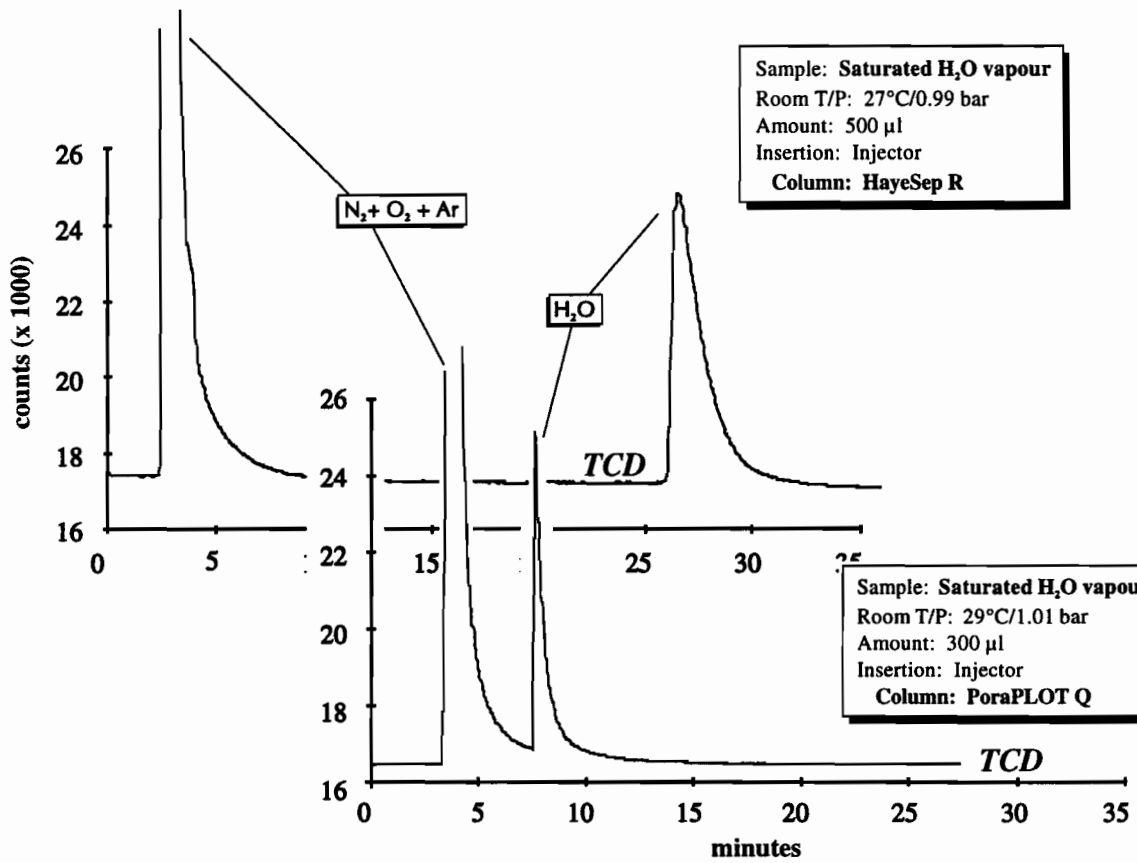
definition is much sharper, with widths  $1/2$  to  $1/10$  of those produced by the same species on the packed column (compare Tables 2 and 4). This greatly improved resolution, and allowed more precise determination of peak areas. Finally, water generates a signal with a width/height ratio  $\sim 1/4$  of that observed on the packed column for similar concentrations, and does not produce anywhere near as large a tail, although it does not show a perfect gaussian shape (Fig. 13). Most importantly, with the packed column we needed to inject at least 100  $\mu\text{l}$  of water-saturated vapour in order to obtain a peak, whereas 20  $\mu\text{l}$  at the same conditions are sufficient using the capillary column.

In contrast to the results obtained using the packed column, there were a number of extra peaks on the PID traces from empty crusher runs as well as from those in which Brazilian quartz and silica tubing were crushed. The most important of these are two unidentified peaks at 29.1 min and 31.6 min, and two more at 37.2 min and 41.5 min, tentatively assigned to ethanol and acetone, respectively (Fig. 12B). Andrawes *et al.* (1984) found that allowing the piston and the body of the crusher to come in contact produced significant  $\text{H}_2$  and  $\text{CH}_4$ . Methane was not observed in our blanks ( $\text{H}_2$  was not detected using He as carrier gas, see below), either because its concentration was below the detection limit of the TCD or because the material from which our crushers were constructed does not produce the same gases. However, since the contaminants found in our blanks occur independently of whether a sample is crushed or the piston is just moved without touching the shaft, we consider it likely that they originate from the silicone O-rings, rather than from degassing of the stainless steel. Moreover, the same peaks, although much smaller, are produced by inserting a needle through the silicone rubber septum in the injection port.

Small quantities of  $\text{H}_2\text{O}$  were detected on all blank runs and even by simply starting the temperature program. As suggested by Bray *et al.* (1991), this probably reflects the presence of trace quantities of  $\text{H}_2\text{O}$  in the carrier gas that collect in the column during the subzero part of the run and then are released at higher temperatures. However, unlike these authors, we did not detect  $\text{CO}_2$  in our blanks, since the oven temperature is always well above the freezing point of  $\text{CO}_2$ . The amount of water contributed by the carrier gas is a very small proportion of the amount released from a sample, and was found not to vary

FIGURE 13

Chromatograms showing the signals from the micro-thermal conductivity (TCD) of aliquots of H<sub>2</sub>O saturated vapour, analysed at 80°C on the packed and capillary columns.



Carrier: He @ 20 ml/min  
 TCD aux gas: He @ 30 ml/min  
 Injector T: 120°C  
 TCD T: 150°C  
 PID T: 105°C

Oven program:  80°C

significantly over a number of blank runs. This quantity can therefore be subtracted from the amount measured in a sample. A more precise analysis of H<sub>2</sub>O can be obtained by performing a second crush of the sample at an oven temperature above the freezing temperature of H<sub>2</sub>O. The results from the two crushes are normalised by using a species which can be measured in both runs (e.g. CH<sub>4</sub>).

On the segment of the run at -20°C, the TCD detects the N<sub>2</sub> ± CO ± Ar ± O<sub>2</sub> peak at 2.4 min. CH<sub>4</sub> elutes at 2.9 min and CO<sub>2</sub> at 5.6 min (Fig. 14A). The PID detects C<sub>2</sub>H<sub>4</sub>, C<sub>2</sub>H<sub>2</sub> and C<sub>2</sub>H<sub>6</sub> at 9.9 min, 10.3 min and 11.6 min, respectively. Compared to runs with the packed column, acetylene and ethane are well isolated. Despite the fact that the oven temperature is ramped at 10°C/min in this interval of the run, the background remains flat (Fig. 14B), allowing clean resolution of these gases.

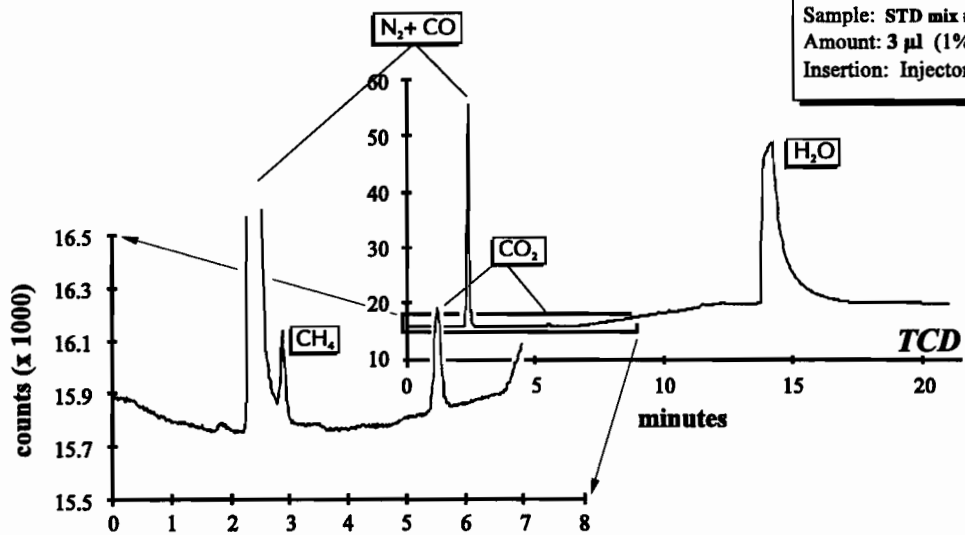
Water is separated at 14.5 min, on the 35°C plateau. Elution typically lasts about 2 to 4 minutes (vs. 5 to 10 min with the packed column) depending on the concentration, after which, especially on the PID trace, the signal returns immediately to baseline background values. After elution of H<sub>2</sub>O, data collection is stopped on the TCD, as species not yet eluted are detected on the PID. It is worth noting that if a species were to elute at the same time as water, the retention time of H<sub>2</sub>O could be easily changed, and the two peaks neatly resolved, by simply holding the oven temperature below zero for a slightly longer/shorter time.

At the beginning of the second temperature program, the C<sub>3</sub> species elute on a flat background (Fig. 15; compare with Fig. 11B). Although the C<sub>3</sub> hydrocarbons, propane (C<sub>3</sub>H<sub>8</sub>), propylene (C<sub>3</sub>H<sub>6</sub>), propadiene (C<sub>3</sub>H<sub>4</sub>) and propyne (C<sub>3</sub>H<sub>4</sub>) have been separated from standards mixes, C<sub>3</sub>H<sub>8</sub>, at 24.7 min, was the only C<sub>3</sub> species detected in the natural samples that were examined. The signal produced by elution of propane from the capillary column is much sharper than the same signal that was obtained from runs with the packed column; propane-peak width/height ratios for similar aliquots of sample 56-A-1 are at least three times greater for the packed column than for the capillary column.

After elution of the unknown peaks that were produced by the blank runs (at 29.1 min and 31.6 min), isobutane (C<sub>4</sub>H<sub>10</sub>) elutes at 34.5 min, and at 36.3 min n-butane exits the

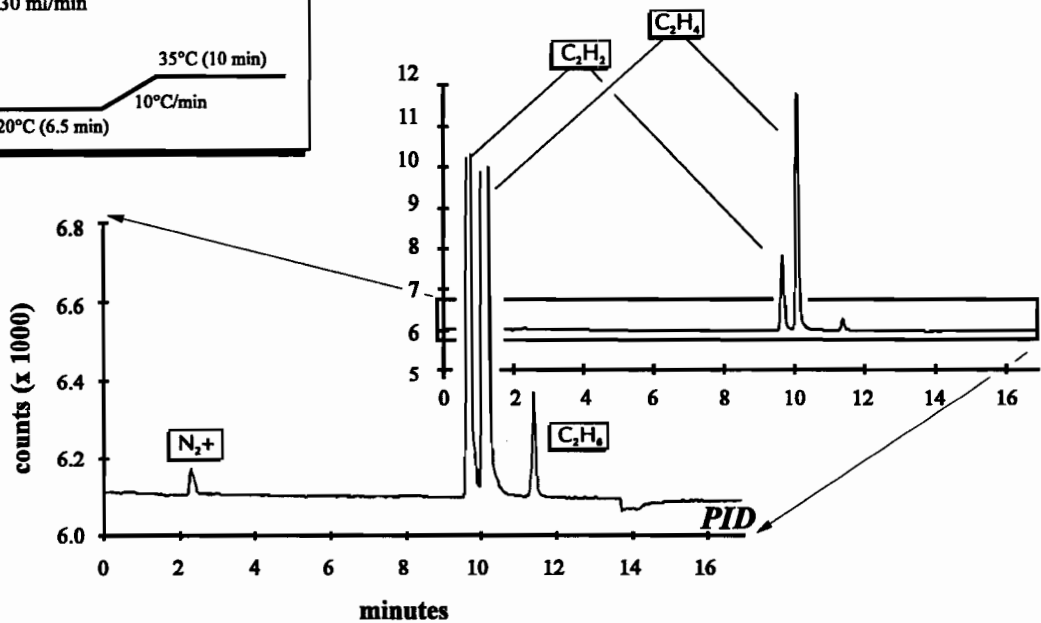
FIGURE 14

Chromatograms showing the signals from the micro-thermal conductivity (TCD) and photoionisation (PID) detectors after injection of 3  $\mu\text{l}$  of standard mixture #216, into the PoraPLOT<sup>®</sup>-Q capillary column.



Carrier: He @ 20 ml/min    Column: PorAPLOT Q  
TCD aux gas: He @ 30 ml/min  
Injector T: 120°C  
TCD T: 150°C  
PID T: 105°C

Oven program:  $-20^\circ\text{C}$  (6.5 min)  $\xrightarrow{10^\circ\text{C}/\text{min}}$   $35^\circ\text{C}$  (10 min)



column followed immediately by the ethanol peak detected in the blank (see above). Isopentane and n-pentane ( $C_5H_{12}$ ) elute after the oven has reached  $115^\circ\text{C}$ , at 44.5 min and 46.8 min, respectively (Fig. 15). As with the  $C_3$  species, most of the  $C_4$  and  $C_5$  hydrocarbons have been separated from injections of standard mixtures on this temperature program, but only the  $C_4$  and  $C_5$  alkanes have so far been found in fluid inclusions. Butanes and pentanes produce high, sharp peaks (width/height ratios on the order of  $10^{-4}$  to  $10^{-5}$ ) in all samples that, when previously analysed on the packed column, were shown not to contain species heavier than propane. Because the detector was the same in both cases, it is evident that the PoraPLOT<sup>®</sup> Q capillary column permits a much improved detection of organic volatiles in inclusions over the HayeSep<sup>®</sup> R packed column.

Peaks at 66.8 min, 69.2 min and 75.0 min were observed for some samples. The last peak corresponds to n-hexane ( $C_6H_{14}$ ), and although the other two are uncalibrated, based on their boiling points, they are tentatively assigned to isohexane and neohexane, respectively. The poorer shape (width/height ratios  $\geq 10^{-3}$ ) of the hexane signals is due to the late elution of these isomers and can be improved by running the samples isothermally at  $115^\circ\text{C}$ , which shortens retention times of these species to  $\sim 30$  min. After the hexanes exit the column the run is stopped, at about 80 min, and the oven is returned to  $-20^\circ\text{C}$ . Because of the nature of its construction material, this column reaches thermal equilibration with the oven almost immediately, which is convenient, especially when making sub-ambient runs.

Heavier aliphatic and some aromatic hydrocarbons (*e.g.*, benzene, chlorobenzenes, toluene) also were separated on this column at  $115^\circ\text{C}$ , but their retention times are extremely long, causing very wide peaks ( $\gg 5$  min) which drastically limit detectability. This could be improved by fitting the PID with the 10.2 eV lamp which would allow an oven temperature of up to  $300^\circ\text{C}$ , and reduce dramatically the elution times of species with boiling points higher than  $\sim 100^\circ\text{C}$  (*e.g.* octane b.p. =  $125^\circ\text{C}$ ), as well as provide at least a ten-fold increase in detector sensitivity for aromatics (*cf.* Driscoll and Duffy, 1987). However, as mentioned earlier, the 10.2 eV lamp cannot detect the  $C_2$  alkanes.

FIGURE 15

Chromatograms showing the signals from the micro-thermal conductivity (TCD) and photoionisation (PID) detectors of fluid-inclusion volatiles released by crushing 1.5 g of pegmatite quartz from the Strange Lake peralkaline complex. The analysis was carried out using the PoraPLOT<sup>®</sup>-Q capillary column.

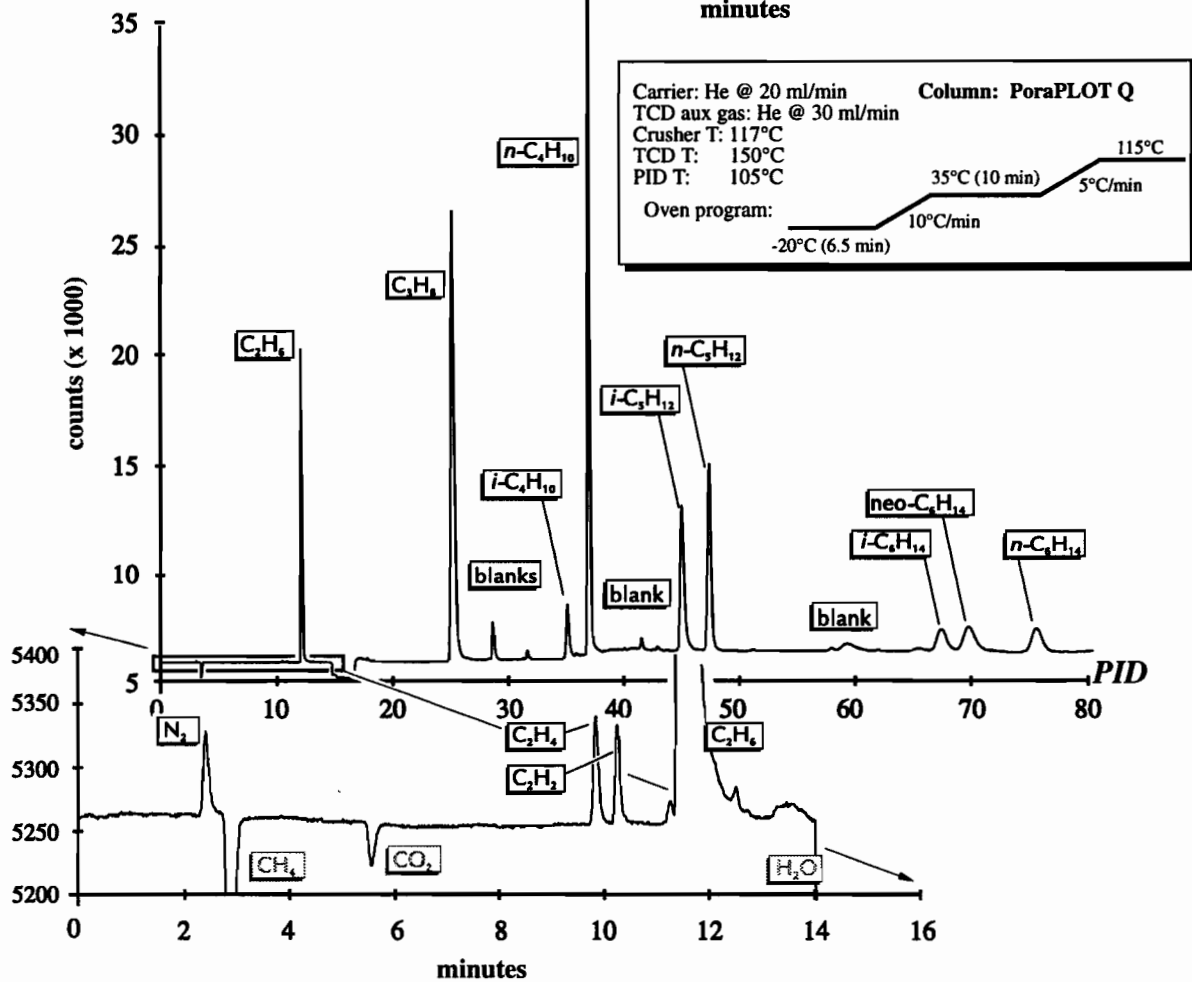
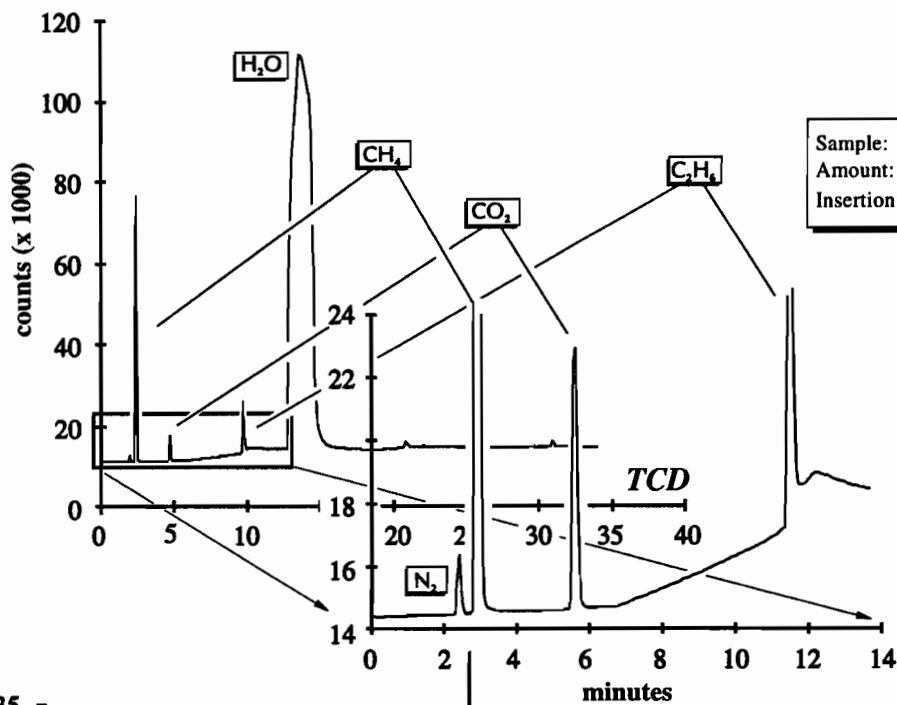


FIGURE 16

A plot of measured peak areas versus different injected amounts of H<sub>2</sub> injected from standard mixtures. The line has slope = 1.

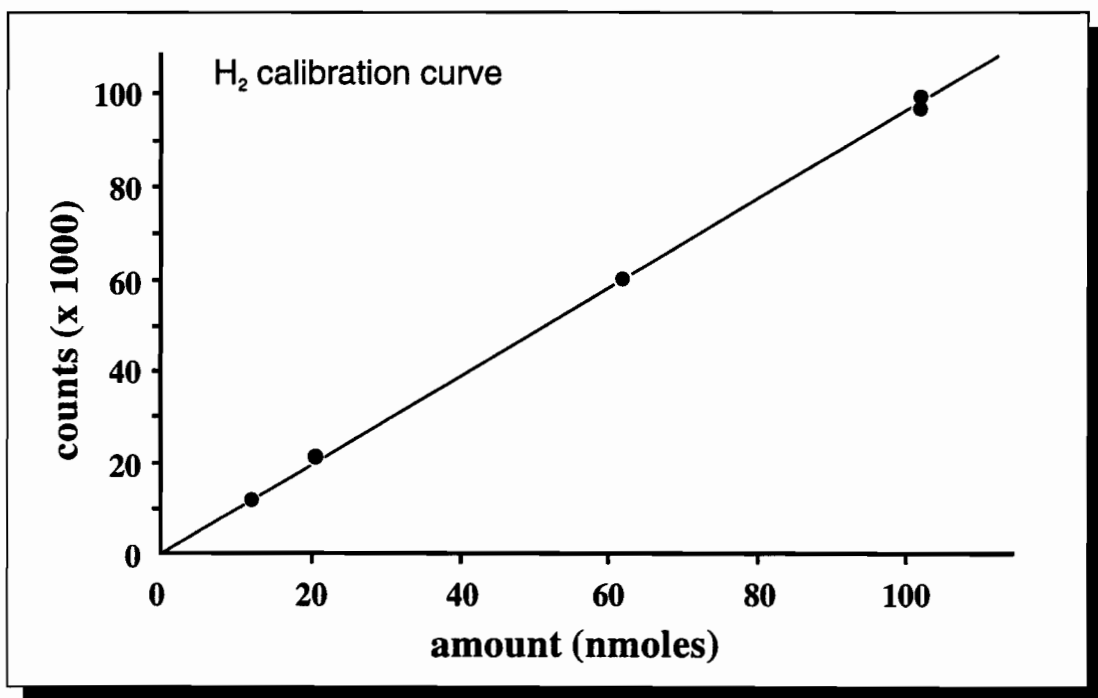


FIGURE 17

Chromatograms showing the response of the micro-thermal conductivity detector (TCD) to gases released from crushing two aliquots of quartz from sample TTR-22 using (A) helium and (B) nitrogen as carrier gases.

Carrier: N<sub>2</sub> @ 20 ml/min

Column: PoraPLOT Q

TCD aux gas: N<sub>2</sub> @ 30 ml/min

Crusher T: 107°C

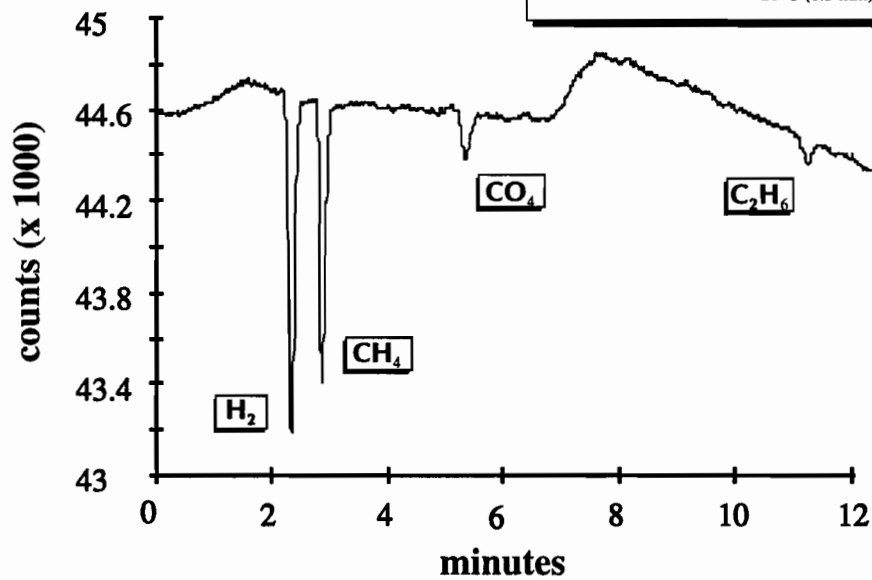
TCD T: 150°C

Oven program: -20°C (6.5 min)

35°C (10 min)

10°C/min

-20°C (6.5 min)



Sample: TTR-22, quartz  
Amount: 1.2 g  
Insertion: Crusher 1

Carrier: He @ 20 ml/min

Column: PoraPLOT Q

TCD aux gas: He @ 30 ml/min

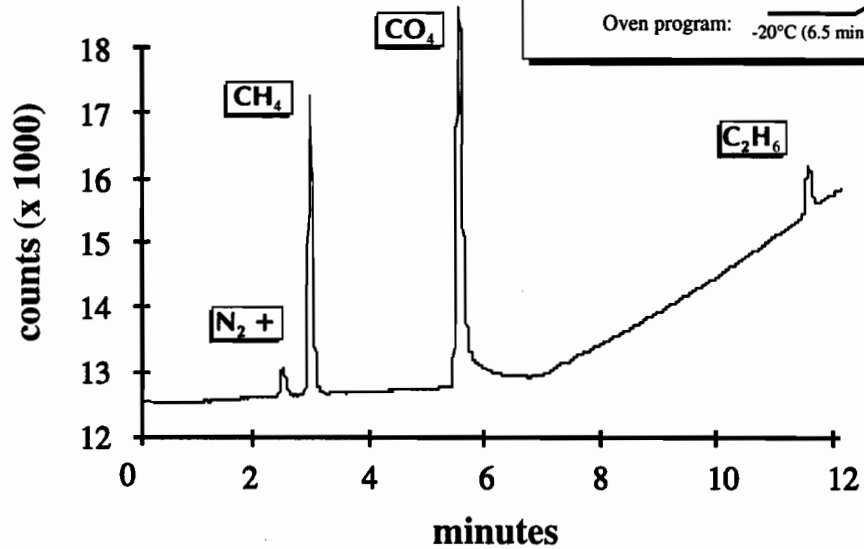
Crusher T: 112°C

TCD T: 150°C

Oven program: -20°C (6.5 min)

35°C (10 min)

10°C/min



Sample: TTR-22, quartz  
Amount: 1.2 g  
Insertion: Crusher 1

### Analysis of Hydrogen

Analysis of H<sub>2</sub> by gas chromatography has been problematic owing to peak overlap with N<sub>2</sub>, Ar, CO and O<sub>2</sub>, and poor retention of this gas using porous polymer columns. Some authors have tried to resolve this problem by analysing H<sub>2</sub> using molecular sieve packed columns (*e.g.*, Andrawes and Gibson, 1979), and although H<sub>2</sub> is detected at low concentrations with such columns, most other gases cannot be detected at the required levels. Consequently the result for H<sub>2</sub> generally cannot be related to those for the remaining gases, which must be analysed on another column.

We succeeded in analysing for H<sub>2</sub> with the PoraPLOT<sup>®</sup> capillary column by changing the carrier to N<sub>2</sub>. These two species differ in thermal conductivity by 1 order of magnitude, and thus the TCD is able to detect very low concentrations of H<sub>2</sub> (Fig. 16). By contrast, He and H<sub>2</sub> have very similar thermal conductivity making detection for H<sub>2</sub> very poor. The problem of N<sub>2</sub> and H<sub>2</sub> peak overlap is resolved by using N<sub>2</sub> as the carrier gas. Use of this carrier also allows H<sub>2</sub> to be separated from Ar, because Ar produces a peak with inverted polarity. Finally, the detection limit for CO is  $\sim 5 \times 10^{-2}$   $\mu$ moles with N<sub>2</sub> as the carrier, making it essentially undetectable in fluid inclusions, and the extremely low partial pressure of O<sub>2</sub> in even the most oxidising hydrothermal fluids, rules out the possibility of it contributing to the H<sub>2</sub> peak.

Figure 17 shows chromatograms for sample TTR-22 collected with the TCD using He and N<sub>2</sub> as carrier gases. The peak at 2.4 minutes with He as the carrier is due to N<sub>2</sub> possibly with a small contribution from H<sub>2</sub>, whereas the same peak with N<sub>2</sub> as the carrier is due entirely to H<sub>2</sub>. Although all peaks with N<sub>2</sub> as the carrier, except Ar, are negative (due to the low thermal conductivity of N<sub>2</sub>), the TCD showed a good linear response during calibration for most species analysed. An exception is CO<sub>2</sub>, which can only be analysed to  $\sim 10^{-2}$   $\mu$ moles. Changing the carrier gas did not seem to have an effect on PID sensitivity (Fig. 18). The quantities of H<sub>2</sub> (and Ar) analysed with N<sub>2</sub> as the carrier can therefore be related to the bulk gas composition analysed with He as the carrier, by normalising the H<sub>2</sub>

**Table 5**  
*Concentrations (absolute and normalised to 100) and standard deviations,  $\sigma$ , for the volatile content of fluid inclusions in two splits of sample 56-A-1.*

		yields (nmoles)		moles %		$\sigma$
		split 1	split 2	split 1	split 2	
(g crushed)		(1.5)	(0.4)			
N <sub>2</sub>	nitrogen	3.098	0.614	0.438	0.451	0.010
CH <sub>4</sub>	methane	569.353	113.226	80.442	83.215	1.961
CO <sub>2</sub>	C dioxide	58.147	11.152	8.215	8.196	0.014
C <sub>2</sub> H <sub>4</sub>	ethylane	0.030	0.005	0.004	0.003	0.001
C <sub>2</sub> H <sub>2</sub>	acetylane	0.084	0.076	0.012	0.056	0.031
C <sub>2</sub> H <sub>6</sub>	ethane	60.324	8.838	8.336	6.495	1.301
C <sub>3</sub> H <sub>8</sub>	propane	12.022	1.425	1.699	1.047	0.461
i-C <sub>4</sub> H <sub>10</sub>	isobutane	0.552	0.077	0.078	0.056	0.015
n-C <sub>4</sub> H <sub>10</sub>	n-butane	4.320	0.494	0.610	0.363	0.175
n-C <sub>5</sub> H <sub>12</sub>	n-pentane	1.174	0.158	0.166	0.116	0.035

FIGURE 18

A chromatogram showing the response of the photoionisation detector (PID), using nitrogen as the carrier gas, to gases released from crushing quartz from sample 55-A-1.

Sample: 56-A-1, quartz  
 Amount: 1.5 g  
 Insertion: Crusher I

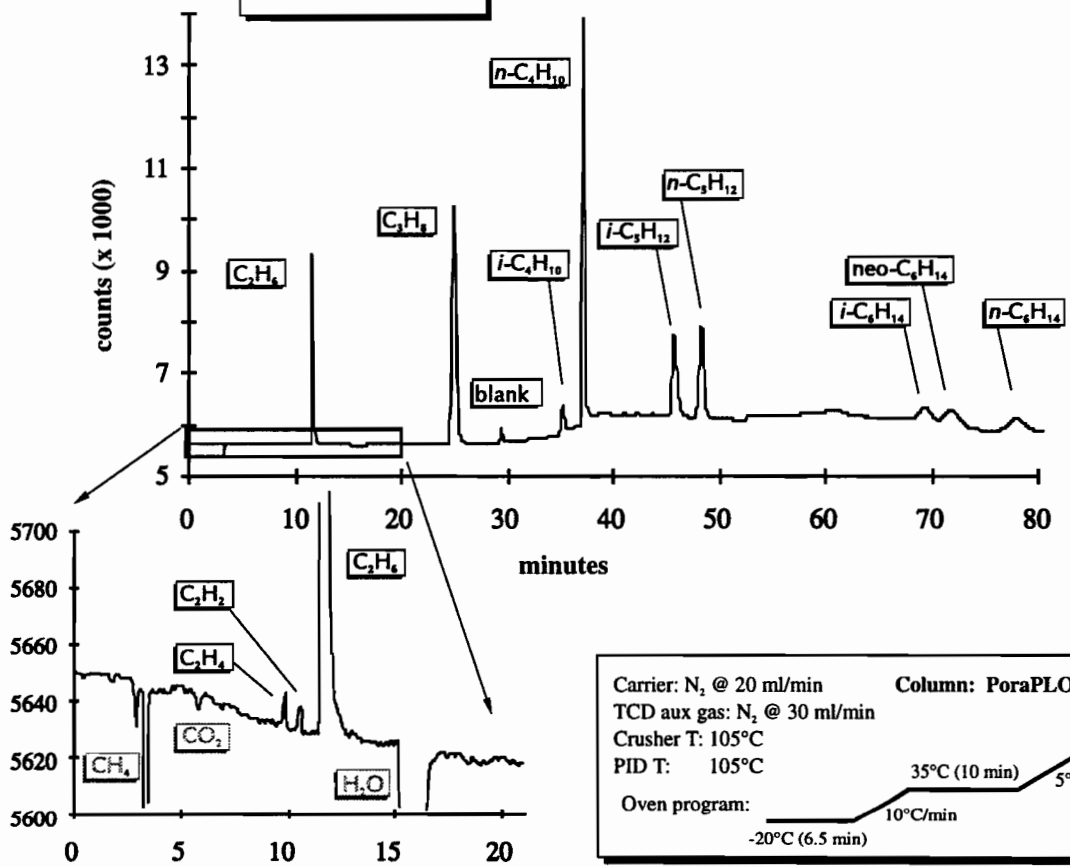
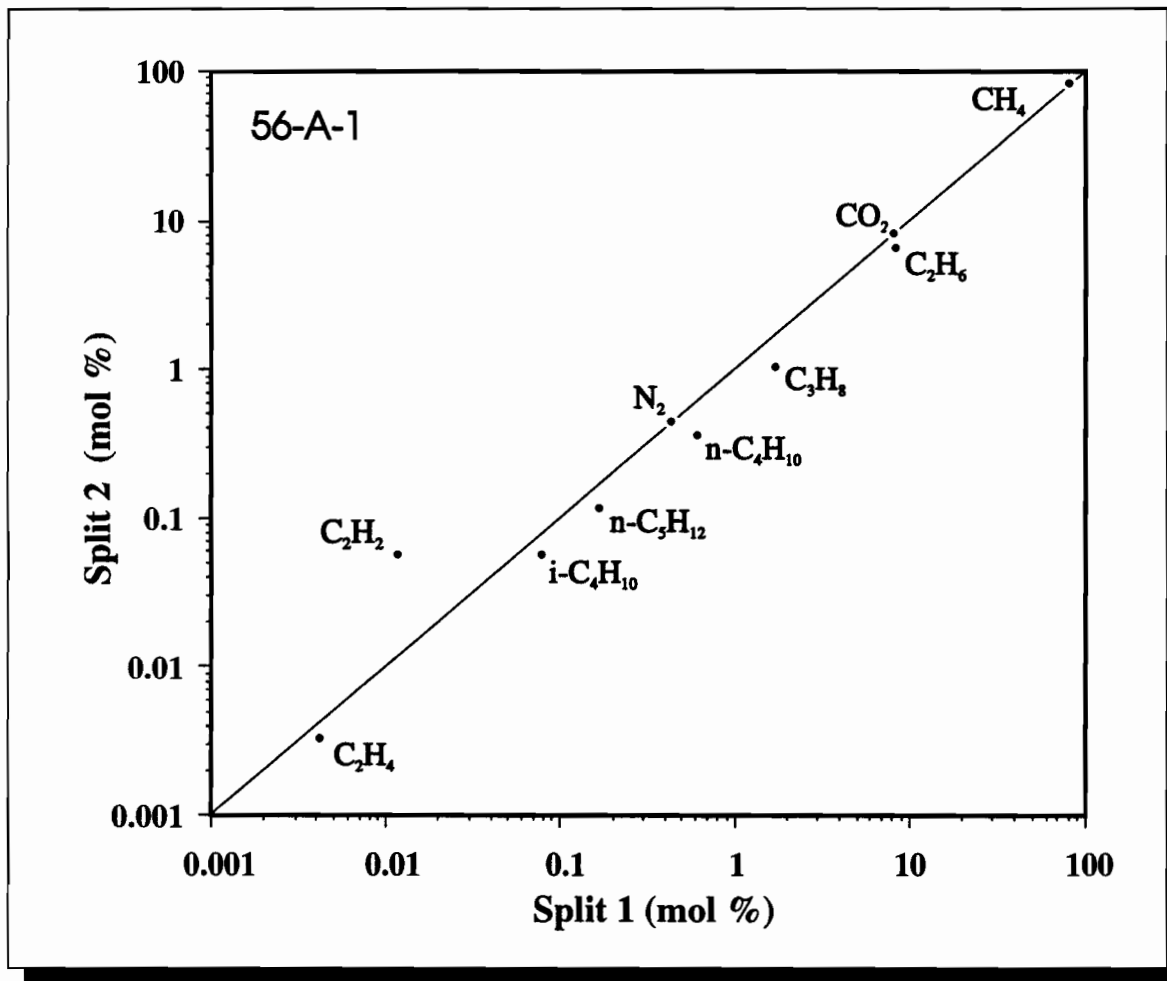


FIGURE 19

Logarithmic plot of species concentration expressed as mol %, for two separate splits of sample 56-A-1. The diameters of the dots correspond to an error of about 5% and the line has slope = 1.



content against those of species such as  $\text{CH}_4$  or  $\text{C}_2\text{H}_6$  which are detected with both carrier gases.

## Reproducibility of Gas Chromatographic Analysis

In order to test reproducibility of the bulk analysis, we performed repeat analyses of sample 56-A-1 using He as the carrier gas. The sample was cut in half, and each portion treated as a separate sample throughout the whole procedure of sieving, picking, cleaning, and analysing. In addition, we weighed different amounts for the two splits (0.41 g and 1.52 g), and did the analyses about one month apart.

The analyses of each portion of the sample, calculated both as absolute concentrations and normalised as percentages, together with the standard deviations are listed in Table 5, and are shown graphically in Fig. 19. Overall, the agreement between the two splits is very good, considering all the variables involved. Most compounds reproduced to  $\pm 15$  mol %, and for the more abundant elements, *i.e.*,  $\text{CH}_4$  and  $\text{CO}_2$  the error was less than one order of magnitude smaller than the reported value. The largest discrepancy between the two analyses was for acetylene ( $\text{C}_2\text{H}_2$ ), which yielded 0.012 mol % and 0.056 mol % in splits 1 and 2, respectively. The poor reproducibility of acetylene analysis could be due to fact that it was present in concentrations close to its detection limit.

## Conclusions

1. The gas chromatographic system developed for the analysis of fluid inclusions at the Department of Earth and Planetary Sciences of McGill University is based on a system in the Department of Geology at the University of Toronto (cf. Bray and Spooner, 1989). It is equipped with in-series photoionisation and micro-thermal conductivity detectors. Heated crushing ( $\sim 120^\circ\text{C}$ ) causes immediate release of volatiles, limiting gas adsorption onto newly created surfaces (e.g., Barker and Torkelson, 1975), but the

temperature is low enough to avoid chemical reactions among released gases. On-line crushing maximises the proportion of the released volatiles entering the column, thereby reducing detection limits ( $\leq 10^{-4}$  mmoles).

2. It has been shown that using a wide-bore capillary column (25 m x 0.53 mm ID fused silica) coated with PoraPLOT<sup>®</sup> Q greatly improves detection of hydrocarbons over the 10' x 1/8" (3.05 m x 3.2 mm)-OD HayeSep<sup>®</sup>-R packed column, reported to date to be the most efficient column for fluid-inclusion volatile analysis. The optimal conditions for analyses using the PoraPLOT<sup>®</sup> Q capillary column were found to be with a 20-ml/min (at 35°C) carrier-gas flow rate and an oven temperature programmed to start at -20°C, subsequently raised (10°C/min) to 35°C and held for 10 min, then raised again (5°C/min), to 115°C. Runs lasted ~80 min.
3. The capillary column allows analysis of N<sub>2</sub>, CO<sub>2</sub>, H<sub>2</sub>O, CH<sub>4</sub>, C<sub>2</sub>H<sub>4</sub>, C<sub>2</sub>H<sub>6</sub>, C<sub>2</sub>H<sub>2</sub>, C<sub>3</sub>H<sub>6</sub>, C<sub>3</sub>H<sub>8</sub> and C<sub>3</sub>H<sub>4</sub> to the same or higher degrees of accuracy than with the packed column. Butanes, pentanes and hexanes could not be analysed or were not detected with the packed column, but produced sharp peaks on the capillary column. Width/height ratios for these gases were of the order of 10<sup>-5</sup> to 10<sup>-3</sup>.
4. H<sub>2</sub> and Ar have been analysed successfully using N<sub>2</sub> as the carrier gas. Detection limits are ~10<sup>-5</sup> μmoles for H<sub>2</sub>, and ~10<sup>-4</sup> μmoles for Ar. Under these operating conditions, the TCD has lower sensitivity to gases other than H<sub>2</sub>, and for obvious reasons, cannot detect N<sub>2</sub>. On the other hand, the sensitivity of the PID is relatively unaffected. The results of analyses with N<sub>2</sub> as the carrier gas can be related to those with He as the carrier, by normalising with respect to CH<sub>4</sub> or C<sub>2</sub>H<sub>6</sub>.
5. Water produces a peak with the capillary column which has a width/height ratio ~1/4 that of the peak produced by similar amounts of water analysed with the packed column. This permits a more precise analysis of H<sub>2</sub>O, and lowers the limit for its detection by a factor of about four.

6. Starting the runs at sub-ambient temperatures, combined with the lower retention of H<sub>2</sub>O in the capillary column, allowed clean resolution of the propane peak, whereas with the packed column, propane could not be analysed due to interference with the water signal.
7. Aliphatic species, heavier than hexane, and aromatic hydrocarbons can be separated on the PoraPLOT<sup>®</sup> column, but in order to detect these gases at the low levels generally encountered in natural fluids, the oven temperature has to be increased above 115°C, which is the highest temperature at which the system can presently operate.

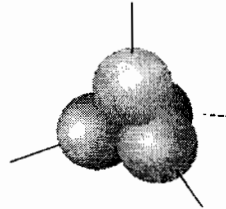
## References

- Abell, P.I., Draffen, C.H., Eglinton, G., Hayes, J.M., Maxwell, J.R. and Pillinger, C.T., 1970.** Organic analysis of the Apollo 11 lunar sample. *Proc. Apollo 11 Lunar Sci. Conf.*, 1757-1773.
- Andrawes, F.F. and Gibson, E.K. Jr., 1979.** Release and analysis of gases from geological samples. *Am. Mineral.*, 64, 453-463.
- Andrawes, F.F., Holzer, G., Roedder, E. Gibson, E.K. Jr., and Oro, J., 1984.** Gas chromatographic analyses of volatiles in fluid and gas inclusions. *J. Chromatogr.*, 302, 181-193.
- Barker, C.G. and Torkelson, B.E., 1975.** Gas adsorption on crushed quartz and basalt. *Geochim. Cosmochim. Acta*, 39, 212-218.
- Behar, F. and Pineau, F., 1979.** Analyse de CO<sub>2</sub>, H<sub>2</sub>O, hydrocarbures des inclusions fluides par chromatographie en phase gazeuse: application aux fentes alpines et aux roches métamorphiques. *Bull. Minéral.*, 102, 611-621.
- Bray, C.J. and Spooner, E.T.C., 1989.** Fluid inclusion volatile analysis using heated crushing (~105°C)/gas chromatography with in-series photoionization/thermal conductivity detectors and digital peak processing [abs]. *2<sup>nd</sup> Biennial Pan-Am Conf. Res. Fluid Inclusions*, 2, 12-13.
- Bray, C.J. and Spooner, E.T.C., 1992.** Fluid inclusion volatile analysis by gas chromatography with photoionization/micro-thermal conductivity detectors: Applications to magmatic MoS<sub>2</sub> and other H<sub>2</sub>O-CO<sub>2</sub> and H<sub>2</sub>O-CH<sub>4</sub> fluids. *Geochim. Cosmochim. Acta*, 56, 261-272.
- Bray, C.J., Spooner, E.T.C. and Thomas, A.V., 1991.** Fluid inclusion volatile analysis by heated crushing, on-line gas chromatography; applications to Archean fluids. *J. Geochem. Exploration*, 42, 167-193.
- Channer, D.M.DeR. and Spooner, E.T.C., 1994.** Combined gas and ion chromatographic analysis of fluid inclusions: Applications to Archean granite pegmatite and gold-quartz vein fluids. *Geochim. Cosmochim. Acta*, 58, 1101-1118.
- Cuney, M., Pagel, M. and Touret, J., 1976.** L'analyse des gaz des inclusions fluides par chromatographie en phase gazeuse. *Bull. Soc. Fr. Minéral. Crystallogr.*, 99, 169-177.

- Driscoll, J.N. and Duffy, M., 1987.** Photoionization Detector: A versatile tool for environmental analysis. *Chromatography*, 2, 21-27.
- Eugster, H.P. and Skippen, G.B., 1967.** Igneous and metamorphic reactions involving gas equilibria. In *Researches in Geochemistry*, P.H. Abelson ed., 2, Wiley, New York, 492-520.
- Goguel, R., 1963.** Die chemische Zusammensetzung der in den mineralen einiger Granite und ihrer Pegmatite eingeschlossenen Gase und Flüssigkeiten. *Geochim. Cosmochim. Acta*, 27, 155-181.
- Gough, T.A. and Simpson, C.F., 1972.** Water adsorption by porous polymer bead gas chromatographic columns. *J. of Chromatogr.*, 68, 31-45.
- Jennings, W., 1987.** *Analytical Gas Chromatography*, Academic Press, Orlando, FA., 259 p.
- Hewlett-Packard Co., 1991.** *HP 5890 Series II Reference Manual*, Printed in Pennsylvania, U.S.A.
- Hollis, L.O., 1966.** Separation of gaseous mixtures using porous polyaromatic polymer beads. *Anal. Chem.*, 38, 309-316.
- Hollis, L.O. and Hayes, W., 1966.** Water analysis by gas chromatography using porous polymer columns. *J. Gas Chromatogr.*, 4, 235-239.
- Kaliskan, R., 1987.** *Quantitative Structure-Chromatographic Retention Relationships*. Chemical Analysis Series, 93, J.D. Winefordner and I.M. Kolthoff, eds., Wiley-Interscience, New York, N.Y., 303 p.
- Kesler, S.E., Haynes, P.S., Creech, M.Z. and Gorman, J.A., 1986.** Application of fluid inclusion and rock-gas analysis in mineral exploration. *J. Geochem. Explor.*, 25, 201-215.
- Kreulen, R. and Schuiling, R.D., 1982.** N<sub>2</sub>-CH<sub>4</sub>-CO<sub>2</sub> fluids during formation of the Dôme d'Agout, France. *Geochim. Cosmochim. Acta*, 46, 193-203.
- Merle d'Aubigné, J. and Guiochon, G., 1970.** Etude du comportement thermique des polystyrènes réticulés, type porapak. *Chromatographia*, 3, 153-162.
- Miller, R.R., 1986.** Geology of the Strange Lake Alkalic Complex and the associated Zr-Y-REE mineralization. *Current-Research, Newfoundland Dept. of Mines and Energy*, Report 86-1, 11-19.

- Mironova, O.F., Naumov, V.B. and Salazkin, A.N., 1972.** Chromatographic analysis of gases trapped in rocks (in Russian). *Geokhimiya*, 10, 1514-1521.
- Petersilie, I.A. and Sørensen, H., 1970.** Hydrocarbon gases and bituminous substances in rocks from the Ilímaussaq alkaline intrusion, south Greenland. *Lithos*, 3, 59-76.
- Piperon, N.B. and Penchev, N.P., 1973.** A study on gas inclusions in minerals. Analysis of the gases from micro-inclusions in allanite. *Geochim. Cosmochim. Acta*, 37, 2075-2097.
- Pollock, G.E., O'Hara, D. and Hollis, O.L., 1984.** Gas chromatographic separation of nitrogen, oxygen, argon, and carbon monoxide using custom-made porous polymers from high purity divinyl-benzene. *J. Chromatography Science*, 22, 343-347.
- Roedder, E., 1972.** Composition of fluid inclusions. *U.S. Geol. Surv. Prof. Pap.* 440 JJ, 164 p.
- Salvi, S. and Williams-Jones A.E., 1992.** Reduced orthomagmatic C-O-H-NaCl fluids in the Strange Lake rare-metal granitic complex, Quebec/Labrador, Canada. *Eur. J. Mineral.*, 4, 1155-1174.
- Shepherd, T.J., Rankin, A.H. and Alderton, D.H.M., 1985.** *A Practical Guide to Fluid Inclusion Studies*, Blakie, 239 p.
- Smith, T.J., Cloke, P.L. and Kesler, S.E., 1984.** Geochemistry of fluid inclusions from the McIntyre-Hollinger gold deposit, Timmins, Ontario, Canada. *Econ. Geol.*, 79, 1265-1285.
- Thomas, A.V., Pasteris, J.D., Bray, C.J. and Spooner, E.T.C., 1990.** H<sub>2</sub>O-CH<sub>4</sub>-NaCl-CO<sub>2</sub> inclusions from the footwall contact of the Tanco granitic pegmatite: Estimates of internal pressure and composition from microthermometry, laser Raman spectroscopy, and gas chromatography. *Geochim. Cosmochim. Acta*, 54, 559-573.
- Welhan, J.A., 1988.** Methane and hydrogen in mid-ocean-ridge basalt glasses: analysis by vacuum crushing. *Can. J. Earth Sci.*, 25, 38-48.
- Ypma, P., 1974.** Analysis of fluid inclusions by gas chromatography. *Nato advanced study*, Nancy, N.P. Report.
- Zajac, I.S., Miller, R.R., Birkett, T., Nantel, S., 1984.** Le gîte de Zr, Y, Nb, et Be du complexe alcalin de Strange Lake, Québec-Labrador. *Ministère de l'Énergie et des Ressources, Québec*, DV 84-18, 127-142.

## CHAPTER IV



# MAGMATIC HYDROCARBONS AND THEIR ALTERATION IN THE STRANGE LAKE PERALKALINE GRANITE, QUEBEC/LABRADOR: EVIDENCE FROM FLUID INCLUSIONS

---

STEFANO SALVI

AND

ANTHONY E. WILLIAMS-JONES

*Department of Geological Sciences  
McGill University  
Montreal, QC  
Canada*

## Abstract

The volatile content of fluid inclusions in pegmatite quartz from the Strange Lake peralkaline complex has been analysed by gas chromatography using on-line extraction of inclusion contents and a PoraPLOT<sup>®</sup> Q capillary column. The measured gas species are, in order of abundance, CH<sub>4</sub>, H<sub>2</sub>, C<sub>2</sub>H<sub>6</sub>, CO<sub>2</sub>, N<sub>2</sub>, C<sub>3</sub>H<sub>8</sub>, *n*-C<sub>4</sub>H<sub>10</sub>, *n*-C<sub>5</sub>H<sub>12</sub>, C<sub>2</sub>H<sub>2</sub>, *i*-C<sub>4</sub>H<sub>10</sub>, and C<sub>2</sub>H<sub>4</sub>. Minor amounts of *i*-C<sub>5</sub>H<sub>12</sub>, *n*-C<sub>6</sub>H<sub>14</sub>, *i*-C<sub>6</sub>H<sub>14</sub> and *neo*-C<sub>6</sub>H<sub>14</sub> were also detected (but not quantified) in some of the inclusions. A suite of quartz samples from Ca-metasomatised pegmatites contains fluid inclusions with a similar distribution of hydrocarbons but much higher proportions of CO<sub>2</sub>.

The carbonic fluid coexisted immiscibly with a brine (Salvi and Williams-Jones, 1992), which on the basis of field and petrographic evidence, was interpreted to have originated from the magma. However, thermodynamic calculations indicate that the above gas species, specifically the hydrocarbons, could not have co-existed at equilibrium in the proportions measured, at any geologically reasonable conditions either prior to or post entrapment. We propose, instead, that the gas compositions measured in the Strange Lake inclusions, and in inclusions from other alkalic complexes, resulted from the production of H<sub>2</sub> during the alteration of arfvedsonite to aegirine, and the subsequent reaction of this H<sub>2</sub> with orthomagmatic CO<sub>2</sub> and CO to form hydrocarbons in a magnetite-catalysed Fischer-Tropsch synthesis.

Locally, influx of an oxidised calcic brine, derived externally from the pluton, altered the original composition of the fluid by converting hydrocarbons to CO<sub>2</sub>.

*“The inorganic theory [for the origin of petroleum] has some importance... also as a contribution to the synthetic theory for the origin of life. If inorganic ‘fuel oils’ escaped from the crust into the primitive ocean, ... the oil will have floated, and eventually been washed ashore in the same way that present-day fuels oils, discharged from ships at sea, besmear the coasts of Europe. Complex hydrocarbons are thus automatically concentrated and delivered to the environment ... The interface between oil and mud would form an ideal environment for [organic] synthesis, for the decomposition of relatively heavy hydrocarbons in a reducing environment would be exothermal, with the emission of methane, and would thus not only provide the materials for the synthesis of complex molecules but also the energy. Colloidal clay minerals would also be available ... as catalytic agents (‘proto-enzymes’).”<sup>1</sup>*

---

<sup>1</sup> Sylvester-Bradley, P.C. and King, R.J., 1963. Evidence for abiogenic hydrocarbons, *Nature*, vol. 198, pp. 728-731.

## Introduction

THE reduced nature of carbonic fluids in silica-undersaturated alkalic igneous systems has long been recognised (Petersilie, 1958 and 1963; Heinrich and Anderson, 1965; Petersilie and Sørensen, 1970; Ikorskii and Romanikhin, 1964; Kogarko, 1974; Sobolev *et al.*, 1974; Konnerup-Madsen *et al.*, 1979, Kogarko *et al.*, 1986) and, recently, reduced fluids have also been found in peralkaline granite (Salvi and Williams-Jones, 1992). These fluids are dominated by methane, almost invariably contain significant proportions of heavier alkanes (C<sub>2</sub> to C<sub>5</sub> and higher) and, less frequently, contain unsaturated aliphatic hydrocarbons. They are also characterized by an unusually high hydrogen content and commonly contain significant nitrogen.

Although there is still no clear consensus on the provenance of the carbon, *i.e.*, whether it originated from inorganic gases produced by the magma (*e.g.*, Petersilie and Sørensen, 1970; Kogarko *et al.*, 1986), or represents organic carbon, graphite (Lytkevich, 1967) or carbonate (*e.g.*, Konnerup-Madsen *et al.*, 1988) introduced into the magma, the majority of researchers appear to favour the orthomagmatic hypothesis. Advocates of a magmatic origin all envisage initial separation of a CO<sub>2</sub>-bearing fluid which then transforms to methane and higher hydrocarbons. Various equilibrium mechanisms have been proposed which satisfactorily explain production of the methane. However, it not clear that any of these mechanisms can explain the occurrence of higher hydrocarbons.

In this contribution, we report the results of a gas chromatographic study of fluid inclusions gases in pegmatite quartz from the Strange Lake peralkaline granite, on the Quebec/Labrador border. These inclusions, first described by Salvi and Williams-Jones (1992) as being orthomagmatic, contain immiscible saline-aqueous and carbonic fluids, the volatile composition of which is dominated by hydrogen (this study), methane and heavier hydrocarbons. Locally, where sodic minerals in the pegmatite have been altered at low temperature (<200°C; Salvi and Williams-Jones, 1990) to calcium-bearing minerals, the CO<sub>2</sub> content of the fluid is sharply higher.

Evidence presented in this paper shows that the heavier hydrocarbons and hydrogen in these inclusions could not have formed in equilibrium at any condition between those of magma emplacement and fluid entrapment, and could not have been produced during post-entrapment cooling of the fluid. Instead, we propose that the occurrence of these species at Strange Lake, and in other alkalic complexes, reflects the production of H<sub>2</sub> during wall-rock alteration, and its reaction with orthomagmatic CO<sub>2</sub> and CO to form hydrocarbons in a magnetite-catalysed Fischer-Tropsch syntheses. We attribute the increase in CO<sub>2</sub> of fluid inclusions in calcium-metasomatised samples to oxidation of the hydrocarbons by externally derived waters.

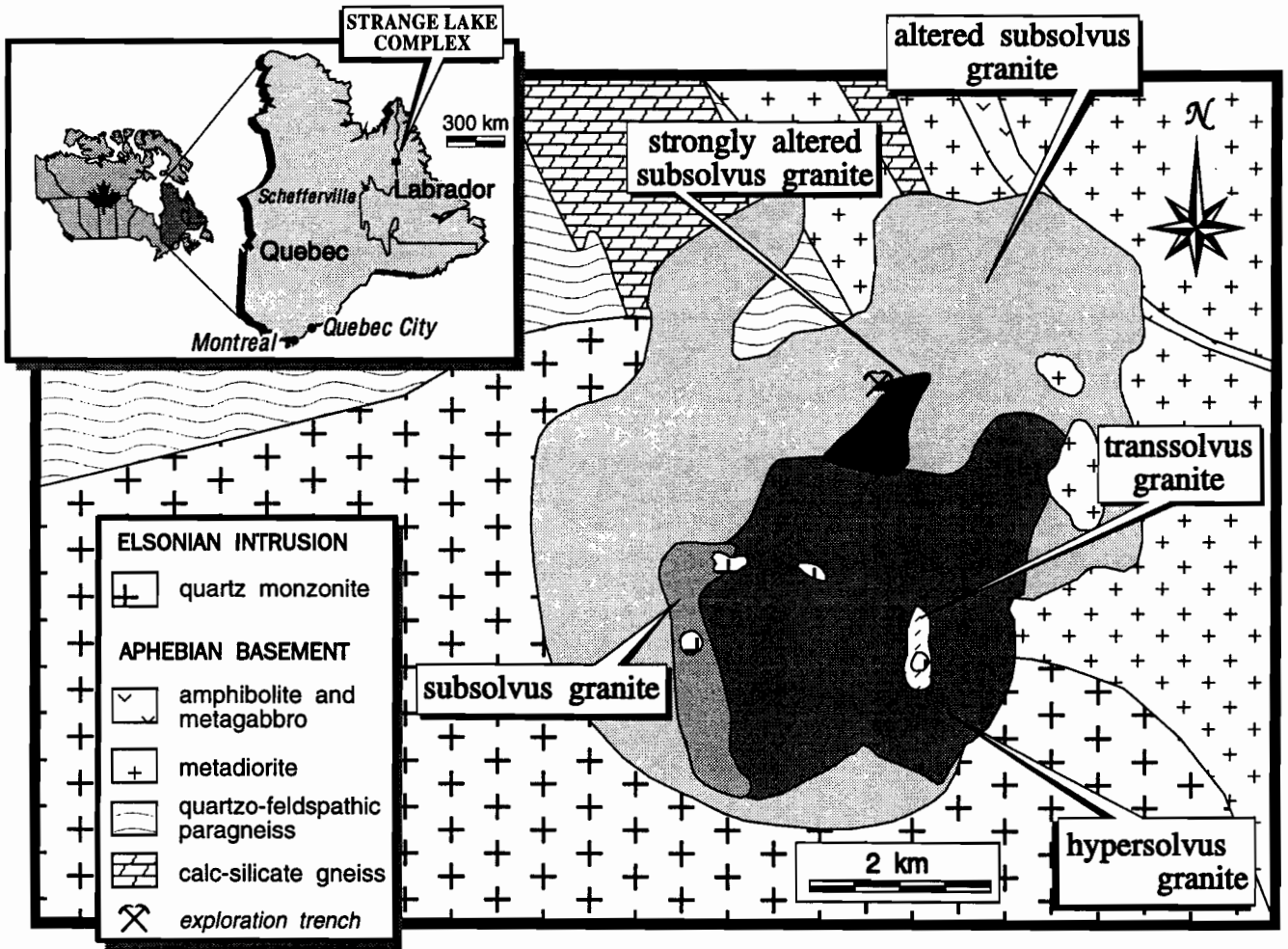
## Geological Setting

The Strange Lake pluton is an isolated intrusion of peralkaline granite, located in the Rae tectonic Province of the Canadian Shield, at the contact between Archean basement and Elsonian quartz monzonite (Fig. 1) (Currie, 1985; Pillet, 1985; Miller, 1986). The Archean host rocks comprise intercalated quartzo-feldspathic, calc-silicate, graphitic, dioritic, gabbroic and anorthositic gneisses, which were metamorphosed to upper-amphibolite facies during the Aphebian Hudsonian orogeny (Taylor, 1979; Bélanger, 1984); the quartz monzonite is post-tectonic. The age of the pluton ( $1189 \pm 32$  Ma; Pillet *et al.*, 1989), and its peralkaline character suggest that it represents part of the anorogenic Gardar province of southern Greenland.

The pluton is about 6 km in diameter and consists of several roughly-concentric intrusive phases of hypersolvus, subsolvus and transsolvus granites (Nassif and Martin, 1991), most of which contain large xenoliths and roof pendants of the host rock (Fig. 1). An outwardly-dipping ring fracture, marked by a heterogeneous breccia in a fluorite-filled matrix, surrounds the pluton. Pegmatites are concentrated mainly in the subsolvus granite. They form thin (10 to 50 cm) bodies, generally strike east-west and have subvertical dips. Field evidence (roof pendants, miarolitic cavities) and the low trapping

FIGURE 1

Location and simplified geological map of the Strange Lake pluton (modified after Salvi and Williams-Jones, 1992).



pressure estimated for primary orthomagmatic fluid inclusions (Salvi and Williams-Jones, 1992), suggest a shallow level of emplacement for the pluton.

The hypersolvus granite is composed mostly of early-crystallised perthite, interstitial quartz and late arfvedsonite, whereas the subsolvus granite is characterised by idiomorphic quartz, arfvedsonite, albite and microcline. The transsolvus granite contains perthite phenocrysts but is otherwise similar to the subsolvus granite, *i.e.*, the groundmass contains two alkali feldspars. The pegmatites are composed of quartz, microcline, albite, arfvedsonite, aegirine, and rare-metal minerals, which range in grain size from 1 to 10 cm. The rare-metal minerals comprise between 5% and 30% of the rock by volume, with their highest concentrations occurring in units of subsolvus granite and pegmatites (Miller, 1986).

Most units of the subsolvus granites have undergone at least two episodes of alteration. An early, widely distributed event, involved replacement of arfvedsonite by aegirine plus magnetite and quartz (Salvi and Williams-Jones, 1990; Nassif, 1993). This alteration is interpreted, on the basis of fluid inclusion data, to have been caused by orthomagmatic fluids released during crystallisation of the subsolvus granite (Salvi and Williams-Jones, 1992). The second alteration event was accompanied by pervasive hematisation and by a strong enrichment in calcium relative to the fresh subsolvus rocks (Salvi and Williams-Jones, 1995c). This event was particularly important in the centre of the complex (Fig. 1) where a potential ore body is located, containing  $30 \times 10^6$  tons grading 3.25%  $ZrO_2$ , 1.3% REE oxides, 0.66%  $Y_2O_3$ , 0.56%  $Nb_2O_5$  and 0.12% BeO (Iron Ore Company, unpublished report). The principal ore minerals are gittinsite, armstrongite ( $Ca_2ZrSi_6O_{15} \cdot 3H_2O$ ), kainosite ( $Ca_2[Ce, Y, HREE]_2 Si_4O_{12}[CO_3] \cdot H_2O$ ), bastnäsite ( $[La, Ce, Nd]CO_3F$ ), gagarinite ( $Na[Y, Ca, Na, REE]_2F_6$ ), monazite, pyrochlore, and gadolinite ( $Y_2FeBe_2Si_2O_{10}$ ). Several of these minerals occur mainly as pseudomorphs representing replacement of sodium in primary minerals by calcium, and are interpreted to be products of interaction of the rock with a low temperature ( $<200^\circ C$ ) brine derived externally from the pluton (Salvi and Williams-Jones, 1990 and 1995b).

The Pegmatites are interpreted to have formed pene-contemporaneously with fluid phase separation during crystallisation of the subsolvus granite (Nassif 1993; Boily and Williams-Jones, 1994), and, without exception, show extensive alteration of arfvedsonite to aegirine. In many cases, narrow zones in which primary arfvedsonite was replaced by aegirine can be observed adjacent to pegmatite in otherwise fresh granite. The calcium-metasomatised pegmatites in the ore zone are also more intensely altered than the surrounding granites, which may reflect greater porosity of the pegmatites (due perhaps to the development of miarolitic cavities) and thus preferential channelling of the later calcium-bearing fluid.

## Fluid Inclusion Characteristics

### “Fresh” Pegmatites

The orthomagmatic fluid inclusions described by Salvi and Williams-Jones (1992) are hosted in quartz crystals from several small pegmatites which outcrop in the southern part of the complex (although referred to as “fresh”, these pegmatites display alteration in which arfvedsonite was partially or wholly replaced by aegirine). Quartz was the last mineral to crystallise in these pegmatites, as indicated by cross-cutting relationships with other minerals, its preferential occurrence in the cores of zoned pegmatitic veins, and the common presence of terminated quartz crystals inside vugs. Some of these euhedral to subhedral crystals show evidence of growth zoning. The occurrence of fluid inclusions along growth zones and along planes truncated by inclusion-free overgrowths indicates a primary and pseudosecondary origin, respectively, of the inclusions. Fluid inclusions were also found concentrated in the cores of anhedral quartz grains and aligned along short planes that parallel each other. These inclusions were likewise interpreted to be primary or pseudosecondary. The inclusions were classified into three major groups: I) two-phase aqueous, II) one-phase carbonic, and III) two-phase aqueous-carbonic. The compositions of type II inclusions and the carbonic phase in type III inclusions are very

similar. Also similar, are the salinities and the species dissolved in type I inclusions and in the aqueous phase of type III inclusions. This evidence, together with variable phase ratios in type III inclusions, and their spatial association, suggests that type III fluid inclusions probably represent heterogeneous entrapment of immiscible aqueous (trapped by type I inclusions) and carbonic (type II inclusions) fluids.

Type I inclusions and the aqueous phase of type III inclusions formed hydrohalite crystals upon cooling. Initial and final ice melting occurred at almost the same temperature, around  $-20^{\circ}\text{C}$ , and hydrohalite dissolved mostly between this temperature and a few degrees above zero. These data indicated that NaCl was the only salt dissolved in significant quantities in the fluid and that its concentration was approximately 25 wt. %, *i.e.*, between the eutectic and peritectic points of the  $\text{H}_2\text{O}$ -NaCl system. This conclusion was confirmed by SEM-EDS analyses of residues from decrepitated inclusions which detected only Na and Cl. Most type I inclusions homogenised by vapour disappearance at temperatures between  $300^{\circ}\text{C}$  and  $360^{\circ}\text{C}$ , with a mode of  $340^{\circ}\text{C}$ . The homogenisation of type III inclusions took place over a wide range of temperature ( $130^{\circ}\text{C}$  to  $>600^{\circ}\text{C}$ ), consistent with the interpretation that they represent heterogeneous entrapment of immiscible aqueous and carbonic phases.

Methane was the only species detected in the carbonic phase of types II and III inclusions. Nonetheless, under ultra-violet illumination several of these inclusions were seen to contain an orange or green fluorescing phase, in the form of a ring surrounding the methane-dominated carbonic vapour. This suggested that these inclusions contain unsaturated aliphatic and/or aromatic hydrocarbons (cf. Rao, 1975), an interpretation which was confirmed by the presence of peaks representing possible C-H stretching of higher order aliphatic hydrocarbons in the region between  $3000\text{ cm}^{-1}$  and  $2800\text{ cm}^{-1}$  of Fourier transform infrared (FTIR) spectra (cf., Wopenka *et al.*, 1990). Unfortunately, the high detection limits of FTIR ( $>1\text{ mol } \%$ , *e.g.*, Wopenka and Pasteris, 1987) and strong fluorescence of the inclusions during Raman analysis, precluded identification of the heavier hydrocarbon species using these techniques.

### Altered Pegmatites

In the strongly altered subsolvus granites and mineralised pegmatites at the centre of the intrusion (Fig. 1), some of the ore minerals form pseudomorphs with quartz after earlier sodic minerals, the outlines of which are commonly defined by trains of fluid inclusions in the quartz (Salvi and Williams-Jones, 1990). The type of inclusion most commonly observed in the pseudomorphs contains aqueous liquid and vapour, and was interpreted to represent a moderately saline (13 to 24 wt. % NaCl eq.), Ca-rich (Te < -50°C) liquid, trapped at temperatures of  $\leq 200^{\circ}\text{C}$ . Some of these inclusions contain a small daughter crystal of one of the ore minerals, bastnäsite. The fluid is considered to have originated in the paragneisses which surround the pluton. Similar aqueous fluid inclusions also occur in quartz crystals in pegmatites and associated quartz veins, together with a population of lower-salinity NaCl-dominated, aqueous fluid inclusions, which were trapped at lower temperatures (100°C to 165°C), and were interpreted to have originated in the granite.

Coexisting with these inclusions, both in pseudomorphs, and in the veins and pegmatites, is a group of methane-only and aqueous-methane inclusions. These were interpreted to represent an immiscible carbonic fluid and, like the Ca-rich aqueous fluid, to have originated externally from the pluton (Salvi and Williams-Jones, 1990). This latter conclusion has been reconsidered in light of the evidence reported by Salvi and Williams-Jones (1992) and discussed in this paper, that an apparently similar carbonic fluid of magmatic origin is present in fluid inclusions trapped by “unaltered” pegmatites.

### Gas Chromatography

As discussed above, fluid inclusions in both fresh and altered pegmatites sampled immiscible aqueous liquid and carbonic fluid containing methane and heavier hydrocarbons. The nature of the latter could not be detected by the techniques available to us at the time of our original study (Salvi and Williams-Jones, 1990, 1992). Since then,

we have acquired a gas chromatograph and constructed an extraction system for the analysis of fluid-inclusion volatiles, including hydrocarbons heavier than methane (Salvi and Williams-Jones, 1995a). Such systems avoid the problems of fluorescence encountered with Raman spectroscopy, and have much lower detection limits (down to  $10^{-6}$   $\mu$ moles; cf. Bray *et al.*, 1991) than both Raman and FTIR spectroscopic methods. However, because gas chromatographic techniques involve analysis of the bulk fluid released by crushing or decrepitation, an average fluid inclusion composition is obtained. In some cases, this is problematic because of the occurrence of multiple inclusion populations.

As indicated previously, the “fresh” pegmatites host three types of primary fluid inclusions, and any of these may contain a UV-fluorescent phase. In addition, trains of secondary fluid inclusions commonly cross-cut the quartz grains. Nonetheless, the inclusions containing a UV-fluorescent phase (high order hydrocarbons) are all primary, and all of the fluid inclusions of clearly secondary origin, which were investigated microthermometrically and by Raman spectroscopy, contain only an aqueous phase. There is also good evidence that type II and III inclusions contain the same carbonic fluid. We therefore believe that, although the gas chromatographic analyses reported below provide the average composition of more than one generation of inclusions, they reliably reconstruct the composition of the primary hydrocarbon fluid that was present in the pluton. Furthermore, because these two types of inclusions trapped different aliquots of immiscible fluids, a bulk study probably more closely represents the original composition of the fluid than analyses of only a few, individual inclusions. A similar argument can be applied to the fluid inclusions contained in the altered pegmatites.

### **Analytical Procedure**

The analytical system used in this study (see Salvi and Williams-Jones, 1995a, for a detailed description) is similar to the system in the Department of Geology at the University of Toronto (cf. Bray and Spooner, 1989; Bray *et al.* 1991; Bray and Spooner, 1992). The gas chromatograph is an HP<sup>®</sup>-5890 Series-II gas chromatograph,

manufactured by Hewlett-Packard<sup>®</sup>, equipped with a micro-thermal conductivity detector (TCD). A photoionisation detector (PID) (PI-52-02A model of HNU<sup>®</sup> Systems) with an 11.7 eV lamp, was retrofitted and connected in-series to the TCD. Analyses were performed using a 25 m x 0.53 mm inside-diameter fused-silica column, coated with a 20- $\mu$ m-thick layer of PoraPLOT<sup>®</sup> Q, a porous-polymer manufactured by Chrompack International (NL). The raw data were collected and digitised by an HP<sup>®</sup> 35900C dual-channel interface. Spectra were integrated with the aid of the PC-operated software package Chromatographic ChemStation<sup>®</sup>, purchased from Hewlett-Packard<sup>®</sup>. The system plumbing is designed to allow switching among four ports of introduction into the gas chromatographic column, *i.e.*, from one of three sample crushers or an injector.

The crushers, built after the design of Andrawes and Gibson (1979; see also Bray and Spooner, 1989), are constructed of heat-treated stainless steel, and consist of a basal block and an upper portion containing the cylindrical piston. The basal block hosts the sample chamber and two cartridge heaters. Silicone O-rings seal the chamber from the external atmosphere, and allow the upper part of the crusher to be pressurised with the same gas used as the carrier (ultra-high-purity zero grade He). This provides added protection in case the sample chamber should leak, especially when the piston is lowered during crushing (*cf.* Andrawes *et al.*, 1984).

The gas chromatographic system described above is superior in several respects to other gas chromatographic systems commonly used in the analysis of fluid-inclusion volatiles. Crushing is carried out at a temperature ( $\sim 110^{\circ}\text{C}$ ) that is high enough to cause immediate release of volatiles, limiting the potential of gas adsorption onto newly created surfaces (*e.g.*, Barker and Torkelson, 1975), yet low enough to avoid chemical reactions among released gases (*e.g.*, Kesler *et al.*, 1986). On-line crushing allows release of the volatiles into the column as a single batch instead of aliquots, as is the case when gas extraction is carried out off-line (*e.g.*, Welhan, 1988). This minimises volatile losses and maximises detectability. The PoraPLOT<sup>®</sup> Q capillary column can separate both polar and non-polar compounds, enabling analysis of common fluid-inclusion volatiles ( $\text{CO}_2$ ,  $\text{CH}_4$ ,  $\text{N}_2$ ),  $\text{H}_2\text{O}$ , as well as other aliphatic hydrocarbons, to trace levels ( $< 10^{-4}$   $\mu\text{moles}$ ) in a

single run (Salvi and Williams-Jones, 1995a). Aromatic hydrocarbons can also be separated on this column, but in order to detect these species at the low levels generally encountered in fluid inclusions, the oven temperature would have to be increased above the present upper operational limit (~115°C).

### Sample Preparation

In preparation for analysis, the selected samples were fragmented, sieved to a size fraction between 0.75 mm and 2 mm, and hand-picked. Cleaning was performed using doubly distilled H<sub>2</sub>O to avoid any possibility of contamination from acids and/or organic solvents. Samples were then dried in an oven (~80°C) or on a hot plate (~50°C) under a fumehood, and ~0.5 to ~2 g were loaded into the crushers. Prior to analysis, the crushers were heated to ~110°C, and both sample and confining chambers were flushed with a low flow of He ( $\leq 1$  ml/min), for a duration of at least 12 hours (overnight). This procedure allows removal of all air and H<sub>2</sub>O that may be absorbed onto the sample. Preceding the analysis, the carrier gas flow was increased to 20 ml/min and reference gas flow to the TCD was set at 30 ml/min. Crushing was accomplished by suddenly releasing a pressure of ~350 bar on the piston, via an Enerpac<sup>®</sup> hydraulic ram powered by a manually operated oil pump. This sharp stroke, coupled with the internal pressure build-up in the fluid inclusions due to the heating, causes an immediate release of the inclusion volatile content into the stream of He. Analysis on the gas chromatograph was started synchronously with crushing.

In analysing a sample, we initially performed two or more consecutive crushes, using increasingly higher pressures on the ram. The results of these multiple crushes were identical, except that the yield from the first crush was larger and the peaks correspondingly higher. This indicated that there was no preferential opening of compositionally different sets of inclusions. In order to maximise detectability, we subsequently performed only a single crush on each sample, with fairly high ram pressure (~350 bar).

## Standardisation and Identification of Species

Identification of peaks and standardisation was achieved by injecting different amounts of known gas mixtures (available commercially from Scott Speciality Gases Co., Plumsteadville, PA) into the gas chromatograph, except for water, which was injected as saturated vapour at known temperature and pressure. Blanks were run by crushing inclusion-free Brazilian quartz crystals and pure-silica rods, fragmented, sieved, and cleaned exactly as would be regular samples.

The contents of N<sub>2</sub>, CO<sub>2</sub>, CH<sub>4</sub>, H<sub>2</sub>O and H<sub>2</sub> were analysed using the TCD, whereas hydrocarbons heavier than methane were analysed with the PID; NH<sub>3</sub> could not be analysed because of poor detectability. The samples were run for ~80 min, as longer runs did not produce any peaks. The last hydrocarbons to elute were the hexanes, which exited the column between ~67 min and ~75 min into the run. Although the TCD signal in all samples produced large H<sub>2</sub>O peaks, we did not routinely analyse this component because of the presence of secondary aqueous inclusions in the samples. On average, water represented about 80 to 90 mol % of the total volatile yield.

Analysis of hydrogen by gas chromatography using porous polymer columns presents difficulties due to its co-elution with N<sub>2</sub>, O<sub>2</sub>, CO and Ar. Moreover, the TCD has very low sensitivity to this species with He as carrier gas. However, N<sub>2</sub> has a much lower thermal conductivity than H<sub>2</sub>, and using it as a carrier, we were able to detect H<sub>2</sub> to better than 10<sup>-5</sup> μmoles on the TCD (cf. Salvi and Williams-Jones, 1995a). The problem of peak overlapping is largely eliminated because N<sub>2</sub>, as the carrier gas, is not detected, Ar produces a signal with the inverse polarity of H<sub>2</sub>, O<sub>2</sub> has extremely low fugacity at the conditions considered in this study, and the detection limits of CO are very poor (>10<sup>-2</sup> μmoles). Moreover, as discussed below, CO, even at the most favourable conditions for its formation (temperature > 500°C and *f*O<sub>2</sub> < QFM), is unlikely to have constituted > 1% of the carbonic species. Figure 2 shows chromatograms for analyses of a sample and a blank using N<sub>2</sub> as the carrier gas.

Gas chromatographic analyses are reproducible to better than ±15 % (Salvi and Williams-Jones, 1995a).

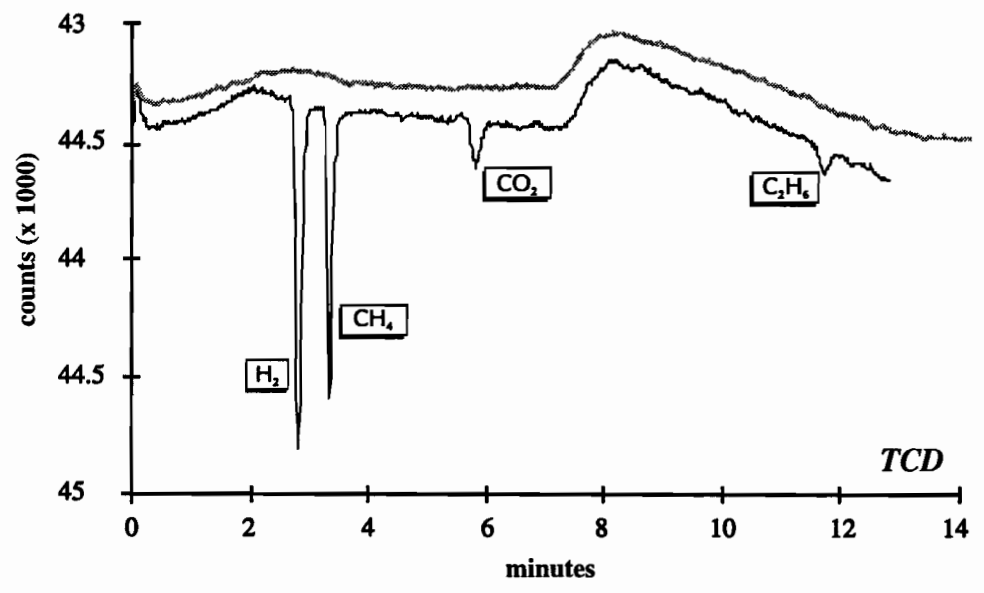
FIGURE 2

A chromatogram demonstrating the detection of H<sub>2</sub> in quartz from sample TTR-22 using the micro-thermal conductivity (TCD) detector, and nitrogen as the carrier gas. Also shown is the chromatogram for the blank, Brazilian quartz.

Carrier: N<sub>2</sub> @ 20 ml/min  
TCD aux gas: N<sub>2</sub> @ 30 ml/min  
Crusher T: 107°C  
TCD T: 150°C

Oven program: -20°C (6.5 min) / 10°C/min / 35°C (10 min)

Legend:  
Brazilian quartz  
TTR-22, 1.5 g



## Results

### “Fresh” Pegmatites

Six outcrop samples of quartz from pegmatites that were not subject to calcium metasomatism, and one from drill core, were analysed by gas chromatography. The outcrop samples were collected in the southern part of the pluton, from pegmatites hosted in units of hypersolvus and unaltered subsolvus granites. The drill core sample consists of quartz from an “unaltered” pegmatite intersected at the bottom of DDH SL-178, located near the centre of the pluton. Results from these analyses are reported as mole % in Table 1, and the chromatogram for a representative sample is shown in Figure 3.

To estimate H<sub>2</sub> contents, three representative samples were re-analysed using N<sub>2</sub> as the carrier gas (see above). The concentrations of H<sub>2</sub> measured during these runs were corrected to allow comparison with the gas composition previously determined by normalising with methane. Proportions of volatiles recalculated to include H<sub>2</sub> are shown in Table 1.

Because significant H<sub>2</sub> is present in these inclusions, and because this gas and N<sub>2</sub> cannot be distinguished in runs with He as the carrier, the yields of N<sub>2</sub> obtained with the He carrier must be considered maximum values. However, the fact that poor sensitivity of the TCD to H<sub>2</sub> in He coincides with excellent sensitivity of this detector to N<sub>2</sub> in the same carrier, encourages us to believe that the N<sub>2</sub> concentrations were probably not grossly over-estimated. The occurrence of samples that yielded low N<sub>2</sub> and large amounts of H<sub>2</sub> (e.g., TTR-22, Table 2) support this conclusion.

If we exclude water, the volatile compositions of the crushed samples are dominated by CH<sub>4</sub>, comprising between ~54 mol % and ~80 mol % of the fluid (Table 1). The content of H<sub>2</sub> ranges from 1 mol % to 35 mol %, ethane (C<sub>2</sub>H<sub>6</sub>) between ~4 mol % and ~8 mol %, CO<sub>2</sub> between ~0.4 mol % and ~8 mol %, and N<sub>2</sub> ≤ 1.5 mol % of the fluid. The remaining 1% to 3% are made up of propane (C<sub>3</sub>H<sub>8</sub>), straight- and branched-chain butanes (C<sub>4</sub>H<sub>10</sub>), *n*-pentane (C<sub>5</sub>H<sub>12</sub>), and the C<sub>2</sub> unsaturated hydrocarbons, *i.e.*, ethylene

**Table 1**

*Mole proportions of gases (excluding H<sub>2</sub>O) in the bulk fluid extracted from quartz in "fresh" pegmatites.*

		He carrier gas							N <sub>2</sub> carrier gas**		
		SL-178*									
Samples:		48-A-7	56-A-1	SL2-1	SL4-12	SL4-14	SL4-15	206.7 m	56-A-1	SL4-14	SL4-15
(g crushed)		(0.95)	(1.5)	(1.6)	(0.6)	(1.0)	(0.7)	(0.5)			
H <sub>2</sub>	hydrogen	-	-	-	-	-	-	-	1.074	35.023	21.163
N <sub>2</sub>	nitrogen	1.491	0.438	1.730	4.235	2.284	1.226	4.930	0.433	1.484	0.966
CH <sub>4</sub>	methane	88.036	80.442	90.439	89.783	83.143	91.823	84.628	79.578	54.024	72.391
CO <sub>2</sub>	C dioxide	1.907	8.215	0.466	2.669	4.683	0.491	7.575	8.127	3.043	0.387
C <sub>2</sub> H <sub>4</sub>	ethylane	n/d	0.004	0.177	0.005	0.098	0.006	0.018	0.004	0.064	0.005
C <sub>2</sub> H <sub>2</sub>	acetylane	n/d	0.012	0.220	0.089	0.134	0.101	0.139	0.012	0.087	0.080
C <sub>2</sub> H <sub>6</sub>	ethane	7.089	8.336	5.931	2.894	7.378	5.461	0.841	8.246	4.794	4.305
C <sub>3</sub> H <sub>8</sub>	propane	0.986	1.699	0.546	0.191	1.580	0.531	1.575	1.680	1.027	0.419
i-C <sub>4</sub> H <sub>10</sub>	isobutane	0.057	0.078	0.081	0.012	0.107	0.016	0.128	0.077	0.069	0.012
n-C <sub>4</sub> H <sub>10</sub>	n-butane	0.324	0.610	0.232	0.092	0.351	0.295	0.166	0.604	0.228	0.233
n-C <sub>3</sub> H <sub>12</sub>	n-pentane	0.109	0.166	0.178	0.030	0.243	0.050	n/d	0.164	0.158	0.039
Σ yield †		4.472	707.779	50.043	35.588	80.698	74.901	0.529			

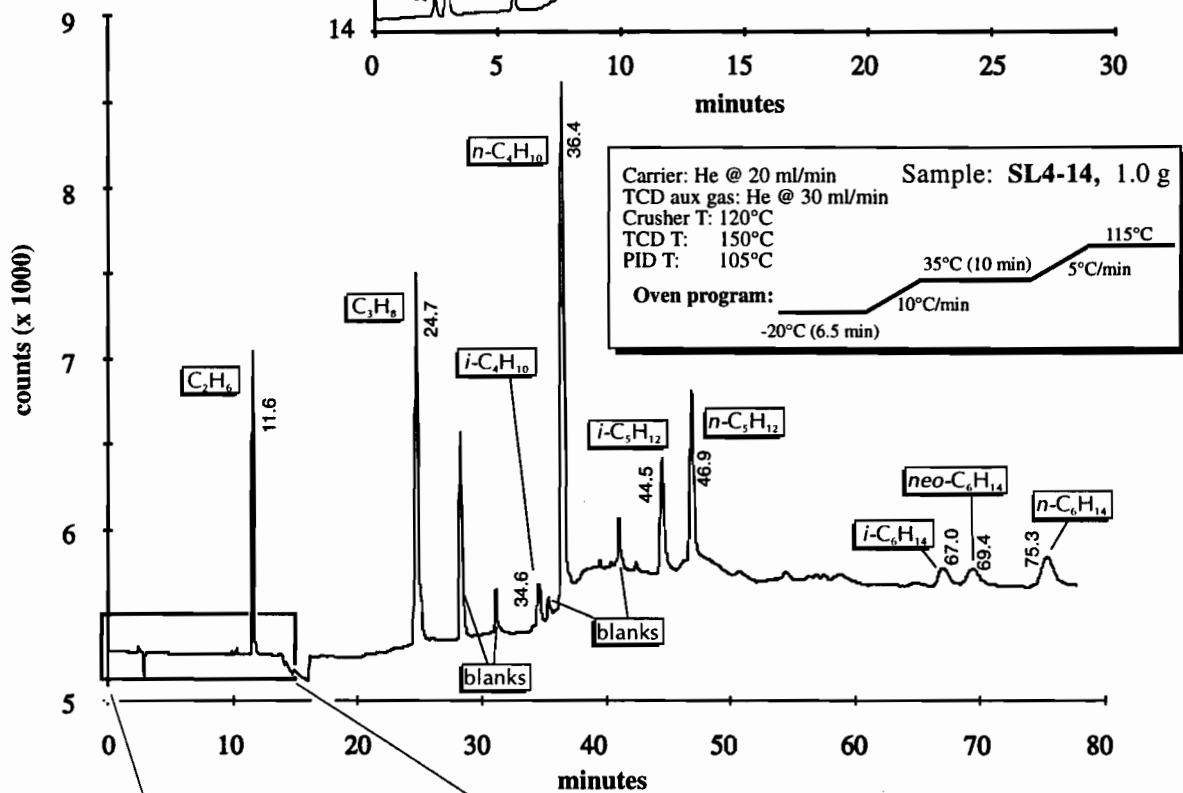
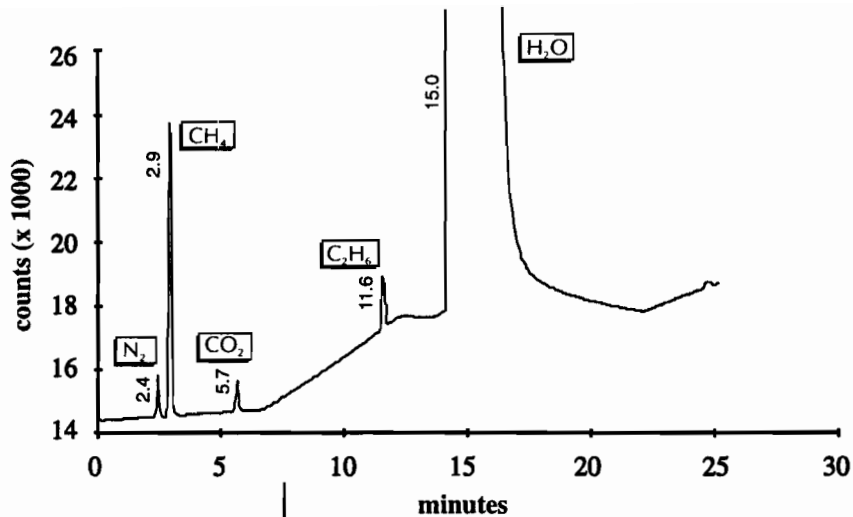
\* : drill core sample

† : nmoles

\*\* : recalculated to 100 from analyses with He as the carrier gas

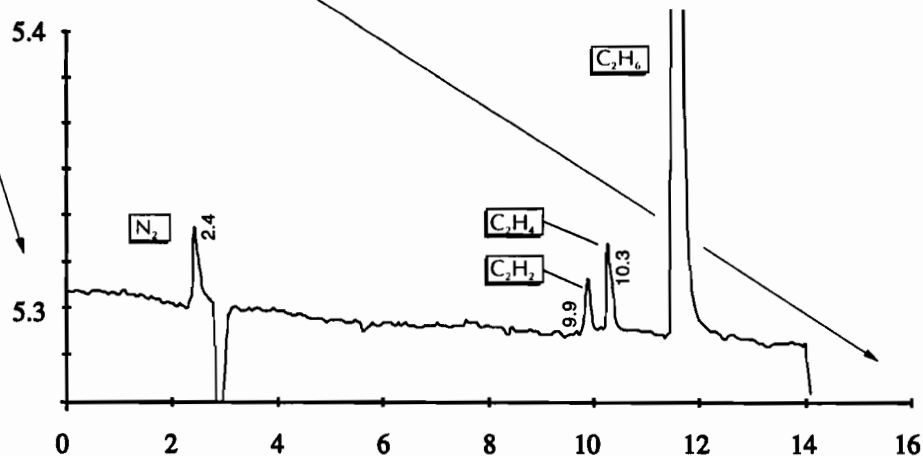
FIGURE 3

Representative chromatograms showing the peaks for species analysed by the microthermal conductivity (TCD) and photoionisation (PID) detectors in fluid-inclusion volatiles released by crushing 1.0 g of quartz from “fresh” pegmatite. The analysis was carried out using He as the carrier gas, and a PorapLOT<sup>®</sup>-Q capillary column.



Carrier: He @ 20 ml/min      Sample: SL4-14, 1.0 g  
 TCD aux gas: He @ 30 ml/min  
 Crusher T: 120°C  
 TCD T: 150°C  
 PID T: 105°C

Oven program:  $-20^\circ C$  (6.5 min)  $\rightarrow$   $10^\circ C/min$   $\rightarrow$   $35^\circ C$  (10 min)  $\rightarrow$   $5^\circ C/min$   $\rightarrow$   $115^\circ C$



and acetylene. The proportions of hydrocarbon species in the different samples are remarkably similar, *i.e.*, they show a decrease in abundance with increasing molecular weight, and a predominance of the alkanes over alkenes and alkynes. This homogeneity supports the conclusion drawn earlier that the hydrocarbon inclusions in these samples represent a single fluid generation.

Isopentane and the hexanes (C<sub>6</sub>H<sub>14</sub>) (Fig. 3) were identified from their boiling points, since a standard containing these species was not available to us. For the same reason we could not quantify them, however, since *n*-pentane averages ~0.1 mol %, and isopentane produces a similar peak, this gas probably makes up ≤0.1 mol % of the total volatile content of the inclusions. Similarly, the small size of the hexane peaks and the fact that the other hydrocarbons occur in decreasing amounts with increasing number of carbons in their structure, lead us to believe that these species total <0.1 mol %. Not all analysed samples produced peaks for hexanes. However, this is probably because their yield was below the detection limit, rather than being evidence of a different trace-hydrocarbon signature.

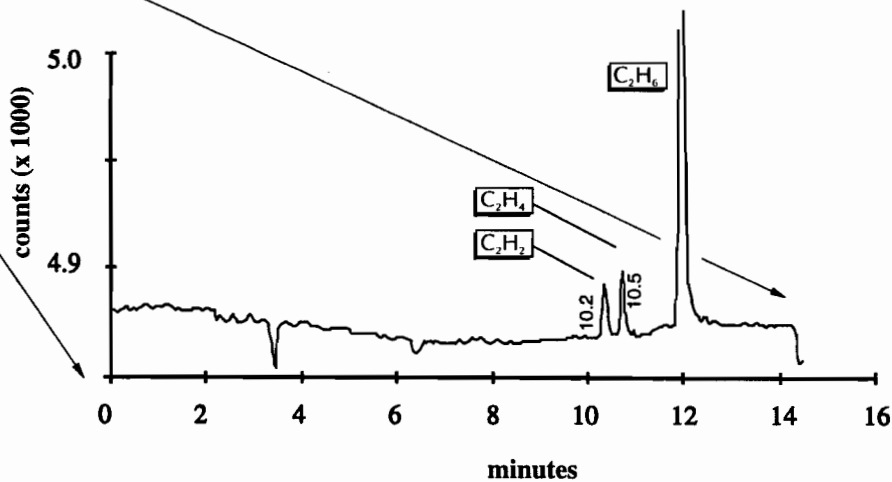
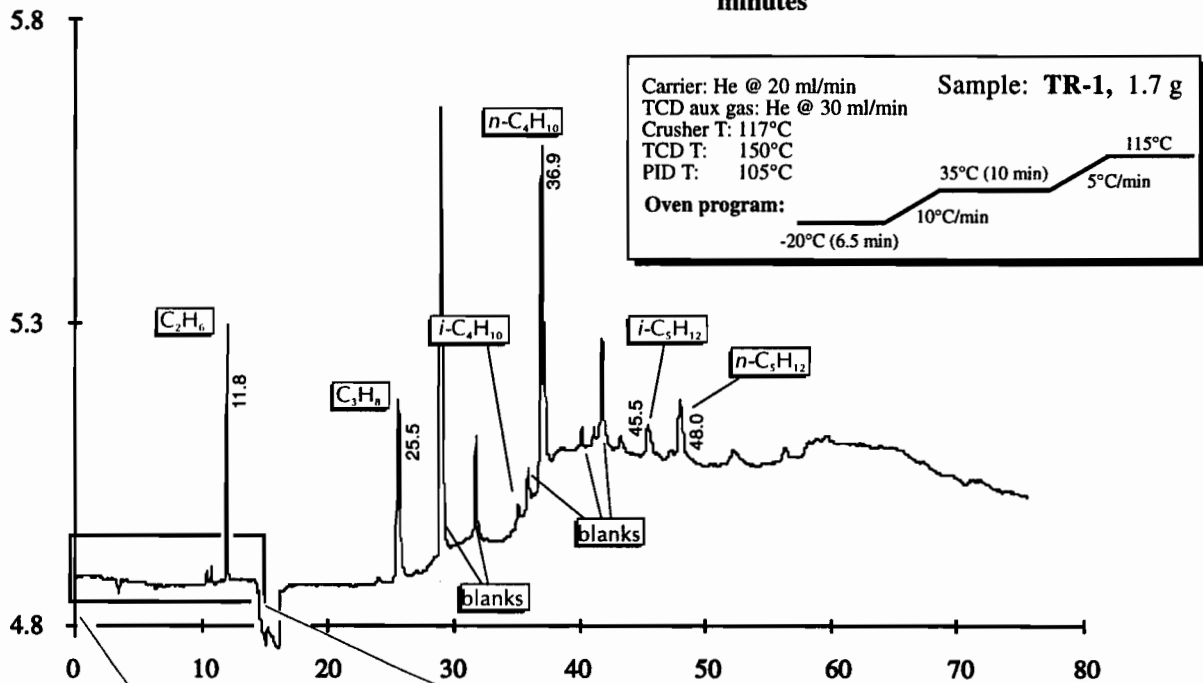
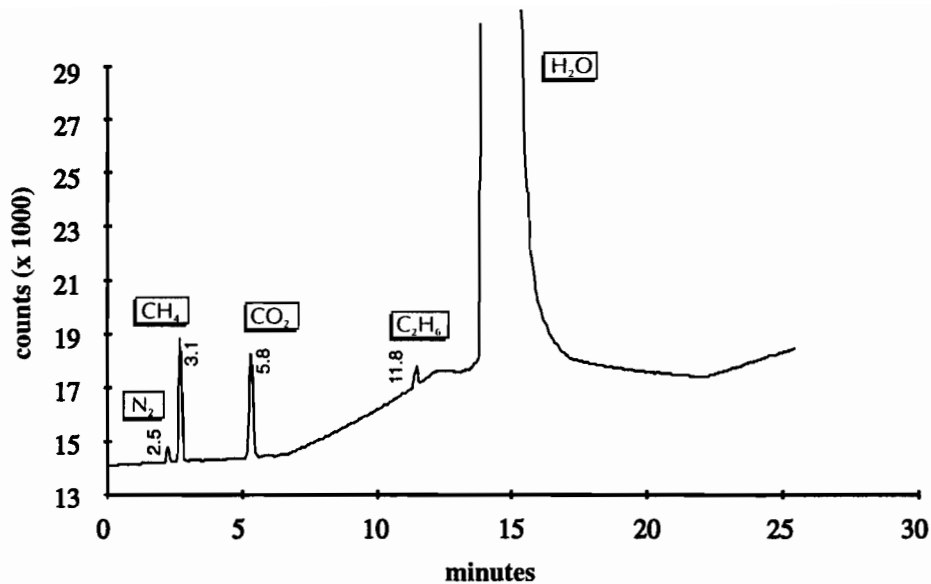
### Altered Pegmatites

Six samples of quartz from altered pegmatites were analysed; two of these were from an exploration trench located in the main ore zone in the centre of the complex, two were from outcrop, and two were from DDH SL-182 (cf. Salvi and Williams-Jones, 1995b), located about 1 km southeast of the trench (Fig. 1). Results of these analyses are presented in Table 2, and an example of a chromatogram is shown in Figure 4. Table 2 also lists compositions of three samples recalculated to include H<sub>2</sub> contents.

The volatile species detected in these rocks were the same as those identified in samples from “fresh” pegmatite, however, the relative proportions of these species in the two types of pegmatites differ substantially (Fig. 5). Moreover, the volatile yield from the altered pegmatites was generally lower, and the gas composition more heterogeneous than those of the “fresh” pegmatites. The concentrations of CO<sub>2</sub> and CH<sub>4</sub> are similar, ranging from 25 to 62 mol %, and from ~ 8 to ~ 40 mol % respectively. Hydrogen varies

FIGURE 4

Representative chromatograms showing the peaks for species analysed by the microthermal conductivity (TCD) and photoionisation (PID) detectors in fluid-inclusion volatiles released by crushing 1.7 g of quartz from altered pegmatite. The analysis was carried out using He as the carrier gas, and a PorapLOT<sup>®</sup>-Q capillary column.



in abundance from 14 mol % to 27 mol %, and the N<sub>2</sub> content varies between 0.6 mol % and ~10 mol %, and is generally higher than that of the “fresh” pegmatites. The sum of the C<sub>2</sub> and higher hydrocarbons is between ~0.5 mol % and ~5 mol % of the total gas content.

The distribution of the hydrocarbon species is similar to that in the “fresh” pegmatites, *i.e.*, they decrease in amount with increasing carbon number, and the straight-chain alkanes are more abundant than their branched isomers. Unsaturated compounds also occur in subordinate proportions to the alkanes. An exception to this is sample 54-A-3, which has the highest molecular proportion of *n*-butane among all the samples analysed (2.8 mol %; Table 2). Significantly, this sample also has the lowest percentage of methane and relatively low ethane (< 1 mol %). The hydrocarbon proportions are also anomalous in sample DDH SL-182, 48.2, where C<sub>2</sub>H<sub>6</sub>/C<sub>2</sub>H<sub>2</sub> < 1 (Fig. 6 and Table 2). Interestingly, these two samples also contain the highest proportions of N<sub>2</sub> and CO<sub>2</sub>.

## Discussion

The most striking difference between the analysed volatile composition of the “fresh” and altered pegmatites is undoubtedly the CH<sub>4</sub>/CO<sub>2</sub> ratio (Fig. 5). This ratio changes from greater than 10 in samples from “fresh” pegmatites, to close to or less than unity in samples from altered pegmatites. However, with one exception (sample 54-A-3), the distribution of hydrocarbons in the two sample suites is very similar, as shown by ratios of the average contents of various pairs of *n*-alkanes (Table 3). The lower proportion of hydrocarbons in the altered pegmatites seems therefore to simply reflect dilution by CO<sub>2</sub>. This, in turn, suggests that the hydrocarbons in both “fresh” and altered pegmatites had a similar source.

### Source of Hydrocarbons

The presence of elevated concentrations of hydrocarbons in the fluid inclusions of the Strange Lake granitic pegmatites was unexpected, as, to our knowledge, fluid

**Table 2**  
Mole proportions of gases (excluding  $H_2O$ ) in the bulk fluid extracted from quartz in the altered pegmatites.

		He carrier gas				N <sub>2</sub> carrier gas**				
						SL-182*				
		46-I-2	54-A-3	TTR-22	TR-1	48.2 m	51.7 m	54-A-3	TTR-22	TR-1
(g crushed)		(1.6)	(1.6)	(1.2)	(1.7)	(2.0)	(0.6)			
H <sub>2</sub>	hydrogen	-	-	-	-	-	-	14.554	16.073	27.053
N <sub>2</sub>	nitrogen	0.620	12.297	0.943	4.202	17.389	6.639	10.507	0.791	3.065
CH <sub>4</sub>	methane	64.657	9.402	40.440	54.102	11.217	48.074	8.034	33.940	39.465
CO <sub>2</sub>	C dioxide	28.953	73.032	54.187	34.471	70.647	40.801	62.403	45.478	25.146
C <sub>2</sub> H <sub>4</sub>	ethylane	0.007	0.302	0.002	0.019	0.009	0.016	0.258	0.002	0.014
C <sub>2</sub> H <sub>2</sub>	acetylane	0.580	0.408	0.053	0.316	0.329	1.124	0.349	0.044	0.230
C <sub>2</sub> H <sub>6</sub>	ethane	4.279	0.688	3.597	5.689	0.249	2.631	0.588	3.019	4.150
C <sub>3</sub> H <sub>8</sub>	propane	0.659	0.202	0.470	0.813	0.111	0.425	0.173	0.394	0.593
i-C <sub>4</sub> H <sub>10</sub>	isobutane	0.024	0.131	0.021	0.027	0.010	0.032	0.112	0.018	0.020
n-C <sub>4</sub> H <sub>10</sub>	n-butane	0.142	3.292	0.230	0.294	n/d	0.129	2.813	0.193	0.214
n-C <sub>5</sub> H <sub>12</sub>	n-pentane	0.081	0.246	0.057	0.067	0.040	0.129	0.210	0.048	0.049
Σ yield †		12.783	27.186	63.022	24.467	10.725	6.613			

\* : drill core sample

† : nmoles

\*\* : recalculated to 100 from analyses with He as the carrier gas

**Table 3**  
*Volume proportions and ratios of the n-alkanes, in gases from Strange Lake and other alkalic complexes*

Locality	environment	N <sub>2</sub>	CO <sub>2</sub>	H <sub>2</sub>	C <sub>1</sub>	C <sub>2</sub>	C <sub>3</sub>	C <sub>4</sub>	C <sub>5</sub>	C <sub>1/2</sub>	C <sub>2/3</sub>	C <sub>3/4</sub>	C <sub>4/5</sub>	References	
Strange Lake complex	"fresh" peg*	1.92	3.76	19.086	68.66	5.78	1.04	0.35	0.12	14.84	6.01	3.34	2.15	This study <sup>†</sup>	
	altered peg*	6.27	48.35	19.227	36.70	3.58	0.49	0.20	0.05	13.29	6.64	2.50	2.65		
Himaussaq complex	syenite*	-	0.01	12.59	83.72	2.50	0.23	0.04	-	33.49	10.68	5.57		Peterliyle & Sorensen, 1970 <sup>†</sup>	
	naujaite*	-	0.04	5.04	80.82	9.90	1.74	0.31	-	8.16	5.69	5.63			
	foyaite*	-	0.06	12.64	70.95	7.37	1.34	0.37	-	9.63	5.50	3.62			
	lujavrite*	-	0.02	68.44	24.44	3.15	0.21	0.01	-	7.76	15.00	21.00			
	sodalite		8.10	0.40	4.20	75.40	9.10	1.90	0.60	-	8.29	4.79	3.17		Konnerup-Madsen & Rose-Hansen, 1979 <sup>†</sup>
			13.00	4.00	3.50	70.00	7.30	1.10	0.28	0.07	9.59	6.64	3.93	4.00	
	arfvedsonite		10.00	0.50	23.00	57.00	5.60	0.71	0.17	0.02	10.18	7.89	4.18	9.44	
	nepheline		3.60	0.40	6.20	80.00	8.50	1.10	0.26	0.03	9.41	7.73	4.23	8.67	
eudialyte		4.00	0.40	34.00	43.00	13.00	2.00	0.49	0.06	3.31	6.50	4.08	8.17		
Khibina massif	khlebnite*	-	0.03	1.16	95.69	2.93	0.15	0.002	-	32.66	19.53	75.00		Peterliyle & Sorensen, 1970 <sup>†</sup>	
		-	0.02	1.08	95.55	3.15	0.16	0.001	-	30.33	20.06	157.00			
	urtite*	-	-	1.16	96.75	1.93	0.05	0.02	-	50.13	42.89	2.25			
	ritschorrite*	-	0.17	4.02	90.04	3.59	0.17	0.01	-	25.09	21.11	21.25			
Lovozero massif	syenite*	-	0.33	13.67	79.47	4.10	0.85	0.05	-	19.38	4.82	17.35		Kogarko et al., 1986 <sup>‡</sup>	
	urtite*	-	0.41	6.74	84.36	5.45	3.04	-	-	15.48	1.79				
	foyaite*	-	0.12	4.21	91.36	2.77	1.29	0.24	-	32.99	2.14	5.39			
	eudialyte	22		25	53										

- : denotes not reported or analysed

\* : averages

† : analysed by gas chromatography

‡ : analysed by Raman spectroscopy

FIGURE 5

A histogram showing the proportions of the major volatile species (excluding H<sub>2</sub>O and H<sub>2</sub>) in fluid inclusions from samples of “fresh” and altered pegmatites.

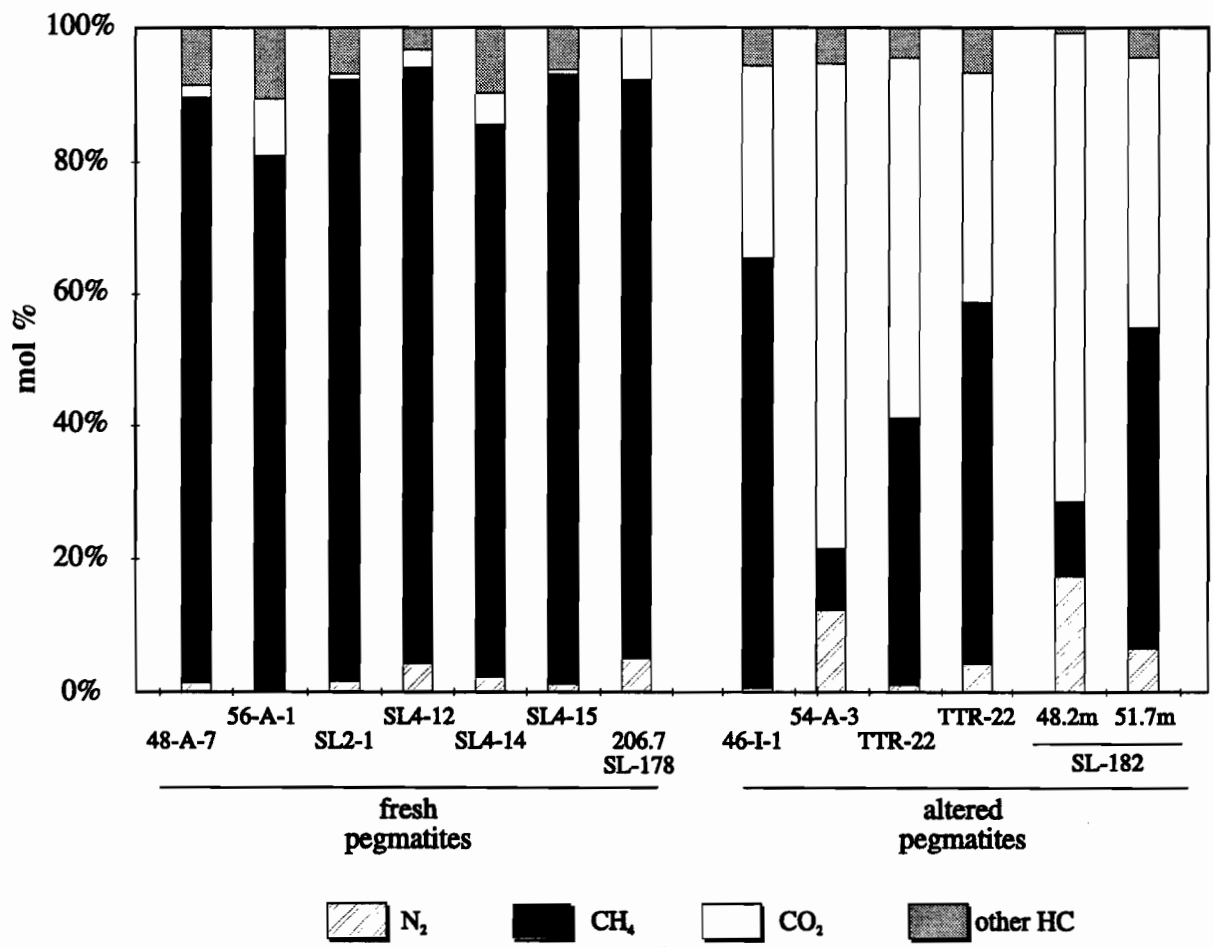
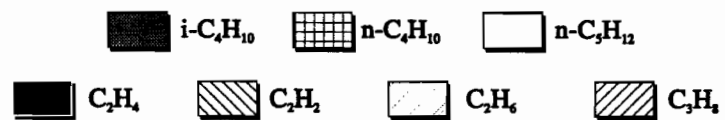
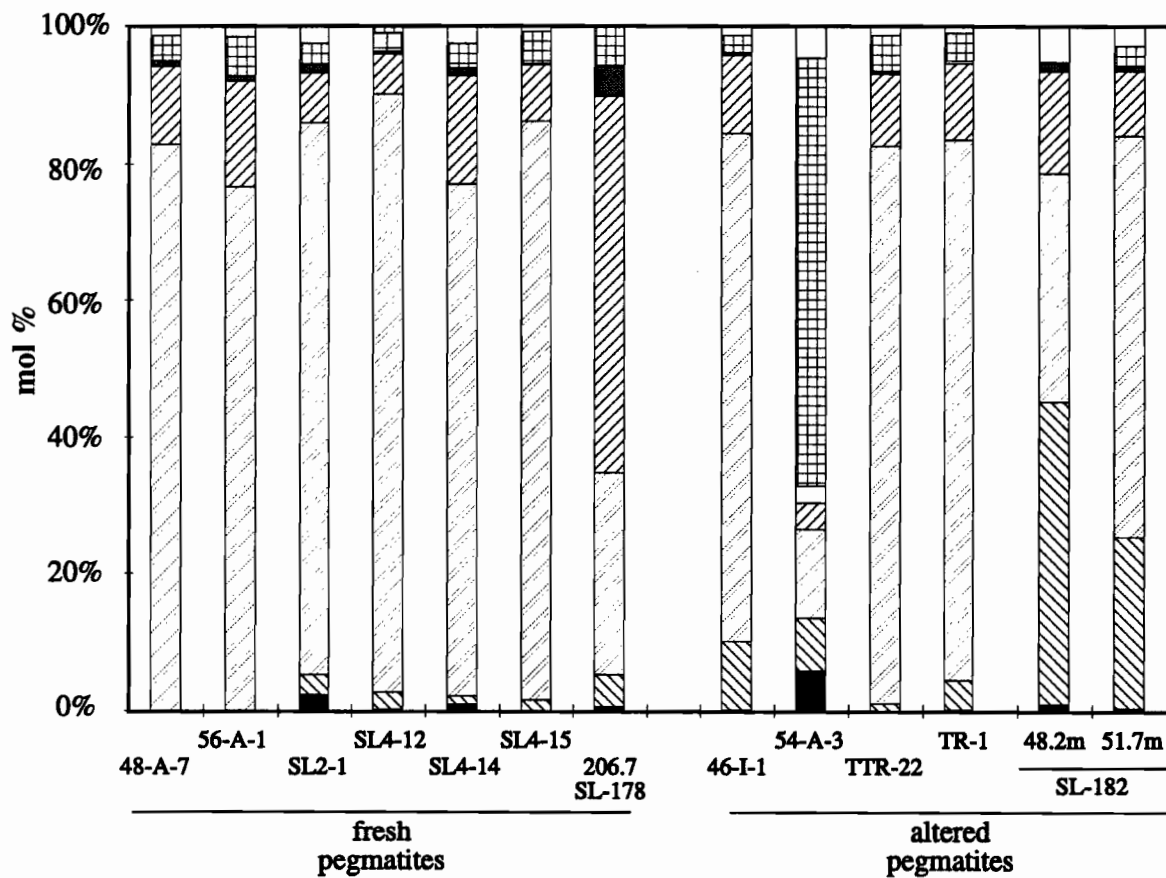


FIGURE 6

A histogram showing the proportions of the higher hydrocarbon species ( $C_2$  to  $C_5$ ) in fluid inclusions from samples of “fresh” and altered pegmatites



inclusions with such compositions have not been reported from other granitic systems. However, fluid inclusions with high contents of CH<sub>4</sub> and higher hydrocarbons have been widely reported from silica-undersaturated rocks in peralkaline igneous provinces, *e.g.*, the Ilímaussaq intrusion in Greenland (Petersilie and Sørensen, 1970; Konnerup-Madsen *et al.*, 1979), the Khibina and Lovozero massifs in the Kola Peninsula, Russia (*e.g.*, Petersilie 1963; Ikorskii and Romanikhin, 1964; Sobolev *et al.*, 1974), and the McClure Mountain-Iron Mountain alkalic complex, Colorado (Heinrich and Anderson, 1965).

Although there have been some suggestions that the source of these hydrocarbon-rich fluids is sedimentary-derived organic matter incorporated in the intrusion (*e.g.*, Lyutkevich, 1967), most authors favour an abiogenic origin because of the location of many of the intrusions in crystalline basement where there was no access to organic carbon (*e.g.*, Petersilie, 1963; Heinrich and Anderson, 1965; Sørensen, 1965). However, among proponents of an abiogenic origin, opinion is divided over whether the hydrocarbons are magmatic or the product of reaction of aqueous fluids in the intrusion with externally introduced graphite. In some cases, the latter explanation is supported by the existence of graphite-bearing shists and gneisses in the vicinity of the intrusion, but in other cases, notably the Kola peninsula, the low carbon content of the country rocks and a juvenile carbon isotopic signature seem to require a magmatic interpretation (Petersilie and Sørensen, 1970). Magmatic interpretations typically envisage exsolution of a C-O-H fluid from the magma which evolves to become hydrocarbon-enriched. For example, Gerlach (1980), attributed the CH<sub>4</sub>-rich gas composition of fluid inclusions reported from alkaline igneous complexes in the Kola Peninsula in Russia, to cooling of an orthomagmatic fluid that maintained equilibrium with the rock and was therefore buffered to lower oxygen fugacities. He showed that a fluid rich in CO<sub>2</sub> at magmatic conditions will evolve to a CH<sub>4</sub>-dominated fluid below ~ 600°C, if the system is allowed to maintain equilibrium with QFM (see also Kogarko *et al.*, 1986). However, as far as we are aware, none of the published orthomagmatic explanations have addressed the question of how hydrocarbons heavier than methane form in this environment.

*Equilibrium Models*

In order to evaluate the abiogenic hypothesis for the hydrocarbon-dominated fluid inclusions at Strange Lake, we started by carrying out thermodynamic calculations designed to determine the equilibrium composition of an evolving orthomagmatic carbon-bearing fluid.

The pressure and temperature of trapping were estimated to be approximately 700 bar and 340°C (Salvi and Williams-Jones, 1992) and  $fO_2$  was estimated to be  $\sim 2$  log units below the quartz-fayalite-magnetite (QFM) buffer, based on the near-end-member composition of arfvedsonite (Salvi and Williams-Jones, 1992).

For the sake of simplicity, and because nitrogen-bearing carbonic compounds or ammonia were not or could not be detected, respectively, we restricted calculations to the system C-O-H. We also assumed that, because the aqueous brine and carbonic fluids are immiscible at the above temperature and pressure, the activity of  $H_2O$  in the carbonic phase was determined by its solubility and that, NaCl was contained entirely in the aqueous phase (cf. Bowers and Helgeson, 1983). The species considered were  $H_2O_v$ ,  $H_2$ ,  $O_2$ ,  $CO_2$ ,  $CO$ ,  $CH_4$ ,  $C_2H_6$  and  $C_3H_8$ . The independent equilibria that describe this system can be expressed as follows:



where  $K_1$ ,  $K_2$ ,  $K_3$ ,  $K_4$  and  $K_5$  represent the equilibrium constants of reactions (1) through (5). In addition, because  $\sum P_i = P_{tot}$ , we can write:

$$P_g = PH_2O_v + PH_2 + PCO_2 + PCO + PCH_4 + PC_2H_6 + PC_3H_8$$

$$= f_{\text{H}_2\text{O}_v}/\gamma_{\text{H}_2\text{O}_v} + f_{\text{H}_2}/\gamma_{\text{H}_2} + f_{\text{CO}_2}/\gamma_{\text{CO}_2} + f_{\text{CO}}/\gamma_{\text{CO}} + f_{\text{CH}_4}/\gamma_{\text{CH}_4} + \\ + f_{\text{C}_2\text{H}_6}/\gamma_{\text{C}_2\text{H}_6} + f_{\text{C}_3\text{H}_8}/\gamma_{\text{C}_3\text{H}_8}, \quad (6)$$

where  $P_g$  is the total gas pressure,  $P_i$  is the partial pressure,  $f_i$  the fugacity, and  $\gamma_i$  the fugacity coefficient of species  $i$ . Oxygen has been excluded from equation (6) because its contribution to the total pressure, at the studied conditions, is negligible.

Equilibrium constants for reactions (1) through (5) were calculated using the Lewis-Randall approximation, *i.e.*,

$$K_i = K_{p_i} K \gamma_i, \quad (7)$$

where  $K_{p_i}$  is the equilibrium constant at 1 atm and temperature, and  $K \gamma_i$  is the corresponding ratio of the fugacity coefficients of the pure gases at pressure and temperature. The values of  $\Delta G_f^\circ$  (1 atm, T) for these gases were taken from Stull *et al.* (1969), and the fugacity coefficients were calculated from the empirical relationship

$$\gamma_i = 1 + aP_R + bT_R P_R + cT_R^2 P_R + dP_R^2 + eT_R^2 P_R + fT_R P_R^2 + gT_R^2 P_R^2$$

using the reduced pressures ( $P_R = P/P_{C_i}$ ) and temperatures ( $T_R = T/T_{C_i}$ ), and parameters a to g tabulated in Ryzhenko and Volkov (1971). Owing to the complexity of the system, equations of state to calculate the fugacity coefficients for mixtures of these components could not be used. However, because of the relatively low temperatures and pressures in question, and extensive immiscibility of aqueous and carbonic phases, due to the high salt content, and the similar molecular properties of  $\text{N}_2$  and the carbonic species (e.g., polarisability; Prausnitz, 1969), the gases are expected to have behaved *quasi* ideally. In the absence of data on the solubility of  $\text{H}_2\text{O}$ -25 wt. %  $\text{NaCl}$  in  $\text{CH}_4$ , it was assumed that this value was the same as that for  $\text{CH}_4$  in the corresponding brine ( $X_{\text{H}_2\text{O}} \sim 0.01$  at  $350^\circ\text{C}$ , Duan *et al.*, 1992). The partial pressures and mole fractions of the various gas species

listed above were calculated by solving equations (1) to (6) simultaneously, as discussed in Appendix 2.

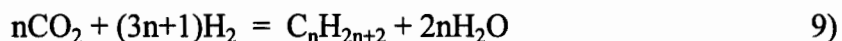
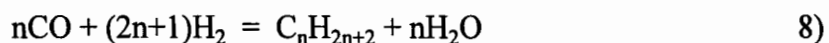
The calculations described above showed that the composition of the bulk carbonic fluid in the Strange Lake samples could not represent the equilibrium gas composition at the conditions of entrapment;  $H_2$ ,  $C_2H_6$  and  $C_3H_8$  are at least 1, 2 and 3 orders of magnitude less abundant than measured, respectively (Table 4). Moreover, increasing  $fO_2$  to QFM or decreasing it to 5 log units below QFM, and/or increasing the temperature to 500°C, did not improve the fit to the measured composition (Table 4).

It could be argued that the present composition of the fluid inclusions reflects re-equilibration of the gases at lower temperature. However, since  $fO_2$  is not buffered in the inclusions and the high temperature  $fO_2$  conditions represent states of extreme oxidation at low temperature (Fig. 7), we can assume that the dominant fluid at room temperature would be  $CO_2$ . One possibility that cannot be excluded is that  $H_2$  diffused into the inclusions some time after entrapment (cf. Mavrogenes and Bodnar, 1994), but even in the unlikely event that this did occur, it still does not explain the elevated levels of higher hydrocarbons.

In view of the fact that the Strange Lake pluton is intruded into upper amphibolite to granulite facies gneisses that are locally graphitic, we also considered the possibility that the hydrocarbons were produced by reaction of the aqueous orthomagmatic fluid with graphite. However, the fit of the calculated equilibrium gas composition at 350°C to the measured composition is even worse than that discussed above. It must therefore be concluded that the gas species in the carbonic inclusions are not, and never were, in equilibrium.

### **Hydrocarbon Formation by Fischer-Tropsch Synthesis**

An alternative abiogenic explanation for the presence of the higher hydrocarbons species in the Strange Lake fluid inclusions is that they were produced by the disequilibrium reactions:



These reactions are the basis for a well-known industrial process, the Fischer-Tropsch synthesis, which is used to convert coal to petroleum (e.g. Anderson, 1984). The process originated from the work of Sabatier and Senderens (1902) who showed that, in the presence of nickel, carbon monoxide reacts with hydrogen to produce methane.

The overall reaction consists of a series of steps, including breaking of the C-O bond and replacing it by a C-C or C-H bond. In the case of reaction (9), CO<sub>2</sub> is first transformed to CO, which is then hydrogenated to form hydrocarbons (Weatherbee and Bartholomew, 1984). The process of breaking the C-O bond is catalysed by a group VIII metal in its native form or as an oxide (e.g., Anderson 1984), and could occur naturally in the presence of wustite or magnetite (e.g., Madon and Taylor, 1981; Röper, 1983).

The length of the carbon chain in F-T synthesis is dictated by the probability of the addition to the chain of a carbon or hydrogen atom. As a result, complex mixtures are produced, but the lighter hydrocarbons (shorter chains) are always favoured (e.g., Anderson *et al.*, 1976; Satterfield and Huff, 1982). Chain growth probability is a function of reaction temperature, pressure, and the ratio of H<sub>2</sub> to C species; higher temperature and H<sub>2</sub>/CO favour the formation of shorter chains, and higher pressure produces low olefin/paraffin ratios (unsaturated/saturated aliphatics). Within a given product, the molecular ratios of hydrocarbons with successive carbon numbers are ~constant ( $C_{n+1}/C_n = C_{n+2}/C_{n+1}$ ), resulting in the Schulz-Flory distribution of hydrocarbons (they decrease linearly on a log  $X_i$  vs  $C_n$  plot). Since the purpose of the industrial application of the Fischer-Tropsch synthesis is to produce oil, *i.e.*, relatively long-chain unsaturated and cyclic compounds, most syntheses are conducted at temperatures <400°C and pressures below 100 bars. However, Anderson (1984) has shown that significant yields of hydrocarbons up to at least C<sub>6</sub> are obtained at temperatures as high as 600°C.

**Table 4**  
*Molecular proportions of gaseous species for the system C-O-H obtained from equilibrium thermodynamic calculations.*

T°C	graphite not present *					graphite present **
	QFM-2			QFM	QFM-5	QFM-2
	200 <sup>†</sup>	350	500	350	350	350
CO <sub>2</sub>	0.000	0.549	74.471	98.149	0.000	0.043
CO	0.000	0.003	1.582	0.061	0.000	0.000
H <sub>2</sub>	0.087	0.155	0.244	0.015	4.898	0.597
CH <sub>4</sub>	99.913	99.236	23.658	1.775	95.100	99.359
C <sub>2</sub> H <sub>6</sub>	0.001	0.057	0.045	0.000	0.002	0.015
C <sub>3</sub> H <sub>8</sub>	0.000	0.000	0.000	0.000	0.000	0.000

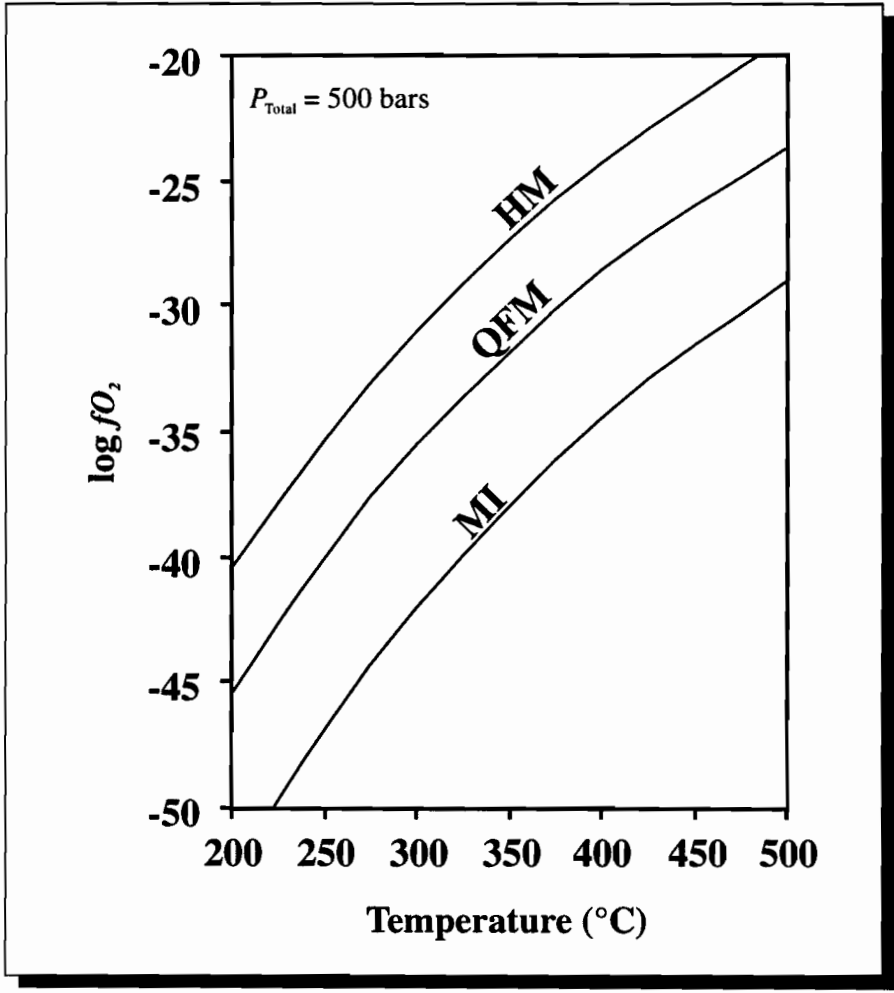
\* calculated from reactions (1) through (5) using method in appendix

\*\* calculated from reactions involving graphite, as in French, 1966

<sup>†</sup> after entrainment,  $f_{O_2}$  is not buffered by the rock, however, this calculation was performed assuming  $f_{O_2}$  buffered to QFM - 2 at 200°C. Higher values of  $f_{O_2}$  would produce CO<sub>2</sub> and even lower ethane contents.

FIGURE 7

Temperature- $\log fO_2$  conditions for the hematite-magnetite (HM), quartz-fayalite-magnetite (QFM), and magnetite-iron (MI) oxygen buffering systems. Equilibrium boundaries were calculated using the computer software package SUPCRT92 ( Johnson *et al.*, 1992).



The ratios of the mole fractions of pairs of progressively heavier hydrocarbons in the “fresh” pegmatites at Strange Lake are, on average,  $C_2/C_1 = 0.084$ ,  $C_3/C_2 = 0.180$ ,  $C_4/C_3 = 0.340$ ,  $C_5/C_4 = 0.339$ . As can be seen, with increasing carbon number these ratios level off to a constant value of approximately 0.34 and thus conform with the Schultz-Flory distribution rule; the low ethane/methane ratio is explained by the fact that some methane was present at equilibrium. Moreover, the limiting ratio of 0.34 is consistent with the finding that synthetic product mixtures dominated by light hydrocarbons have  $C_{n+1}/C_n$  values below  $\sim 0.6$  (e.g., Szatmari, 1989).

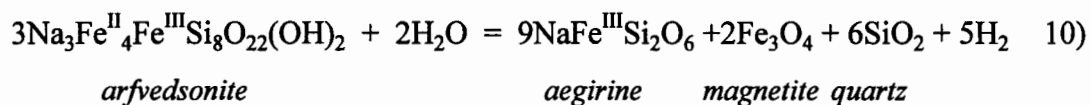
The question that next needs to be addressed is whether  $CO_2$ ,  $CO$  and  $H_2$  were potentially present in sufficient concentrations to produce the measured concentrations of the heavier hydrocarbons. From Table 1 it can be seen that the total content of heavier hydrocarbons in inclusions in “fresh” pegmatite ranges from  $\sim 5$  to  $\sim 10$  mol % of the volatile content of the inclusions (excluding  $H_2O$ ). Assuming equilibrium in the system C-O-H, it can be readily demonstrated, using the calculations described earlier, that the amounts of  $CO_2$ ,  $CO$  and  $CH_4$  are more than sufficient to produce the measured hydrocarbons at temperatures between  $500^\circ C$  and  $600^\circ C$  and at  $fO_2$  2 to 3 log units below QFM. However, at all the above conditions,  $H_2$  constitutes  $< 1$  mol % of the volatile content. By contrast, at least 30 mol %  $H_2$  are required to produce the ethane and heavier hydrocarbons, plus a further 20 mol % that was unreacted and is now present in the inclusions. It therefore follows that an independent source of  $H_2$  would have been necessary to account for the measured hydrocarbon content by Fischer-Tropsch synthesis.

One such source of  $H_2$  may have been the alteration of arfvedsonite to aegirine which, as discussed earlier, is believed to have occurred as a result of interaction of the subsolvus granite with orthomagmatic fluids during pegmatite emplacement. Initially we suggested that this alteration represented sodium metasomatism (Salvi and Williams-Jones, 1990, 1992). However, mass balance calculations have shown that Na was conserved during this alteration process (Salvi and Williams-Jones, 1995c). Therefore, if we write this reaction conserving sodium, and balance it using  $H_2O$  instead of  $O_2$  we obtain:

**Table 5**

*Calculated molecular proportions of major species for the system C-O-H obtained from equilibrium thermodynamic calculations.*

T°C	500			600		
	<i>QFM-2</i>	<i>QFM-2.5</i>	<i>QFM-3</i>	<i>QFM-2</i>	<i>QFM-2.5</i>	<i>QFM-3</i>
CO <sub>2</sub>	74.471	23.564	3.015	90.765	65.585	18.542
CO	1.582	0.890	0.203	5.097	6.550	3.293
CH <sub>4</sub>	23.658	74.859	95.779	3.755	27.132	76.708
H <sub>2</sub>	0.244	0.434	0.772	0.380	0.676	1.201



which, as is readily evident, produces 5 moles of H<sub>2</sub> for every mole of arfvedsonite altered. Moreover, the stoichiometry of equation (10) indicates that 1) if all the arfvedsonite initially in the rock (4 wt. % or ~0.04 mol /kg) was altered to aegirine, 0.2 moles of H<sub>2</sub> would have been produced per kg of rock altered, and 2) that, at a water/rock volume ratio of ¼, the H<sub>2</sub> produced by this reaction could constitute 25 - 50 mol % of the gas phase or 5 mole % of gas plus aqueous liquid (~80 - 90 mol % of the inclusion fluid is H<sub>2</sub>O, see above). The magnetite produced in reaction (10) could have acted as the catalyst for reactions (8) and/or (9).

Although the Fischer-Tropsch reaction has not been proposed previously to explain the occurrence of hydrocarbons in alkalic complexes, several investigators, especially in the Russian literature, have used it to explain the presence of oil in deep-seated environments containing ultramafic rocks (see Porfir'ev, 1974 for extensive review, also, Friedel and Sharkey, 1963; Gold and Soter, 1982). According to their theory, the H<sub>2</sub> necessary for the synthesis is produced by serpentinisation and the carbon is juvenile (*e.g.*, Apps, 1985; Morency *et al.*, 1986; Szatmari, 1989). Fischer-Tropsch synthesis has also been invoked to explain the presence of hydrocarbons in meteorites, *i.e.*, it has been proposed that they are produced by cosmic-particle catalysed reactions of H<sub>2</sub> and/or NH<sub>3</sub> with inorganic carbon (*e.g.*, Studier, *et al.*, 1972; Lancet and Anders, 1970).

Thus in summary, we propose that the hydrocarbons analysed in pegmatite quartz from Strange Lake were formed from an orthomagmatic fluid, which when it separated from the magma was composed mainly of a mixture of CO, CO<sub>2</sub> and CH<sub>4</sub>, and was in equilibrium with the rock at 500°C to 600°C and *f*O<sub>2</sub> between 2 and 3 log units below QFM. According to our model, this fluid, *i.e.*, the CO and CO<sub>2</sub>, reacted with H<sub>2</sub> derived from the oxidation of arfvedsonite to aegirine, and as a result of Fischer-Tropsch synthesis catalysed by magnetite, produced the hydrocarbons presently preserved in the

Strange Lake fluid inclusions. Once formed and trapped these species remained in a continual state of disequilibrium for the same kinetic reasons that necessitates the use of catalysts in the commercial production of light alkanes from crude oil.

### Alteration of Gas Composition

As noted earlier, the major feature of the gas-rich fluid inclusions in altered (Ca-metasomatised) pegmatite which distinguishes them from gas-rich inclusions in “fresh” pegmatite, is their much higher CO<sub>2</sub> content; the CO<sub>2</sub>/CH<sub>4</sub> ratio in altered pegmatite is 1/1, whereas it is 1/10 in the “fresh” pegmatite. There are two obvious explanations for the measured CO<sub>2</sub>, either it was added by the metasomatising fluid or the hydrocarbons were oxidised. If the former explanation is the correct one, we would have expected to find inclusions with variable CO<sub>2</sub>-CH<sub>4</sub> ratios (or CO<sub>2</sub>-H<sub>2</sub>O inclusions), reflecting incomplete mixing of the external CO<sub>2</sub>-bearing fluid with the hydrocarbon fluid, which was not the case; no CO<sub>2</sub>-rich gas inclusions or CO<sub>2</sub>-H<sub>2</sub>O inclusions were detected either microthermometrically or using Raman spectroscopy. On the other hand, oxidation of hydrocarbons to produce the increase in CO<sub>2</sub> is supported by the fact that calcium metasomatism was accompanied by extensive hematization (Salvi and Williams-Jones, 1990, 1995c), and is not inconsistent with the observation that the hydrocarbon proportions in the two sample suites did not change substantially; it is reasonable to expect that they would have been oxidised in proportion to their initial concentrations, thus preserving the *n*-alkane ratios.

It is therefore proposed that the higher CO<sub>2</sub> content of fluid inclusions in the altered pegmatites reflects oxidation of the hydrocarbon fluid during alteration by an externally derived Ca-metasomatising fluid.

Earlier we noted that fluids from two samples of the altered pegmatites have anomalously high contents of N<sub>2</sub> (54-A-3; SL-182, 48.2m) and that they also contain the highest proportions of CO<sub>2</sub>. According to the above interpretation a much higher proportion of hydrocarbons was oxidised in these samples than in others in the suite. Thus the most likely explanation for the elevated levels of N<sub>2</sub> in these samples is that they

represent magmatic  $\text{NH}_3$  which was oxidised to  $\text{N}_2$  by the Ca-metasomatising fluid. Unfortunately, however, this hypothesis could not be tested as  $\text{NH}_3$  cannot be detected using the column employed in this study.

## Conclusions

Gas chromatographic analyses of fluid inclusion volatiles in pegmatites from the Strange Lake pluton has revealed a gas composition dominated by methane, containing up to ~10 mol % higher hydrocarbons (saturated and unsaturated aliphatics), and up to 35 mol % hydrogen. A suite of quartz samples from pegmatites that had been exposed to an externally derived Ca-metasomatising fluid was also analysed, and shown to contain fluid inclusions with a similar hydrocarbon composition to those in “fresh” pegmatites, but a much higher proportions of  $\text{CO}_2$ .

Field and petrographic evidence indicate that the hydrocarbons are orthomagmatic, however, thermodynamic calculations reveal that, at equilibrium and under the temperature, pressure and  $fO_2$  conditions independently estimated for the Strange Lake pluton, the composition of the fluid measured in these rocks is impossible. Instead, our observations and thermodynamic calculations suggest that the presence of higher hydrocarbons and hydrogen in the inclusions at Strange Lake, and in other alkalic complexes, reflects the production of  $\text{H}_2$  during alteration of arfvedsonite to aegirine, and its reaction with orthomagmatic  $\text{CO}_2$  and  $\text{CO}$  to form hydrocarbons in a magnetite-catalysed Fischer-Tropsch reaction.

The high  $\text{CO}_2$  content of the calcium metasomatised samples is attributed to oxidation of the hydrocarbons by externally-derived waters.

## References

- Anderson, R.B., Lee, C., and Machiels, J.C., 1976. The thermodynamics of the hydrogenation of oxides of carbon. *Can. J. Chem. Engineer.*, 54, 590-594.
- Anderson, R.B., 1984. *The Fischer-Tropsch Synthesis*. Academic Press, New York, 301 p.
- Andrawes, F.F. and Gibson, E.K. Jr., 1979. Release and analysis of gases from geological samples. *Am. Mineral.*, 64, 453-463.
- Andrawes, F.F., Holzer, G., Roedder, E. Gibson, E.K. Jr., and Oro, J., 1984. Gas chromatographic analyses of volatiles in fluid and gas inclusions. *J. Chromatogr.*, 302, 181-193.
- Apps, J.A., 1985. Methane formation during hydrolysis by mafic rock, Lawrence Berkeley Lab. *Annu. Rep.*, 84, 13-17.
- Barker, C.G. and Torkelson, B.E., 1975. Gas adsorption on crushed quartz and basalt. *Geochim. Cosmochim. Acta*, 39, 212-218.
- Bélanger, M., 1984. Région du lac Brisson: *Ministère Énergie Ressources, Québec*, Document DP 84-20 (carte annotée, scale 1:50,000).
- Boily, M. and Williams-Jones, A.E., 1994. The role of magmatic and hydrothermal processes in the chemical evolution of the Strange Lake plutonic complex (Quebec-Labrador). *Contrib. Mineral. Petrol.*, 118, 33-47.
- Bowers, T. S., and Helgeson, H. C. 1983. Calculation of the thermodynamic and geochemical consequences of non ideal mixing in the system H<sub>2</sub>O-CO<sub>2</sub>-NaCl on phase relations in geological systems: Equation of state for H<sub>2</sub>O-CO<sub>2</sub>-NaCl fluids at high pressures and temperatures. *Geochim. et Cosmochim. Acta*, 47, 1247-1275.
- Bray, C.J. and Spooner, E.T.C., 1989. Fluid inclusion volatile analysis using heated crushing (~105°C)/gas chromatography with in-series photoionization/thermal conductivity detectors and digital peak processing [abs]. *2<sup>nd</sup> Biennial Pan-Am Conf. Res. Fluid Inclusions*, 2, 12-13.
- Bray, C.J. and Spooner, E.T.C., 1992. Fluid inclusion volatile analysis by gas chromatography with photoionization/micro-thermal conductivity detectors: Applications to magmatic MoS<sub>2</sub> and other H<sub>2</sub>O-CO<sub>2</sub> and H<sub>2</sub>O-CH<sub>4</sub> fluids. *Geochim. Cosmochim. Acta*, 56, 261-272.

- Bray, C.J., Spooner, E.T.C. and Thomas, A.V., 1991.** Fluid inclusion volatile analysis by heated crushing, on-line gas chromatography. applications to Archean fluids. *J. Geochem. Exploration*, 42, 167-193.
- Currie, K.L., 1985.** An unusual peralkaline granite near Lac Brisson, Quebec-Labrador. *Geological Survey of Canada, Report 85-1A*, 73-90.
- Duan, Z., Møller, N., Greenberg, J. and Weare, J.H., 1992.** The prediction of methane solubility in natural waters to high ionic strength from 0 to 250°C and from 0 to 1600 bar. *Geochim. Cosmochim. Acta*, 56, 1451-1460.
- Friedel, R.A. and Sharkey, A.G., 1963.** Alkanes in natural and synthetic petroleum: Comparison of calculated and actual compositions. *Science*, 139, 1203-1205.
- French, B.M., 1966.** Some geologic implications of equilibrium between graphite and a C-O-H gas phase at high temperatures and pressures. *Rev. Geophys.*, 4, 223-253.
- Gerlach, T.M., 1980.** Chemical characteristics of the volcanic gases from Nyiragongo lava Lake and the generation of CH<sub>4</sub>-rich fluid inclusions in alkaline rocks. *J. Volcanol. Geotherm. Res.*, 8, 177-189.
- Gold, T. and Soter, S., 1982.** Abiogenic methane and the origin of petroleum. *Energy Explor. Exploit.*, 1, 1-19
- Heinrich, E. Wm. and Anderson, R.J., 1965.** Carbonatites and alkalic rocks of the Arkansas River area, Fremont County, Colorado. 2. Fetid gas from carbonatite and related rocks. *Am. Mineral.*, 50, 1915-1916.
- Ikorskii, S.V. and Romanikhin, A.M., 1964.** The mode of occurrence of hydrocarbon gases in nepheline of the Khibina alkalic massif. *Geokhimiya*, 3, 276-281.
- Johnson, J.W., Oelkers, E.H, and Helgeson, H.C., 1992.** SUPCRT92: A software package for calculating the standard molal thermodynamic properties of minerals, gases, aqueous species, and reactions from 1 to 5000 bars and 0° and 1000°C. *Computers and Geosciences*, 18, 899-947.
- Kesler, S.E., Haynes, P.S., Creech, M.Z. and Gorman, J.A., 1986.** Application of fluid inclusion and rock-gas analysis in mineral exploration. *J. Geochem. Explor.*, 25, 201-215.
- Kogarko, L.N., 1974.** The role of volatiles. In *The Alkaline Rocks*, H. Sørensen ed., John Wiley & Sons, London, 474-487.

- Kogarko, L.N., Kosztolanyi, Ch. and Ryabchikov, I.D., 1986.** Geochemistry of the reduced fluid in alkali magmas. *Geokhimiya*, 12, 1688-1986. Translated in *Geochem. Int.* 24, (7), 1987, 20-27.
- Konnerup-Madsen, J., Larsen, E. and Rose-Hansen, J., 1979.** Hydrocarbon-rich inclusions in minerals from the alkaline Ilímaussaq intrusion, South Greenland. *Bull. Minéral.*, 102, 642-653.
- Konnerup-Madsen, J., Kreulen, R. and Rose-Hansen, J., 1988.** Stable isotope characteristics of hydrocarbon gases in the alkaline Ilímaussaq complex, south Greenland. *Bull. Minéral.*, 111, 567-576.
- Lancet, M. and Anders, E., 1970.** Carbon isotope fractionation in the Fischer-Tropsch synthesis and in meteorites. *Science*, 170, 980-982.
- Lyutkevich, Ye.M., 1967.** O Bitumo- i gazoproyavleniakh na Kolskom poluostrove i prirode ikh ishodnykh veshchestv (On bitumen and gas shows of Kola Peninsula and nature of original matter). In *Genesis Nefti i Gaza* (Genesis of oil and gas), Moscow, Izd. Nedra, 255-261.
- Madon, R.J. and Taylor, W.F., 1981.** Fischer-Tropsch synthesis on precipitated iron catalyst. *Journal of Catalysis*, 69, 32-43.
- Mavrogenes, J.A. and Bodnar, R.J., 1994.** Hydrogen movement into and out of fluid inclusions in quartz: Experimental evidence and geologic implications. *Geochim. Cosmochim. Acta*, 58, 141-148.
- Miller, R.R., 1986.** Geology of the Strange Lake Alkalic Complex and the associated Zr-Y-Be-REE mineralization. *Newfoundland Department of Mines and Energy, Mineral Development Division Report 86-1*, 11-19.
- Morency, M, Mineau, R., Zeller, E. and Dreschhoff, 1986.** Are all fossil fuels really fuels? *Oil & Gas Journal*, 84, 92-95.
- Nassif, G.J., 1993.** *The Strange Lake Peralkaline Complex, Québec-Labrador: The Hypersolvus-Subsolvus Granite Transition and Feldspar Mineralogy*, M.Sc. thesis, McGill University, Montreal, Quebec. 104 p.
- Nassif, G.J. and Martin R.F., 1991.** The hypersolvus granite-subsolvus granite transition at Strange Lake, Québec-Labrador [abs.]. In *program with abstracts, GAC-MAC-CSPG joint annual meeting*, Toronto, A89.

- Petersilie, I.A., 1958.** Hydrocarbon gases in the intrusive massifs of the central part of the Kola Peninsula. *Dokl. Akad. Nauk SSSR*, 122, 1086-1089 (in Russian).
- Petersilie, I.A., 1963.** Organic matter in igneous and metamorphic rocks of the Kola peninsula, in A.P. Vinogradov, ed., *Chemistry of the Earth's Crust*, 1, 178-184.
- Petersilie, I.A. and Sørensen, H., 1970.** Hydrocarbon gases and bituminous substances in rocks from the Ilímaussaq alkaline intrusion, south Greenland. *Lithos*, 3, 59-76.
- Pillet, D., 1985.** Le granite peralkalin du lac Brisson, Territoire du Nouveau-Québec: résultats préliminaires. *Ministère de l'Énergie et des Ressources, Québec*, MB 85-87, 51 p.
- Pillet, D., Bonhomme, M.G., Duthou, J.L. and Chenevoy, M., 1989.** Chronologie Rb/Sr et K/Ar du granite peralkalin du lac Brisson, Labrador central, Noveau-Québec: *Can. J. Earth Sci.*, 26, 328-332.
- Porfir'ev, V.B., 1974.** Inorganic origin of petroleum. *A.A.P.G. Bulletin*, 58, 3-33.
- Prausnitz, J.M., 1969.** *Molecular Thermodynamics of Fluid-Phase Equilibria*. Prentice-Hall, Englewood Cliffs, N.J., 524 p.
- Rao, C.N.R., 1975.** *Ultra-violet and Visible Spectroscopy*. 3<sup>rd</sup> edition, Butterworths & Co., London, 242 p.
- Röper, M., 1983.** Fischer-Tropsch synthesis. In *Catalysis in C<sub>1</sub> Chemistry*, W. Keim, ed. Dordrecht, Holland, D. Reidel; 41-88.
- Ryzhenko, B.N. and Volkov, V.P., 1971.** Fugacity coefficients of some gases in a broad range of temperatures and pressures. *Geokhimiya*, 7, 769-773.
- Sabatier, P. and Senderens, J.D., 1902.** C.R. Hebd, Seance, *Acad. Sci.*, 134, 514-680.
- Salvi, S. and Williams-Jones, A.E., 1990.** The role of hydrothermal processes in the granite-hosted Zr, Y, REE deposit at Strange Lake, Quebec/Labrador: Evidence from fluid inclusions. *Geochim. Cosmochim. Acta*, 54, 2403-2418.
- Salvi, S. and Williams-Jones A.E., 1992.** Reduced orthomagmatic C-O-H-NaCl fluids in the Strange Lake rare-metal granitic complex, Quebec/Labrador, Canada. *Eur. J. Mineral.*, 4, 1155-1174.
- Salvi, S. and Williams-Jones, A.E., 1995a.** Fluid-inclusion volatile analysis by gas chromatography: Application of a wide-bore porous-polymer capillary column. *Anal. Chem.* (to be submitted).

- Salvi, S. and Williams-Jones A.E., 1995b.** Zirconosilicate phase relations in the Strange Lake (Lac Brisson) pluton, Quebec-Labrador, Canada. *Am. Mineral.* (accepted for publication).
- Salvi, S. and Williams-Jones A.E., 1995c.** The role of hydrothermal processes in concentrating HFSE in the Strange Lake peralkaline complex, Quebec/Labrador. *Chem. Geol.* (to be submitted).
- Satterfield, C.N. and Huff, G.A., Jr., 1982.** Carbon number distribution of Fischer-Tropsch products formed on an iron catalyst in a slurry reactor. *Journal of Catalysis*, 73, 187-197.
- Sobolev, V.S., Bazarova, T.Yu. and Kostyuk, V.P., 1974.** Inclusions in the minerals of some types of alkaline rocks. In *The Alkaline Rocks*, H. Sørensen ed., John Wiley & Sons, London, 389-401.
- Sørensen, H., 1965.** On the magmatic evolution of the alkaline province of South Greenland (in Russian). In *Problemy Geochimiji*. Izd. 'Nauka', Moskva, 338-349. English translation: *Rapp. Grønlands Geol. Unders.*, 7, 1-19.
- Studier, M.H., Hayatsu, R. and Anders, E., 1972.** Origin of organic matter in early solar system—V. Further studies of meteoritic hydrocarbons and a discussion of their origin. *Geochim. et Cosmochim. Acta*, 36, 189-215.
- Stull, D.R., Westrum, E.F., Jr. and Sinke, G.C., 1969.** *The Chemical Thermodynamics of Organic Compounds*, John Wiley & Sons, Toronto, 865 p.
- Szatmari, P., 1989.** Petroleum formation by Fischer-Tropsch synthesis in plate tectonics, *A.A.P.G. Bulletin*, 73, 989-998.
- Taylor, F.C., 1979.** Reconnaissance geology of a part of the Precambrian shield, northeastern Quebec, northern Labrador and Northwest Territories. *Geol. Survey Canada, Memoires*, vol. 393.
- Weatherbee, G.D. and Bartholomew, C.H., 1984.** Hydrogenation of CO<sub>2</sub> on group VIII metals. *Journal of Catalysis*, 87, 352-362.
- Welhan, J.A., 1988.** Methane and hydrogen in mid-ocean-ridge basalt glasses: analysis by vacuum crushing. *Can. J. Earth Sci.*, 25, 38-48.
- Wopenka, B. and Pasteris, J.D., 1987.** Raman intensities and detection limits of geochemically relevant gas mixtures for a laser Raman microprobe. *Anal. Chem.*, 59, 2165-2170.

**Wopenka, B., Pasteris, J.D. and Freeman, J.J., 1990.** Analysis of individual fluid inclusions by Fourier transform infrared and Raman microspectroscopy. *Geochim. Cosmochim. Acta*, 54, 519-533.

## CHAPTER V



# ZIRCONOSILICATE PHASE RELATIONS IN THE STRANGE LAKE (LAC BRISSON) PLUTON, QUEBEC-LABRADOR, CANADA

---

STEFANO SALVI

AND

ANTHONY E. WILLIAMS-JONES

*Department of Geological Sciences  
McGill University  
Montreal, QC  
Canada*



## Introduction

**I**N most igneous rocks, zirconium is an incompatible trace element present in amounts ranging from <10 ppm to several hundreds of ppm, and is accommodated as the accessory mineral zircon. However, in peralkaline igneous rocks its concentration is commonly orders of magnitude higher and may be locally sufficient to constitute a potentially exploitable deposit (*e.g.*, in Greenland the Ilímaussaq complex, Gerasimovsky, 1969; in Russia the Lovozero deposit, Kogarko, 1990; and, in Canada, the Strange Lake complex, Miller, 1986, the Kipawa complex, Allan, 1992, and the Thor Lake deposit, Trueman *et al.*, 1988). The zirconium mineralogy of peralkaline rocks is also unusual. Although most contain some zircon, the bulk of the zirconium commonly occurs as one or more of a large family of alkali and alkaline-earth zirconosilicate minerals. The most important of these are catapleite ( $\text{Na}_2\text{ZrSi}_3\text{O}_9 \cdot 2\text{H}_2\text{O}$ ), dalyite ( $\text{K}_2\text{ZrSi}_6\text{O}_{15}$ ), elpidite ( $\text{Na}_2\text{ZrSi}_6\text{O}_{15} \cdot 3\text{H}_2\text{O}$ ), eudialyte ( $\text{Na}_4(\text{Ca}, \text{Ce})_2(\text{Fe}^{2+}, \text{Mn}, \text{Y})\text{ZrSi}_8\text{O}_{22}(\text{OH}, \text{Cl})_2$ ), and vlasovite ( $\text{Na}_2\text{ZrSi}_4\text{O}_{11}$ ), any of which may be the principal zirconosilicate mineral in a particular setting, *e.g.* eudialyte at Lovozero (Vlasov *et al.*, 1966), catapleite at Mt. Saint-Hilaire (Horváth and Gault, 1990) and vlasovite on Ascension Island (Fleet and Cann, 1967).

Little is known about the factors controlling the distribution of zirconosilicate minerals and there is little documentation of their parageneses. The only reversed experimental study that provides data on their stability, at geologically meaningful conditions, is that of Currie and Zaleski (1985) on the dehydration reaction of elpidite to vlasovite and quartz. Marr and Wood (1992) have constructed theoretical P-T diagrams for sodium and Ca-zirconosilicate minerals using the results of Currie and Zaleski (1985), molar volume data and the few constraints available from natural systems. Further advances in our understanding of zirconium mineral petrogenesis will require basic thermodynamic data for the major phases and careful documentation of field occurrences. The latter is the objective of the present contribution.

In the Strange Lake pluton, zirconium occurs mainly in the form of the zirconosilicate minerals elpidite (*cf.* Cannillo *et al.*, 1973), armstrongite ( $\text{CaZrSi}_6\text{O}_{15} \cdot 3\text{H}_2\text{O}$ )

(cf. Jambor *et al.*, 1987) and gittinsite ( $\text{CaZrSi}_2\text{O}_7$ ) (cf. Ansell *et al.*, 1980). These minerals vary greatly in their relative proportions and, locally, any one of them may be the principal or sole zirconium phase. The highest concentrations of zirconium are in rocks containing only gittinsite. Salvi and Williams-Jones (1990) observed that gittinsite plus quartz form pseudomorphs after an unidentified phase; based on the morphology of the pseudomorphs and on fluid-inclusion evidence, they suggested that a Ca-bearing fluid at  $\sim 200^\circ\text{C}$  caused the metasomatic transformation of the Na-zirconosilicate, elpidite, to gittinsite plus quartz. Birkett *et al.* (1992) subsequently proposed that gittinsite replaced the Ca-zirconosilicate armstrongite, which they claimed occurs both as a phenocryst and as a replacement of elpidite.

We re-examine the genesis of elpidite, armstrongite and gittinsite at Strange Lake, in light of textural and mineral chemical data collected from a representative diamond drill hole located near the zone of economic interest. These data, in conjunction with mineral stability relationships and published fluid inclusion data (Salvi and Williams-Jones, 1990), support a model involving low-temperature metasomatic replacement of elpidite by armstrongite and gittinsite.

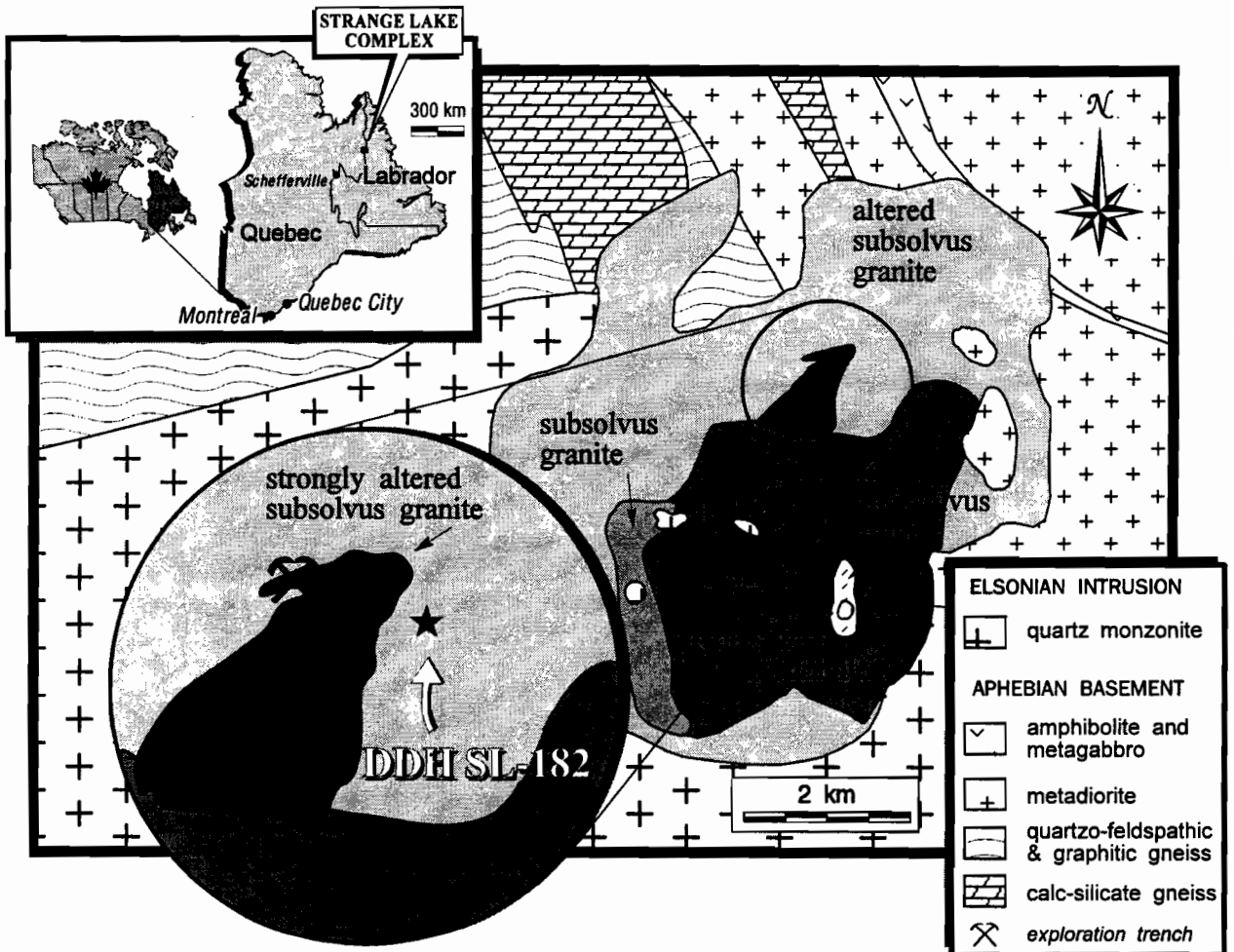
## Geological Setting

The Strange Lake pluton ( $1189 \pm 32$  Ma, Pillet *et al.*, 1989), located in the eastern Rae province of the Canadian Shield, is a peralkaline granite that intruded Aphebian metamorphic rocks (1.8 Ga) and an Elsonian quartz monzonite (1.4 Ga) (Fig. 1). The intrusion is a sub-vertical cylindrical body approximately 6 km in diameter and represents the latest tectonic event in the area. Large roof pendants are commonly observed (Fig. 1) suggesting that the present erosional surface is close to the apical part of the pluton. Based on its peralkalinity, mode of emplacement and age, the pluton may represent the Labrador extension of the Gardar anorogenic igneous event (Currie, 1985; Pillet *et al.*, 1989).

Aphebian rocks north of the pluton consist of upper-amphibolite facies metadiorites, calc-silicate gneisses, meta-amphibolites, and quartzo-feldspathic and graphitic

FIGURE 1

Location and simplified geological map of the Strange Lake pluton (modified after Salvi and Williams-Jones, 1992).



paragneisses (Taylor, 1979; Bélanger, 1984). The quartz monzonite to the south of the pluton has a distinct rapakivi texture, and is believed to be part of the Mistastin Batholith (Bélanger, 1984; Currie, 1985).

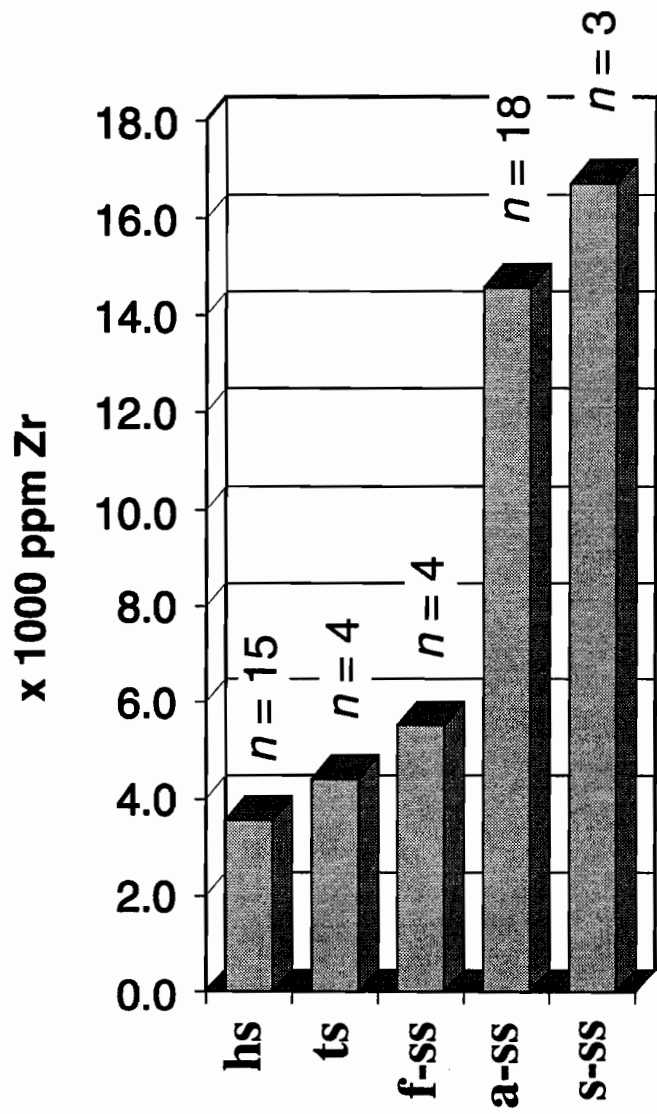
Several concentric intrusive pulses of peralkaline granite formed the Strange Lake pluton, represented by hypersolvus granite, transsolvus granite, and more evolved, volatile-saturated subsolvus granites (Nassif and Martin, 1991) (Fig. 1). All phases are fluorine-rich and contain primary fluorite. They are mainly leucocratic, fine- to medium-grained and quartz-saturated. Pegmatites are common and concentrated mainly in the subsolvus granite. An outwardly-dipping ring fracture, marked by a heterogeneous breccia in a fluorite-filled matrix, surrounds the pluton.

The hypersolvus granite consists mostly of perthite, interstitial quartz and arfvedsonite, and the subsolvus granite is characterised by idiomorphic quartz, arfvedsonite and alkali feldspars. Zirconosilicate minerals comprise up to 5% of the hypersolvus granite and up to 30% of the subsolvus granite and pegmatites. Elpidite is the principal Zr mineral in the hypersolvus granite, whereas elpidite, armstrongite and gittinsite are the dominant Zr minerals in the subsolvus granite and pegmatites. Less common zirconosilicates at Strange Lake include catapleiite, Ca-catapleiite, dalyite, hilairite ( $\text{Na}_2\text{ZrSi}_3\text{O}_9 \cdot 3\text{H}_2\text{O}$ ), vlasovite and zircon (cf. Birkett *et al.*, 1992).

Subsolvus granites commonly display hematitic alteration, and, where altered, have higher zirconium contents than fresh hypersolvus or subsolvus granites (Fig. 2). Hematisation was associated with the development of secondary HFSE minerals, many of which are Ca-bearing. Some of the most intense hematisation is in the centre of the complex where a sub-economic ore zone has been delineated containing some 30 million tonnes grading 3.25%  $\text{ZrO}_2$ , 1.3% REE oxides, 0.66%  $\text{Y}_2\text{O}_3$ , 0.56%  $\text{Nb}_2\text{O}_5$  and 0.12% BeO (Iron Ore Company of Canada, unpublished data). These granites have lower alkali contents, higher  $\text{Fe}^{3+}/\text{Fe}^{2+}$ , and higher Ca contents than fresh or less-altered subsolvus rocks (Miller, 1986; Salvi and Williams-Jones, 1990; Boily and Williams-Jones, 1995). Salvi and Williams-Jones (1990) provided fluid inclusion evidence of the interaction of ore-zone rocks with a low-temperature,  $\text{CaCl}_2$ -dominated brine. The high  $\delta^{18}\text{O}$  of these rocks

FIGURE 2

A histogram showing the average whole-rock content of Zr in the principal varieties of granite at Strange Lake. Abbreviations: hs = hypersolvus; ts = transsolvus; f-ss = fresh subsolvus; a-ss = altered subsolvus; and s-ss = strongly altered subsolvus. Standard deviations are 1.9, 2.4, 1.3, 2.3, 0.3 x 1000 ppm, respectively.



suggests that the fluid was externally derived (cf. Boily and Williams-Jones, 1994). A second episode of alteration is represented by the replacement of arfvedsonite by aegirine. This event is not well constrained temporally, but has been shown to be limited spatially to the subsolvus granite, and is thought to represent an earlier, high-temperature sodium metasomatic event (Salvi and Williams-Jones, 1990). Significantly, this alteration is most strongly developed as halos around pegmatites, which contain primary high-temperature fluid inclusions rich in NaCl and without detectable calcium (Salvi and Williams-Jones, 1992).

### Geology of DDH SL-182

Hole SL-182 was drilled in 1982 by the Iron Ore Company of Canada, in subsolvus granite very near the potential ore zone (Fig. 1). The hole plunges vertically, extends for about 88 m, and intersects several varieties of subsolvus granite, as well as a number of pegmatites.

All the lithologies intersected contain quartz phenocrysts, arfvedsonite, fine-grained alkali feldspars, zirconosilicate minerals and medium- to coarse-grained idiomorphic pseudomorphs of titanite + quartz  $\pm$  fluorite after narsarsukite. Most samples contain rare perthite phenocrysts (replaced almost entirely by microcline and rimmed by albite), at least two generations of fluorite in varied proportions, small octahedra of pyrochlore, locally poikilitic, and one or more of the zirconosilicate minerals elpidite, armstrongite and gittinsite. Small proportions of hematite, zircon, thorite, allanite, bastnäsite, kainosite, yttrian milarite (Cerný *et al.*, 1991), and several unidentified minerals occur locally.

The top half and final 13 m of the hole are composed of fine- to medium-grained granite that is distinguished by a bimodal distribution of arfvedsonite crystal size, *i.e.* phenocrysts ~2 mm to ~8 mm in diameter and groundmass crystals  $\leq$ 1 mm in diameter. This rock unit is also characterised by the presence of inclusions of melanocratic granite, which range from a few centimetres to a few tens of centimetres in diameter; they constitute about 2-5% by volume of the rock. The inclusions are fine to very fine grained, and locally contain scattered phenocrysts of microcline and, less commonly, quartz and arfvedsonite.

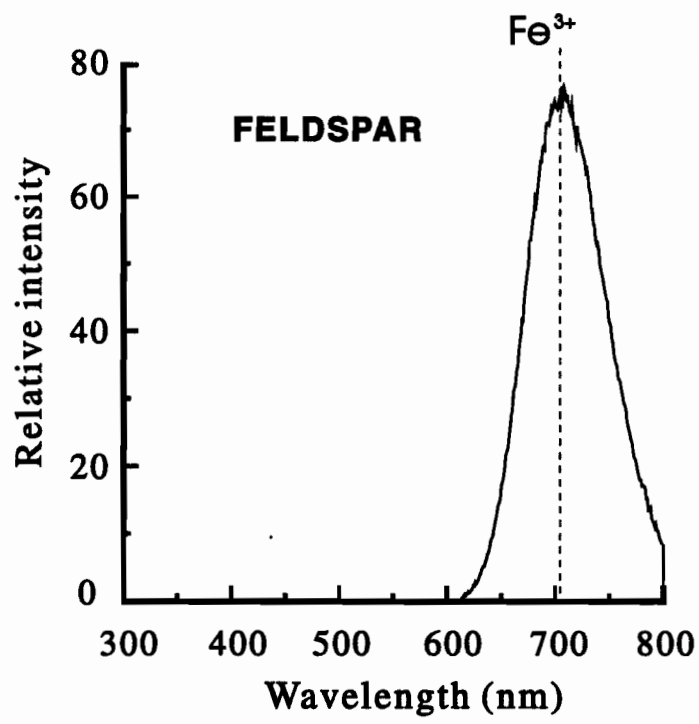
The dark colour of the rock is due to a high proportion of the amphibole in the groundmass. The melanocratic inclusions lack chill margins and in place show evidence of partial resorption and plastic deformation. It has been suggested that the melanocratic granite represents a chilled marginal facies of transsolvus granite (Nassif and Martin, 1991; Boily and Williams-Jones, 1994).

In the central portion of the hole, the granite is also fine- to medium-grained but is non-porphyritic, *i.e.* lacks arfvedsonite phenocrysts. The mafic inclusions, which characterise the porphyritic granite, are also absent. Subhedral to euhedral aegirine occurs locally in this unit. The lower contact between this and the porphyritic granite is transitional and is represented by a zone a few meters in thickness in which the proportion of arfvedsonite phenocrysts gradually decreases towards the equigranular granite, zirconosilicates have two habits (see below), and the melanocratic inclusions are very scarce. The upper contact is more abrupt, although lacking chilled margins. This and the absence of other evidence of intrusive relationships suggest that these two main rock types were roughly coeval. Several metre-wide, flat-lying pegmatites cut the equigranular granite. Based on their quartz contents, the pegmatites can be divided into two groups, one containing abundant quartz (50% to 80% of the rock by volume), and the other containing little (<10% by volume) to no quartz. The equigranular granite is intersected in other drill holes and is exposed in the trench, northwest of DDH SL-182. It can therefore be deduced that this unit forms a sub-horizontal sheet a few tens of meters in thickness, covering an area of approximately 1 km<sup>2</sup> in the central portion of the pluton (cf. Miller, 1990; Birkett *et al.*, 1992).

The granites show varied degrees of alteration, except in the bottom 10 metres of the hole where the rocks are relatively fresh. Alteration is manifested as replacement of arfvedsonite by aegirine ± hematite, replacement textures involving the zirconosilicates (see below), hematite staining, cloudiness and red Fe<sup>3+</sup>-activated cathodoluminescence of feldspars (Fig. 3), appearance of secondary fluorite, and the development of extensive secondary porosity. The strongest replacement of arfvedsonite by aegirine is observed in

FIGURE 3

Cathodoluminescence emission spectrum for alkali feldspar in altered subsolvus granite from Strange Lake. Beam voltage: 10 to 15 keV; beam current: 0.5 to 1 mA; beam diameter: 5 mm. Scanning at 0.5 nm increments, stepping time of 1 second. Photomultiplier high-voltage: 950 V.



and adjacent to the pegmatites, whereas hematite staining of the rock is more pronounced in the top levels.

### **Distribution of Zirconosilicate Minerals in DDH SL-182**

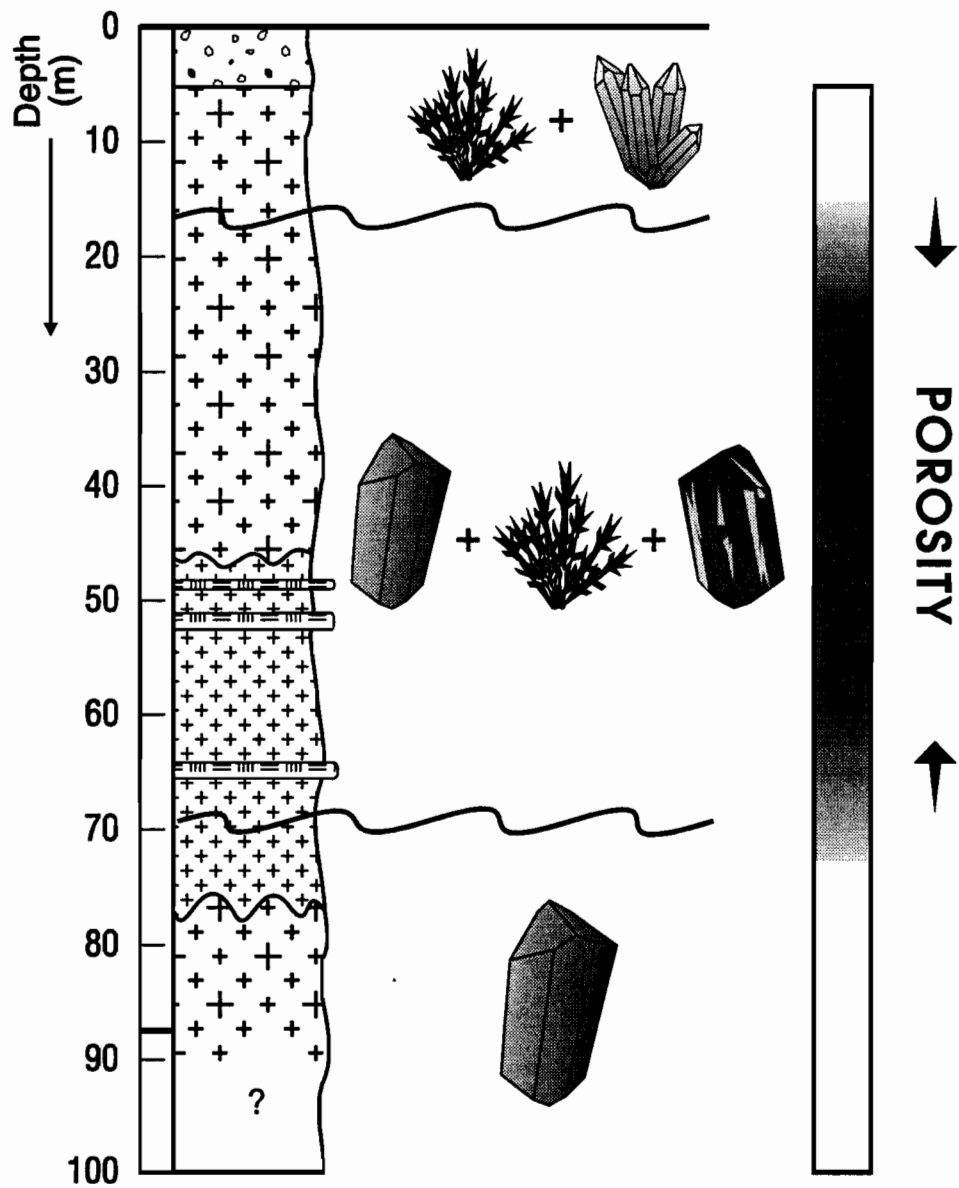
Euhedral elpidite occurs as doubly-terminated orthorhombic prisms, with the typical "boat" shape also observed in rocks from Narssârssuk by Goldshmidt (1918). Euhedral armstrongite has a pseudo-orthorhombic habit indistinguishable from that of elpidite. All observed occurrences of armstrongite show polysynthetic twinning. Gittinsite occurs almost exclusively as narrow feathery crystals forming radiating aggregates.

Elpidite, armstrongite and gittinsite have distinctly different distributions and modes of occurrence (Fig. 4). In the porphyritic granite at the bottom of the hole, elpidite is the principal zirconosilicate mineral and its abundance ranges from a few percent to 20% of the rock by volume; armstrongite is absent, and gittinsite is rare. Elpidite occurs as anhedral up to 3 mm in diameter interstitial to feldspar and quartz grains (Fig. 5A), or as large aggregates of small grains (<0.1 mm diameter), also distributed interstitially to the main rock forming minerals (Fig. 5B).

Elpidite is also the dominant zirconosilicate mineral in the equigranular granite (middle of the hole), but it forms euhedral crystals (Fig. 5C) up to 3 mm long and its abundance varies between 15% and 25% of the rock by volume. Many elpidite crystals display varying degrees of rim and core replacement by armstrongite and gittinsite. The volume proportion of elpidite replaced by these minerals averages 15-20% and increases upwards. Where replacement involved armstrongite alone, volume was conserved (Fig. 5D). However, elpidite crystals replaced by gittinsite, or armstrongite + gittinsite, all contain pore space (Fig. 5E and F). Although armstrongite can be found in contact with both elpidite and gittinsite, the latter minerals rarely occur in contact with each other. In the transitional zone between the two granites, both interstitial and euhedral habits of elpidite are observed.

FIGURE 4

A schematic representation of the geology, the zirconosilicate mineral habits and distribution, and the porosity profile down DDH SL-182. Darker shading corresponds to higher porosity.



over-burden



pegmatite



equigranular granite  
(euhedral elpidite)



porphyritic granite  
(anhedral elpidite)



elpidite



armstrongite



gittinsite



quartz

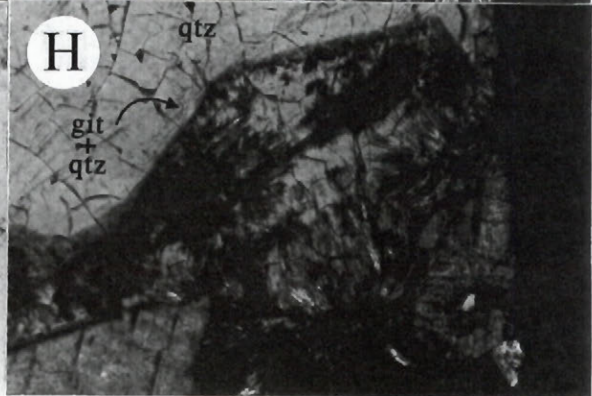
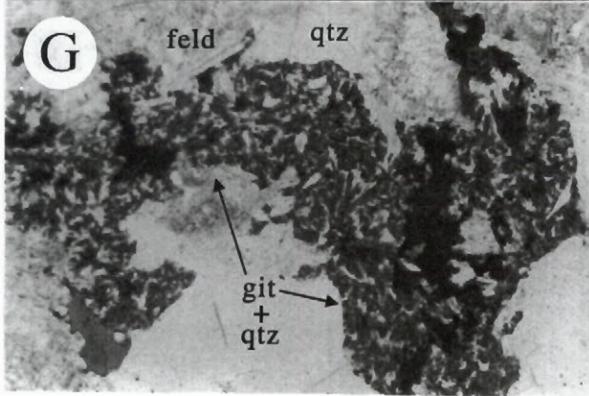
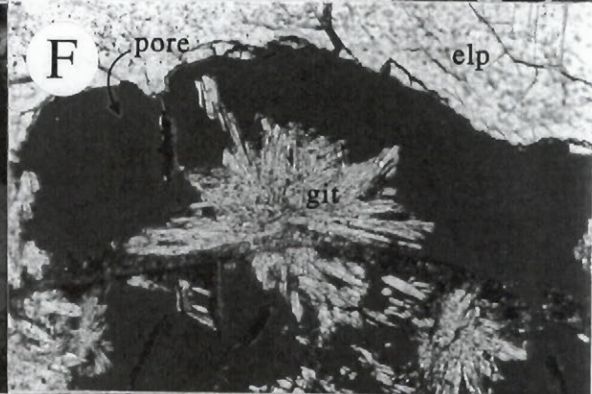
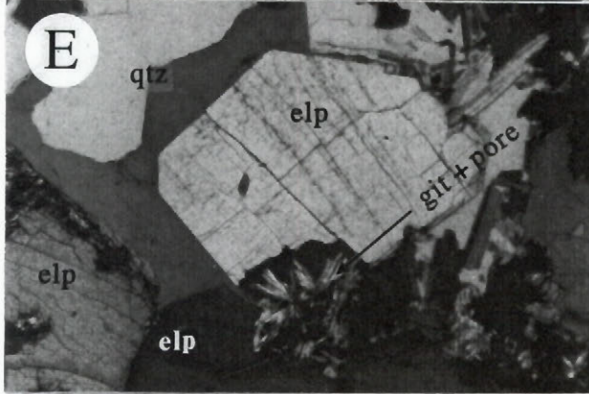
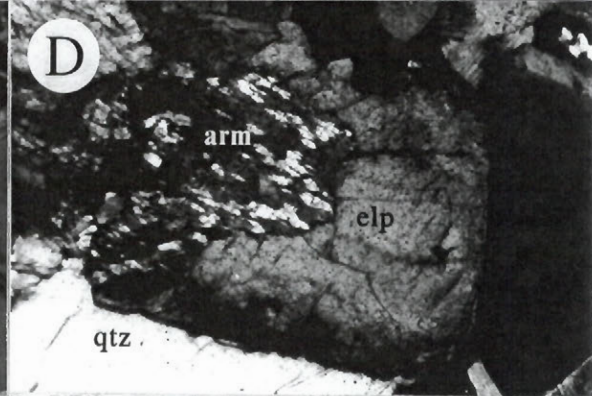
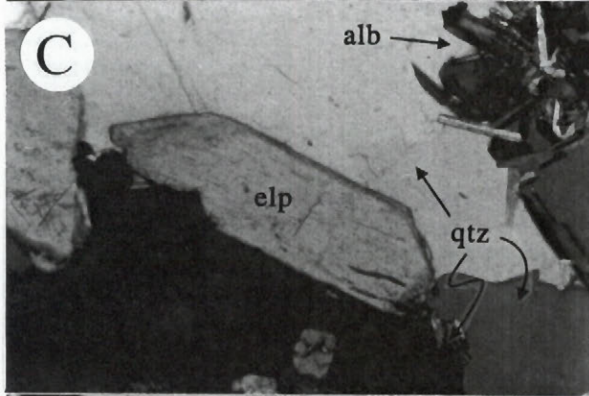
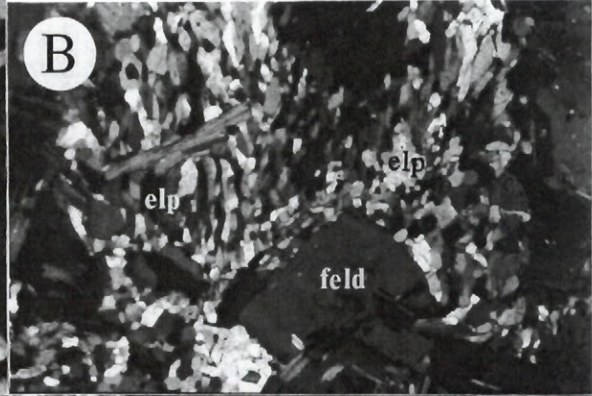
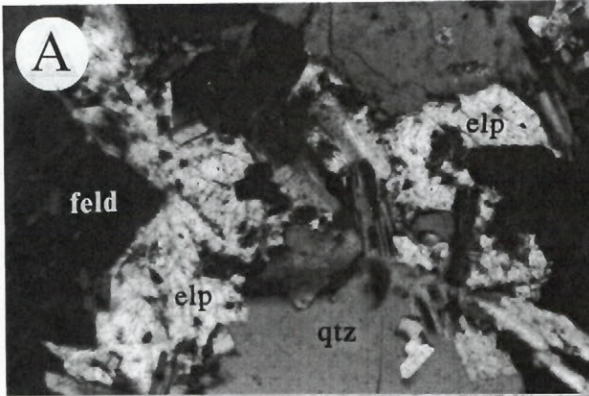
Further up the hole (15-46 m depth), in porphyritic granite, elpidite has a similar habit to elpidite in the deepest part of the hole. However, in this interval it experienced extensive dissolution, leaving behind pore space (up to 10% of the rock), and Ca-zirconosilicates, largely gittinsite (Fig. 5F). Gittinsite rosettes occur in the cavities left by elpidite dissolution, and commonly grow preferentially on surrounding feldspar and arfvedsonite grains, as well as on rare strings of tiny spherical aggregates of radiating zircon crystals (Fig. 5F). The habit of these zircon spherules and the fact that they occur in the pore space suggest that the zircon is secondary. In cases where an entire pocket of elpidite has been replaced, the proportions of gittinsite and pore space are about 40% and 60%, respectively, of the precursor elpidite. Armstrongite is a minor phase, and replaced either cores or rims of elpidite crystals. Replacement of elpidite is more extensive toward the top of the interval.

In the top 10-15 m of drill core, gittinsite is the sole zirconosilicate mineral. It forms feathery radiating crystals up to 0.5 mm in length embedded in tiny anhedral quartz grains. Gittinsite and quartz form coherent aggregates in the groundmass, interstitial to other minerals (Fig. 5G). The sizes, shapes and sharp boundaries of these aggregates suggest that they fill interstitial volumes formerly occupied by crystals of elpidite. In this interval, gittinsite comprises from 5% to 20% of the rock by volume. The granite is almost free of porosity and displays a patchy red coloration due to fine-grained hematite in the gittinsite-quartz aggregates.

Rocks from the exploration trench, similar in texture and mineralogy to the equigranular granite in SL-182, as well as equigranular granite intersected at high levels by other drill holes, also contain aggregates of gittinsite plus quartz and lack porosity. However, in contrast to the upper part of hole SL-182, these aggregates form pseudomorphs after a euhedral phase (Fig. 5H) which we interpret to be elpidite based on the occurrence of elpidite crystals with similar morphology in equigranular granite in DDH SL-182. The volume proportions of gittinsite and quartz in the pseudomorphs, whether after euhedral or interstitial elpidite, vary from 40% to 70% and 30% to 60%, respectively. Interestingly, the

FIGURE 5

Photomicrographs of zirconosilicate mineral textures: A) (74.9 m depth) anhedral crystal of elpidite (elp) and B) aggregate of small elpidite crystals interstitial to quartz (qtz) and feldspar (feld); C) (54.9 m) euhedral crystal of elpidite; D) (53.0 m) partial replacement of elpidite by polysynthetically twinned armstrongite (arm); E) (59.4 m) gittinsite (git) rosettes, accompanied by pore space, partly replacing large elpidite crystals; F) (44.7 m) radiating gittinsite crystals attached to a string of secondary zircon spherules, and growing in pore space adjacent to elpidite; G) (13.5 m) aggregate of feathery gittinsite crystals plus quartz interstitial to quartz and feldspars; H) (trench sample) gittinsite-quartz pseudomorph after an euhedral phase. Photos A, B, C, D, E, H are in crossed polarised light; F and G in plain polarised light. Photos A, B, C, E, G are 2 mm across; D, F, H are 1 mm across.



gittinsite-quartz pseudomorphs in both equigranular or porphyritic granite, occur where hematite alteration is most intense.

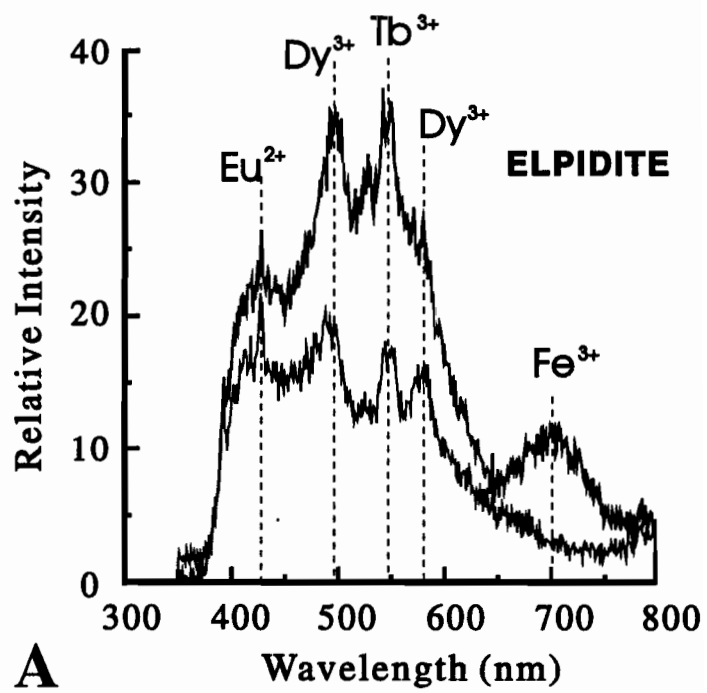
## Geochemistry

Electron microprobe analyses were performed with a Cameca CAMEBAX instrument equipped with an EDS (NORAN high-purity Ge detector, NORVAR window) detector. The analyses were carried out in EDS mode in order to permit use of a low beam current (15 kV, 0.6 Na current, and 2000 to 3500 counts), so as to minimise the volatility of light elements such as sodium (light-element volatility is the major source of error in zirconosilicate mineral analysis; Stephen Aja, personal communication; see also Bonin, 1988; Birkett *et al.*, 1992). Where possible, the beam was defocused to a diameter of 5 mm to further minimise light element volatility. Data reduction was performed with the PROZA version of the phi-rho-z correction routine using internal standards (Bastin and Heijligers, 1992).

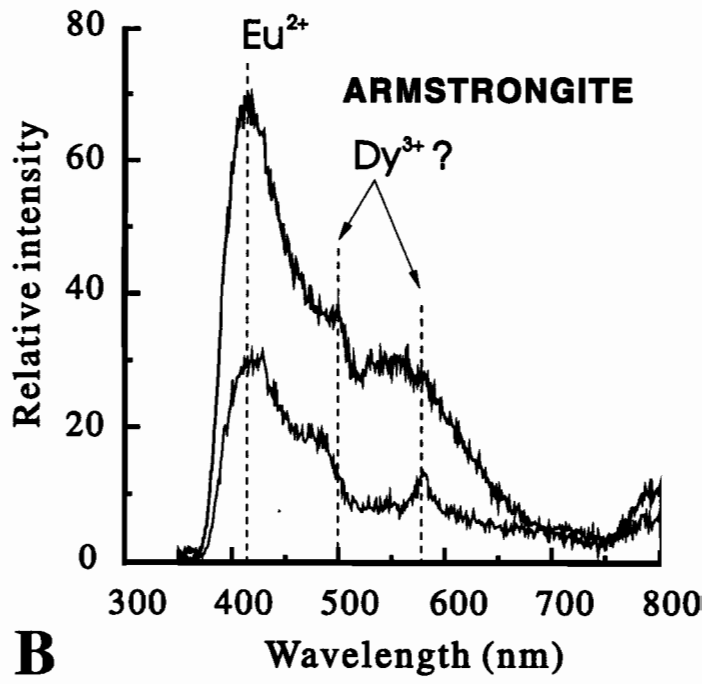
Analyses for each zirconosilicate are listed in Table 1 and are plotted as atomic proportions of Na, Ca and  $Zr/(Zr+Si)$  in Figure 6. The data indicate that elpidite contains up to 37 mol% of Ca zirconosilicate in solid solution. By contrast, most of the gittinsite and armstrongite samples have compositions very close to those of the end-member phases. Generally, cores of elpidite euhedra are more calcic than the rims and fine-grained, late interstitial aggregates such as in Figure 5B.

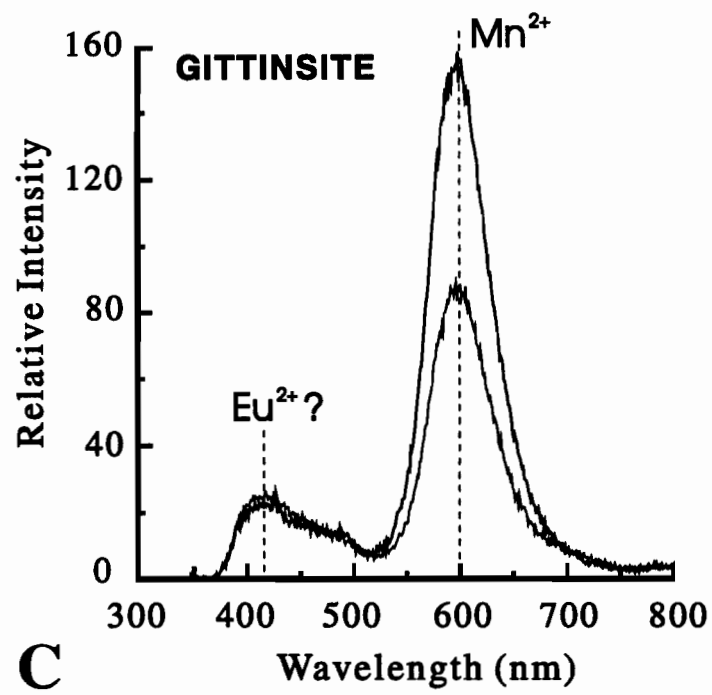
## Cathodoluminescence

Elpidite, armstrongite and gittinsite display strong luminescence when bombarded by an electron beam. Similar but weaker luminescence can be observed under ultraviolet illumination. This allowed the distribution of zirconosilicates to be established in a large number of drill holes.



A





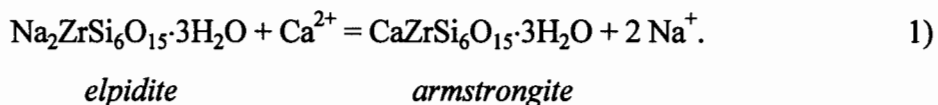
**C**

suggesting that  $Mn^{2+}$  may be the activator in this mineral. Activation at 420 nm is similar to the homologous emission in armstrongite and elpidite, and is therefore attributed to  $Eu^{2+}$ .

## Discussion

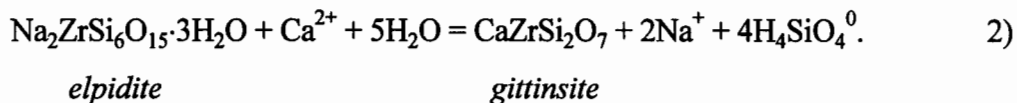
The euhedral habit of elpidite in the equigranular granite suggests that this mineral crystallised relatively early, whereas its occurrence as interstitial anhedral in the porphyritic granite indicates relatively late-stage crystallisation. In both rock types, however, elpidite is clearly a magmatic mineral and was the first zirconosilicate to form. By contrast, the textures described above show that armstrongite and gittinsite occur only as secondary subsolidus minerals, largely as a replacement of elpidite.

The formation of armstrongite is readily explained by the cation-exchange reaction:



This reaction has a very small negative  $\Delta V_S$  ( $-11.01 \text{ cm}^3/\text{mol}$ ; calculated from molar volume data in Marr and Wood, 1992) which corresponds to 4.8% volume reduction and is consistent with the textural evidence of essentially constant volume replacement of elpidite euhedra by armstrongite (Fig. 5D).

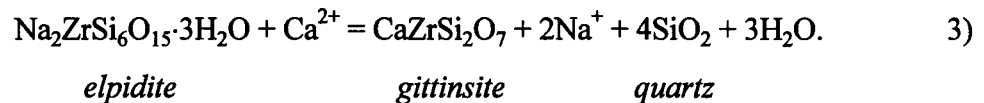
The replacement of elpidite by gittinsite can be explained by the reaction:



Reaction 2 has a large negative  $\Delta V_S$  ( $-149.1 \text{ cm}^3/\text{mol}$  or 65% volume reduction), thereby explaining the considerable porosity associated with replacement of elpidite by gittinsite in the central part of the hole (Fig. 5E and F). In fact, the pore volume predicted by the  $\Delta V_S$  of Reaction 2 compares closely to the observed porosity created where grains of elpidite have

been entirely replaced by gittinsite; 60-70%. The production of silicic acid in Reaction 2 and absence of quartz accompanying gittinsite indicates that the altering fluid was quartz-undersaturated.

In the porphyritic granite in the top 10 m of the hole, as well as in equigranular granite at shallow levels in other holes and exposed in the trench, elpidite is absent, gittinsite is the sole zirconosilicate, and there is no evidence of porosity. Instead, quartz fills the interstices around gittinsite. The similarity of the sizes and shapes of the gittinsite-quartz aggregates and the boat-shaped pseudomorphs to elpidite aggregates and euhedra in similar rocks deeper in DDH SL-182, suggest that gittinsite and quartz formed at the expense of precursor elpidite. This requires that gittinsite replacement of elpidite was accompanied or followed by precipitation of additional quartz. A reaction which might explain coprecipitation of gittinsite and quartz is:



However,  $\Delta V_s$  for this reaction is  $-58.4 \text{ cm}^3/\text{mol}$ . This represents a 25% volume reduction which should be readily evident in the form of pore space. The fact that there is no unfilled volume in the space occupied by gittinsite-quartz aggregates indicates that, if replacement was according to reaction 3, there must have been precipitation of additional quartz. An alternative explanation, supported by preservation of delicate rosettes of gittinsite, is that replacement took place by Reaction 2 and that quartz precipitated later. This implies that the metasomatic fluid was initially undersaturated with respect to quartz, and that at a later stage, silica solubility decreased thereby causing precipitation of quartz in the pores at high levels in the pluton.

The mineralogical relationships in DDH SL-182 occur throughout altered parts of the pluton and suggest that an episode of calcium metasomatism caused extensive replacement of elpidite by Ca-zirconosilicates to a depth of ~70 m below the present erosional surface, and that silica was added in the form of quartz closer to the surface. On

the basis of data from primary fluid inclusions in gittinsite-quartz pseudomorphs Salvi and Williams-Jones (1990) proposed that pseudomorphism was effected by Ca-rich brines at temperatures of ~200°C. The replacement of magmatic elpidite by gittinsite or armstrongite or both, was probably caused by a similar fluid. Such low-temperature formation of gittinsite and armstrongite explains their near-end-member compositions. This contrasts with the extensive solid-solution displayed by elpidite (cf. Fig. 6), which is interpreted to have crystallised under magmatic conditions; magmatic conditions for elpidite crystallisation are also suggested by zoned crystals which, like plagioclase in igneous systems, were initially Ca rich. The activation of luminescence by  $\text{Eu}^{2+}$  in both armstrongite and gittinsite but not elpidite (Fig. 7) is consistent with calcium metasomatism, and the fact that, in its divalent state, europium readily substitutes for calcium.

The questions which now need to be addressed are: whether the calcium metasomatism was caused by orthomagmatic fluids (Birkett *et al.*, 1992) or externally derived formational waters (Salvi and Williams-Jones, 1990); whether or not Zr was mobilised and concentrated by the metasomatism; why armstrongite formed at depth and gittinsite closer to the surface; why quartz addition was restricted to the near surface environment; and ultimately under what conditions and in response to what factors alteration of elpidite to armstrongite and gittinsite occurred.

The orthomagmatic fluid hypothesis can be ruled out by the evidence that the fluids responsible for the deeper alteration were quartz-undersaturated. If the altering fluid were of magmatic origin it would have been in equilibrium with the granite, and therefore saturated with respect to silica (any cooling would have caused deposition of quartz). Moreover, the average calcium concentration observed in altered subsolvus granite (1.5 wt.% vs. 0.5 wt.% in unaltered granites) cannot be explained by magmatic processes alone (cf. Nassif, 1993; Boily and Williams-Jones, 1994).

The restriction of gittinsite to the volume of the precursor phase is strong evidence that Zr acted as an immobile element during metasomatism. However, as reported above, the proportions of gittinsite to quartz in samples from high levels are generally greater than the proportions of gittinsite to pore space lower in the hole. Although the difference is

small, it could be significant as it may indicate that Zr was indeed remobilised by the metasomatic fluid, albeit to a limited degree. This would be consistent with the observed increase of whole-rock Zr in the strongly altered subsolvus granites (Fig. 2), *i.e.*, in rocks containing the gittinsite-quartz pseudomorphs. On the other hand, it is more likely that this correlation reflects late onset of hydrothermal activity coincident with the emplacement of the most evolved and hence Zr-rich phase of the intrusion.

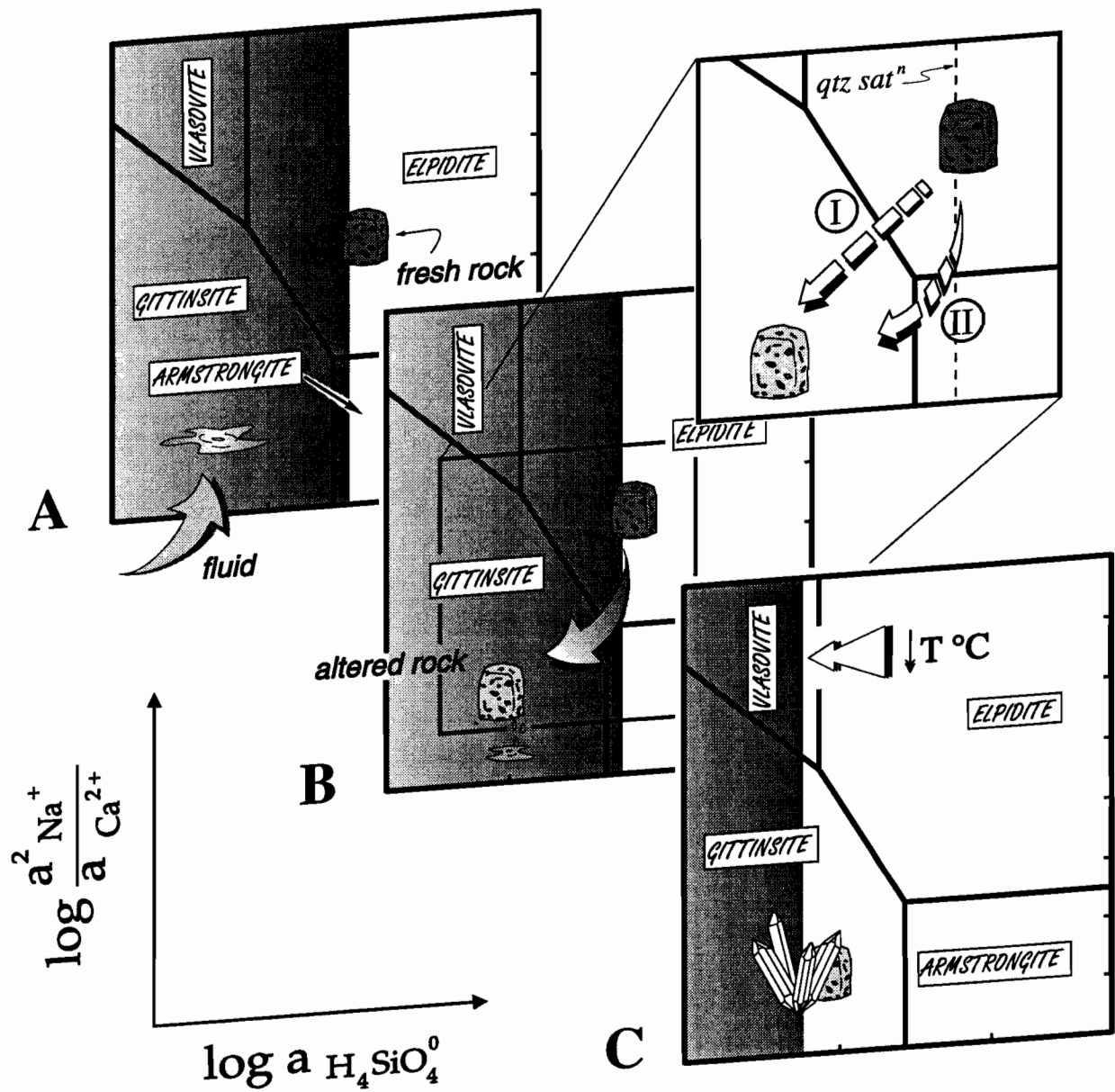
Further insight into this metasomatic process can be gained by examining the stability fields of the zirconosilicate minerals as a function of Na, Ca and Si activity. Unfortunately, there are few thermodynamic data for the alkali and alkaline-earths zirconosilicates (cf. Marr and Wood, 1992). Nonetheless, it is possible to represent phase stability relationships schematically using the principles of chemographic analysis (Schreinemaker, 1915-1925; Korzhinskii, 1959; Zen, 1966). In Figure 8 we present a  $\log a^2_{\text{Na}^+}/a_{\text{Ca}^{2+}}$  vs.  $\log a_{\text{H}_4\text{SiO}_4^0}$  diagram for the system  $\text{Na}_2\text{O}-\text{CaO}-\text{ZrO}_2-\text{SiO}_2-\text{H}_2\text{O}$  and the phases in the system observed in the altered rocks of Strange Lake, plus vlasovite. Also shown on the diagram are possible locations of the boundary of quartz saturation.

We propose that, sometime after crystallisation of at least the apical region of the intrusion, heated groundwaters in equilibrium with adjacent calc-silicate gneisses and gabbros (and therefore Ca-rich and quartz-undersaturated) entered the pluton (Fig. 8A). In the uppermost parts where water/rock ratios were high, the fluids dissolved elpidite, replacing it primarily with gittinsite (Fig. 8B, path I). Deeper in the pluton, fluid/rock ratios were lower permitting the rock to buffer  $a_{\text{H}_4\text{SiO}_4^0}$  to higher values which were sufficient to stabilise gittinsite plus armstrongite and locally armstrongite alone (Fig. 8B, path II).

The presence of quartz with gittinsite near the surface requires either that P-T conditions of alteration changed so as to permit saturation of quartz at lower  $a_{\text{H}_4\text{SiO}_4^0}$ , or that quartz was introduced later. In view of the textures, *i.e.*, feathery gittinsite crystals embedded in quartz, we prefer the latter explanation and propose that quartz was precipitated in response to cooling of the fluids during the waning stages of the hydrothermal system (Fig. 8C).

FIGURE 8

Schematic  $\log a^2\text{Na}^+/a\text{Ca}^{2+}$  vs.  $a\text{H}_4\text{SiO}_4^0$  diagrams showing the stability fields of the zirconosilicate minerals, as well as hypothetical compositions of the unaltered elpidite-bearing granite, the hydrothermal fluid (A), and the altered gittinsite-bearing granite (C). Also shown are possible paths of metasomatic transformation of the rock during alteration (B). The shaded fields represent quartz saturation levels in the fluid, during metasomatism (A and B), and at lower temperature (C).



## Conclusions

Textural relationships in drill core and surface exposures provide the key evidence necessary to interpret the genesis of elpidite, armstrongite and gittinsite in altered granites at Strange Lake. These relationships show that the Na-zirconosilicate, elpidite, crystallised at the magmatic stage, whereas the Ca-zirconosilicates armstrongite and gittinsite are secondary and formed during subsolidus interaction of the rock with a low-temperature, Ca-rich silica-undersaturated brine derived externally from the pluton. The replacement of elpidite by armstrongite occurred at essentially constant volume, whereas the precipitation of gittinsite was accompanied by the creation of significant pore space. Alteration was more pronounced at shallow levels, where elpidite was replaced entirely by gittinsite rosettes, and decreased in importance with depth, where all three zirconosilicate minerals can be observed. We interpret the changing importance of gittinsite and armstrongite with depth to have been controlled by the activity of silica; at shallow depths, high water/rock ratios buffered  $a_{\text{H}_4\text{SiO}_4^0}$  to low levels, favouring the formation of gittinsite, whereas at greater depth and lower water/rock ratios the rock buffered the silica activity to levels high enough to stabilise armstrongite and gittinsite and locally armstrongite alone. At a later stage, cooling of the residual hydrothermal fluid may have induced a decrease in silica solubility, promoting precipitation of quartz in the pore space created by gittinsite replacement of elpidite.

## References

- Allan, J.F., 1992. Geology and mineralization of the Kipawa yttrium-zirconium prospect, Quebec. *Exploration and Mining Geology*, 1, 283-295.
- Ansell, H.G., Roberts, A.C., Plant, A.G. and Sturman, B.D., 1980. Gittinsite, a new calcium zirconium silicate from the Kipawa agpaitic syenite complex, Quebec. *Can. Mineral.*, 18, 201-203.
- Bastin, G.F. and Heijligers, H.J.M., 1992. Quantitative Electron Probe Microanalysis of Ultra-Light Elements (Oxygen-Boron). In *Electron Probe Quantitation*. K.F.J. Heinrich and D.E. Newbury, eds., Plenum Press, 145-162.
- Bélanger, M., 1984. Région du lac Brisson. *Ministère Énergie Ressources, Québec*, Document DP 84-20 (carte annotée, scale 1:50,000).
- Birkett, T.C., Miller, R.R., Roberts, A.C. and Mariano, A.N., 1992. Zirconium-bearing minerals of the Strange Lake intrusive complex, Quebec-Labrador. *Can. Mineral.*, 30, 191-205.
- Boily, M. and Williams-Jones, A.E., 1994. The role of magmatic and hydrothermal processes in the chemical evolution of the Strange Lake plutonic complex (Quebec-Labrador). *Contrib. Mineral. Petrol.*, 118, 33-47.
- Bonin, B., 1988. Peralkaline granites in Corsica: Some petrological and geochemical constraints. *Rendiconti della Società Italiana di Mineralogia e Petrologia*, 73, 1191-1194.
- Cannillo, E. Rossi, G. and Ungaretti, L., 1973. The crystal structure of elpidite. *Am. Mineral.*, 58, 106-109.
- Cerný, P., Hawthorne, F.C., Jambor, J.L. and Grice, J.D., 1991. Yttrian milarite. *Can. Mineral.*, 29, 533-541.
- Currie, K.L., 1985. An unusual peralkaline granite near Lac Brisson, Quebec-Labrador. *Geological Survey of Canada*, Report 85-1A, 73-90.
- Currie, K.L. and Zaleski, Eva., 1985. The relative stability of elpidite and vlasovite: A P-T indicator for peralkaline rocks. *Can. Mineral.*, 23, 577-582.
- Fleet, S.G. and Cann, J.R., 1967. Vlasovite: a second occurrence and a triclinic to monoclinic inversion. *Mineral. Magazine*, 36, 233-241.

- Gerasimovsky, V.I., 1969.** *Geochemistry of the Ilimaussaq Alkaline Massif (South-West Greenland)*. Nauka, Moscow, 174 p. (in Russian) (not seen; extracted from *Lithos*, 26, 167, 1990).
- Goldshmidt, V., 1918.** *Atlas der Krystallformen*, Carl Winters Universitäts-buchhandlung, Heidelberg, 3.
- Herzog, L.F., Marshall, D.J. and Babione, R.F., 1970.** The Luminoscope - a new instrument for studying the electron-stimulated luminescence of terrestrial, extra-terrestrial and synthetic materials under the microscope. In *Space Science Applications of Solid State Luminescence Phenomena*, J.N. Weber and E. White, eds., 79-98. MRL publication 70-101, State College, Pennsylvania.
- Horváth, L. and Gault, R.A., 1990.** The mineralogy of Mont Saint-Hilaire, Quebec. *The Mineral. Record*, 21, 284-359.
- Jambor J.L., Roberts, A.C. and Grice, J.D., 1987.** Armstrongite from the Strange Lake alkalic complex, on the Quebec-Labrador boundary, Canada. *Powder Diffraction*, 2, 2-4.
- Kogarko, L.N., 1990.** Ore-forming potential of alkaline magmas. *Lithos*, 26, 167-175.
- Lazutkina, L.N., Kogarko, L.N. and Krigman, L.D., 1980.** Stability of zirconium minerals in alkali agpaitic magmas. *Geochem. Int.*, 17 (4), 83-86.
- Korzhinskii, D.S., 1959.** *Physicochemical Basis of the Analysis of the Paragenesis of Minerals*, Consultant Bureau, Inc., New York, 142 p.
- Mariano, A.N. and Ring, P.J., 1975.** Europium-activated cathodoluminescence in minerals. *Geochim. Cosmochim. Acta*, 39, 649-660.
- Marr, R.A., Wood, S.A., 1992.** Preliminary petrogenetic grids for sodium and calcium zirconosilicate minerals in felsic peralkaline rocks: The  $\text{SiO}_2\text{-Na}_2\text{ZrO}_3$  and  $\text{SiO}_2\text{-CaZrO}_3$  pseudobinary system. *Am. Mineral.*, 77, 810-820.
- Marshall, D.J., 1988.** *Cathodoluminescence of Geological Materials*, Unwin-Hyman, Boston, 146 p.
- Mason, R.A. and Mariano, A.N., 1990.** Cathodoluminescence activation in manganese-bearing and rare earth-bearing synthetic calcites. *Chem. Geol.*, 88, 191-206.

- Miller, R.R., 1986.** Geology of the Strange Lake Alkalic Complex and the associated Zr-Y-Be-REE mineralization. *Newfoundland Department of Mines and Energy, Mineral Development Division, Report 86-1, 11-19.*
- Miller, R.R., 1990.** The Strange Lake pegmatite-aplite hosted rare metal deposit, Labrador. *Newfoundland Department of Mines and Energy, Geological Survey Branch, Report 90-1, 171-182.*
- Nassif, G.J., 1993.** *The Strange Lake Peralkaline Complex, Québec-Labrador: The Hypersolvus-Subsolvus Granite Transition and Feldspar Mineralogy*, M.Sc. thesis, McGill University, Montreal, Quebec, 104 p.
- Nassif, G.J. and Martin, R.F., 1991.** The hypersolvus granite-subsolvus granite transition at Strange Lake, Quebec-Labrador. In *Abstracts with Program, Geol. Ass. of Canada*, A89.
- Pillet, D., Bonhomme, M.G., Duthou, J.L. and Shenevoy, M., 1989.** Chronologie Rb/Sr et K/Ar du granite peralkalin du lac Brisson, Labrador central, Nouveau-Québec. *Can. J. Earth Sci.*, 26, 328-332.
- Salvi, S. and Williams-Jones, A.E., 1990.** The role of hydrothermal processes in the granite-hosted Zr, Y, REE deposit at Strange Lake, Quebec/Labrador: Evidence from fluid inclusions. *Geochim. Cosmochim. Acta*, 54, 2403-2418.
- Salvi, S. and Williams-Jones, A.E., 1992.** Reduced orthomagmatic C-O-H-N-NaCl fluids in the Strange Lake rare-metal granitic complex, Quebec/Labrador, Canada. *Eur. J. Mineral.*, 4, 1155-1174.
- Schreinemakers, F.A.H., 1915-1925.** *In-, Mono-, and Divalent Equilibria*. Proceedings of Koninklijke Akademie van Wetenschappen Te Amsterdam. Reprinted as Papers by F.A.H. Schreinemakers, vol. 2, The Pennsylvania State University, University Park, Pa., June 1965.
- Taylor, F.C., 1979.** Reconnaissance geology of a part of the Precambrian shield, northeastern Quebec, northern Labrador and Northwest Territories. *Geol. Survey Can. Memoires*, vol. 393.
- Trueman, D.L., Pedersen, J.C., de St. Jorre, L. and Smith, D.G.W., 1988.** The Thor Lake, N.W.T., rare-metal deposits. In *Granite-Related Mineral Deposits: Geology, Petrogenesis and Tectonic Setting*. Taylor, R.P. and Strong, D.F., eds. *Can. Inst. Min. Met.*, Special Volume 39, 279-284.

**Vlasov, K.A., Kuz'menko, M.Z. and Es'kova, E.M., 1966.** *The Lovozero Alkali Massif*, translated by D.G. Fry and K. Syers. S.I. Tomkeiff, M.H. Battey, eds. Hafner Pub. Co., New York, 627 p.

**Zen, E-An., 1966.** Construction of pressure temperature diagrams for multicomponent systems after the method of Schreinemakers - A geometrical approach. *U.S. Geol. Survey Bull.*, 1225, 1-56.

## CHAPTER VI

# THE ROLE OF HYDROTHERMAL PROCESSES IN CONCENTRATING HFSE IN THE STRANGE LAKE PERALKALINE COMPLEX, NORTHEASTERN CANADA

---

STEFANO SALVI

AND

ANTHONY E. WILLIAMS-JONES

*Department of Geological Sciences  
McGill University  
Montreal, QC  
Canada*

## Abstract

The middle-Proterozoic peralkaline pluton at Strange Lake, Quebec/Labrador, consists of several intrusive phases ranging from hypersolvus to more evolved subsolvus granite, which are unusually enriched in Zr, Y, REE, Nb, Be, and F. These elements are most concentrated in the subsolvus granite, and are hosted by a wide variety of exotic alkali and alkaline-earth silicate minerals, comprising up to 20 volume % of the rock. After emplacement, the pluton underwent two episodes of hydrothermal alteration which affected mainly the subsolvus granite. Early alteration is evident in the replacement of arfvedsonite by aegirine, whereas later alteration involved hematisation and the replacement of alkali HFSE minerals by calcic equivalents. The two alteration episodes are interpreted, on the basis of previously published fluid inclusion data, to have occurred at temperatures of approximately 350°C and <200°C, respectively.

Whole-rock chemical analyses indicate that much of the enrichment in HFSE, Y, and REE was primary, *i.e.*, the contents of these elements in the unaltered rocks increase from least to most evolved subsolvus granite. Comparisons of the chemical compositions of fresh and altered rocks, after correcting for any volume or bulk mass changes during alteration, indicate that early alteration was essentially isochemical, except for some depletion in Zr, Y and REE. This alteration is interpreted to reflect oxidation of a relatively reduced primary magmatic mineral assemblage by cooling orthomagmatic brines. Later alteration also involved oxidation, but mainly involved addition of Ca and Mg, and removal of Na. Zirconium, Y and REE were also added in significant amounts to the altered rocks, commonly representing enrichments of >20% relative to the proportions of these elements in the unaltered rocks. Calculations, using available experimental data on the solubility of elpidite, indicate that hydrothermal fluids with modest concentrations of F can transport the amounts of Zr needed to account for the estimated enrichment of this element in the altered rocks. However, these calculations also show that that this would not have been possible in the brine responsible for Ca addition, because F<sup>-</sup> activity would have been buffered to exceptionally low levels as a result of saturation of the fluid with fluorite. A more plausible

candidate for Zr transportation is the sodic, essentially Ca-free, orthomagmatic brine documented by our previously published fluid inclusion studies, and interpreted here to have been responsible for early alteration.

We propose that late alteration and accompanying HFSE enrichment were the result of the mixing, in the apical parts of the pluton, of a F-rich orthomagmatic fluid, containing significant concentrations of Zr and other HFSE, with an externally derived meteoric-dominated fluid, enriched in Ca as a result of interaction with calc-silicate gneisses and gabbros. According to this interpretation, the latter fluid was responsible for the exchange of Ca for alkalis, mainly Na, in zirconosilicate and other HFSE-rich minerals and, by sharply reducing  $F^-$  activity in the mixed fluid through fluorite precipitation and/or increasing pH, destabilised the HFSE-fluoride complexes, causing deposition of HFSE-bearing minerals. An important implication of this study is that major HFSE enrichment may be restricted to those rare cases where F-rich, Ca-free, metal leaching environments and Ca-rich depositional environments are juxtaposed.

## Introduction

**E**NRICHMENT in high-field strength elements (HFSE) is a common feature of alkalic igneous rocks (*e.g.*, Sørensen, 1974; Karup-Møller, 1978; Fitton and Upton, 1987; Wooley, 1987), and can be attributed mainly to the high solubility of HFSE in peralkaline melts, which have a much higher proportion of non-bridging oxygens than metaluminous or peraluminous melts, thereby allowing them to accommodate more of these highly charged cations (*e.g.*, Scarfe, 1977). However, it is not clear that igneous processes alone can explain the extraordinarily high concentrations of these metals in alkalic igneous bodies like the Strange Lake granitic pluton in northern Canada, which contains among the highest contents of Zr, Y, rare-earth elements (REE) and other high-field strength metals reported anywhere (Zajac, 1992). Although peralkaline character, fractional crystallisation and halogen complexation are likely to have been major factors in the primary magmatic concentration of these elements, certain features of the pluton, notably the intense hematization of the most highly mineralised zone and the positive correlation of Ca content with HFSE content (Boily and Williams-Jones, 1994), suggest that hydrothermal processes may also have played a role in HFSE mineralization. This possibility is strengthened by the observations of Salvi and Williams-Jones (1990 and 1995b) that the principal Zr ore mineral is a calcium zirconosilicate, gittinsite, which replaced a sodium zirconosilicate precursor, elpidite, and fluid inclusion evidence that this replacement was caused by a low temperature ( $\leq 200^{\circ}\text{C}$ ) Ca-rich brine (Salvi and Williams-Jones, 1990). The latter study also demonstrated that REE were mobile during the influx of this brine, from the occurrence of bastnäsite in the inclusions as a daughter mineral. However, the scale of this mobility, and whether or not other HFSE were mobilised during this hydrothermal event, was not established by the above or subsequent papers on the Strange Lake pluton.

In this paper we report results of whole-rock chemical analyses and present mass balance calculations which show that, although igneous processes were responsible for much of the HFSE enrichment in the Strange Lake pluton, significant proportions of at least Zr, Y and REE (typically greater than 20% of their masses) were concentrated

hydrothermally. This concentration is explained by transportation of these elements as fluoride complexes in an orthomagmatic fluid, and their subsequent deposition in the apical parts of the pluton as a result of mixing with an externally derived Ca-rich meteoric fluid. The study suggests that HFSE may be relatively mobile in other fluorine-rich geological environments at relatively low temperature, but only if the hydrothermal fluids have exceptionally low contents of calcium. Even minor concentrations of Ca are sufficient to cause precipitation of fluorite and buffer  $F^-$  activities to levels impossibly low for HFSE transportation. It therefore follows that, if conditions are suitable for HFSE transportation, deposition of HFSE minerals is most likely to occur when the hydrothermal fluid encounters a calcium-bearing environment. This may explain why many of the occurrences of hydrothermal HFSE deposits reported in the literature are hosted by carbonate rocks, typically in close proximity to a fluorine-rich igneous body.

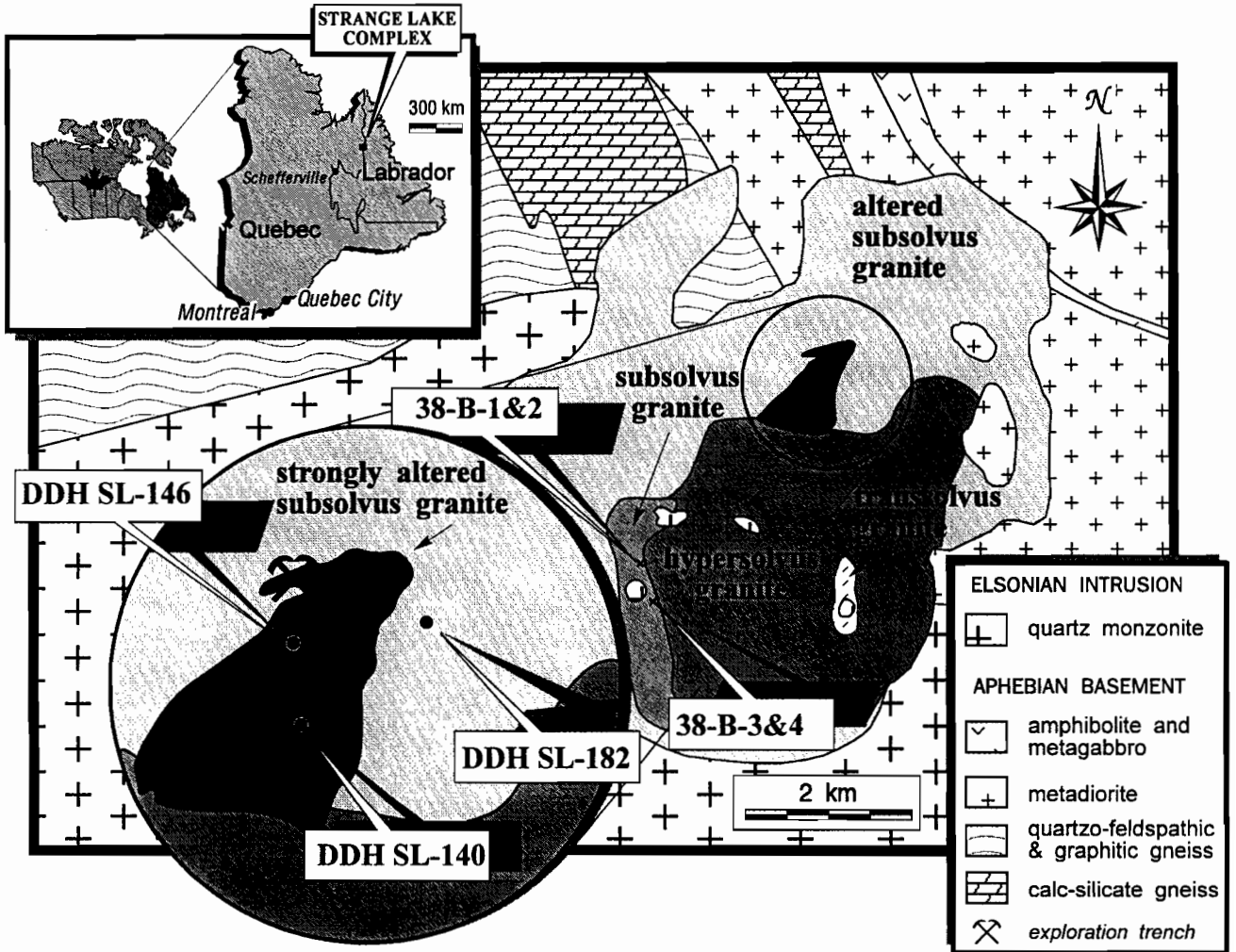
## Geological Setting

The Strange Lake pluton ( $1189 \pm 32$  Ma; Pillet *et al.*, 1989) is a small cylindrical body about 6 km in diameter, intruded in Archean basement in the eastern reaches of the Rae tectonic Province, on the border between Quebec and Labrador, in north-eastern Canada. The country rock, in the vicinity of the pluton, consists of intercalated upper-amphibolite to granulite facies gneisses of Aphebian age, and an Elsonian rapakivi quartz-monzonite intrusion (Taylor, 1979; Bélanger, 1984).

Surface exposure is poor, however, extensive drilling was carried out on the property between 1979 and 1985, which allowed Miller (1986) to produce the first surface map of the pluton. This work led to the recognition of a potential ore zone in the central part of the intrusion containing some 30 million tonnes grading 3.25%  $ZrO_2$ , 1.3% REE oxides, 0.66%  $Y_2O_3$ , 0.56%  $Nb_2O_5$  and 0.12% BeO (Iron Ore Company of Canada, unpublished data; see also Zajac *et al.*, 1984). Further field work, and drill core logging carried out by researchers from McGill University, identified several phases of peralkaline granite, which, on the basis of their feldspar mineralogy, were classified as hypersolvus, transsolvus and

FIGURE 1

Geological map of the Strange Lake pluton, showing the locations of the drill holes and outcrop samples (modified after Salvi & Williams-Jones, 1992).



more evolved subsolvus granite (Nassif and Martin, 1991) (Fig. 1). In addition to these major intrusive facies, there are also numerous pegmatite dykes, located mainly in the subsolvus granite, and rare aplites. Roof pendants are common in the northern part of the pluton, and suggest that the present level of exposure is close to the top of the intrusion.

The hypersolvus granite consists of phenocrysts of quartz and perthite, interstitial arfvedsonite, plus subordinate amounts of albite, aenigmatite, astrophyllite, vlasovite, dalyite and other exotic phases (cf. Salvi and Williams-Jones, 1990) in the ground-mass (see Table 1 for mineral compositions). The transsolvus granite has a similar mineralogy to the hypersolvus granite, except that microcline is a common phase. Arfvedsonite in this unit occurs predominantly as fine-grained anhedral, imparting a melanocratic appearance to the rock.

The subsolvus granite occupies more than 60 % of the complex. It is composed of quartz, two alkali feldspars and arfvedsonite. In addition, in some units of subsolvus granite, the zirconosilicate mineral elpidite ( $\text{Na}_2\text{ZrSi}_6\text{O}_{15}\cdot 3\text{H}_2\text{O}$ ) can comprise up to 15 - 20% of the rock by volume. Commonly, arfvedsonite has a bimodal grain-size distribution, *i.e.*, it forms phenocrysts, and is also part of the groundmass. Accessory phases include hematite, fluorite, thorite, bastnäsite, monazite, pyrochlore, kainosite, allanite, yttrian milarite, and several unidentified minerals (Table 1). The subsolvus granite is interpreted to have crystallised at a late stage, as indicated by the common presence of inclusions of the other granite types, and by the feldspar mineralogy, *i.e.*, the presence of microcline and near-end-member albite (Nassif, 1993).

All these granite types display some degree of heterogeneity due mainly to flow differentiation, which locally concentrated arfvedsonite and some of the denser exotic minerals, notably elpidite, in thin discontinuous layers. Inclusions in the subsolvus granite are aligned parallel to this layering, which generally is subvertical, except in the north-central part of the pluton, where it is subhorizontal (consistent with the location of these rocks near the top of the pluton).

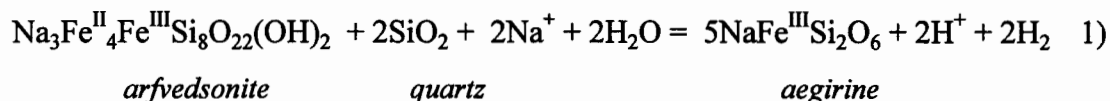
**Table 1**  
*Mineral formulae and abbreviations for selected minerals  
 occurring in the Strange Lake pluton.*

Mineral name	Formula	Abbreviation
Aegirine	$\text{NaFe}^{+3}\text{Si}_2\text{O}_6$	Aeg
Albite	$\text{NaAlSi}_3\text{O}_8$	Ab*
Arfvedsonite	$\text{Na}_3\text{Fe}_4^{+2}\text{Fe}^{+3}\text{Si}_8\text{O}_{22}(\text{OH})_2$	Arf*
Armstrongite	$\text{CaZrSi}_6\text{O}_{15} \cdot 2\text{H}_2\text{O}$	Arm
Bastnäsité	$(\text{La}, \text{Ce}, \text{Nd}, \text{Y})\text{CO}_3\text{F}$	Bst
Chlorite	$\text{Mg}_8\text{FeSi}_{5,3}\text{Al}_{5,5}\text{O}_{20}(\text{OH})_{16}$	Chl
Dalyite	$\text{K}_2\text{ZrSi}_6\text{O}_{15}$	Dal
Elpidite	$\text{Na}_2\text{ZrSi}_6\text{O}_{15} \cdot 3\text{H}_2\text{O}$	Elp
Fluorite	$\text{CaF}_2$	Fl*
Gadolinite	$\text{Y}_2\text{Fe}^{+2}\text{Be}_2\text{Si}_2\text{O}_{10}$	Gad
Gittinsite	$\text{CaZrSi}_2\text{O}_7$	Git
Hematite	$\text{Fe}^{+3}_2\text{O}_3$	Hem*
K-feldspar	$\text{KAlSi}_3\text{O}_8$	Kfs*
Magnetite	$\text{Fe}^{+2}\text{Fe}_2^{+3}\text{O}_4$	Mag*
Monazite	$(\text{Ce}, \text{La}, \text{Th})\text{PO}_4$	Mnz*
Narsarsukite	$\text{Na}_2(\text{Ti}, \text{Fe}^{+3})\text{Si}_4\text{O}_{10}(\text{O}, \text{F})_{11}$	Nsk
Pyrochlore	$(\text{Ca}, \text{Na})_2(\text{Nb}, \text{Ta})_2\text{O}_6(\text{O}, \text{OH}, \text{F})$	Pyc
Quartz	$\text{SiO}_2$	Qtz*
Thorite	$\text{ThSiO}_4$	Thr
Titanite	$\text{CaTiSiO}_5$	Ttn*

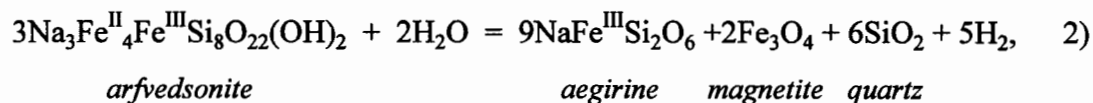
\*Abbreviation according to Kretz, 1983

## Alteration

Two episodes of alteration have been recognised, both of which affected mainly the subsolvus granite (cf. Salvi and Williams-Jones, 1990). The first episode is manifested chiefly by partial or complete replacement of arfvedsonite by aegirine, and is more intense in and adjacent to pegmatites; it is common to observe altered pegmatites in fresh granite. The extent of this alteration cannot be easily mapped, as it occurs very sporadically and to varying degrees of intensity, but generally, it is developed more extensively in the northern part of the pluton. This alteration is believed to have occurred at relatively high temperatures, in the presence of a sodic orthomagmatic brine (Salvi and Williams-Jones, 1992), and was initially interpreted to represent sodium metasomatism accompanied by oxidation according to a reaction of the type:



(Salvi and Williams-Jones, 1990). However, the presence of iron oxides (generally magnetite), and mass balance calculations presented below, suggest that the reaction was more probably of the type:

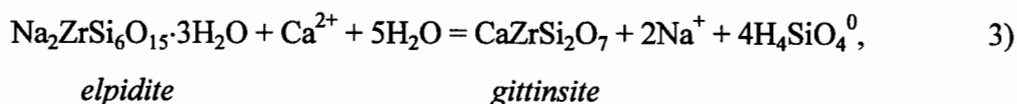


(Salvi and Williams-Jones, 1995a). Similar replacement textures have been observed in the peralkaline granites of Corsica, and explained by an oxidation reaction equivalent to reaction (2) (Bonin, 1986).

The second alteration episode is manifested macroscopically by hematisation of the rock and the pseudomorphic replacement of alkali minerals by calcic minerals, in particular, the formation of gittinsite-quartz pseudomorphs after the sodium zirconosilicate, elpidite,

and titanite-quartz after narsarsukite. Commonly, aegirine pseudomorphs of arfvedsonite, and albite crystals, contain sub-microscopic hematite grains which give a red coloration to these minerals; gittinsite and titanite crystals are invariably coated by hematite. The most intense expression of this alteration is in the central part of the pluton, and coincides with the potential ore zone referred to above. With depth, the intensity of the alteration generally decreases (in some holes, zones of relatively unaltered core were observed within intervals of strongly altered core), and, on the basis of a careful study of available drill core, the granite appears to have been unaffected by this latter alteration below a depth of about 80 to 100 m.

For the most part, the rocks exposed at surface or intersected at shallow levels in drill core, display the most intense hematisation, and the calcium zirconosilicate, gittinsite, is the only zirconium mineral present, typically in the form of pseudomorphs, with quartz, after elpidite. At greater depth, hematisation becomes patchy, and the distribution of the zirconosilicate minerals more varied. Elpidite is present, but is partially to completely replaced by gittinsite and, less commonly, by armstrongite. Where the replacement is by gittinsite, it is invariably accompanied by pore space, and, unlike at higher levels, quartz does not accompany gittinsite, *i.e.*, does not occupy the pore space. Salvi and Williams-Jones (1995b) have attributed the creation of porosity to silica-undersaturation of the altering fluid, and replacement of elpidite by a reaction of the type:



which has a large negative  $\Delta V$  (65% volume reduction). The local formation of armstrongite is explained by a low water/rock ratio wherein the activity of silica in the fluid was buffered by the rock. Below ~80 m rocks only show evidence of the first alteration event, *i.e.*, the replacement of arfvedsonite by aegirine, and elpidite is the only zirconosilicate mineral.

## Chemical Changes During Alteration

### Introduction

In order to evaluate the chemical changes during alteration, *i.e.*, determine the masses of material added and/or removed to or from the rock, and establish whether the hydrothermal processes that caused alteration could have been responsible for concentrating the HFSE, we compared the chemical compositions of altered and fresh rock samples of otherwise equivalent lithologies.

Major and most trace elements, including the REE, were analysed by X-ray fluorescence in the Geochemical Laboratories of the Department of Earth and Planetary Sciences of McGill University. Analysis of Zr required setting up a special calibration routine, because of the unusually high amounts of this element in the Strange Lake rocks. Detection limits are 100 ppm or less for major elements and 1 ppm for trace elements other than IREE and HREE. The analyses for the IREE and HREE are semi-quantitative, and their detection limit is 20 ppm. Be, Li and F were analysed by ACME<sup>®</sup> Analytical Laboratories Ltd. in Vancouver, B.C. Beryllium was analysed by induced coupled plasma-mass spectrometry, Li by atomic adsorption spectrometry and F using a specific ion-sensitive electrode. Rock pulp samples were treated by multi-acid digestion for Be and Li, and by NaOH fusion for F. Detection limits for these analyses are 100 ppm for F, and <0.1 ppm for Be and Li.

With the exception of four samples from surface, all material was selected from drill core. In addition, because of the relatively large sizes of many of the HFSE-bearing minerals, and because of evidence of flow differentiation, the drill core samples used in mass balance calculations consisted of composites of at least one and commonly several metres of continuous drill core to avoid bias because of local heterogeneities (Table 2).

The results of whole-rock major and trace element analyses for the outcrop and composite drill-core samples are presented in Table 3, except for the REE which are

presented in Table 4. In addition, analyses for all elements in 10 hand-samples from DDH SL-182 are given in Appendix 4.

### **Description of Lithologies**

The chemical changes that may have accompanied early alteration, *i.e.*, the replacement of arfvedsonite by aegirine, were evaluated using two unaltered/altered sample pairs (38-B-1, 38-B-2; and 38-B-4, 38-B-5) collected away from the zones affected by the later alteration (Fig. 1). All these samples are from outcrops of the least evolved subsolvus granite, located near the contact with hypersolvus granite in the southern part of the pluton. The rocks are medium to coarse grained, and contain phenocrysts of microcline; quartz, albite and arfvedsonite make up the remaining major mineralogy. In addition, all samples contain small proportions of dalyite and fluorite. The only differences that we could discern between fresh and altered samples were that, in the latter, arfvedsonite had been partially or completely replaced by aegirine, and the feldspars were cloudy. Based on visual estimates, the fresh samples contain about 10 volume % arfvedsonite.

Identifying equivalent samples that had undergone the later alteration was not as straight forward. Although there are relatively few map units in Figure 1, there are numerous small, local variations in primary lithology, especially within subsolvus granite near the centre of the pluton, *i.e.*, the most altered part. We could not, therefore, simply compare samples from unaltered and altered units in outcrop, but had to depend entirely on carefully logged drill core. Fortunately, as mentioned above, the intensity of the later alteration diminishes with depth, and thus, in the case of deeper drill holes, it was possible to find rocks unaffected by alteration, which in terms of primary textures, were indistinguishable from intensely altered rock in the hole.

Chemical changes that may have accompanied the later alteration were evaluated using composite samples from diamond drill holes SL-140, SL-146 and SL-182. These drill holes contain one or more of at least three different subsolvus granitic units plus several

**Table 2**

*Locations and the zirconium mineralogy of rock samples chemically analysed and employed in calculations of mass changes during alteration.*

label	sample#	depth(m)	granite type	alteration	dominant Zr-mineral
B1	38-B-1	<i>outcrop</i>	subsolvus*	<i>fresh</i>	dal
B2	38-B-2	<i>outcrop</i>	subsolvus*	<i>fresh</i>	dal
B4	38-B-4	<i>outcrop</i>	subsolvus*	early	dal
B5	38-B-5	<i>outcrop</i>	subsolvus*	early	dal
A	SL-182	81.4 - 85.7	porphyritic	<i>fresh</i>	elp
B	SL-182	56.9-57.9	equigranular	late	elp + arm + git
C	SL-182	37.0 - 41.0	porphyritic	late	elp + arm + git
D	SL-182	6.2 - 15.5	porphyritic	late	git (+qtz)
E	SL146	97.6-106.5	porphyritic	<i>fresh</i>	elp
F	SL146	74.0-82.0	porphyritic	late	git (+qtz)
G	SL146	56.0-59.7	transitional	late	git (+qtz)
H	SL146	3.4-13.0	transitional	<i>fresh</i>	elp
I	SL140	95.6-104.8	transitional	<i>fresh</i>	elp
J	SL140	21.7-26.5	transitional	late	git (+qtz)

\* : least evolved subsolvus granite

**Table 3***Contents of major oxides and selected minor elements in outcrop and composite drill core samples.*

		Outcrop Samples				SL-182				SL-146				SL-140	
		B1	B2	B4	B5	A	B	C	D	E	F	G	H	I	J
SiO <sub>2</sub>	wt%	71.72	70.73	71.28	71.56	70.04	74.70	71.06	69.97	70.98	69.39	69.46	69.40	70.88	70.74
TiO <sub>2</sub>		0.24	0.25	0.22	0.22	0.38	0.54	0.37	0.35	0.32	0.42	0.47	0.52	0.35	0.34
Al <sub>2</sub> O <sub>3</sub>		11.49	11.42	10.73	10.84	9.56	7.30	9.29	9.44	10.09	9.51	8.68	8.97	8.37	8.76
Fe <sub>2</sub> O <sub>3</sub>		5.29	5.59	6.66	6.24	5.61	3.49	6.23	5.67	5.41	6.02	4.52	5.13	4.68	4.46
MnO		0.09	0.11	0.12	0.10	0.15	0.14	0.15	0.15	0.15	0.17	0.12	0.15	0.18	0.17
MgO		0.00	0.00	0.00	0.01	0.02	0.00	0.01	0.40	0.16	0.49	0.72	0.44	0.21	0.62
CaO		0.49	0.73	0.71	0.68	0.97	0.90	0.88	1.74	0.89	1.70	2.31	1.57	1.00	1.82
Na <sub>2</sub> O		5.32	5.31	5.10	5.29	4.97	3.96	4.97	4.17	4.80	3.85	2.57	3.26	3.88	3.12
K <sub>2</sub> O		4.68	4.54	4.57	4.72	4.14	3.75	3.89	4.16	4.48	4.46	4.42	3.86	4.14	4.39
P <sub>2</sub> O <sub>5</sub>		0.02	0.02	0.02	0.02	0.01	0.02	0.01	0.01	0.02	0.02	0.00	0.01	0.02	0.00
BaO	ppm	29	74	35	21	48	72	46	63	52	101	96	114	265	115
Cr <sub>2</sub> O <sub>3</sub>		0	2	0	2	12	18	17	22	0	0	0	0	0	nd
LOI	wt%	0.37	0.51	0.55	0.50	1.06	1.39	0.79	0.91	0.74	1.18	1.35	1.31	1.80	0.99
<b>Total</b>		99.71	99.21	99.96	100.18	96.91	96.19	97.65	96.97	98.04	97.21	94.62	94.62	95.51	95.41
F	ppm	5400	6100	6200	5400	5800	3600	6000	7400	4000	7600	5200	7000	3400	2500
Be		39	53	18	10	161	215	118	126	175	226	218	152	401	336
Li		162	182	215	136	215	176	220	215	236	224	195	178	202	138
Y	ppm	550	618	538	240	1868	1850	1414	1716	1652	1934	2658	2259	2254	2830
Zr		2583	1111	2732	990	12328	19686	9885	13659	10116	11594	22818	16600	19375	19647
Nb		257	331	184	205	1147	1725	832	891	952	1160	1450	2200	1350	1700
Ga		44	40	41	43	47	45	49	47	40	35	38	42	40	37
Pb		161	162	126	153	237	418	311	342	549	482	441	426	804	198
Th		63	73	nd	nd	289	282	172	252	229	284	342	507	322	403
U		nd	nd	nd	nd	130	177	100	128	nd	nd	nd	nd	nd	nd
Rb		410	422	430	458	735	905	706	759	771	781	879	902	869	998
Sr		102	115	100	53	343	329	266	313	297	359	487	478	403	482
Co		42	49	55	58	19	27	14	21	41	43	62	59	55	67
Cu		49	131	37	98	nd	nd	nd	nd	60	0	28	nd	29	nd
Ni		7	3	0	0	29	9	10	12	9	7	7	5	11	12
Sc		7	0	2	7	3	0	0	0	6	2	0	0	1	4
V		17	17	14	7	14	19	15	11	15	11	15	14	16	17
Zn		467	518	519	368	1218	1064	1097	1175	1228	1354	1114	1051	1621	1098

pegmatites. The granite types are: a porphyritic granite, which is characterised by phenocrysts of arfvedsonite and interstitial elpidite, a fine- to medium-grained equigranular granite in which elpidite forms euhedral crystals, and a medium-grained granite which, both in terms of grain size and habit of elpidite, is transitional between the other two granite types, *i.e.*, it is medium-grained but contains the odd arfvedsonite phenocryst, and displays interstitial as well as subhedral-euhedral habits of elpidite. The three granite types form discrete sub-horizontal units and have gradational contacts. On the basis of the habit of elpidite in these rocks, porphyritic granite is interpreted to have crystallised first followed by the transitional and equigranular varieties. The last named rock type was intersected in only one of the three holes studied (SL-182), where it occurs over a relatively narrow interval (15 m), and is cut by several subhorizontal pegmatite dykes. For this reason we focused our study on units of the porphyritic and transitional granites.

Despite their textural differences, the granites discussed above are very similar in their mineralogy. They contain quartz, two alkali feldspars, arfvedsonite ( $\pm$ aegirine), zirconosilicates (mainly elpidite and/or gittinsite), plus minor amounts of fluorite, titanite-fluorite-quartz pseudomorphs after narsarsukite, pyrochlore, thorite, bastnäsitite, and other exotic minerals (Table 1). The locations of the drill holes are shown in Figure 1, and the locations of the samples within the drill holes are illustrated in Figure 2 and listed in Table 2.

### **Chemical Compositions of Unaltered Rocks**

Silica is the most abundant oxide in the fresh rocks, comprising about 70% of each sample by weight. Alumina makes up between 8 and 10 wt.% of the rock in the drill core samples, but around 11 wt.% in the surface samples. The sum of  $K_2O$  and  $Na_2O$  has a similar distribution, *i.e.*, 7 to 9 wt.% in the core samples and ~10 wt.% in outcrop samples. However, the proportions of  $K_2O$  and  $Na_2O$  are approximately equal in both sample suites. The content of  $Fe_2O_3$  is essentially the same in core and outcrop samples at roughly 5 wt.%. Other major oxides make up <0.5 wt.% of the rock, except for  $CaO$  which generally has a content of about 1 wt.%. The most important of the trace elements is Zr which constitutes

FIGURE 2

Logs of drill holes SL-140, SL-146 and SL-182, depicting the geology, predominant Zr minerals and intensity of alteration. The bars, A to J, indicate the lengths and locations of the composite samples.

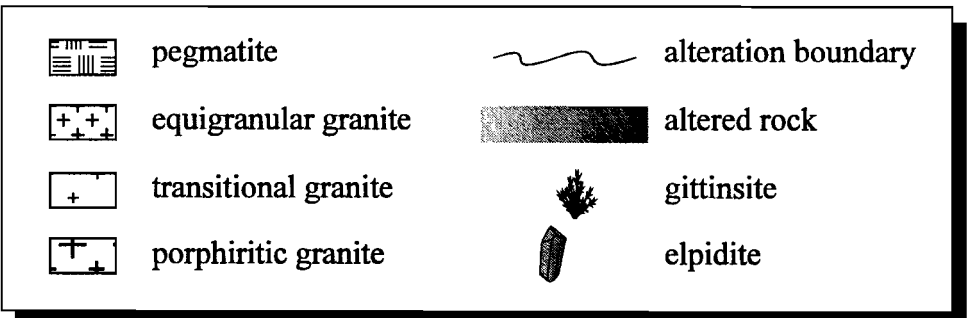
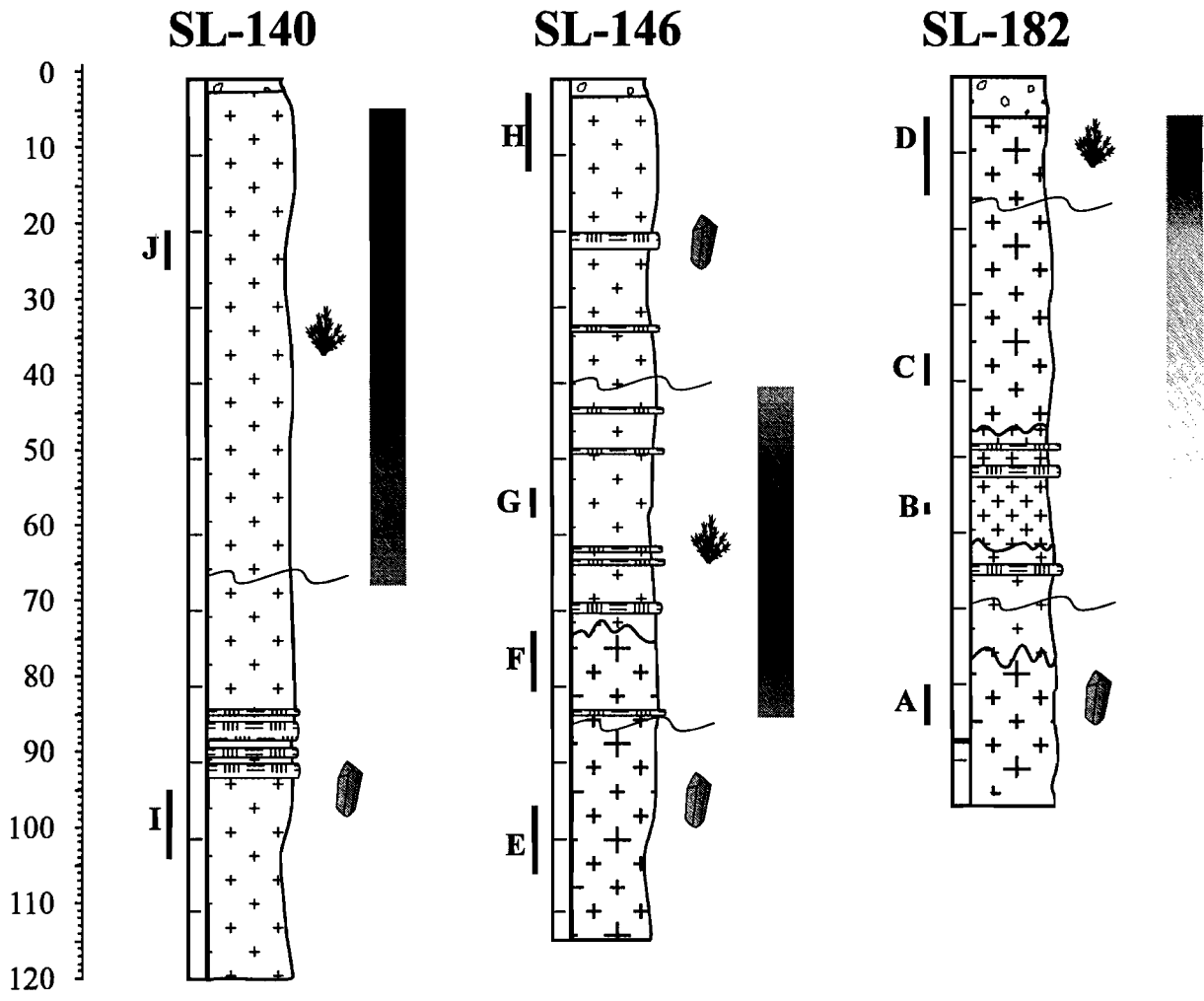


**Table 4***Contents of REE and selected trace elements in outcrop and drill core samples.*

	Outcrop Samples				SL-182				SL-146				SL-140	
	B1	B2	B4	B5	A	B	C	D	E	F	G	H	I	J
<b>La</b>	nd	nd	nd	nd	795	nd	935	1020	773	948	762	nd	797	834
<b>Ce</b>	516	791	448	402	1836	1312	1863	1698	1628	1750	1729	1399	1822	1862
<b>Nd</b>	nd	nd	nd	nd	774	641	738	734	898	918	970	690	958	1100
<b>Sm</b>	nd	nd	nd	nd	nd	nd	nd	nd	nd	307	nd	nd	nd	nd
<b>Gd</b>	nd	nd	nd	nd	nd	nd	nd	nd	nd	nd	111	nd	nd	117
<b>Dy</b>	nd	nd	nd	nd	390	nd	nd	nd	nd	449	10	498	nd	408
<b>Ho</b>	nd	nd	nd	nd	nd	nd	nd	nd	nd	nd	nd	10	nd	10
<b>Er</b>	nd	nd	nd	nd	nd	nd	nd	nd	nd	nd	nd	221	nd	115
<b>Tm</b>	nd	nd	nd	nd	nd	nd	nd	nd	nd	nd	nd	nd	nd	nd
<b>Yb</b>	nd	nd	nd	195	nd	296	nd	nd	148	156	25	22	17	189
<b>Lu</b>	nd	nd	nd	nd	nd	nd	nd	nd	nd	nd	nd	nd	nd	nd
<b>As</b>	36	34	27	43	41	46	26	27	136	121	110	107	156	72
<b>Hf</b>	nd	115	75	nd	220	431	166	251	183	203	490	294	412	406
<b>Mo</b>	nd	nd	nd	111	2430	4220	1950	2850	nd	nd	nd	nd	nd	nd
<b>Sn</b>	nd	nd	nd	180	315	263	nd	nd	216	303	400	330	421	364
<b>Ta</b>	nd	nd	nd	nd	nd	309	nd	nd	nd	nd	nd	337	307	333
<b>W</b>	161	173	190	214	65	196	nd	nd	nd	nd	nd	nd	nd	nd

nd : not detected

up to 2 wt.% of the rock in core samples, but is about an order of magnitude less abundant in the outcrop samples. Niobium, Y and the REE, although less abundant, show similar distributions. The only other important trace element is F which occurs in amounts of up to 0.8 wt.%, although higher values have been reported elsewhere in the complex (*e.g.* Boily and Williams-Jones, 1994).

Among the drill core samples, the equigranular granite (only an altered equivalent of this rock has been analysed) has the highest SiO<sub>2</sub>, Zr and Nb contents and the lowest contents of Al<sub>2</sub>O<sub>3</sub> and Fe<sub>2</sub>O<sub>3</sub>. In other respects it is compositionally similar to porphyritic and transitional granite. The last named granite is intermediate in composition, with respect to the other two granites, in terms of Zr, Nb, Al<sub>2</sub>O<sub>3</sub> and Fe<sub>2</sub>O<sub>3</sub>, and has a lower alkali content than the porphyritic granite (the alkali content of the equigranular granite is similarly low, but this could conceivably be an artefact of alteration; see below). The REE are more abundant in the transitional and equigranular granites than in the porphyritic granite.

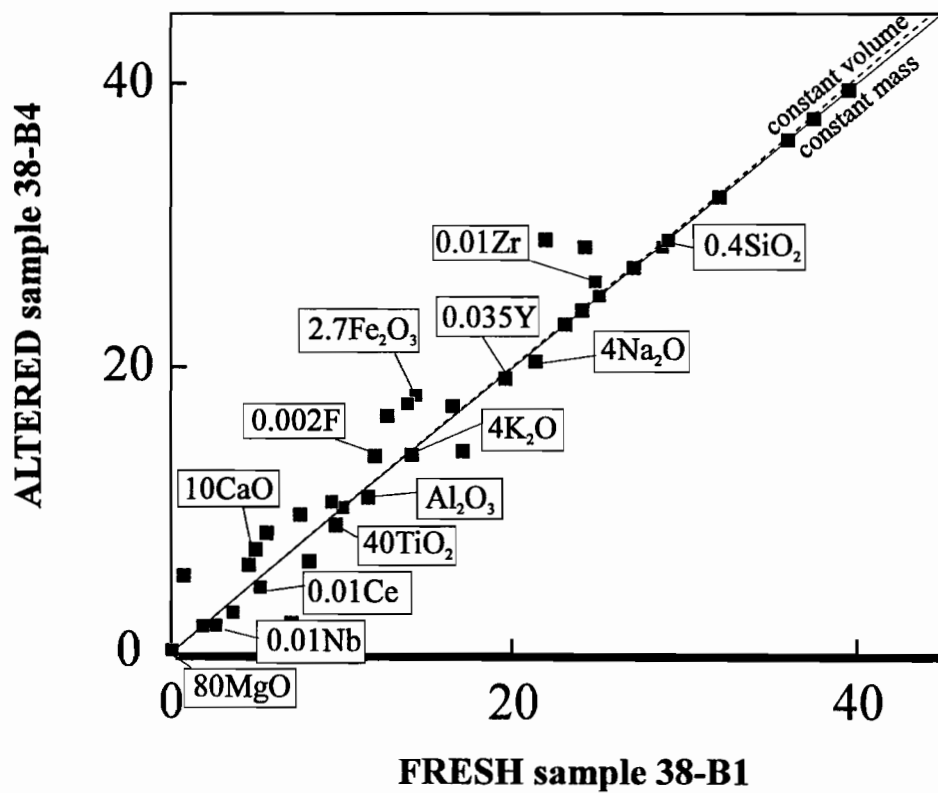
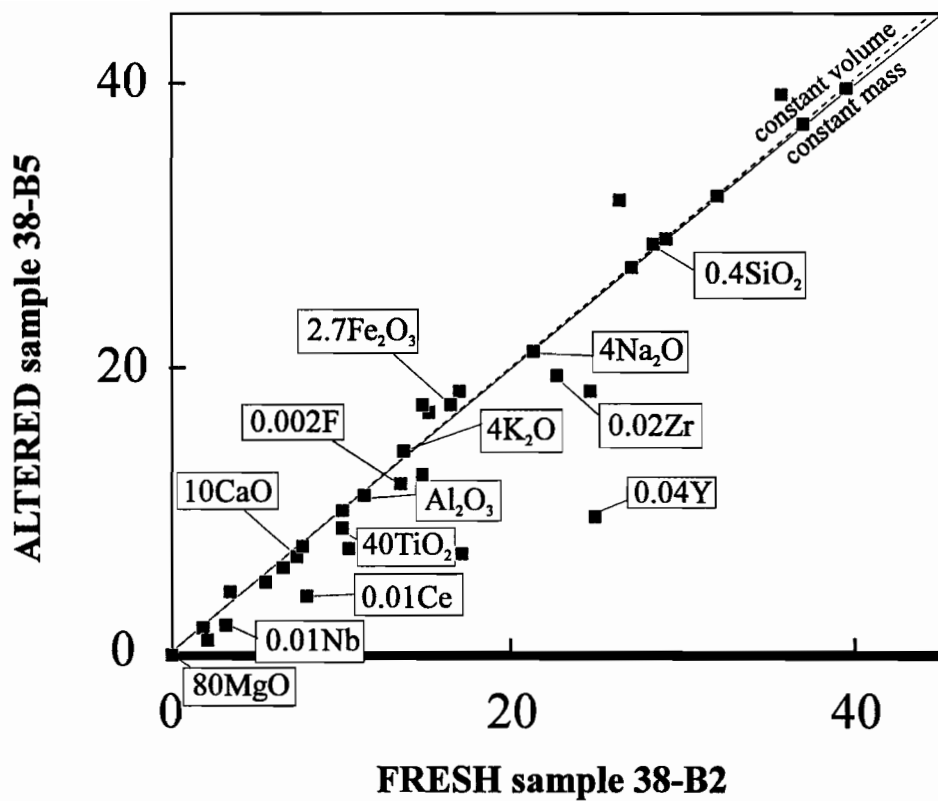
### **Metasomatic Changes in Composition**

Owing to the fact that hydrothermal alteration is commonly accompanied by mass and/or volume changes, it is necessary to identify one or more immobile elements to use as an index of comparison in order to determine which elements have been added to or lost from the rock. The method of identifying these immobile elements which seems best suited to this study, given the number of samples and high degree of primary heterogeneity, is that of Grant (1986), which involves a pairwise graphical comparison of the compositions of altered and unaltered rocks. Elements that have not been gained or lost by the rock, *i.e.*, which are immobile, should define a line (isocon) passing through the origin, the slope of which represents the ratio of the masses of the altered to the fresh rock; a slope of 1 indicates that there has been no mass change, whereas higher or lower slopes imply a gain or loss of mass, respectively (or loss or gain of volume, respectively).

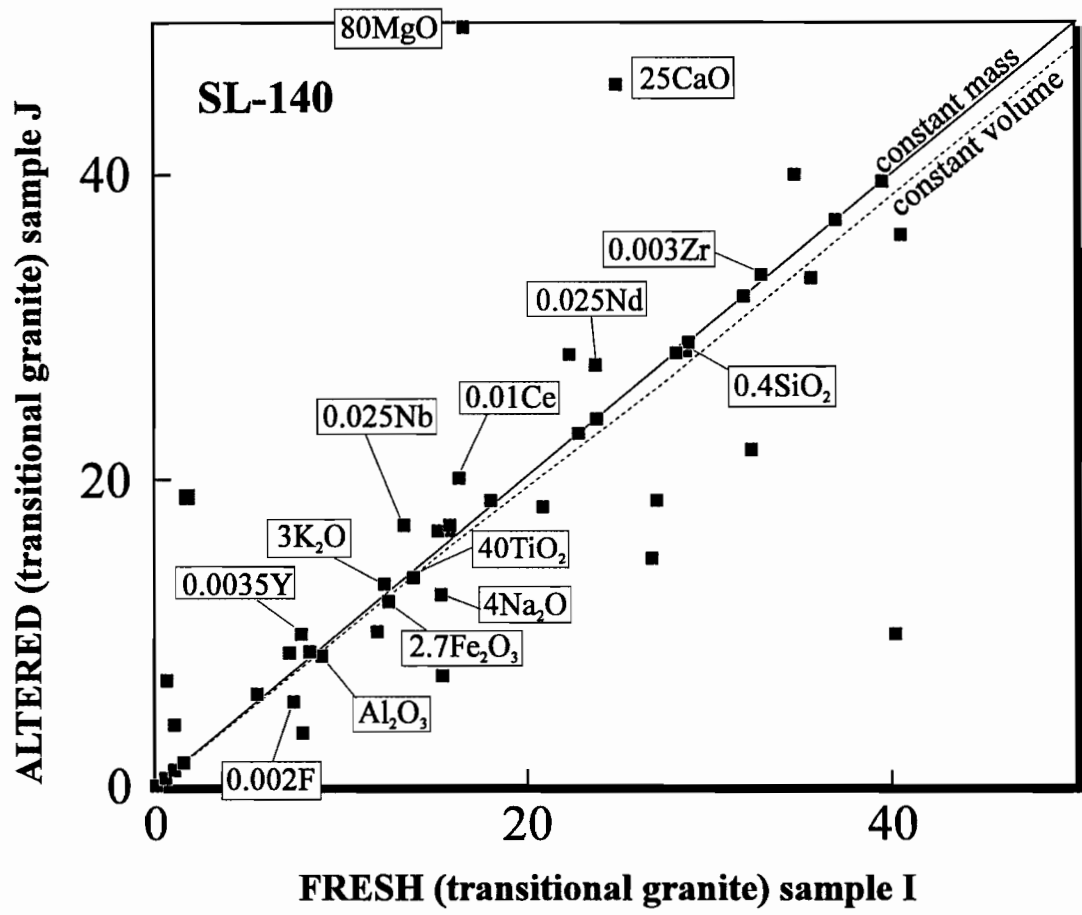
The isocons (lines from the origin passing through or closest to the greatest number

FIGURE 3

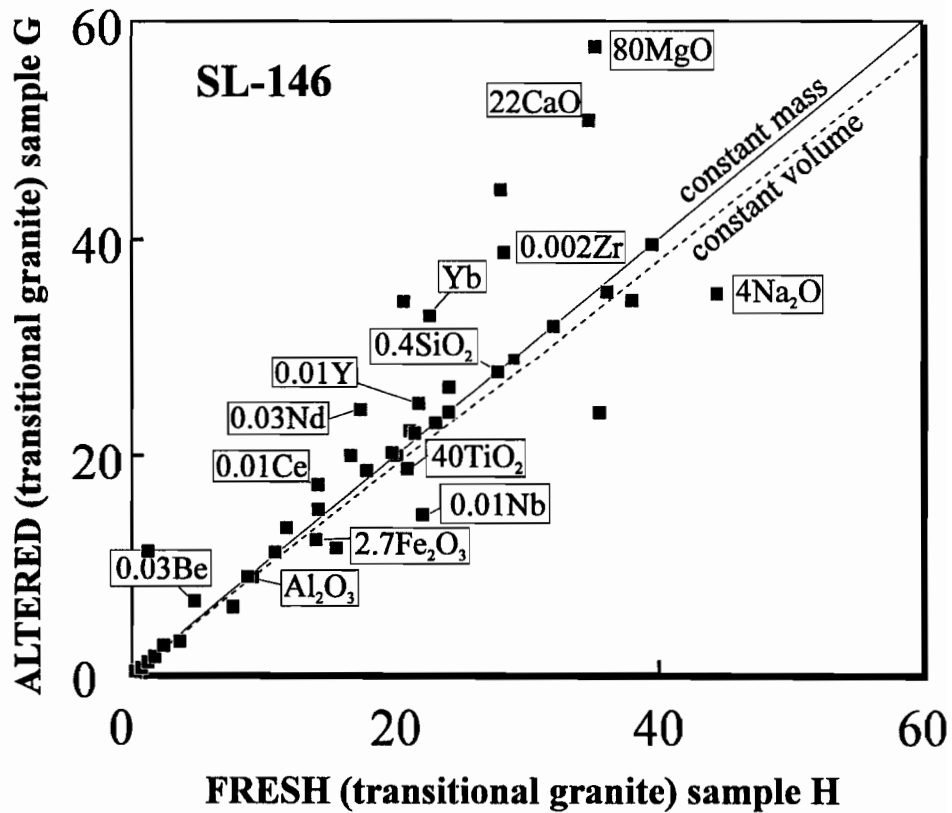
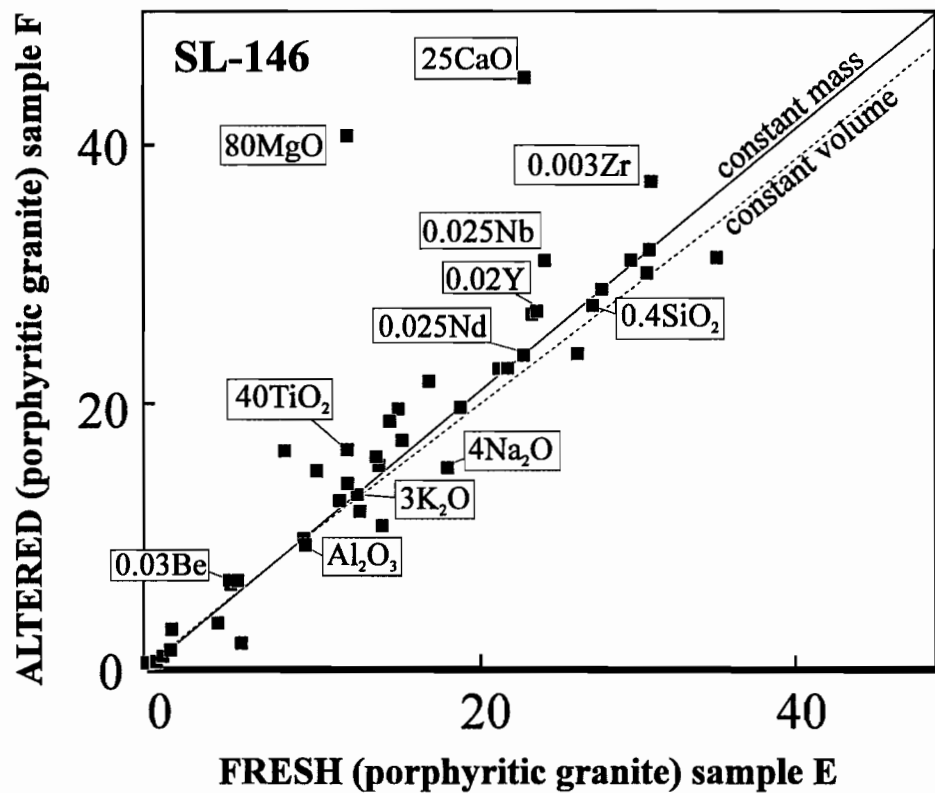
Isocon diagrams comparing the chemistry of rock subjected to early alteration with fresh rock, in outcrop samples (A), and rock subjected to later alteration with equivalent fresh rock, in composite core samples from diamond drill holes SL-140 (B), SL-146 (C), and SL-182 (D). The locations of the samples are indicated in Figures 1 and 2. Also shown are lines representing zero mass change (solid line) and constant volume (dashed line), calculated from the mass and density of the rocks. For clarity, only the major and most important trace elements are labelled.



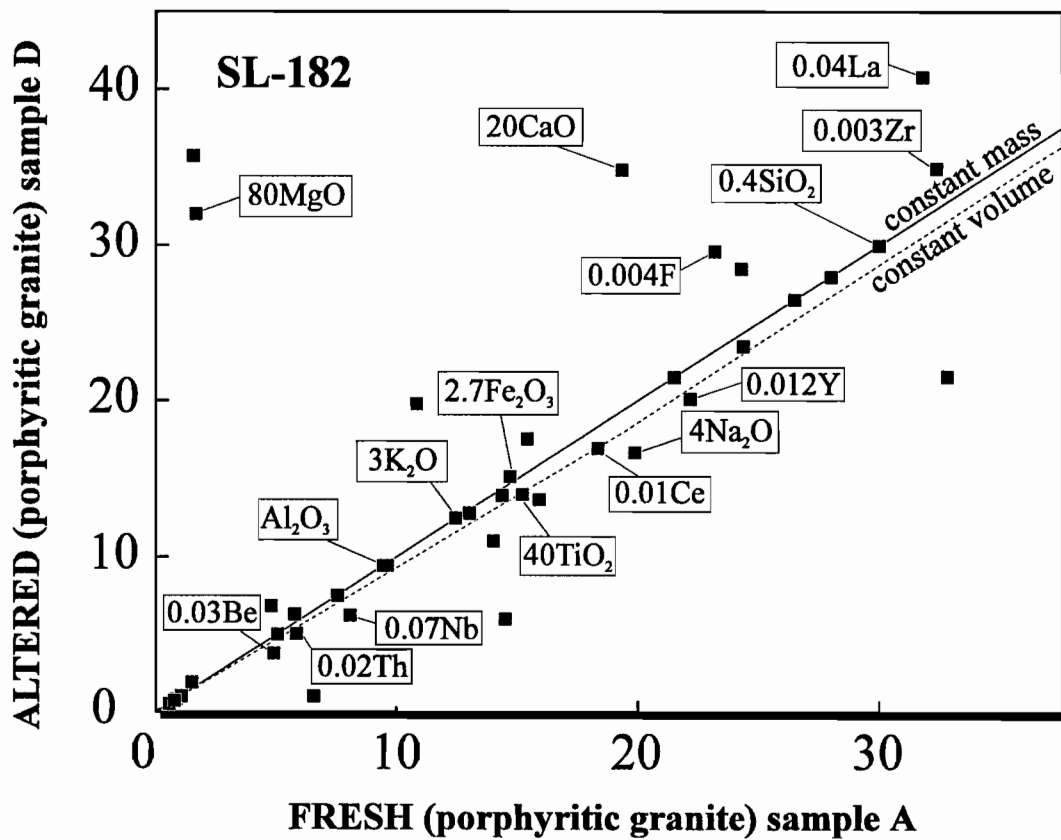
A



**B**



C



**D**

of elements) for the two pairs of samples representing early alteration (38-B-1, 38-B-2; and 38-B-4, 38-B-5) both have slopes of 1, indicating that the early alteration occurred without an overall change in the mass of the rock (Fig. 3A). Furthermore, all major elements, including the alkalis, and most trace elements plot on or close to the isocons, which suggests that this alteration was isochemical and that, as discussed above, the conversion of arfvedsonite to aegirine probably occurred as a result of H<sub>2</sub>O-mediated oxidation. Significantly, however, Zr, Y and several of the REE are depleted in 38-B-2 relative to its unaltered equivalent, 38-B-1.

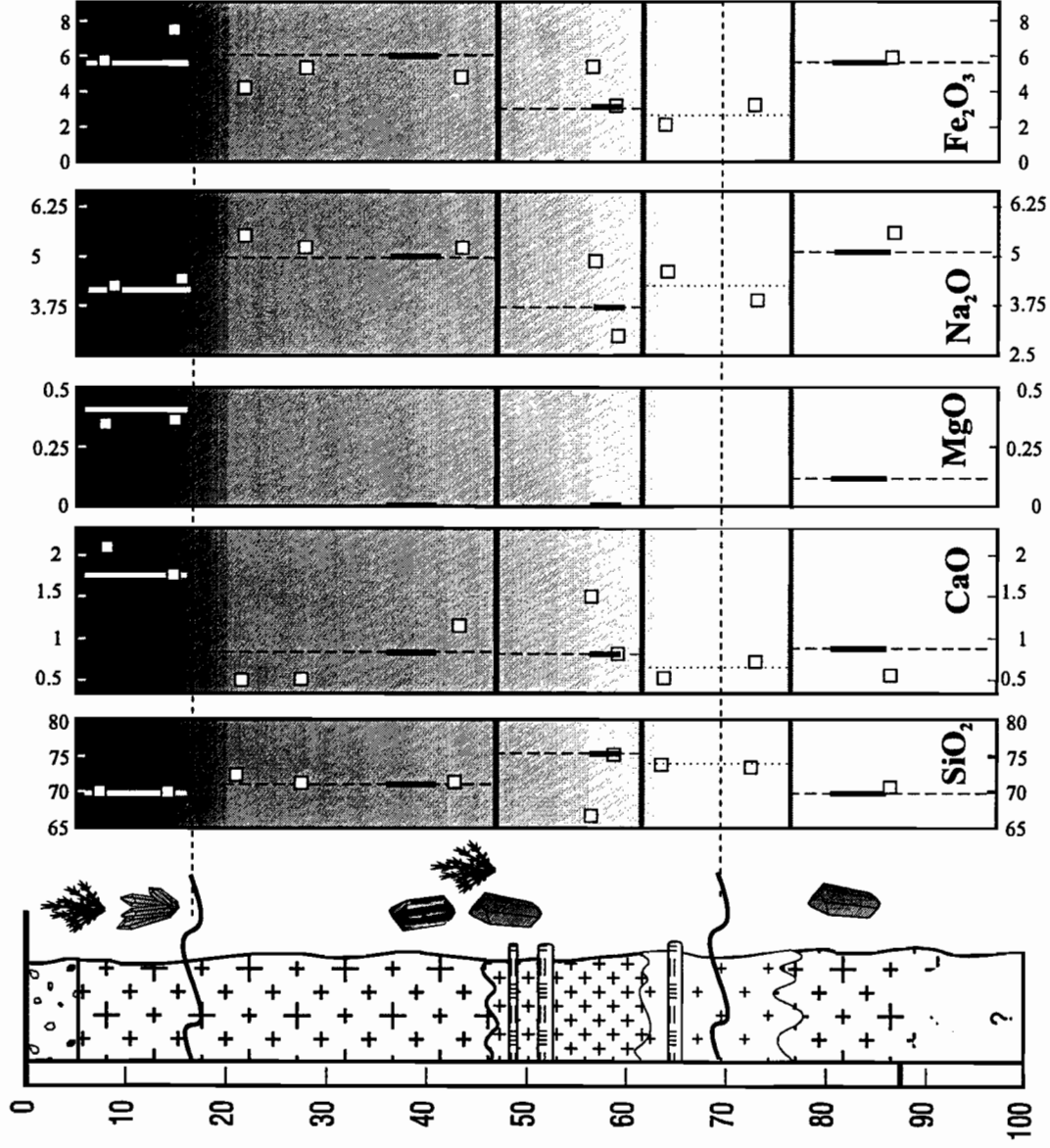
There is much greater scatter of data on the isocon diagrams for the sample pairs representing the later alteration (Figs. 3B to D; see Fig. 2 for sample locations). Nonetheless, in all cases, the isocons have slopes of approximately 1, indicating that this alteration too, occurred without a change in the overall mass of the rock. Interestingly, silica is the only major element oxide that plots on the isocon of all sample pairs. This largely reflects the very high abundance of this oxide, and thus the need for very large exchanges in mass between fluid and rock in order to produce an appreciable change in the proportion of silica in the altered rock. Given the relatively low solubility of most silicate minerals in hydrothermal solutions, particularly at low temperature, the latter would require extremely high water/rock ratios. The other important conclusions that can be drawn from these isocon diagrams are that Ca and Mg were consistently added to the rock during later alteration, Na was consistently removed and that, in many cases Zr, was added (Figs. 3B to D).

In view of the fact that mass was conserved during alteration, *i.e.*, that no correction needs to be applied to the data, we can investigate the relative importance of igneous processes and alteration in controlling the composition of rocks subjected to the second alteration by plotting the abundance of selected elements along the drill logs (Fig. 4). As mentioned above, the three types of granites have different primary compositions. However, some of the changes in chemical composition cannot be attributed solely to changes in rock type. In SL-182, the content of CaO is consistently low irrespective of rock type or alteration, except in altered porphyritic granite at the top of the hole, where gittinsite is the only zirconium mineral and porosity is filled by quartz (Fig. 4A). The behaviour of MgO is

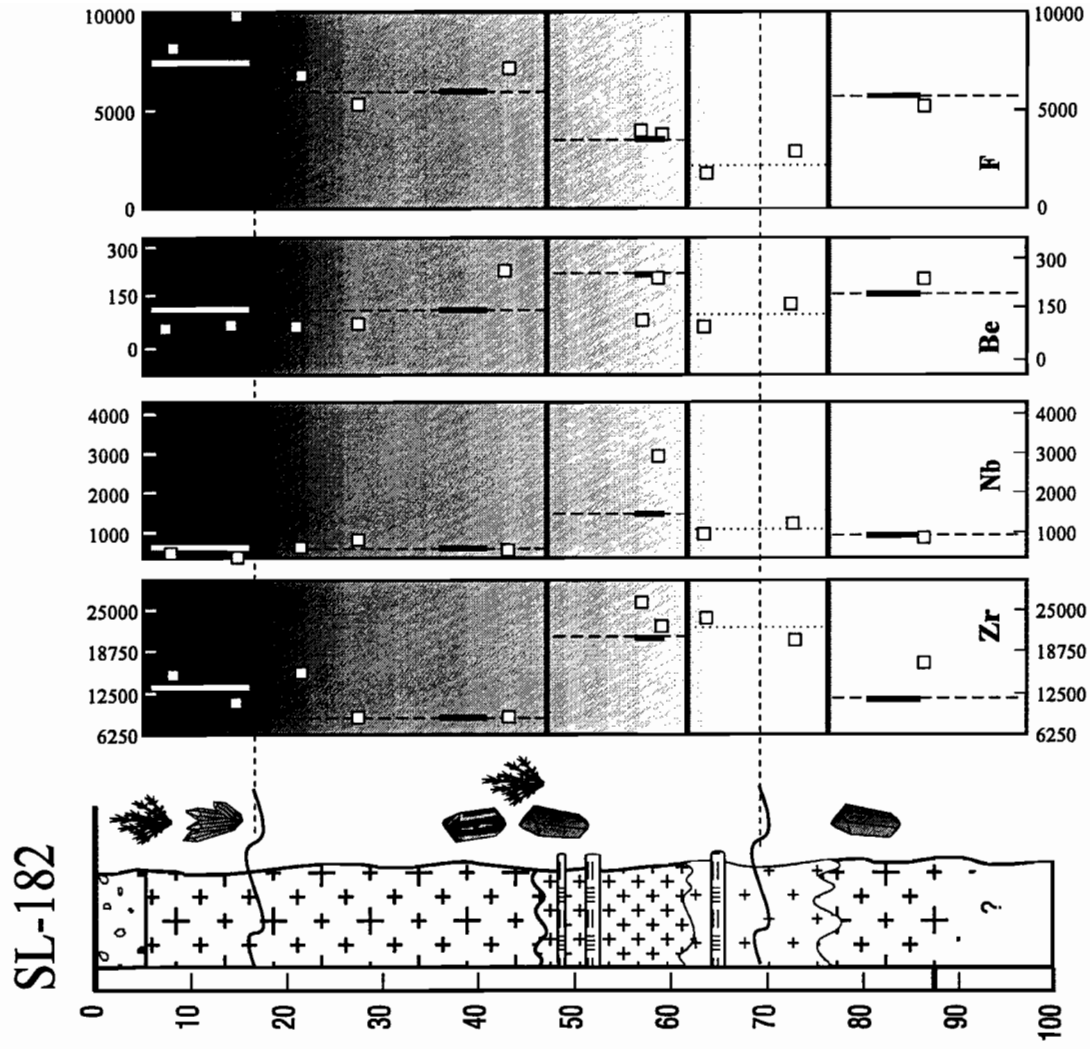
FIGURE 4

Logs of drill holes SL-182 (A to C) and SL-146 (D to F) showing the proportions of selected major oxides and trace elements. The intervals of the composite samples are represented by heavy bars, dashed lines represent extrapolated values within the same lithological/alteration interval. The thick horizontal lines match the changes in lithology and the intensity of the shading represents the degree of alteration. The squares in SL-182 represent compositions of hand-samples.

SL-182

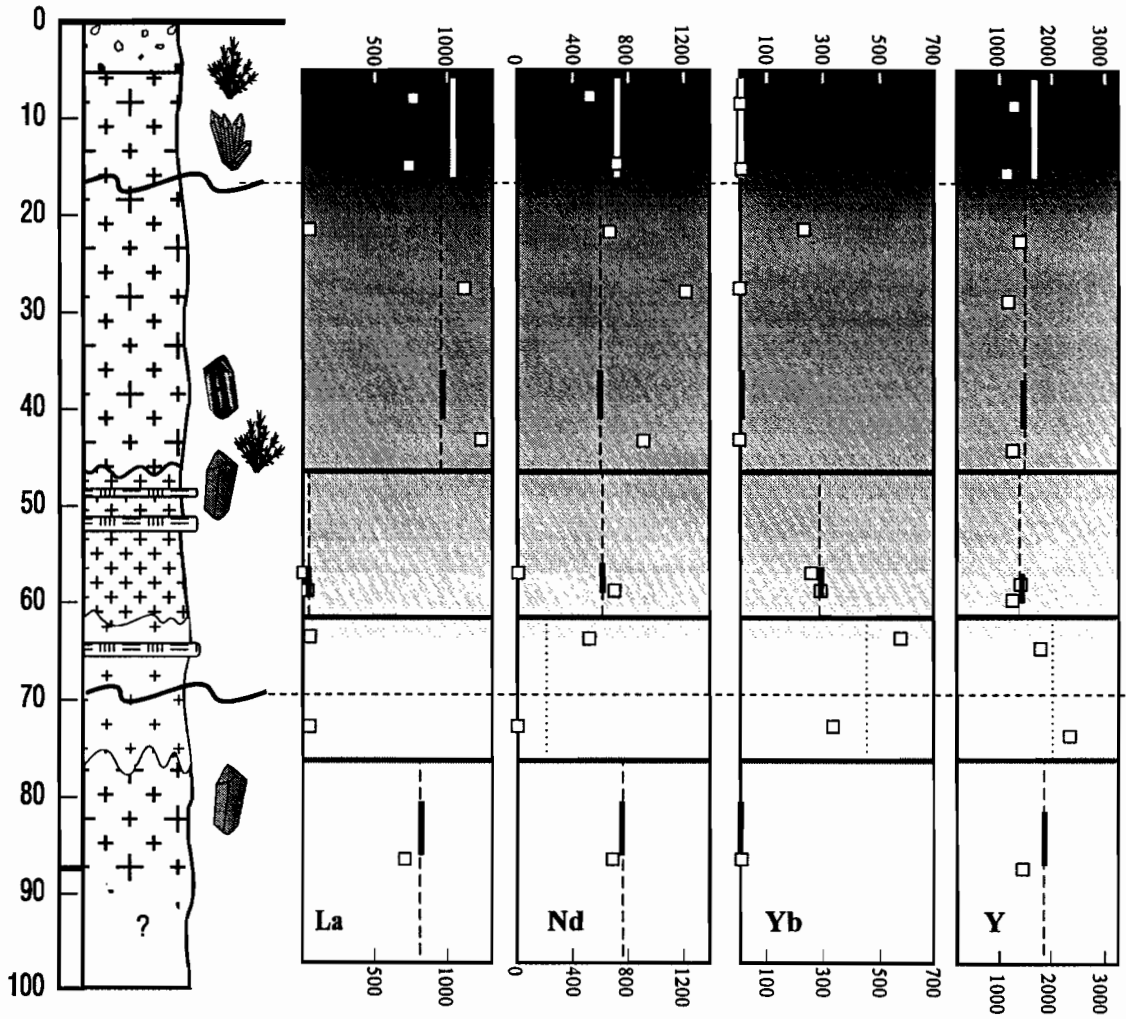


A



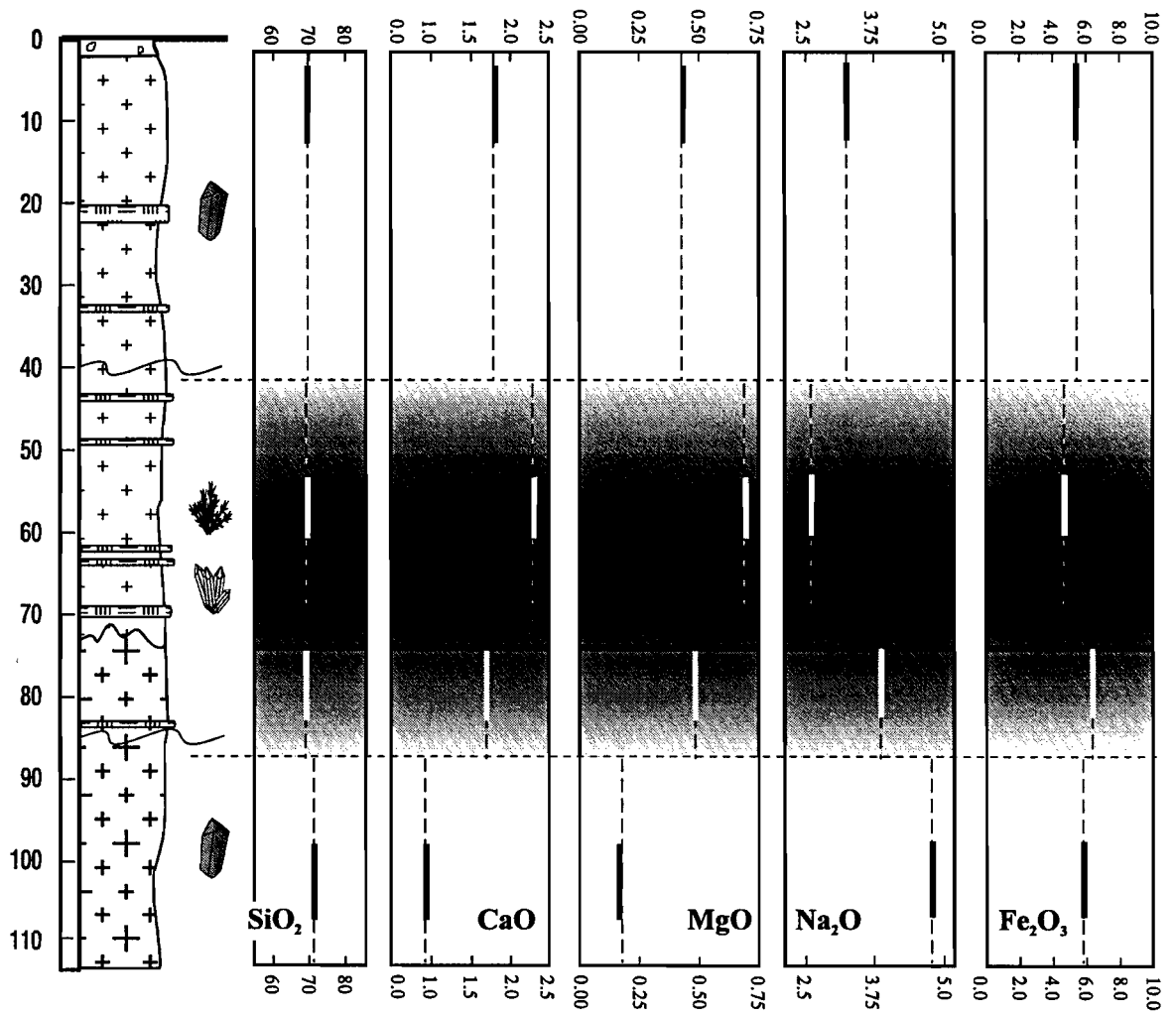
**B**

# SL-182



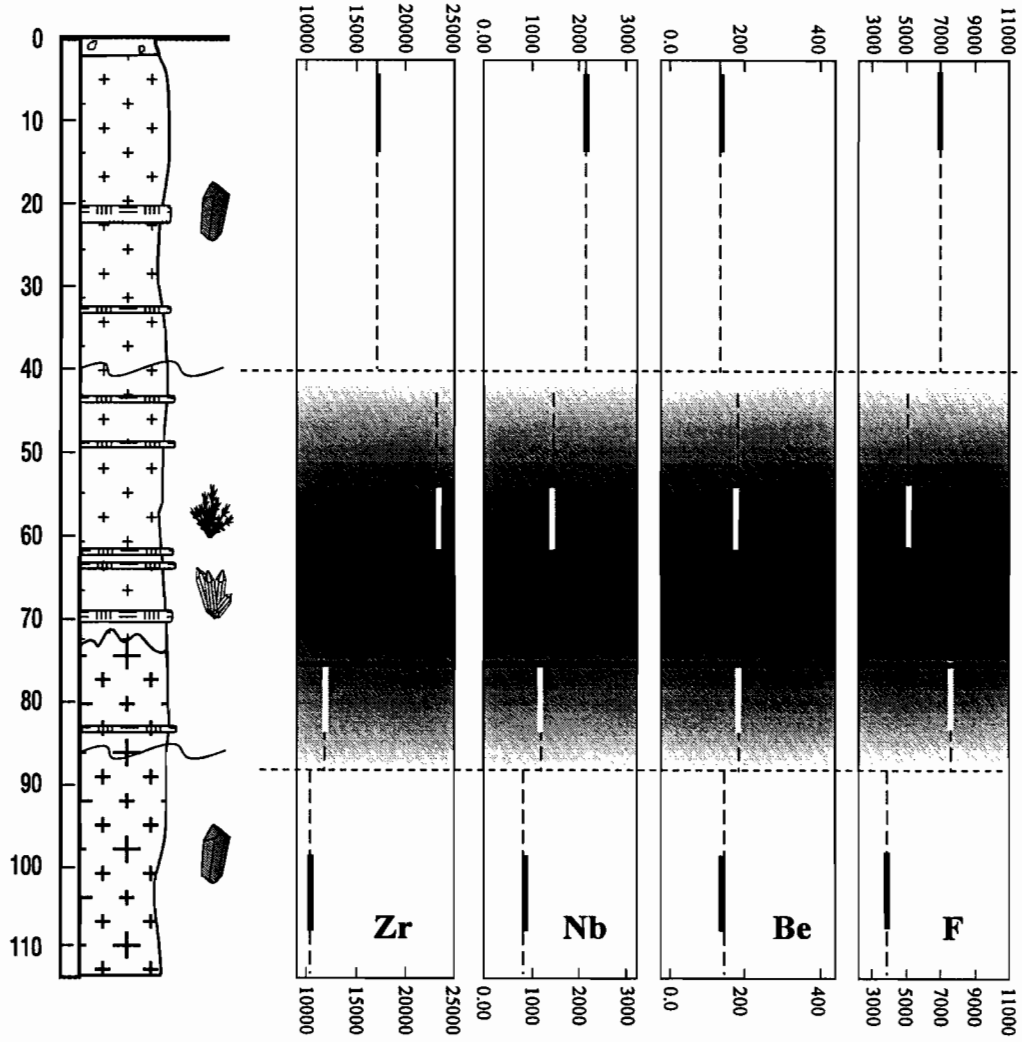
C

# SL-146



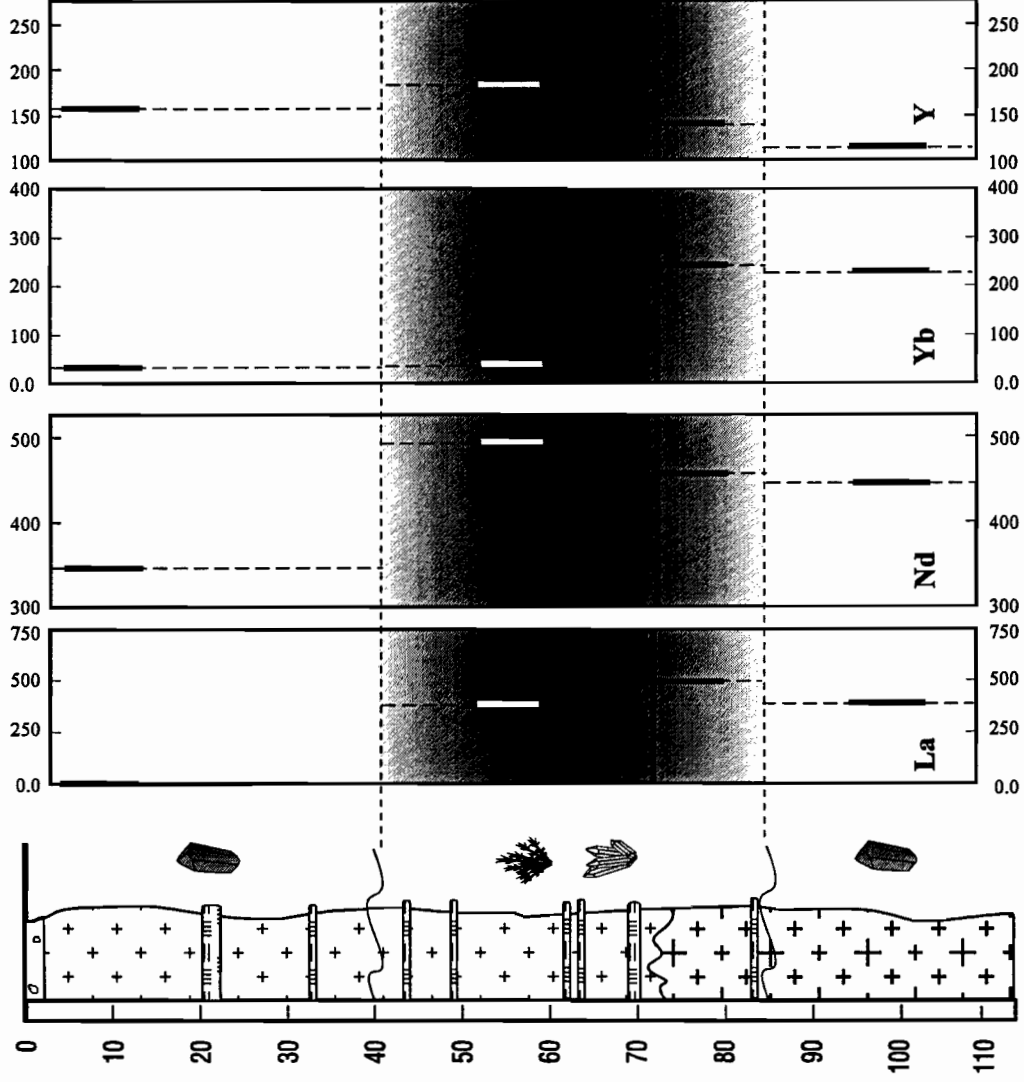
D

# SL-146



# E

SL-146



F

similar. By contrast,  $\text{Na}_2\text{O}$  is depleted in the porphyritic granite at the top of the hole, but only relative to other altered and unaltered porphyritic granite. These patterns are repeated in the profile for SL-146, in the alteration of both porphyritic and transitional granites (Fig. 4D), and in transitional granite of SL-140 (profile not shown). Other major elements display minor and inconsistent variations with alteration. Among the HFSE, only Zr displays entirely consistent behaviour with alteration. Its content in all three holes (SL-140, SL-146, and SL-182) increases significantly in both porphyritic and transitional granite, from fresh granite to granite in which elpidite has been replaced by gittinsite plus quartz (Figs. 4B and E). However, in hole SL-182, where the zone of gittinsite plus quartz alteration overlies a porous zone containing armstrongite and/or gittinsite without quartz after elpidite, the content of this element decreases slightly below its level in the fresh rock (Fig. 4B), *i.e.*, the zone of Zr enrichment at the top of the hole appears to be preceded by one of depletion. The content of Nb also increases with alteration in SL-140, and SL-146 for both porphyritic and transitional granite, but decreases in the two altered zones of porphyritic granite in SL-182, relative to unaltered porphyritic granite. Somewhat surprisingly, Ti does not vary significantly with alteration in any of the holes. The behaviour of the REE is quite variable (Figs. 4C and F). Lanthanum, increases in abundance with alteration in all three holes and for both porphyritic and transitional granite. In contrast to Zr, it does not display depletion in the porous zone, although its content in this zone is lower than that of the overlying gittinsite-plus-quartz alteration zone. Other LREE show inconsistent behaviour. Cerium and neodymium increase significantly with alteration in both rock types intersected in SL-146, and Nd with alteration in SL-140. Both elements show effectively no change with alteration in SL-182, and Ce no change with alteration in SL-140. Ytterbium, representing the HREE, undergoes a large increase with alteration in the transitional granite of SL-140. However, in SL-146 the changes are insignificant, and in SL-182, Yb is below detection in both altered and unaltered varieties of porphyritic granite. Yttrium, which is generally considered an analogue of the HREE, increases substantially with alteration in both SL-140 and SL-146. In SL-182, it is depleted in the porous alteration zone, but increases significantly in the overlying alteration zone, although not to its content in fresh porphyritic granite at the

bottom of the hole. The most important of the remaining trace elements are probably F and Be. Fluorine decreases with alteration in the transitional granites of SL-140 and SL-146, but increases strongly with alteration in the porphyritic granite of SL-146. In SL-182, its behaviour mimics that of Zr and Y, *i.e.*, it is depleted in the porous alteration zone and enriched in the gittinsite plus quartz alteration zone above it. Beryllium contents decrease with alteration in SL-140 and SL-182, but increase in SL-146.

Thus, in summary, it would appear that, although there were significant differences in the pre-alteration chemistry of the different granite types, particularly in the concentrations of Zr, Y and some of the REE, later alteration had the effect of adding significant Ca and Mg at the expense of Na, and generally enriching the gittinsite plus quartz alteration zone in Zr, Y and REE. Moreover, in the case of Zr and to a lesser extent Y, there is evidence from SL-182 that the source of enrichment may have been the underlying porous zone.

The qualitative conclusions summarised above are quantified in Figures 5A and B for hole SL-182 and in Figures 5C to E for SL-146 and SL-140. The addition of CaO ranges between 50 and ~90% of its original values, whereas MgO more than doubles its original content in most cases. The losses of Na represent ~20% of its content in the fresh rocks. About 20% of the Zr is lost in the porous section of SL-182, and 11% added in the most altered rock at the top of the hole; relative to the porous rock this represents an addition of nearly 40%. A similar increase of ~20 to 40% for this element is also observed in the alteration of both porphyritic and transitional granites in SL-146, whereas, in SL-140, Zr addition is <5%. As discussed above, the only other elements that behaved consistently with alteration are La and Y, which are added in proportions varying from 5 to 30% and 17 to 25%, respectively.

### **Normative Calculations and Mineralogical Variations**

The chemical composition of a rock can be used to obtain a normative composition based on the minerals that are present in the sample by solving the matrix equation:

$$A \cdot X \approx B,$$

where  $A$  is the matrix containing the stoichiometry of the elements in each mineral,  $B$  is the matrix containing the molar proportions of the elements obtained from whole rock analyses, and  $X$  is the desired matrix of the molar abundances of each mineral (e.g. Bölke, 1989). The matrix is solved by linear least squares regression (Spear *et al.*, 1982). Weight and volume percentages are obtained using the molecular weights and the densities of the minerals, respectively.

Normative compositions were calculated for the outcrop samples and the composites from SL-146 and SL-182, using the analyses reported in Tables 3 and 4. Representative microprobe analyses for selected minerals in the holes are given in Appendix 5, and compositions for the zirconsilicates are given in Appendix 3. For the minerals not listed in these appendices, the compositions were assumed to be stoichiometric (see Table 1 for some of the more exotic minerals).

The normative mineralogy obtained in this manner for the outcrop samples representing the early alteration is reported in Table 5. The compositions of the two fresh samples are very similar, except for the absence of pyrochlore in 38-B-2. The abundance of HFSE-bearing minerals is low in these rocks, as is expected from the whole-rock chemical data. Arfvedsonite makes up ~10% by volume of the fresh rocks. The most striking change that occurred with alteration was the formation of 3.5 to 4.5 volume % aegirine and a decrease in arfvedsonite by the same amount. Excess iron produced during this alteration also led to the formation of 0.5 to 1.5 volume % magnetite. The only other significant changes with alteration were minor increases and decreases, respectively, in the contents of quartz and albite.

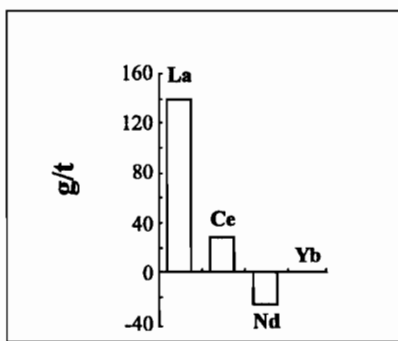
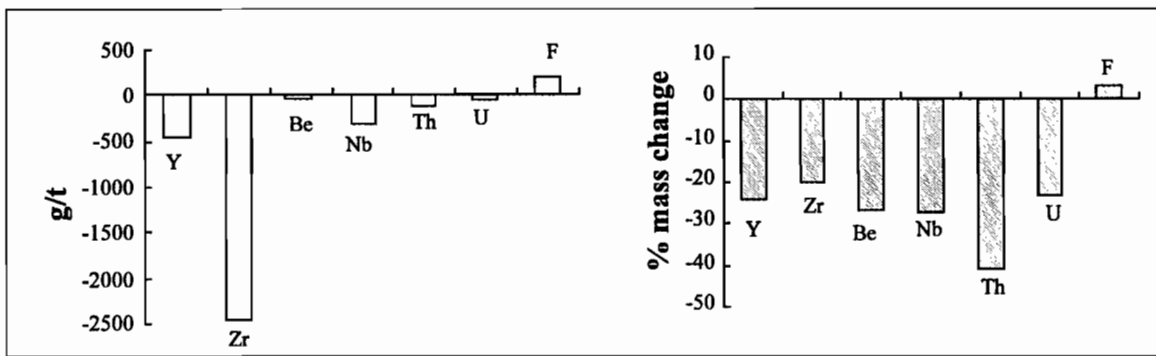
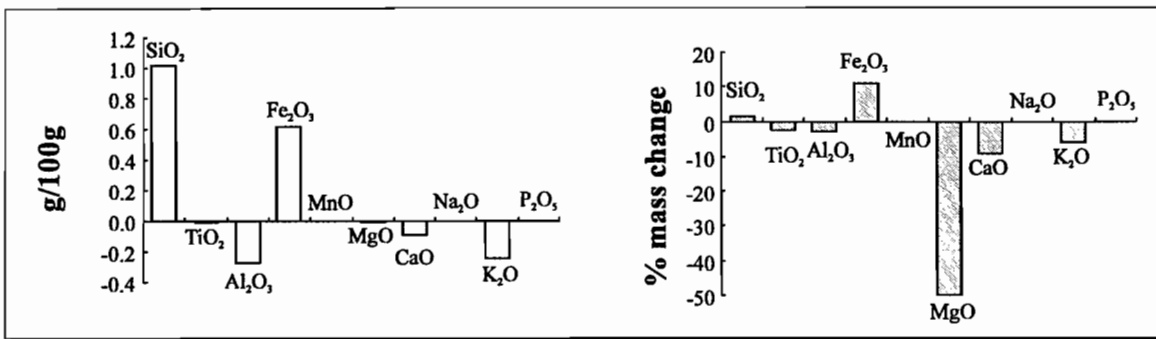
The results of the normative calculations for the samples in drill holes are shown in Figure 6A for SL-182 and in Figure 6B for SL-146. The mineral chlorite was used as the site for Mg in these calculations, as the only mineral found in these rocks, which contains substantial Mg, is an unidentified phase that has a composition similar to chlorite (J.N.

FIGURE 5

Bar diagrams showing the gain and losses of major oxides and selected trace elements in drill holes SL-182 (A and B), SL-146 (C and D) and SL-140 (E). For sample locations refer to Figure 2 or 4.

# SL-182 porphyritic granite

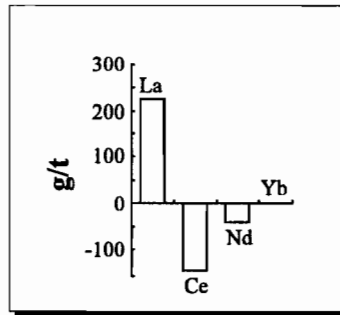
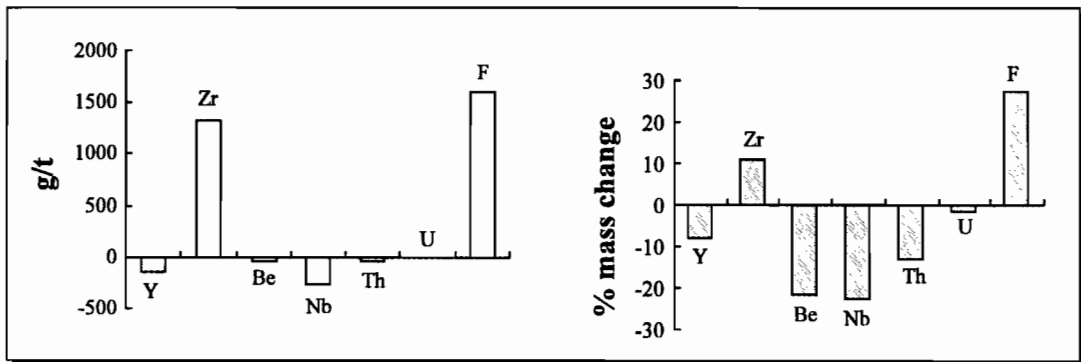
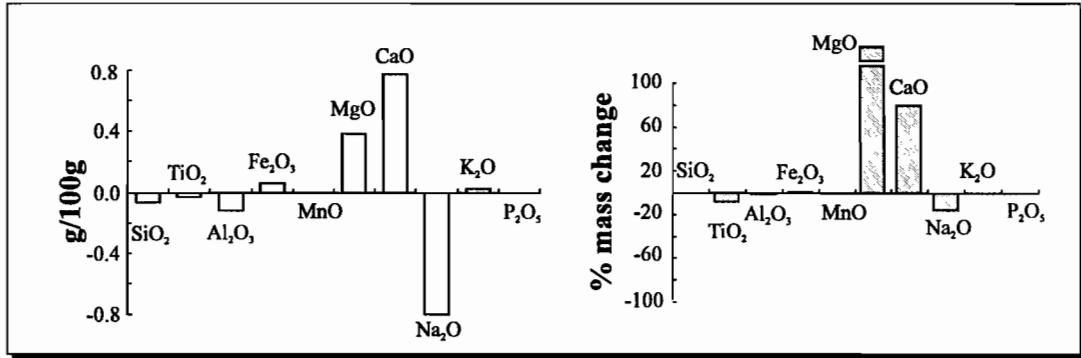
## sample A vs C



**A**

# SL-182 porphyritic granite

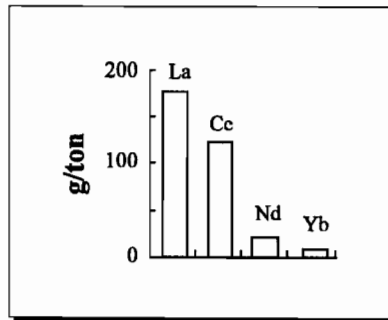
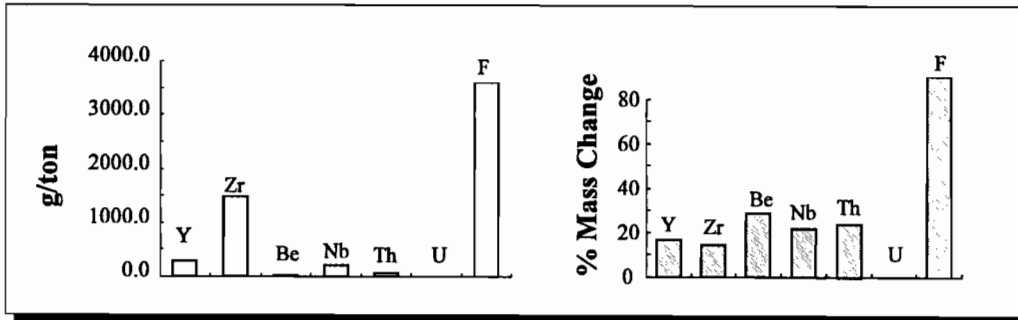
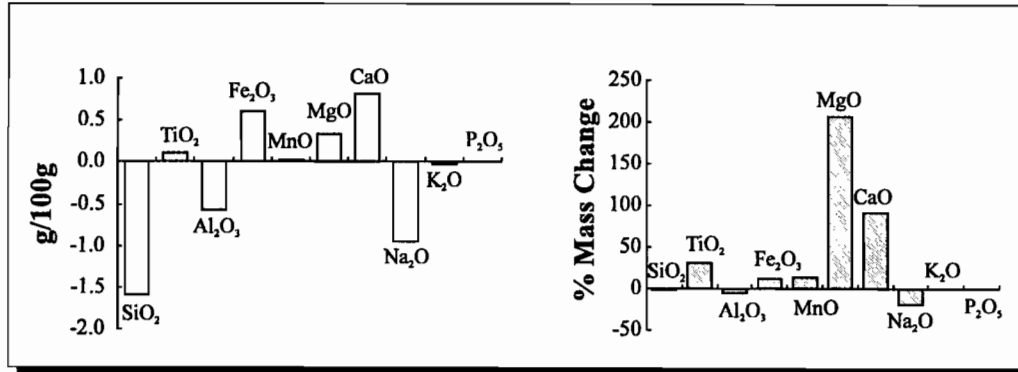
## sample A vs D



**B**

# SL-146 porphyritic granite

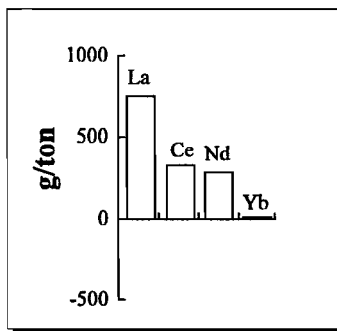
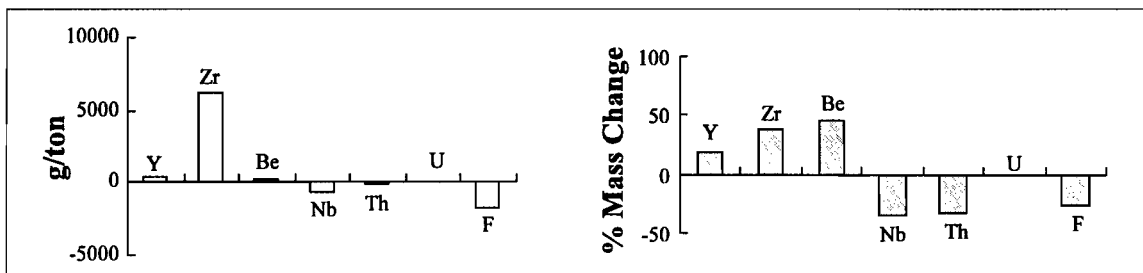
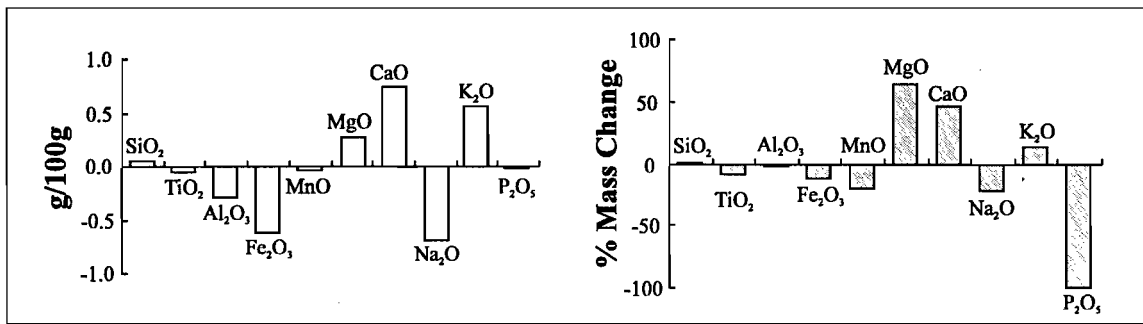
sample E vs F



C

# SL-146 transitional granite

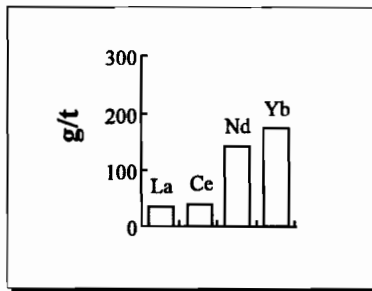
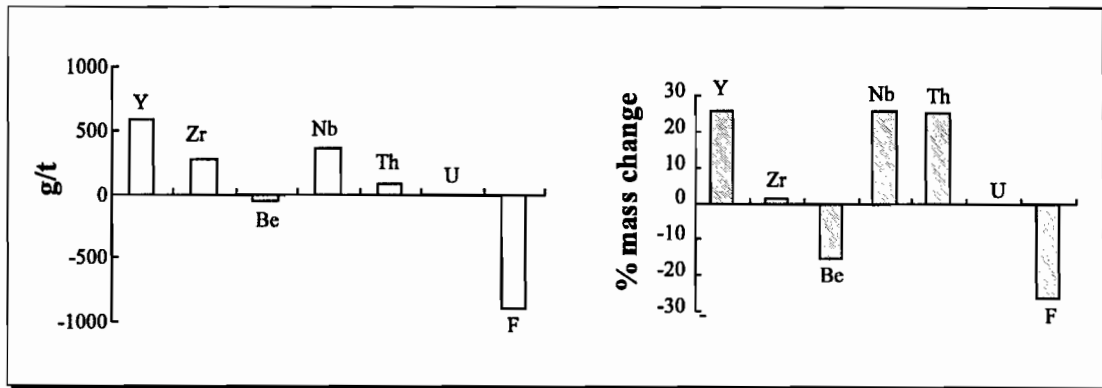
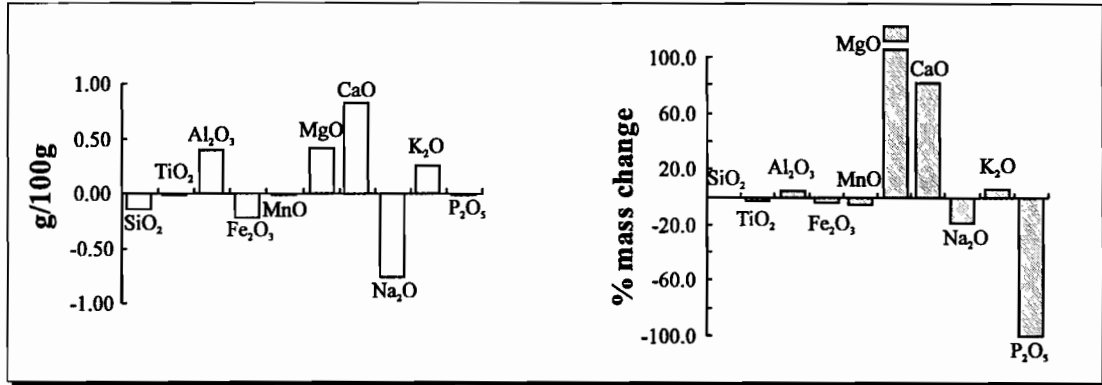
## sample H vs G



**D**

# SL-140 transitional granite

## sample H vs I

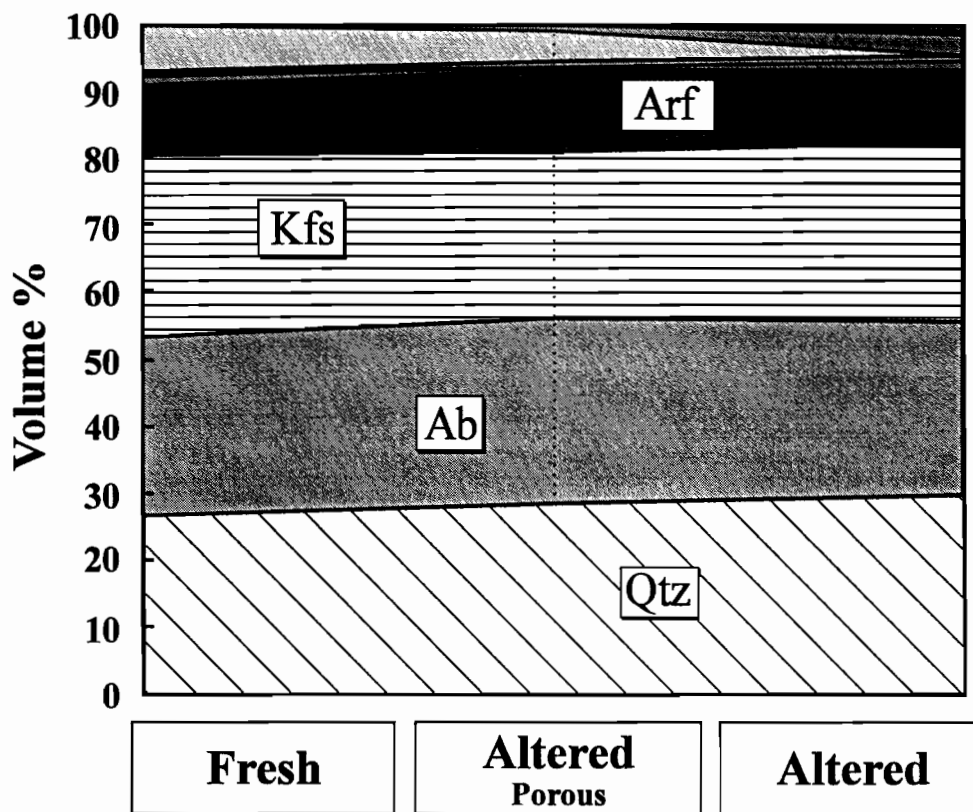


**E**

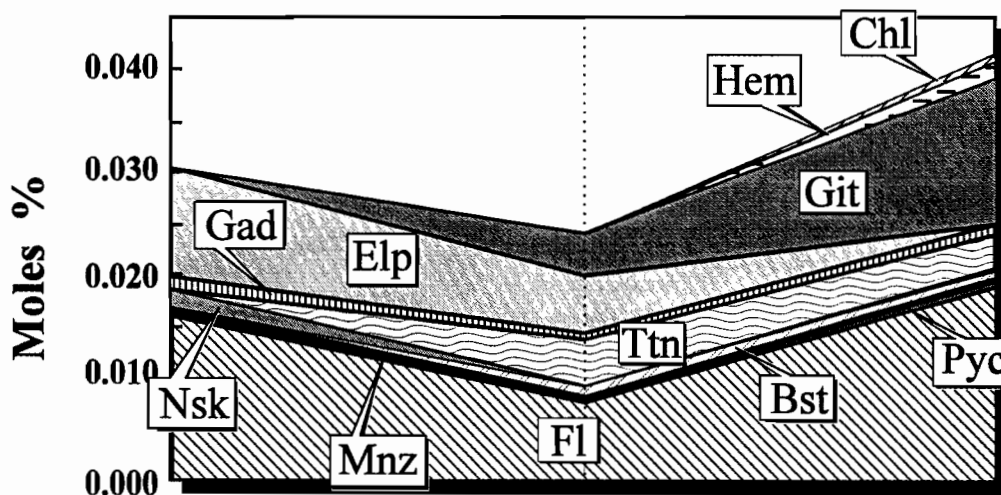
FIGURE 6

Calculated mineral abundances in volume percent, and in the case of the minor and accessory minerals, also in mole percent (shown separately), as a function of depth in SL-182 (A) and SL-146 (B). Mineral abbreviations are given in Table 1. Only the composite samples were used in constructing this figure and, in SL-182, only porphyritic granite is represented.

# D.H. SL-182



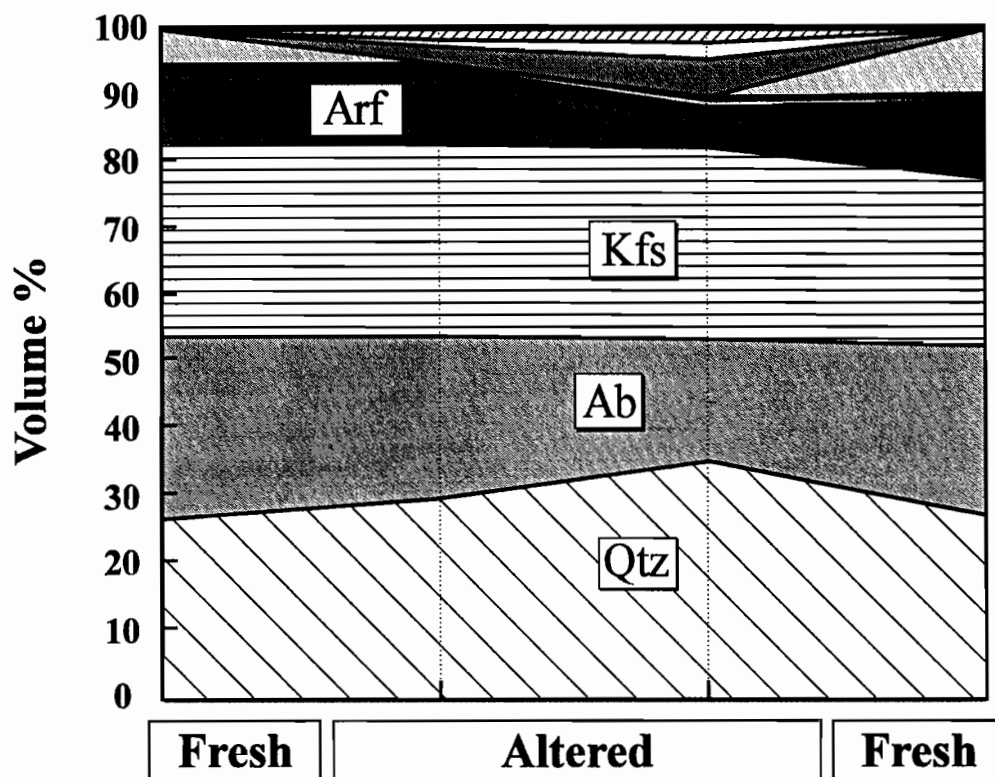
## Molar proportions of trace minerals



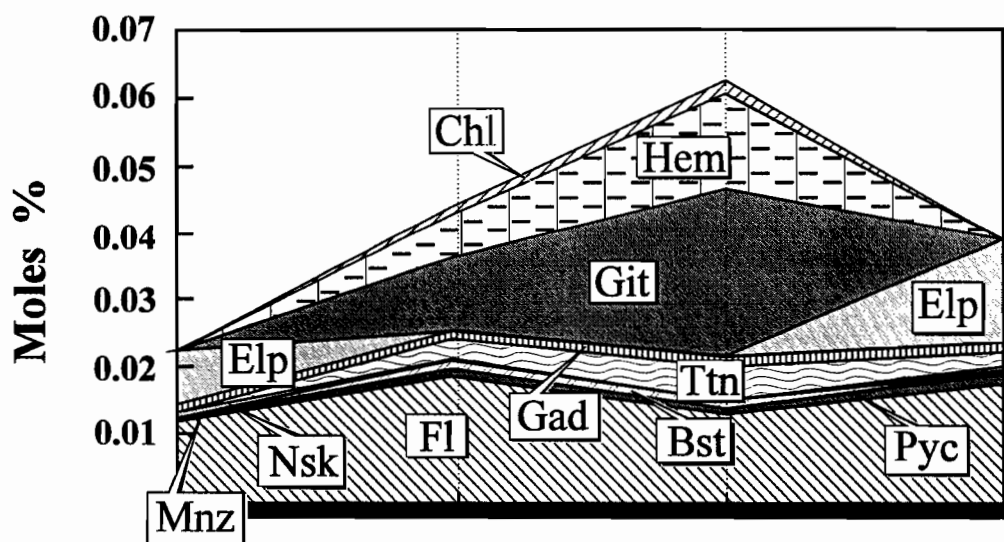
A

← Depth

# D.H. SL-146



## Molar proportions of trace minerals



B

← Depth

Roelofsen, pers. comm.). In addition, the presence of chlorite has been mentioned in several unpublished Iron Ore Co. reports. In constructing Fig. 6A, we did not include the rock samples from the equigranular granite, as the composition of this rock type differs substantially from those of the other granites. In the absence of data on the proportions of  $\text{Fe}^{2+}$  and  $\text{Fe}^{3+}$  in the rocks and the complexity of the mineralogy, we were not able to determine the changes in arfvedsonite/aegirine proportions in these rocks and represent both minerals as arfvedsonite in the diagrams.

As expected, the major rock-forming minerals do not vary substantially in both profiles, although the slight increase in quartz content in the altered rocks at the top of SL-182 may be significant, as we know from textural observations that elpidite was replaced by gittinsite plus quartz in this zone and without quartz lower down. The distribution of zirconosilicate minerals is consistent with their anticipated distribution based on petrographic observation. Thus, as expected, elpidite is the only zirconosilicate mineral in the fresh rocks, co-exists with gittinsite in the porous zone and disappears in the zone above. Hematite and chlorite occur only in the most altered rocks, again consistent with petrographic observations. Following a trend similar to that of the zirconium-bearing silicates, titanite (which, with fluorite and quartz, forms pseudomorphs after the sodium-titanium silicate, narsarsukite) takes the place of narsarsukite in the altered rocks. Other minerals do not display significant variations.

## Discussion

### Introduction

The main conclusions which emerge from our analysis of the whole-rock chemical data reported above are that: the HFSE, notably Zr, vary mainly with granite type; early alteration was essentially isochemical; and later alteration involved addition of Ca, removal of Na, and significant enrichment of Zr, REE and Y. There is also evidence that the source of HFSE enrichment, at least in the case of Zr and perhaps Y, was from immediately

adjacent granite, whereas fluid inclusion data presented in Salvi and Williams-Jones (1990) suggest that Ca and associated Mg had their sources in the gneisses hosting the pluton. The fact that the HFSE vary mainly with granite type, indicates that igneous processes were the principal cause of HFSE enrichment in the Strange Lake pluton. The importance of these processes is further emphasised by the observation that HFSE contents increase progressively from porphyritic granite (70 wt.% SiO<sub>2</sub>), in which zirconosilicate minerals are interstitial, to equigranular granite (75 wt.% SiO<sub>2</sub>), in which these minerals are euhedral, *i.e.* from least to most evolved granite. Nevertheless it is also apparent that the late alteration, in locally enriching HFSE by at least 20%, may have played a key role in forming a deposit with high enough concentration of metals for eventual economic exploitation.

### Early Alteration

As mentioned above, transformation of arfvedsonite to aegirine is most common in and adjacent to pegmatites, which, as also mentioned, formed during exsolution of an orthomagmatic NaCl-rich aqueous fluid. For this reason, we earlier envisaged (Salvi and Williams-Jones, 1992) that sodium metasomatism was the driving force for this alteration (*cf.* reaction 1 above). However, the mass balance calculations reported in this paper show that sodium was conserved, as were essentially all other major element oxides that could have been involved in the reaction. We thus now believe that this early high temperature alteration is better explained by a simple oxidation reaction involving H<sub>2</sub>O and the production of H<sub>2</sub> (*cf.* reaction 2 above). The near-end-member composition of arfvedsonite restricts the magmatic conditions to have been extremely reducing (at 500°C the upper stability of end-member arfvedsonite in terms of  $fO_2$  is ~5 log units below QFM; Ernst, 1962). However, on cooling, assuming that  $fO_2$  remained constant (*i.e.*,  $fO_2$  was not buffered to lower values) conditions would have become progressively more oxidising and, in the presence of an aqueous phase, the Fe<sup>2+</sup> in arfvedsonite would have been oxidised to Fe<sup>3+</sup>, thereby leading to the formation of aegirine and magnetite. Consumption of H<sub>2</sub> to produce methane and higher hydrocarbons (commonly observed in Strange Lake fluid inclusions) through a Fischer-Tropsch reaction with orthomagmatic CO<sub>2</sub> (Salvi and

Williams-Jones, 1995a) could have provided an additional driving force for the alteration. It should be mentioned that Boily and Williams-Jones (1994) appear to imply, on the basis of high  $\delta^{18}\text{O}$  values of mineral separates, that the alteration of arfvedsonite to aegirine occurred at low temperature. However, as was pointed out earlier, fluid inclusion data in Salvi and Williams-Jones (1992) indicate that this early alteration was a high temperature phenomenon. Moreover, most of the samples with high  $\delta^{18}\text{O}$  values are hematized, suggesting that they re-equilibrated with the later calcium-metasomatising fluid (see below), whereas samples without hematite have low  $\delta^{18}\text{O}$  values which is consistent with their higher temperature formation. A minor but significant feature of the early alteration is that, at least in the case of sample 38-B-1, it appears to have been associated with depletion of Zr, Y and REE (Fig. 3A).

#### **Late alteration**

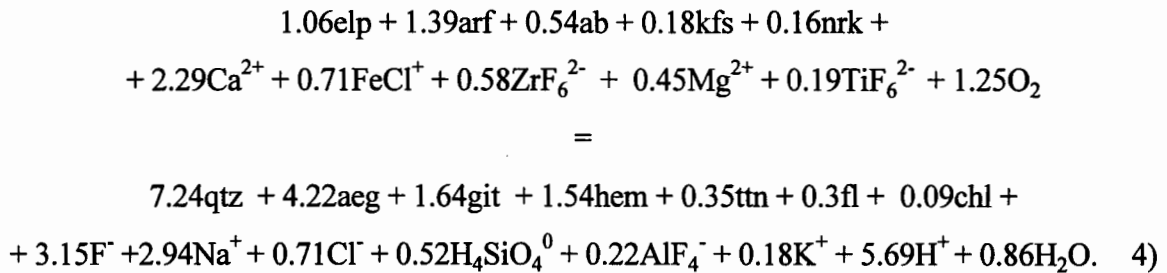
In contrast to early alteration, later alteration, as shown by Salvi and Williams-Jones (1990) occurred at comparatively low temperature ( $\leq 200^\circ\text{C}$ ), and consisted essentially of the replacement of Na-bearing HFSE minerals by Ca-bearing analogues (see also Salvi and Williams-Jones, 1995b). The source of this Ca was shown to be a Ca-rich brine which, it was concluded, originated in the country rocks surrounding the pluton. Interestingly, no other Na-bearing phases seem to have been affected by this metasomatism. Something which was not clear until the present study is that not only was Ca introduced and exchanged for Na, but there was also appreciable mobilisation and local enrichment of Zr, REE and Y during this event.

The mobility of Zr, in particular, was quite unexpected as this element is generally recognised to be about the most immobile of the elements commonly found in earth materials. Indeed, this property of Zr has been widely used in a variety of petrological applications, including estimation of mass and volume changes during hydrothermal alteration. However, there is growing evidence that in some geological settings, Zr may be relatively mobile, and, indeed, be concentrated by hydrothermal processes. For example, at Bergell, Switzerland, Zr occurs as zirconolite ( $\text{CaZrTi}_2\text{O}_7$ ) in skarn near the contact between

a granodiorite intrusion and marble (Gi re, 1986); in Italy, Zr is found, also as zirconolite, in hydrothermal veins cutting dolomite adjacent to the Adamello batholith (Gi re and Williams, 1992); and in the Trans-Pecos igneous province in Texas, zircon is present in limestone-hosted fluorite replacement bodies next to subvolcanic rhyolite intrusions (Rubin *et al.*, 1989, 1993). In the last example, the content of  $ZrO_2$  is locally as high as 4 wt.%. Zirconium daughter minerals have been also found in fluid inclusions (baddeleyite ( $ZrO_2$ ), Philippot and Selverstone, 1991; weloganite ( $Sr_3Na_2Zr(CO_3)_6 \cdot 3H_2O$ ), Vard and Williams-Jones, 1993). Two features which these examples of hydrothermal enrichment have in common are that the associated intrusions are F-rich and the rocks hosting the zirconium minerals are Ca-rich.

#### *Changes in chemical parameters*

Although, as shown above, there have been a number of reports of occurrences in which Zr was demonstrably mobilised by hydrothermal fluids, there have been no attempts to quantify this mobilisation, *i.e.*, to estimate the masses of Zr mobilised and relate these masses to the solubility of the corresponding Zr minerals in the hydrothermal fluids. In this paper, we have estimated the masses of Zr added to the altered rocks at Strange Lake relative to their unaltered equivalents and provided evidence that this Zr was locally derived, *e.g.*, the occurrence of Zr-enriched rocks at the top of SL-182, overlying Zr-depleted rocks. Using the normative calculations reported above to quantify the alteration reactions, we are also able to identify intensive parameters that may have been involved in this mobilisation and, by using reasonable assumptions of water/rock ratios, make order of magnitude estimates of the concentrations of Zr in the hydrothermal fluids. If we use the fresh porphyritic rock at the bottom of SL-182 and the altered porphyritic rock at the top of the hole to characterise reactants and products, respectively, and further assume that the fresh rock does not contain aegirine and the altered rock does not contain arfvedsonite (indicated petrographically but not calculable because of a lack of whole-rock  $Fe^{2+}/Fe^{3+}$  data), we obtain the following reaction (expressed as moles/10 kg of rock):



(Owing to the relatively small proportions of pyrochlore and other REE- and Y-bearing minerals, it has been possible to omit these minerals without significantly affecting the overall stoichiometry of the reaction). The aqueous species in reaction (4) were the predominant species established from consideration of the probable complexation of these cations in the Strange Lake fluids. With the exception of the cations of the HFSE and  $\text{Al}^{3+}$ , all the cations considered in this reaction tend to form their strongest complexes with  $\text{Cl}^-$ . We therefore determined the predominant species involving the latter cations, for  $\text{Cl}^-$  activities corresponding to those of the Strange Lake fluids at temperatures  $<200^\circ\text{C}$ , using the computer code SUPCRT92 and the associated thermodynamic data base (Johnson *et al.*, 1992). In the case of the alkali and alkaline-earth elements, the simple ion is predominant, whereas the 1:1 complex is the predominant Fe-species. The HFSE, Zr and Ti were assumed to be present as octahedrally co-ordinated fluoride-complexes and Al as a tetrahedrally co-ordinated fluoride-complex, all with maximum ligand numbers (see below). At the temperature and pH (see below) conditions of alteration, HF and HCl are essentially dissociated (calculated using SUPCRT92, and given in Ruaya and Seward, 1986).

From reaction (4) it is evident that later alteration, in addition to being accompanied by large changes in the masses of Na, Ca, Mg, Fe, Zr and F, also involved consumption of significant  $\text{O}_2$  and production of  $\text{H}^+$ , *i.e.*, the fluid responsible for alteration was oxidising but relatively alkaline. This implies a pH greater than that required for neutrality, which, at a temperature of  $200^\circ\text{C}$  would be 5.5. The latter conclusion is consistent with the fact that alkali feldspars rather than muscovite or paragonite were the stable phases during alteration,

implying a minimum pH of 5.7 (calculated using SUPCRT92, and the composition of the late fluid estimated by Salvi and Williams-Jones, 1990).

### *HFSE mobilisation*

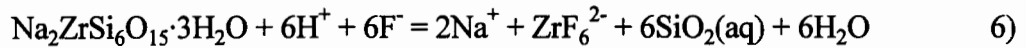
As noted above, the reaction describing late alteration (reaction 4) can also be employed to estimate the concentration of Zr in the fluid, if a reasonable assumption can be made of the probable water/rock ratio. Using oxygen isotope analyses, Taylor (1974) estimated that integrated water-rock ratios for granitoid-related hydrothermal systems range up to values of 3 or 4 but are more typically <1. If we arbitrarily assume a water/rock ratio of one, it follows that the consumption of 0.58 m  $\text{ZrF}_6^{2-}$  per 10 Kg of rock implies a solubility of 0.058 m Zr in the fluid. In order to evaluate whether this estimate is reasonable we have compared it with solubilities predicted by thermodynamic data for hydroxide and fluoride complexes ( $\text{OH}^-$  and  $\text{F}^-$  are the most likely ligands to complex with a hard ion like  $\text{Zr}^{4+}$  in this environment; cf. Crerar *et al.*, 1985) presented in Aja *et al.* (1995). These authors measured the solubility of several Zr-bearing minerals, including elpidite in HF-bearing and HF-free aqueous fluids, and presented equilibrium constants for reactions involving Zr-fluoride and -hydroxide complexes at temperatures of 50 and 150°C. Calculations, using extrapolations of their data, show that, if elpidite dissolved according to the reaction:



(the most stable Zr-hydroxide complex is  $\text{Zr}(\text{OH})_4^0$ ) in a fluid with a NaCl content comparable to those estimated for any of the Strange Lake fluids and a silica activity corresponding to quartz saturation, the Zr concentration will be  $<10^{-28}$  m at 200°C at any geologically reasonable pH. Clearly this concentration is far too low to account for the estimated additions of Zr at any reasonable water/rock ratio.

Calculation of Zr solubility as a fluoride-complex requires information on the activity of  $\text{F}^-$  in the fluids, in addition to those of  $\text{Na}^+$  and  $\text{SiO}_2(\text{aq})$ . Although this parameter

has not been measured, it can be estimated assuming that the fluid was in equilibrium with fluorite. Using the fluid inclusion compositions reported in Salvi and Williams-Jones (1990) for the late fluids (16 wt.% NaCl eq. and  $X_{Ca} = 0.5$ ) and the solubility product calculated for fluorite with SUPCRT92, the  $F^-$  concentration is estimated to be  $3.6 \times 10^{-5}$  and, assuming that elpidite dissolved according to the reaction:



(cf. Aja *et al.*, 1995) the concentration of Zr in solution is  $1.2 \times 10^{-27}$ . This concentration is similar to that calculated assuming dissolution of Zr as  $Zr(OH)_4^0$ , supporting the conclusion of Salvi and Williams-Jones (1990) that calcium addition and transport of Zr involved separate fluids.

The most obvious candidate for the Zr-transporting fluid is the fluid which, as discussed above, is interpreted to have been responsible for early alteration (evidence presented earlier suggests that this alteration involved depletion of Zr, Y and REE), and from fluid inclusion data presented in Salvi and Williams-Jones (1992), was a NaCl brine containing negligible  $CaCl_2$ ; the content of Ca in the residues of decrepitated fluid inclusions is below detection. According to this interpretation, the latter fluid, which is thought to have originated through degassing of the most evolved magmas, either at depth or conceivably close to the site of late alteration (pegmatites and the more evolved equigranular granite are intersected in SL-182, 30 m below the Zr enrichment zone), would have deposited its Zr when it mixed with the Ca-rich fluid in the Zr-rich gittinsite plus quartz alteration zone. If we assume that the Zr-bearing fluid contained no calcium, then any restriction on its potential  $F^-$  content is removed. We can thus use the equilibrium constant for reaction (6), in conjunction with the estimated Na content of the fluid (5.5 m; Salvi and Williams-Jones, 1992) and an assumed pH, to estimate the concentration of  $F^-$  required to yield the concentration of Zr in solution estimated from reaction (4) and our assumed water/rock ratio of 1 (0.058 m Zr). At a pH of 5.7 (the minimum pH required to stabilise K-feldspar in the presence of the late fluid) and a temperature of 200 °C, the

calculated  $F^-$  concentration is 1.2 m. Although this concentration is high, it may not be totally unreasonable given the overall high salinity of the fluid (5.5 m). However, it is more likely that the temperature of the fluid was closer to that estimated for entrapment of the corresponding inclusions, *i.e.* around 350 °C, and that it cooled only upon mixing with the Ca-rich fluid. In this case the minimum pH required to stabilise K-feldspar would have been lower, *i.e.* 4.7, and the corresponding concentration of  $F^-$  needed to account for the estimated Zr content of the fluid would have been only 0.1 m. Thus, in summary, it would appear that a slightly acidic orthomagmatic fluid (pH high enough to stabilise K-feldspar) with low to moderate concentrations of  $F^-$ , would have been easily capable of transporting the amounts of Zr required to account for the enrichment in this element due to hydrothermal processes.

Although the amounts involved are much smaller, there is nevertheless strong evidence that Y and REE were also enriched hydrothermally, and that, as proposed for Zr, these elements were transported as fluoride complexes in the early orthomagmatic fluid (Wood, 1990 has shown that these elements form their most stable aqueous complexes with  $F^-$ ).

#### *Alteration model*

The model which we favour for later alteration and associated HFSE enrichment envisages two fluids, namely a NaCl-dominated fluorine-bearing orthomagmatic fluid which leached Zr from alkali zirconosilicate minerals, mainly elpidite, in earlier crystallised rocks (it may also have fractionated significant Zr directly from the magma), and a Ca-rich fluid which originated in the country rocks. It is proposed that emplacement of the pluton initiated a meteoric-water dominated hydrothermal system which introduced calcium into the apical parts of the pluton and, as a result, transformed elpidite and other HFSE- and REE-bearing minerals into Ca-bearing analogues. It is further proposed that introduction of the Ca-bearing fluid coincided with late stage magma degassing (the orthomagmatic brine referred to above) and that mixing of these two fluids led to precipitation of fluorite and

destabilisation of the Zr, REE and other HFSE-fluoride complexes due to the sharp reduction in ligand concentration and/or an increase in pH.

A feature of the late alteration which occurs locally, notably in SL-182, and is not explained by the above model, is a zone below the main alteration zone in which replacement of elpidite by gittinsite involved the creation of pore space, and there was apparently depletion of Zr and Y. We propose that this zone (preserved because of its greater depth) reflects the initial stages of late stage alteration by a Ca-rich silica-undersaturated fluid (produced by equilibration of meteoric waters with calc-silicate gneisses and gabbros) and proceeded according to reaction (3) which caused a 65% volume reduction (see above and Salvi and Williams-Jones, 1995b). At more advanced stages of the alteration and particularly during mixing with the orthomagmatic fluid (silica-saturated), the external fluid was no longer able to remove all the silica created by the elpidite breakdown reaction and the pore space was consequently filled by quartz. This interpretation is consistent with the overall alteration reaction (4) in which  $\text{SiO}_{2(\text{aq})}$  is a product.

It is less easy to explain the depletion of Zr and Y which accompanied the onset of late-stage alteration. However, we suggest that the porosity creation initially enhanced leaching of Zr and Y by greatly improving access of the rising orthomagmatic fluid to sites containing minerals rich in these elements, and that deposition of Zr- and Y-bearing minerals only commenced when the orthomagmatic fluid entered the overlying main alteration zone and mixed extensively with the Ca-rich fluid which was being circulated into the pluton from above.

## Conclusions

The following are the principal conclusions of this study.

1. HFSE enrichment in the Strange Lake pluton was primarily a magmatic phenomenon.

2. After emplacement, the pluton underwent alteration in which arfvedsonite was oxidised to aegirine plus magnetite by a mildly acidic, Na-rich, Ca-poor, F-bearing orthomagmatic fluid. There was no significant change in the major element composition of the granite as a result of this alteration, however, there was significant HFSE mobilisation.
3. Later alteration was caused by an externally derived fluid, enriched in calcium as a result of interaction with calc-silicate and gabbroic gneisses, which entered the pluton from above. This alteration involved the replacement of mainly Na-bearing HFSE silicate minerals by Ca-bearing equivalents, and was accompanied by addition of Ca and Mg, and removal of Na.
4. The rocks subjected to late stage alteration were enriched in Zr, Y and REE by proportions generally representing at least 20% of their masses in the unaltered granites. This enrichment was caused by mixing of the rising orthomagmatic fluid, which transported the HFSE as fluoride complexes, with the Ca-rich fluid responsible for alteration. Deposition of HFSE minerals occurred as a result of the sharp decrease in F<sup>-</sup> activity which accompanied saturation of the fluid with fluorite, and/or an increase in pH.
5. The results of this study suggest that hydrothermal deposits of HFSE, particularly Zr, are rare because of the unusual nature of the fluid required for the transportation of these elements, *i.e.*, F-bearing and essentially devoid of Ca. In order to cause deposition of HFSE minerals, this fluid should enter an environment promoting increases in Ca activity and/or pH, which may explain why the few documented examples of Zr deposits are almost all hosted by limestones and dolomites or their metamorphosed equivalents.

## References

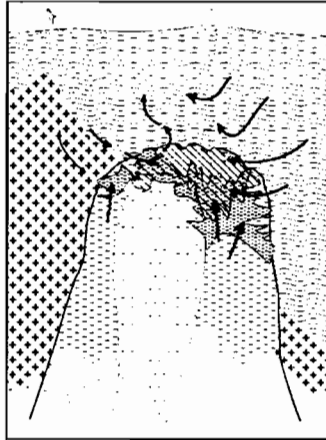
- Aja, S.U., Wood, S.A. and Williams-Jones, A.E., 1995.** The aqueous geochemistry of Zr and the solubility of some zirconium-bearing minerals. *Appl. Geochem.* (submitted).
- Bélanger, M., 1984.** Région du lac Brisson. *Ministère Énergie Ressources, Québec*, Document DP 84-20 (carte annotée, scale 1:50,000).
- Boily, M. and Williams-Jones, A.E., 1994.** The role of magmatic and hydrothermal processes in the chemical evolution of the Strange Lake plutonic complex (Quebec-Labrador). *Contrib. Mineral. Petrol.*, 118, 33-47.
- Bölke, J.K., 1989.** Comparison of metasomatic reactions between a common CO<sub>2</sub>-rich vein fluid and diverse wall rocks: intensive variables, mass transfers, and Au mineralization at Alleghany, California. *Econ. Geol.*, 84, 291-327.
- Bonin, B., 1986.** *Ring Complex Granites and Anorogenic Magmatism*: Elsevier Science Publishing Co., New York, 188 p.
- Crerar, D.A., Wood, S.A., Brantley, S. and Bocarsly, A., 1985.** Chemical controls on solubility of ore-forming minerals in hydrothermal solutions: *Can. Mineral.*, 23, 333-352.
- Ernst, W.G., 1962.** Synthesis, stability relations, and occurrence of riebeckite and riebeckite-arfvedsonite solid solution. *J. Geol.*, 70, 689-736.
- Fitton, J.G. and Upton, B.G.J. (eds), 1987.** *Alkaline Igneous Rocks*. Geological Society Special Publication No. 30, 568 p.
- Gieré, R., 1986.** Zirconolite, allanite and hoegbomite in a marble skarn from the Bergell contact aureole: Implication for mobility of Ti, Zr and REE. *Contrib. Mineral. Petrol.* 65, 459-470.
- Gieré, R. and Williams, C.T., 1992.** REE-bearing minerals in a Ti-rich vein from the Adamello contact aureole (Italy). *Contrib. Mineral. Petrol.* 112, 83-100.
- Grant, J.A., 1986.** The isocon diagram: A simple solution to Gresens' equation for metasomatic alteration. *Econ. Geol.*, 81, 1976-1982.
- Johnson, J.W., Oelkers, E.H, and Helgeson, H.C., 1992.** SUPCRT92: A software package for calculating the standard molal thermodynamic properties of minerals,

- gases, aqueous species, and reactions from 1 to 5000 bars and 0° and 1000°C. *Computers and Geosciences*, 18, 899-947.
- Karup-Møller, S., 1978.** The ore minerals in the Ilímaussaq intrusion: Their mode of occurrence and their conditions of formation. *Bull. Grøn. Geol. Unders.*, 127, 1-51.
- Kretz, R., 1983.** Symbols for rock-forming minerals. *Am. Mineral.*, 68, 277-279.
- Miller, R.R., 1986.** Geology of the Strange Lake Alkalic Complex and the associated Zr-Y-Be-REE mineralization. *Newfoundland Department of Mines and Energy, Mineral Development Division Report 86-1*, 11-19.
- Nassif, G.J. and Martin R.F., 1991.** The hypersolvus granite-subsolvus granite transition at Strange Lake, Québec-Labrador [abs]. In *Program with Abstracts GAC-MAC-CSPG joint annual meeting*, Toronto, A89.
- Nassif, G.J., 1993.** *The Strange Lake Peralkaline Complex, Québec-Labrador: The Hypersolvus-Subsolvus Granite Transition and Feldspar Mineralogy*, M.Sc. thesis, McGill University, Montreal, Quebec. 104 p.
- Philippot, P. and Selverstone, J., 1991.** Trace-element-rich brines in eclogitic veins: Implications for fluid composition and transport during subduction. *Contrib. Mineral. Petrol.*, 106, 417-430.
- Pillet, D., Bonhomme, M.G., Duthou, J.L. and Chenevoy, M., 1989.** Chronologie Rb/Sr et K/Ar du granite peralkalin du lac Brisson, Labrador central, Nouveau-Québec: *Can. J. Earth Sci.*, 26, 328-332.
- Ruaya, J.R. and Seward, T.M., 1986.** The stability of chlorozinc (II) complexes in hydrothermal solutions up to 350°C. *Geochim. Cosmochim. Acta*, 50, 651-661.
- Rubin, J.N., Henry, C.D. and Price, J.G., 1989.** Hydrothermal zircons and zircon overgrowths, Sierra Blanca Peaks, Texas. *Am. Mineral.*, 74, 865-869.
- Rubin, J.N., Henry, C.D. and Price, J.G., 1993.** The mobility of zirconium and other “immobile” elements during hydrothermal alteration. *Chem. Geol.*, 110, 29-47.
- Salvi, S. and Williams Jones, A.E., 1990.** The role of hydrothermal processes in the granite hosted Zr, Y, REE deposit at Strange Lake, Quebec/Labrador: Evidence from fluid inclusions. *Geochim. Cosmochim. Acta*, 54, 2403-2418.

- Salvi, S. and Williams-Jones A.E., 1992.** Reduced orthomagmatic C-O-H-NaCl fluids in the Strange Lake rare-metal granitic complex, Quebec/Labrador, Canada. *Eur. J. Mineral.*, 4, 1155-1174.
- Salvi, S. and Williams-Jones A.E., 1995a.** Magmatic hydrocarbons and their alteration in the Strange Lake peralkaline granite, Quebec/Labrador: Evidence from fluid inclusions. *Geochim. Cosmochim. Acta* (to be submitted)
- Salvi, S. and Williams-Jones A.E., 1995b.** Zirconosilicate phase relations in the Strange Lake (Lac Brisson) pluton, Quebec-Labrador, Canada. *Am. Mineral.*, (accepted for publication).
- Scarfe, C.M., 1977.** Viscosity of a pantellerite melt at one atmosphere. *Can. Mineral.*, 15, 185-189.
- Sørensen, H. (ed), 1974.** *The Alkaline Rocks*: Wiley Interscience. New York, 622 p.
- Spear, F.S., Rumble III, D. and Ferry, J.M., 1982.** Linear algebraic manipulation of n-dimensional composition space. In Characterization of Metamorphism through Mineral Equilibria, J.M. Ferry Ed., *Reviews in Mineralogy*, 10, *Mineralogical Society of America*. 53-104.
- Taylor, F.C., 1979.** Reconnaissance geology of a part of the Precambrian Shield, northeastern Quebec, northern Labrador and Northwest Territories: *Geological Survey of Canada Mémoire* 393, 99 p, with 17 maps scale 1:250,000.
- Taylor, H.P., Jr., 1974.** The application of oxygen and hydrogen isotope studies to problems of hydrothermal alteration and ore deposition. *Econ. Geol.*, 69, 843-883.
- Vard, E. and Williams-Jones, A.E., 1993.** A fluid inclusion study of vug minerals in dawsonite-altered phonolite sills, Montreal, Quebec: Implications for HFSE mobility. *Contrib. Mineral. Petrol.* 113, 410-423.
- Wood, S.A., 1990.** The aqueous geochemistry of the rare-earth elements and yttrium 2. Theoretical predictions of speciation in hydrothermal solutions to 350°C at saturation water vapor pressure. *Chem. Geol.*, 88, 99-125.
- Woolley, A.R. (ed), 1987.** *Alkaline Rocks and Carbonatites of the World. Part 1: North and South America*. British Museum (Natural History), London, 216 p.
- Zajac, I.S., 1992.** The Strange Lake Complex and its yttrium and zirconium mineralization [abs]. *Society for Mining Metallurgy and Exploration Abstracts with Program*, 69.

**Zajac, I.S., Miller, R.R., Birkett, T., Nantel, S., 1984.** Le gîte de Zr, Y, Nb, et Be du complexe alcalin de Strange Lake, Québec-Labrador. *Ministère de l'Énergie et des Ressources, Québec*, DV 84-18, 127-142.

## CHAPTER VII



## CONCLUSIONS

---

## General Conclusions

THE formation of methane- and higher-hydrocarbon-dominated fluid inclusions in the Strange Lake pluton, alteration of arfvedsonite to aegirine, and the enrichment of Zr, Y and REE in the most altered rocks, were intimately related. The enrichment in HFSE, as demonstrated by the correlation of HFSE content with parameters reflecting magma evolution, was largely primary. However, mass balance calculations show that Zr, Y and the REE, were concentrated in amounts corresponding to at least 20% of their primary contents, during low temperature alteration which was accompanied by addition of Ca to and removal of mainly Na from the rocks. Similarly, the conditions of entrapment suggest that the carbonic fluid was of orthomagmatic origin, but that hydrocarbon species did not escape from the magma or form spontaneously on cooling. Rather, their formation required a source of hydrogen, which was provided when orthomagmatic brines oxidised arfvedsonite to aegirine plus magnetite, leading to production of aliphatic hydrocarbons as a result of hydrogenation of the juvenile carbonic fluid.

The hydrothermal history of the pluton commenced with exsolution of an aqueous brine and an immiscible, reduced C-O-H-N fluid, at temperatures above 350°C and pressures ~700 bar, respectively. Analyses of fluid inclusion gas compositions in bulk samples, using a gas chromatographic system built by the author, showed that the carbonic fluid is now dominated by CH<sub>4</sub>, H<sub>2</sub>, N<sub>2</sub>, and C<sub>2</sub>H<sub>6</sub> and contains lesser amounts of CO<sub>2</sub> and aliphatic hydrocarbons as heavy as hexane. However, thermodynamic calculations revealed that the carbonic species could not have coexisted in equilibrium at the time of entrapment. Nor could they have formed during post-entrapment cooling. Instead, the calculations suggest that, at magmatic conditions, the carbonic fluid consisted dominantly of CO<sub>2</sub> and contained some CH<sub>4</sub> or CO. The most plausible explanation for the heavier hydrocarbons is that they formed at subsolidus conditions from a carbonic fluid dominated by CO<sub>2</sub>, as a result of magnetite-catalysed Fischer-Tropsch synthesis. Whole-rock geochemical data and petrographic observations suggest that the source of the hydrogen and the catalyst for this synthesis, and the excess hydrogen in fluid inclusions, was

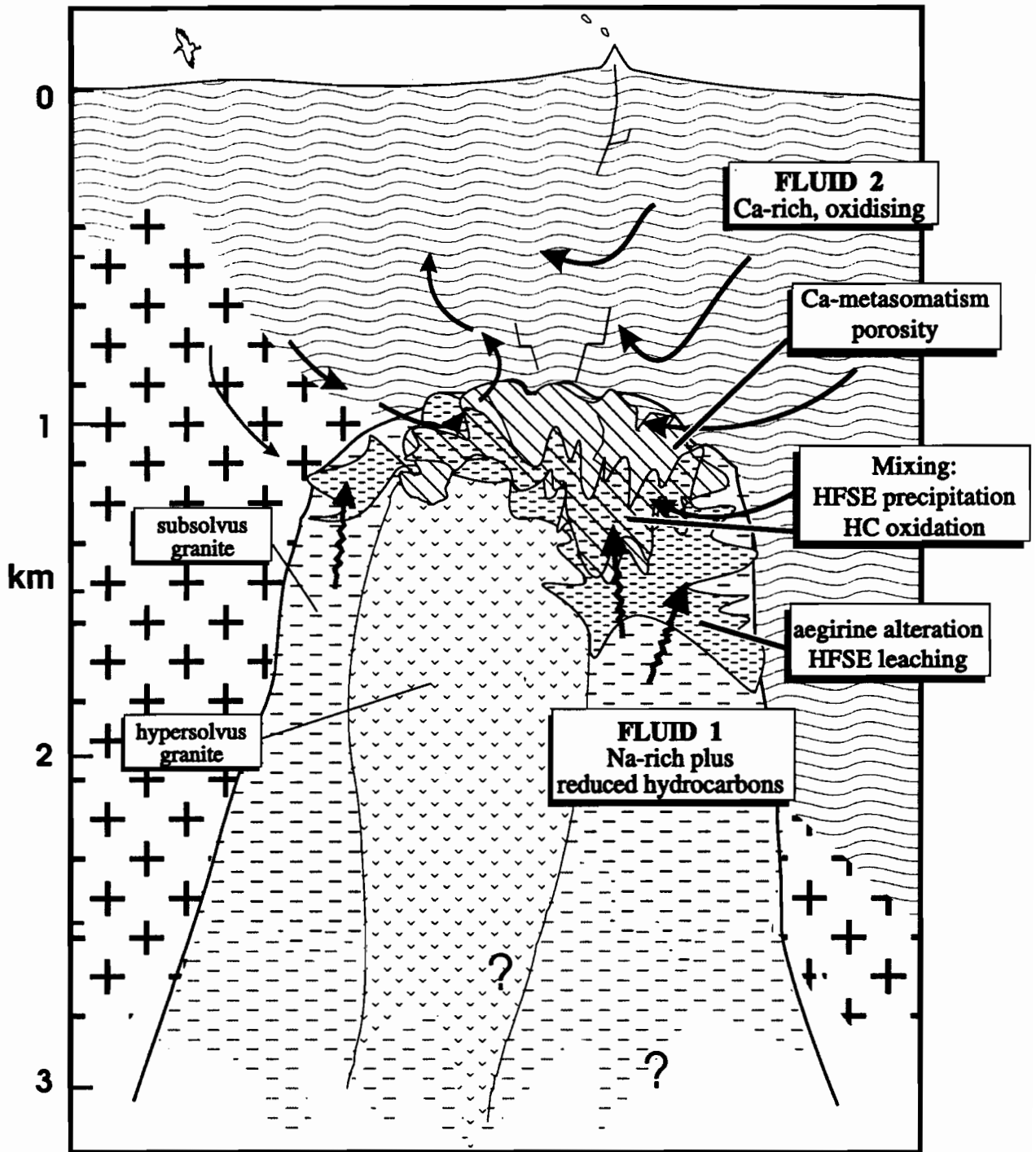
an isochemical reaction in which orthomagmatic brine and primary arfvedsonite reacted to produce aegirine, magnetite and hydrogen.

In addition to altering arfvedsonite, the orthomagmatic brine also leached Zr, Y and REE from primary minerals. These highly charged metals were kept in solution as fluoride complexes at mildly acidic conditions (pH above 4.7, *i.e.*, high enough to prevent the reaction of k-feldspar to muscovite at ~350°C). Pene-contemporaneously with the release of the orthomagmatic fluid, a low-temperature, oxidising, ground-water-dominated convective system, initiated by heat from the pluton, developed in the apical region of the intrusion. This later fluid gained significant amounts of Ca from interaction with the host gneisses, but was undersaturated in quartz. Upon reacting with the granites, this fluid added Ca and Mg and removed Na from the rock, causing the transformation of sodic HFSE-bearing minerals, notably elpidite, to calcic equivalents, primarily gittinsite, and to a lesser extent armstrongite. This alteration, because of the much smaller molar volume of gittinsite relative to elpidite, was accompanied by a 65% reduction in the volume of solids at zirconium mineral sites, and thus creation of significant porosity. Near the base of the alteration zone, the increased porosity enhanced leaching of Zr and Y by greatly improving access of the rising orthomagmatic fluid to sites containing minerals rich in these elements, which explains the depletion of Zr and Y immediately below the main gittinsite plus quartz alteration zone. At higher levels, however, there was extensive mixing of the orthomagmatic fluid with the Ca-rich, meteoric fluid, which caused precipitation of Zr, Y and REE minerals, as a result of decreased ligand concentration due to saturation of the fluid with fluorite and/or an increase of pH. This mixing also promoted partial oxidation of the carbonic fluid, as indicated by the higher CO<sub>2</sub>/CH<sub>4</sub> ratio of fluid inclusions in Ca-metasomatised rocks, and increased silica activity to quartz saturation, thereby filling pores and sealing the rock to further fluid circulation (Fig. 1).

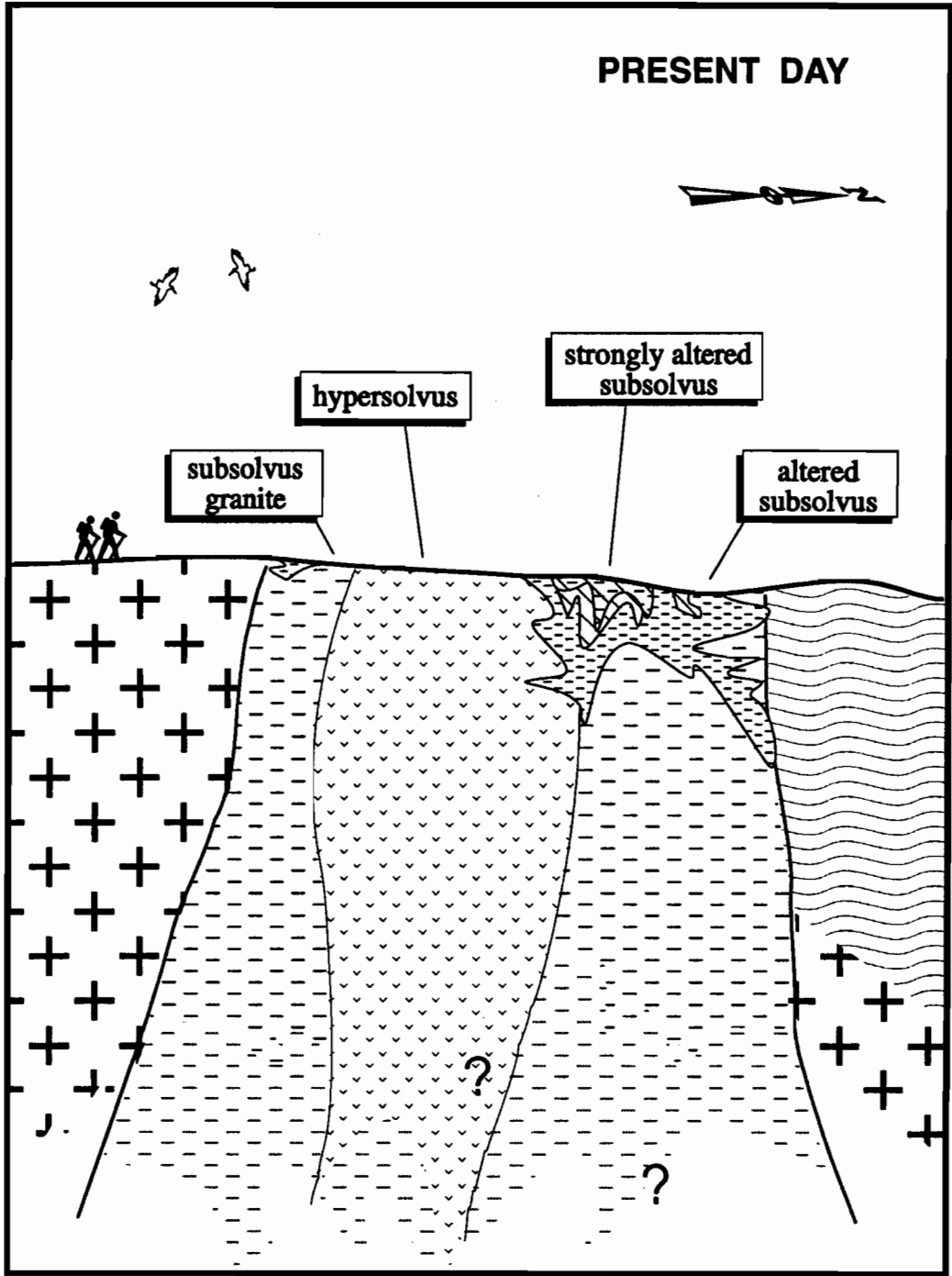
The study suggests that an essential condition for hydrothermal mobility of HFSE, particularly Zr, is the availability of free fluoride ions and the near absence of Ca in the hydrothermal fluid. The fact that elevated HFSE concentrations, of interpreted hydrothermal origin, commonly occur in limestones or marble adjacent to fluorine-rich igneous bodies

FIGURE 1

Schematic cross-sections through the Strange Lake pluton depicting the main events envisaged during sub-solidus hydrothermal alteration (A), and the resulting present-day erosional profile (B).



A



**B**

**C**

(e.g., in marble skarn, Gière, 1986; in veins in dolomitic marble, Gière and Williams, 1992; and in fluor spar deposits in limestone, Rubin *et al.*, 1989) suggests further, that subsequent access to a Ca-rich environment may be an essential requirement for focused deposition of HFSE minerals from hydrothermal fluids.

## Contributions to Knowledge

The following represent the most important original contributions to knowledge of the thesis:

1. This study is one of a relatively small number dealing with fluid inclusions in alkaline granites, and the first to document the coexistence of brine and hydrocarbon inclusions in such rocks.
2. Although the presence of methane and higher hydrocarbon fluid inclusions has been documented previously in alkalic igneous bodies, only the origin of methane in these inclusions has been satisfactorily explained. This study is the first to propose that these higher hydrocarbons are produced by a natural Fischer-Tropsch synthesis, and show that this is made possible by a hydrothermal reaction that occurs commonly in alkalic igneous bodies, namely the oxidation of arfvedsonite to aegirine.
3. The low temperature hydrothermal replacement of sodic HFSE minerals by calcic equivalents was first documented by the author as part of his M.Sc. thesis project. This thesis expands on the observations made in that study and provides a carefully supported qualitative explanation, based on sound thermochemical principles, of the range of zirconosilicate textures observed in the Strange Lake pluton.
4. Several previous studies have provided qualitative evidence of hydrothermal transport of Zr in alkalic igneous systems. However, to the author's knowledge, this is the first investigation that attempts to quantify the Zr enrichment, relate it to parameters controlling Zr-mineral solubility, and provide a plausible model for Zr transport and deposition. The study suggests that post magmatic concentration of Zr and other HFSE

will tend to occur mainly when there is a juxtaposition of fluorine-rich/calcium-poor and calcium-rich hydrothermal environments.

5. The gas chromatographic system developed during the course of this thesis for fluid analysis of fluid inclusion gas species, represents a significant advance over other previously described systems, both in the range of gases that can be simultaneously analysed *e.g.* higher hydrocarbons up to hexane, argon, nitrogen and hydrogen and the quality of the analyses (improved detection and accuracy).

### Recommendation for Future Work

The research presented in the first part of this thesis provides a documentation of and an explanation for the reduced gases associated with the Strange Lake peralkaline pluton, based on fluid inclusion compositions, alteration mineralogy, and thermodynamic calculations. According to the explanation, these gases owe their origin to magma degassing and subsolidus hydrogenation reactions. However, the possibility that these gases somehow originated in the gneisses surrounding the intrusion, *i.e.*, from carbon originally of sedimentary origin, cannot be entirely excluded. This possibility could be further evaluated by analysing the gases for the stable isotopes of carbon and nitrogen, and comparing the analysed ratios with those for magmatic and sedimentary sources of carbon and nitrogen. More work could also be done on the documentation of the hydrocarbons. Although the unsaturated aliphatic hydrocarbon gases detected by gas chromatography in the inclusions (chapter 4) would fluoresce under UV illumination, the fact that some of the inclusions display more than one colour when observed in this manner (chapter 2), suggests that aromatic hydrocarbons and/or bituminous substances may be present in the rocks in addition to the gases. These components could be detected and measured using the gas chromatographic system described in chapter 3, by running the analyses with an oven temperature above that achievable with the present system, and using of a 10.2 eV lamp in the photoionisation detector.

In chapter 5, the textural relationships involving pseudomorphism of elpidite by gittinsite and armstrongite have been carefully documented and explained qualitatively from theoretical considerations of phase equilibria. Unfortunately, there are no thermodynamic data for most of these minerals and consequently, while intensive parameters controlling alteration can be identified, the magnitudes of the changes in these parameters and thus their relative importance cannot be established. Phase equilibrium experiments designed to provide these thermodynamic data are thus needed to permit further evaluation of these replacement. Similar textures have been observed involving narsarsukite, titanite and a number of other exotic minerals, some of which have not been identified. These too need to be properly documented and explained.

The opportunity to quantitatively document the mobility of Zr and other rare metals in hydrothermal fluids was exciting, as was finding a mechanism for transporting these metals which was consistent with geological observations (chapter 6). However, it would be even more satisfying to show that some of these metals are still in solution, albeit in reduced amounts, in fluid inclusions associated with the early alteration, *i.e.*, which are interpreted to have leached the metals. This could be attempted, using a recent refinement of the bulk fluid-inclusion leachate technique, which allows detection down to very low ppb levels (Banks *et al.*, 1994), or synchrotron X-ray fluorescence, which has recently been applied to the non-destructive analysis of trace elements in single inclusions (R. Bodnar, pers. comm. to A. W.-J., 1994). Finally, as was clearly evident from the discussion in chapter 6, there is great need for more data on the solubility of HFSE minerals, and on the aqueous speciation of the HFSE.

## References

- Banks, D.A., Yardley, B.W.D., Campbell, A.R. and Jarvis, K.E., 1994.** REE composition of an aqueous magmatic fluid: A fluid inclusion study from the Capitan Pluton, New Mexico, U.S.A. *Chem. Geol.*, 113, 259-272.
- Gieré, R., 1986.** Zirconolite, allanite and hoegbomite in a marble skarn from the Bergell contact aureole: Implication for mobility of Ti, Zr and REE. *Contrib. Mineral. Petrol.* 65, 459-470.
- Gieré, R. and Williams, C.T., 1992.** REE-bearing minerals in a Ti-rich vein from the Adamello contact aureole (Italy). *Contrib. Mineral. Petrol.* 112, 83-100.
- Rubin, J.N., Henry, C.D. and Price, J.G., 1989.** Hydrothermal zircons and zircon overgrowths, Sierra Blanca Peaks, Texas. *Am. Mineral.*, 74, 865-869.

# APPENDIX 1

---

## **Fluid Inclusion Microthermometric Data**

(cf. Chapter 2)

AQUEOUS INCLUSION DATA

Incl. Type	Sample#	Tf	Te	Tm(ice)	Tm(hydr)	ThL	Td (NaCl)
I	SL4-14#1	-27.0	-22.0	-20.2	5.6		
I		-52.0	-22.0	-20.8	7.3	266.0	
I		-50.0	-25.0	-20.6	3.0	341.2	
I		-80.0	-24.0	-21.0	3.0	450.0	
I		-80.0	-25.6	-24.1	2.0	340.0	
I*	SL-4-15#2	-70.0	-23.0	-21.7	5.2	460.0	170.0
I*		-70.0	-23.0	-21.7	5.2	430.0	115.0
I*		-50.0	-23.0	-21.8	0.0	570.0	100.0
I*	SL4-14#2	-55.0	-22.0	-21.7	1.1	560.0	165.0
I*		-60.0	-22.0	-21.8	-0.1	580.0	110.0
I	SL4-14A	-55.0	-23.0	-14.8	-22.0	206.0	
I		-50.0	-26.0	-14.0	-22.0	130.0	
I		-58.0	-23.4	-22.9	6.0	322.0	
I		-64.0	-23.0	-21.0	0.0	275.5	
I		-68.0	-22.5	-16.4	-21.0	300.0	
I		-59.0	-23.0	-21.1	5.8	170.0	
I*		-45.0	-25.0	-22.8	5.0	520.0	298.0
I*		-34.0	-26.0	-22.9	2.0	540.0	282.0
I*	SL4-14#3	-50.0	-22.0	-22.0	9.0	130.0	200.0
I		-40.0	-22.0	-22.0	-10.0	120.0	
I*		-40.0	-23.0	-22.4	24.0	450.0	210.0
I		-80.0	-22.0	-20.6	14.5	350.0	
I*		-40.0	-26.0	-22.0	10.0	450.0	240.0
I		-60.0	-22.0	-19.0	11.0	470.0	
I		-62.0	-23.0	-20.0	20.0	500.0	
I		-40.0	-23.0	-21.0	-16.0	263.0	
I	SL2-4#9					512.0	
I		-65.0	-25.0	-21.8	-14.6	355.0	
I		-65.0	-25.0	-21.8	-11.2	220.0	
I		-50.0	-24.0	-21.9	-15.0	320.0	
I		-65.0	-25.0	-21.9	-16.0		
I		-46.0	-23.4	-19.7	-21.8		
I		-52.0	-23.0	-21.8	-13.0	320.0	

I\* with halite

AQUEOUS INCLUSION DATA

Incl. Type	Sample#	Tf	Te	Tm <sub>(ice)</sub>	Tm <sub>(hydr)</sub>	ThL	Td <sub>(NaCl)</sub>
I	SL2-4#9	-45.0	-24.0	-22.0	-9.0	360.0	
I	SL4-14#5A	-55.0	-24.3	-19.2	-22.0	355.0	
I		-46.0	-24.3	-19.0	-21.5	300.0	
I		-47.0	-24.3	-18.8	-21.6	330.0	
I		-70.0	-24.3	-19.2	-19.0	332.0	
I		-58.0	-24.3	-19.1	-21.8	333.0	
I		-58.0	-24.3	-20.0	-21.8	275.0	
I	56-A-1#3	-40.0	-23.0	-21.8	-13.0	350.0	
I	...	-45.0	-24.0	-21.8	-9.0	340.0	
I		-55.0	-24.8	-22.0	-10.0	360.0	
I		-46.0	-23.4	-19.7	-19.7	380.0	
I		-45.0	-23.8	-19.5	-22.0	320.0	
I		-47.0	-24.0	-19.2	-21.5	330.0	
I	SL2-4#7	-70.0	-25.0	-12.3	-21.8	152.2	
I		-50.0	-25.0	-10.8	-21.5	192.0	
I		-60.0	-24.0	-12.3	-21.4	334.2	
I		-58.0	-25.0	-10.5	-21.5	258.0	
I		-60.0	-24.0	-12.3	-21.4	187.8	
I		-58.0	-25.0	-10.5	-21.5	185.0	
I*	SL4-14#B1	-40.0	-24.0	-21.5	6.0	450.0	250.0
I*		-70.0	-25.0	-21.6	6.7	400.0	260.0
I*		-50.0	-23.0	-21.8	8.0	383.5	161.0
I*		-60.0	-23.0	-21.8	10.0	420.0	320.0
I		-58.0	-24.6	-22.1	-11.5	232.0	
I		-60.0	-24.8	-22.2	-13.9	320.0	
I		-58.0	-27.0	-14.2	-21.8	380.0	
I		-40.0	-27.0	-10.0	-21.8	210.0	
I		-60.0	-24.0	-13.9	-20.0	259.8	
I		-58.0	-23.0	-10.0	-21.0	267.0	
I		-40.0	-24.0	-13.9	-19.9	362.0	
I		-70.0	-22.9	-13.9	-20.5	255.3	
I	SL2-4#5	-33.0	-23.0	-22.0	-16.0	315.0	
I		-35.0	-24.0	-22.0	-16.5	350.0	
I		-55.0	-22.0	-20.8	3.0	325.0	
I		-60.0	-22.5	-21.3	-1.6	340.0	

I\* with halite

CARBONIC INCLUSION DATA

Incl. Type	Sample#	Tf(tot)	TmCH <sub>4</sub>	Tm(clath)	Th(carb)	Tf(H <sub>2</sub> O)	Tc(H <sub>2</sub> O)	Tm(ice)	Tm(hydr)	Th(L)	Th(V)	Td(NaCl)
II	SL2-1#1	-199.8	-184		-72							
II		-199.8	-190		-71							
II	SL2-1#2		-188		-76							
II					-76							
III	SL4-14#1	-199.8	-190	-19	-70	-74					360	
III		-199.8	-184.4	-16	-71	-66					400.0	
III	SL2-4#5	-199.8		-11		-74					406	
III		-199.8	-185	-1.8		-60.0				300		
III		-199.8	-184	-2.6	-76.5	-74	-19.4	-5.8	-20	280.0		
III	SL4-14#2	-199	-188	-4.5	-76.8	-60.0					380	
III		-199.8	-186	3.2	-79	-60.0	-19.7				375	
III	SL4-14#3	-199.8	-195	2	-77	-57.0					370	
III		-199.8	-190	6.3	-78.2	-48.0	-20	-13.6	-4.2	250.0		
III		-199.8	-184	19.5	-82						390	
III	SL4-13	-199	-184	8.5	-79.5	-45.0	-19.8	-13.8	-13.5	310.0		
III										350		
III	SL4-12					-40	-19.1		-6.5	350		
III						-40				340.0		
III							-19.3	-13.9	-5.8	325.0		
III	SL4-14A					-40.0	-19.2			300.0		
III						-39.0		-13.5	-3.5	250		
III						-35.0	-19.7			345		
III						-33.0		-2.3		209		
III	SL4-14#B1					-30.0		-1.7		310.0		
III						-38.0				315.0		
III						-40		-2.5			390	
III	SL4-15#2					-40			-20.9	350		
III						-40			-13.8	333.0		
III									-1.1		399	
III						-50.0			-20.2		420	
III						-50.0			-20.8		420	
III						-40			-20.5		392.5	
III	SL4-14#5A									200.0		
III											440	
III											456.5	
III											410	
III										200.0		

CARBONIC INCLUSION DATA

Incl. Type	Sample#	Tf(tot)	TmCH <sub>4</sub>	Tm(clath)	Th(carb)	Tf(H <sub>2</sub> O)	Te(H <sub>2</sub> O)	Tm(ice)	Tm(hydr)	Th(L)	Th(V)	Td(NaCl)
III										130.0		
III										180.0		
III											400	
III										300.0		
III											450.0	
III	SL2-4#9										487.0	
III										300.0		
III						-40					450.0	
III							-23.5	-21.0			450.0	
III*							-23.0	-21.7	5.2		460.0	170.0
III*							-23.0	-21.7			430.0	115.0
III*							-23.0	-21.8			570.0	100.0
III*							-22.0	-20.7			560.0	165.0
III*							-20.9	-20.8			580.0	110.0
III*							-22.0	-21.8			520.0	298.0
III*	SL2-4#7						-20.5	-20.9			540.0	282.0
III*							-20.5	-20.1		130.0		200.0
III*							-20.5	-20.4			450.0	210.0
III*							-20.5	-20.0			450.0	240.0

III\* with halite

## APPENDIX 2

---

### **Thermodynamic Calculations to Determine the Equilibrium Composition of an Orthomagmatic Carbon-Bearing Fluid, for the System C-O-H.**

(cf. Chapter 4)

Equilibrium compositions of the gases analysed in this study (Chapter 4) were calculated assuming that they could be modeled in the system C-O-H and that the gas phase was in equilibrium with an immiscible brine. The latter assumption allowed the fugacity of H<sub>2</sub>O in the gas phase to be fixed by its solubility. Unfortunately this parameter is not well known for methane-dominated systems and had to be estimated from the solubility of CH<sub>4</sub> in brine on the assumption that the solvus is symmetrical.

The mole fraction of a species in the gas phase is given by

$$X_i = P_i / \Sigma P_i \quad 1)$$

where  $P$  the partial pressure and  $i$  a species. Calculations of mole fractions were restricted to the species H<sub>2</sub>O<sub>v</sub>, H<sub>2</sub>, O<sub>2</sub>, CO<sub>2</sub>, CO, CH<sub>4</sub>, C<sub>2</sub>H<sub>6</sub> and C<sub>3</sub>H<sub>8</sub>, and involved simultaneous solving of the five independent mass action equations for the system plus a sixth equation which relates the sum of the partial pressures of the various gas species.

The independent equilibria that describe this system are as follows:



and their equilibrium constants  $K_1$ ,  $K_2$ ,  $K_3$ ,  $K_4$  and  $K_5$  given by the relationships:

$$K_1 = \frac{f_{\text{H}_2} \cdot \sqrt{f_{\text{O}_2}}}{f_{\text{H}_2\text{O}}}$$

$$K_2 = \frac{f_{\text{CH}_4} \cdot f_{\text{O}_2}}{f_{\text{CO}_2} \cdot f_{\text{H}_2}^2}$$

$$K_3 = \frac{f_{CO} \cdot \sqrt{f_{O_2}}}{f_{CO_2}}$$

$$K_4 = \frac{f_{C_2H_6} \cdot f_{H_2}}{f_{CH_4}^2}$$

$$K_5 = \frac{f_{C_3H_8} \cdot f_{H_2}^2}{f_{CH_4}^3}$$

These relationships, plus the gas equation:

$$P_g = PH_2O_v + PH_2 + PO_2 + PCO_2 + PCO + PCH_4 + PC_2H_6 + PC_3H_8,$$

which can be rewritten as:

$$P_g = f_{H_2O_v}/\gamma_{H_2O_v} + f_{H_2}/\gamma_{H_2} + f_{O_2}/\gamma_{O_2} + f_{CO_2}/\gamma_{CO_2} + f_{CO}/\gamma_{CO} + f_{CH_4}/\gamma_{CH_4} + f_{C_2H_6}/\gamma_{C_2H_6} + f_{C_3H_8}/\gamma_{C_3H_8}, \quad 7)$$

provide a system of 6 equations with 8 unknowns. However, since  $f_{H_2O}$  is estimated from the solubility relationship discussed above and  $f_{O_2}$  can be estimated from mineralogical relationships, the system reduces to one of 6 equations and 6 unknowns for which a unique solution can be obtained. This set of equations was solved as follows:

First the mass action relationships were rewritten to yield the fugacities of the various species:

$$f_{H_2} = \frac{K_1 \cdot f_{H_2O}}{\sqrt{f_{O_2}}}$$

$$f_{CO_2} = \frac{f_{CH_4} \cdot f_{O_2}}{K_2 \cdot f_{H_2}}$$

$$f_{CO} = \frac{K_3 \cdot f_{CO_2}}{\sqrt{f_{O_2}}}$$

$$f_{C_2H_6} = \frac{K_4 \cdot f_{CH_4}^2}{f_{H_2}}$$

$$f_{C_3H_8} = \frac{K_5 \cdot f_{CH_4}^3}{f_{H_2}^2},$$

then we can substitute the known values for  $f_{O_2}$  and  $f_{H_2O}$ , i.e., we can let  $a = f_{O_2}$ , and  $b = f_{H_2O}$ , and rearrange the above equations so to express all unknowns as functions of  $f_{CH_4}$ , such as:

$$f_{H_2} = \frac{K_1 \cdot b}{\sqrt{a}} \quad 8)$$

$$f_{CO_2} = \frac{f_{CH_4} \cdot a^2}{K_1^2 \cdot K_2 \cdot b^2} \quad 9)$$

$$f_{CO} = \frac{K_3 \cdot a^2 \cdot f_{CH_4}}{K_1^2 \cdot K_2 \cdot \sqrt{a} \cdot b^2} \quad 10)$$

$$f_{C_2H_6} = \frac{K_4 \cdot \sqrt{a} \cdot f_{CH_4}^2}{K_1 \cdot b} \quad 11)$$

and

$$f_{C_3H_8} = \frac{K_5 \cdot a \cdot f_{CH_4}^3}{K_1^2 \cdot b^2} \quad 12)$$

These fugacities are then converted to partial pressures according to:

$$P_i = f_i / \gamma_i , \quad (13)$$

where  $\gamma$  is the fugacity coefficient, and substituted in the gas equation (8) to obtain:

$$P_g = \frac{a}{\gamma_{O_2}} + \frac{b}{\gamma_{H_2O}} + \frac{K_1 \cdot b}{\sqrt{a} \cdot \gamma_{H_2}} + \frac{a^2 \cdot f_{CH_4}}{K_1^2 \cdot K_2 \cdot b^2 \cdot \gamma_{CO_2}} + \frac{K_3 \cdot a^2 \cdot f_{CH_4}}{K_1^2 \cdot K_2 \cdot \sqrt{a} \cdot b^2 \cdot \gamma_{CO}} + \frac{f_{CH_4}}{\gamma_{CH_4}} + \frac{K_4 \cdot \sqrt{a} \cdot f_{CH_4}^2}{K_1 \cdot b \cdot \gamma_{C_2H_6}} + \frac{K_5 \cdot a \cdot f_{CH_4}^3}{K_1^2 \cdot b^2 \cdot \gamma_{C_3H_8}} \quad (14)$$

where  $P_g$  is the total volatile pressure. Equation (14) can be solved iteratively by inserting values for  $f_{CH_4}$  until the right hand side of the equation is approximately equal to  $P_g$  which in this study was assumed to be 500 bars.

The value of  $f_{CH_4}$  so calculated is used to obtain the fugacities of the other species by substituting it into equations (8) to (12). From these values, and using the equations (1) and (13), we can obtain the mole fraction of the species in question, i.e., the composition of the fluid.

#### *Thermodynamic Data*

Equilibrium constants for reactions (2) through (6) are calculated using the Lewis-Randall approximation, i.e.,

$$K_i = K_{p_i} K \gamma_i,$$

where  $K_{p_i}$  is the equilibrium constant at 1 atm and temperature, and  $K \gamma_i$  is the corresponding ratio of the fugacity coefficients of the pure gases at pressure and temperature. The values of  $\Delta G_f^\circ$  (1 atm, T) for these gases are taken from Stull et al.

(1969), and the fugacity coefficients are calculated using empirically derived relationships such as:

$$\gamma_i = 1 + aP_R + bT_R P_R + cT_R^2 P_R + dP_R^2 + eT_R^2 P_R + fT_R P_R^2 + gT_R^2 P_R^2,$$

using the reduced pressures ( $P_R = P/P_{C_i}$ ) and temperatures ( $T_R = T/T_{C_i}$ ), and parameters a to g tabulated in Ryzhenko & Volkov (1971).  $T_C$  and  $P_C$  represent the critical conditions of species *I*.

#### References

- Ryzhenko, B.N. and Volkov, V.P., 1971.** Fugacity coefficients of some gases in a broad range of temperatures and pressures. *Geokhimiya*, 7, 769-773.
- Stull, D.R., Westrum, E.F., Jr. and Sinke, G.C., 1969.** *The chemical Thermodynamics of Organic Compounds*, John Wiley & Sons, New York, 865 p.

## **APPENDIX 3**

---

### **Electron Microprobe Data for the Zirconosilicate Minerals Elpidite, Armstrongite and Gittinsite.**

(cf. Chapter 5)

Appendices

GITTINSITE

	1	2	3	4	5	6	7	8	9	10
	10.18m		19.43m	40.77m				50.6m		
SiO <sub>2</sub>	41.81	43.20	43.62	43.06	47.49	43.16	42.62	41.92	42.05	42.87
TiO <sub>2</sub>	0.00	0.00	0.00	0.00	0.00	0.66	0.00	0.00	0.50	0.00
ZrO <sub>2</sub>	35.75	35.18	35.29	34.76	28.98	36.11	35.43	35.05	34.64	35.62
FeO	0.26	0.96	0.25	0.00	1.07	0.00	0.20	0.20	1.00	0.74*
MgO	0.18	0.00	0.42	0.13	0.37	0.38	0.23	0.00	0.00	0.26
MnO	0.60	0.99	0.99	0.74	0.70	0.00	0.66	0.66	1.52	0.96
CaO	19.57	18.43	19.01	19.83	15.54	18.77	19.98	19.88	18.08	19.56
Na <sub>2</sub> O	0.00	0.00	0.00	0.00	0.61	0.00	0.00	0.00	0.00	0.00
K <sub>2</sub> O	0.00	0.00	0.00	0.00	0.00	0.00	0.00	0.00	0.00	0.00
Nb <sub>2</sub> O <sub>5</sub>	1.52	0.65	0.00	0.91	4.04	0.93	0.89	0.83	1.52	0.00
Ce <sub>2</sub> O <sub>3</sub>	0.00	0.00	0.00	0.00	1.16	0.00	0.00	1.20	0.84	0.62
Nd <sub>2</sub> O <sub>3</sub>	0.00	0.00	0.00	0.57	0.12	0.00	0.00	0.00	0.00	0.00
Total	99.69	99.41	99.58	100.00	100.08	100.01	100.01	99.74	100.15	99.89

ELPIDITE

	1	2	3	4	5	6	7	8	9	10
	19.43m	40.77m					50.6m			
SiO <sub>2</sub>	62.87	62.00	63.45	62.10	64.43	62.54	63.72	64.48	62.68	63.77
TiO <sub>2</sub>	0.00	0.00	0.00	0.00	0.00	0.00	0.00	0.00	0.00	0.00
ZrO <sub>2</sub>	18.43	18.99	18.89	18.08	17.38	18.81	15.98	16.51	16.03	15.79
FeO	0.00	0.00	0.00	0.00	0.42	0.37	0.00	0.00	0.50	0.00
MgO	0.35	0.60	0.32	0.00	0.00	0.00	0.29	0.00	0.28	0.24
MnO	0.00	0.00	0.00	0.00	0.00	0.00	0.26	0.00	0.00	0.00
CaO	0.32	0.19	0.00	0.43	0.38	0.89	1.06	0.74	0.41	0.67
Na <sub>2</sub> O	7.96	8.83	8.09	8.14	7.64	8.49	9.65	9.71	9.89	9.06
K <sub>2</sub> O	0.00	0.00	0.00	0.00	0.00	0.00	0.00	0.00	0.00	0.00
Nb <sub>2</sub> O <sub>5</sub>	1.15	0.00	0.00	1.90	0.83	0.83	0.00	0.00	0.91	0.00
Ce <sub>2</sub> O <sub>3</sub>	0.00	0.00	0.00	0.00	0.00	0.00	0.00	0.00	0.00	0.00
Nd <sub>2</sub> O <sub>3</sub>	0.00	0.46	0.00	0.00	0.00	0.00	0.00	0.00	0.00	0.00
Total	91.08	91.07	90.75	90.65	91.08	91.93	90.96	91.44	90.70	89.53

AMSTRONGITE

	1	2	3	4	5	6	7	8	9	10
	40.77m			50.6m						51.60
SiO <sub>2</sub>	61.92	60.98	59.67	60.64	61.39	61.10	60.52	61.32	59.62	63.65
TiO <sub>2</sub>	0.16	0.02	0.28	0.00	0.00	0.14	0.00	0.00	0.21	0.00
ZrO <sub>2</sub>	18.44	19.27	19.18	19.56	19.31	19.40	19.73	20.03	25.02	18.03
FeO	0.19	0.22	0.00	0.00	0.53**	0.27**	0.00	0.00	0.00	0.00
MgO	0.16	0.00	0.21	0.00	0.00	0.00	0.00	0.00	0.00	0.00
MnO	0.00	0.00	0.00	0.00	0.00	0.00	0.00	0.00	0.00	0.00
CaO	9.85	10.64	10.45	10.49	9.85	9.55	10.64	9.57	11.76	9.30
Na <sub>2</sub> O	0.13	0.00	0.00	0.00	0.00	0.00	0.09	0.16	0.00	0.00
K <sub>2</sub> O	0.00	0.00	0.00	0.18	0.00	0.00	0.00	0.00	0.00	0.00
Nb <sub>2</sub> O <sub>5</sub>	0.00	0.80	1.46	0.00	0.00	0.57	0.00	0.00	0.00	0.00
Ce <sub>2</sub> O <sub>3</sub>	0.00	0.00	0.00	0.00	0.00	0.00	0.00	0.00	0.00	0.00
Nd <sub>2</sub> O <sub>3</sub>	0.39	0.00	0.00	0.00	0.00	0.00	0.00	0.00	0.00	0.00
Total	91.24	91.93	91.25	90.87	91.08	90.89	90.98	91.08	90.77	90.98

\* = as Fe

\*\* = as Fe<sub>2</sub>O<sub>3</sub>

Appendices

GITTINSITE					
	11	12	13	14	15
	<i>59.4m</i>			<i>71.0m</i>	
SiO <sub>2</sub>	43.43	42.65	50.34	51.23	50.76
TiO <sub>2</sub>	0.00		0.40	0.00	0.00
ZrO <sub>2</sub>	35.58	36.39	33.54	34.81	32.47
FeO	0.30*	0.13*	0.67*	0.00	0.00
MgO	0.17	0.58	0.39	0.32	0.44
MnO	0.89	0.26	0.00	0.00	0.00
CaO	19.49	19.05	12.92	12.02	14.29
Na <sub>2</sub> O	0.00	0.38	0.64	1.51	0.87
K <sub>2</sub> O	0.00	0.00	0.00	0.00	0.00
Nb <sub>2</sub> O <sub>5</sub>	0.00	0.55	0.23	0.12	0.11
Ce <sub>2</sub> O <sub>3</sub>	0.42	0.00	0.65	0.56	0.48
Nd <sub>2</sub> O <sub>3</sub>	0.00	0.00	0.33	0.22	0.04
Total	99.98	99.86	99.44	100.79	99.46

ELPIDITE											
	11	12	13	14	15	16	17	18	19	20	21
	<i>51.6m</i>										
SiO <sub>2</sub>	63.57	63.75	62.57	65.17	63.14	63.75	63.86	63.05	63.66	62.99	63.60
TiO <sub>2</sub>	0.00	0.00	0.00	0.00	0.00	0.00	0.00	0.00	0.00	0.00	0.00
ZrO <sub>2</sub>	16.21	14.38	16.61	14.69	15.39	15.06	15.19	15.46	15.37	15.95	15.46
FeO	0.29	0.00	0.00	0.00	0.00	0.00	0.00	0.49	0.00	0.00	0.38
MgO	0.54	0.00	0.00	0.77	1.43	0.36	0.94	0.99	0.82	0.78	0.42
MnO	0.00	0.20	0.20	0.29	0.40	0.35	0.00	0.00	0.00	0.00	0.00
CaO	2.43	2.93	0.50	1.49	1.55	1.07	1.13	0.32	0.42	0.82	0.71
Na <sub>2</sub> O	8.04	6.76	9.52	8.68	9.16	9.79	9.49	10.76	10.31	9.94	10.49
K <sub>2</sub> O	0.00	0.00	0.00	0.00	0.00	0.00	0.00	0.00	0.00	0.00	0.00
Nb <sub>2</sub> O <sub>5</sub>	0.00	1.23	0.00	0.00	0.00	0.00	0.00	0.00	0.00	0.00	0.00
Ce <sub>2</sub> O <sub>3</sub>	0.00	0.00	0.00	0.00	0.00	0.00	0.00	0.00	0.00	0.00	0.00
Nd <sub>2</sub> O <sub>3</sub>	0.00	0.00	0.00	0.00	0.00	0.00	0.00	0.00	0.00	0.00	0.00
Total	91.08	89.25	89.40	91.09	91.07	90.38	90.61	91.07	90.58	90.48	91.06

ELPIDITE											
	22	23	24	25	26	27	28	29	30	31	32
	<i>59.4m</i>								<i>71.0m</i>		
SiO <sub>2</sub>	64.81	64.13	63.12	63.61	63.68	63.19	63.83	63.03	63.93	60.71	59.95
TiO <sub>2</sub>	0.00	0.00	0.00	0.00	0.00	0.00	0.00	0.00	0.00	0.00	0.00
ZrO <sub>2</sub>	15.57	15.01	16.72	15.58	15.40	15.57	15.80	15.12	15.45	19.47	19.98
FeO	0.34	0.00	0.00	0.00	0.00	0.23	0.26**	0.00	0.00	0.52**	0.00
MgO	0.00	0.59	0.28	0.84	0.30	0.87	0.00	0.00	0.00	0.00	0.00
MnO	0.00	0.00	0.00	0.18	0.21	0.00	0.00	0.00	0.00	0.00	0.24
CaO	3.60	2.83	0.85	0.41	2.42	0.30	0.31	0.33	0.25	0.43	0.57
Na <sub>2</sub> O	6.76	8.51	9.36	10.46	8.58	10.47	10.19	10.08	9.84	9.95	10.14
K <sub>2</sub> O	0.00	0.00	0.00	0.00	0.00	0.44	0.45	0.16	0.54	0.00	0.13
Nb <sub>2</sub> O <sub>5</sub>	0.00	0.00	0.00	0.00	0.00	0.00	0.00	1.43	0.69	0.00	0.00
Ce <sub>2</sub> O <sub>3</sub>	0.00	0.00	0.00	0.00	0.00	0.00	0.00	0.00	0.00	0.00	0.00
Nd <sub>2</sub> O <sub>3</sub>	0.00	0.00	0.00	0.00	0.00	0.00	0.00	0.00	0.00	0.00	0.00
Total	91.08	91.07	90.33	91.08	90.59	91.07	90.84	90.15	90.7	91.08	91.01

\* = as Fe

\*\* = as Fe<sub>2</sub>O<sub>3</sub>

*Appendices*

---

**ELPIDITE**

	33	34	35	36	37	38	39	40	41 <i>81.6m</i>	42	43
SiO <sub>2</sub>	59.75	60.76	59.52	60.09	62.79	61.86	61.50	59.72	63.58	63.15	61.77
TiO <sub>2</sub>	0.00	0.00	0.00	0.00	0.00	0.00	0.00	0.00	0.00	0.00	0.00
ZrO <sub>2</sub>	19.90	19.01	19.47	19.77	20.88	19.76	20.48	19.35	18.11	17.85	18.59
FeO	0.00	0.51**	0.51**	0.00	0.00	0.36**	0.00	0.69**	0.00	0.00	0.92*
MgO	0.00	0.00	0.00	0.00	0.00	0.00	0.00	0.00	0.58	0.75	0.44
MnO	0.30	0.00	0.00	0.00	0.00	0.16	0.00	0.21	0.00	0.00	0.00
CaO	0.56	0.89	1.00	0.90	0.56	0.51	0.45	0.46	1.63	1.42	0.39
Na <sub>2</sub> O	9.85	9.65	9.29	9.91	6.65	7.97	8.29	10.55	6.24	7.69	7.97
K <sub>2</sub> O	0.00	0.14	0.43	0.18	0.00	0.22	0.12	0.10	0.10	0.20	0
Nb <sub>2</sub> O <sub>5</sub>	0.00	0.00	0.00	0.00	0.00	0.00	0.00	0.00	0.84	0.00	0.00
Ce <sub>2</sub> O <sub>3</sub>	0.00	0.00	0.00	0.00	0.00	0.00	0.00	0.00	0.00	0.00	0.00
Nd <sub>2</sub> O <sub>3</sub>	0.00	0.00	0.00	0.00	0.00	0.00	0.00	0.00	0.00	0.00	0.00
<b>Total</b>	<b>90.36</b>	<b>90.96</b>	<b>90.22</b>	<b>90.85</b>	<b>90.88</b>	<b>90.84</b>	<b>90.84</b>	<b>91.08</b>	<b>91.08</b>	<b>91.06</b>	<b>90.08</b>

\* = as Fe

\*\* = as Fe<sub>2</sub>O<sub>3</sub>

## **APPENDIX 4**

---

### **Electron Microprobe Analyses of Selected Minerals, Used for Calculating Normative Mineral Abundances.**

(cf. Chapter 6)

*Appendices*

**Microcline**

wt%	37-A-4*	37-A-4*	37-A-4*	24-B-1**	24-C-1**	25-B-1**
SiO <sub>2</sub>	64.88	65.64	65.34	63.92	63.91	63.14
Al <sub>2</sub> O <sub>3</sub>	17.15	17.42	17.57	17.31	17.15	16.91
K <sub>2</sub> O	16.39	16.36	16.25	16.87	16.18	16.26
Na <sub>2</sub> O	0.52	0.64	0.55	0.40	0.41	0.41
CaO	0.00	0.00	0.00	0.00	0.01	0.00
Fe <sub>2</sub> O <sub>3</sub>	1.13	0.86	0.84	0.98	0.41	0.94
TiO <sub>2</sub>	0.01	0.01	0.01	0.01	0.00	0.08
MgO	0.00	0.00	0.00	0.00	0.00	0.00
BaO	0.01	0.00	0.01	0.00	0.00	0.00
P <sub>2</sub> O <sub>5</sub>	0.00	0.01	0.00	0.00	0.04	0.01
SrO	0.06	0.06	0.07	0.02	0.09	0.04
PbO	0.01	0.06	0.00	0.00	0.23	0.12
TOT	100.16	101.07	100.64	99.50	98.43	97.91

\* : fresh subsolvus

\*\* : altered subsolvus

**Albite**

wt%	37-A-1*	37-D-1*	37-E-4*	24-B-1**	25-C-1**	36-A-1**
SiO <sub>2</sub>	68.79	69.15	68.83	69.08	69.23	69.10
Al <sub>2</sub> O <sub>3</sub>	18.12	19.18	19.22	18.47	18.81	18.79
K <sub>2</sub> O	0.06	0.07	0.18	0.29	0.14	0.18
Na <sub>2</sub> O	11.37	11.64	11.22	11.43	11.50	11.17
CaO	0.00	0.02	0.00	0.00	0.01	0.01
Fe <sub>2</sub> O <sub>3</sub>	0.70	0.32	0.29	0.57	0.15	0.59
TiO <sub>2</sub>	0.02	0.00	0.05	0.02	0.04	0.00
MgO	0.00	0.00	0.03	0.01	0.00	0.00
BaO	0.06	0.00	0.00	0.00	0.00	0.00
P <sub>2</sub> O <sub>5</sub>	0.00	0.00	0.00	0.03	0.00	0.00
SrO	0.11	0.09	0.07	0.05	0.08	0.05
PbO	0.00	0.06	0.09	0.07	0.16	0.08
TOT	99.24	100.53	99.98	100.00	100.12	99.97

\* : fresh subsolvus

\*\* : altered subsolvus

*Appendices*

**Arfvedsonite**

wt%	SL-Arf1	SL-Arf2	SL-Arf3	SL-Arf4	SL-Arf5
SiO <sub>2</sub>	50.23	49.49	51.57	50.14	50.26
TiO <sub>2</sub>	0.74	1.07	0.94	0.90	0.83
Al <sub>2</sub> O <sub>3</sub>	1.12	1.45	1.21	1.19	1.20
FeO*	33.47	34.53	33.41	34.34	34.25
MgO	0.01	0.05	0.01	0.04	0.05
CaO	0.60	0.61	0.41	0.88	0.68
Na <sub>2</sub> O	9.84	9.12	9.07	9.16	9.39
P <sub>2</sub> O <sub>5</sub>	0.01	0.02	0.09	0.00	0.00
ZrO <sub>2</sub>	0.01	0.08	0.03	0.01	0.06
TOT	96.03	96.42	96.74	96.66	96.72

\* : Total iron as FeO

**Aegirine**

wt%	SL-AEg1	SL-AEg2	SL-AEg3
SiO <sub>2</sub>	53.48	52.70	52.79
TiO <sub>2</sub>	0.38	0.65	0.95
Al <sub>2</sub> O <sub>3</sub>	0.28	0.65	0.18
FeO	30.49	31.59	31.24
MgO	0.03	0.01	0.02
CaO	0.19	0.23	0.06
Na <sub>2</sub> O	14.24	13.26	13.97
P <sub>2</sub> O <sub>5</sub>	0.00	0.02	0.02
ZrO <sub>2</sub>	0.02	0.07	0.03
TOT	99.11	99.17	99.26

**Pyrochlore**

wt%	SL-Pc1	SL-Pc2
SiO <sub>2</sub>	0.51	0.32
TiO <sub>2</sub>	4.98	4.32
Al <sub>2</sub> O <sub>3</sub>	0.04	0.06
FeO	0.00	0.00
MgO	0.01	0.00
CaO	2.72	2.72
Na <sub>2</sub> O	7.43	5.04
P <sub>2</sub> O <sub>5</sub>	0.06	0.05
ZrO <sub>2</sub>	0.28	0.11
Nb <sub>2</sub> O <sub>5</sub>	53.54	57.24
Ce <sub>2</sub> O <sub>3</sub>	12.12	11.45
Y <sub>2</sub> O <sub>3</sub>	0.29	0.32
<b>TOT</b>	<b>81.98</b>	<b>81.63</b>

**Monazite**

wt%	SL-Mnz1	SL-Mnz2
SiO <sub>2</sub>	0.78	0.70
Sm <sub>2</sub> O <sub>3</sub>	4.35	3.98
P <sub>2</sub> O <sub>5</sub>	31.28	31.00
ZrO <sub>2</sub>	0.00	0.00
Nd <sub>2</sub> O <sub>3</sub>	6.93	7.55
Ce <sub>2</sub> O <sub>3</sub>	37.78	37.35
La <sub>2</sub> O <sub>3</sub>	22.01	20.73
<b>TOT</b>	<b>103.13</b>	<b>101.31</b>

**Titanite**

wt%	SL-Ttn1	SL-Ttn2
SiO <sub>2</sub>	30.54	29.27
TiO <sub>2</sub>	30.92	31.31
Al <sub>2</sub> O <sub>3</sub>	0.49	0.46
FeO	3.99	5.07
MgO	0.00	0.00
CaO	26.54	26.20
Na <sub>2</sub> O	0.32	3.09
P <sub>2</sub> O <sub>5</sub>	0.03	0.00
ZrO <sub>2</sub>	0.18	0.43
Nb <sub>2</sub> O <sub>5</sub>	2.80	2.03
Ce <sub>2</sub> O <sub>3</sub>	0.00	0.00
Y <sub>2</sub> O <sub>3</sub>	0.20	0.20
<b>TOT</b>	<b>96.01</b>	<b>98.06</b>

## **APPENDIX 5**

---

**Whole-Rock Data for Hand Samples of Drill Hole SL-182.**

(cf. Chapter 6)

**Table 1**  
*Concentration of major oxides and selected minor elements in hand-samples from drill hole SL-182*

		SL-182									
		1	2	3	4	5	6	7	8	9	10
SiO <sub>2</sub>	wt%	70.12	70.24	71.88	71.26	71.24	67.40	74.77	73.25	73.15	70.17
TiO <sub>2</sub>		0.56	0.28	0.19	0.22	0.26	0.83	0.42	0.19	0.33	0.13
Al <sub>2</sub> O <sub>3</sub>		9.15	8.26	9.72	9.84	9.85	9.43	6.93	9.28	8.45	8.85
Fe <sub>2</sub> O <sub>3</sub>		5.83	7.68	4.49	5.47	5.14	4.58	3.42	2.48	3.58	4.69
MnO		0.16	0.20	0.11	0.14	0.13	0.21	0.13	0.08	0.13	0.12
MgO		0.33	0.34	0.00	0.00	0.00	0.00	0.00	0.00	0.00	0.00
CaO		2.10	1.76	0.59	0.61	1.20	1.46	0.92	0.61	0.80	0.61
Na <sub>2</sub> O		4.29	4.47	5.53	5.35	5.23	5.01	3.24	4.65	4.11	4.92
K <sub>2</sub> O		3.49	3.33	3.23	3.47	3.38	3.93	4.03	3.99	4.13	4.48
P <sub>2</sub> O <sub>5</sub>		0.00	0.01	0.04	0.04	0.03	0.00	0.02	0.01	0.00	0.01
BaO	ppm	67	39	26	26	53	87	57	35	32	24
Cr <sub>2</sub> O <sub>3</sub>		21	25	17	12	16	1	24	24	18	17
LOI	wt%	0.80	0.78	1.15	0.86	0.90	1.32	1.33	1.40	1.41	1.72
<b>Total</b>		<b>96.83</b>	<b>97.35</b>	<b>96.93</b>	<b>97.26</b>	<b>97.36</b>	<b>94.17</b>	<b>95.21</b>	<b>95.94</b>	<b>96.09</b>	<b>95.70</b>
F	ppm	8200	9800	6600	5400	7200	4000	3800	1900	2800	5100
Be		59	68	67	76	227	81	190	60	135	64
Li		225	295	180	220	210	245	142	105	192	190
Y		1358	1190	1371	1259	1314	1489	1282	1773	2234	1502
Zr		15188	11557	16124	10283	10250	25392	21840	22658	19864	23092
Nb		781	655	905	1068	825	3993	3092	1242	1469	351
Ga		48	44	53	56	55	68	45	58	47	45
Pb		278	235	159	1126	187	490	564	178	844	464
Th		124	111	97	88	226	137	71	91	56	83
U		126	93	142	113	100	260	212	202	202	209
Rb		636	563	584	689	603	908	1030	990	850	824
Sr		256	234	272	259	252	276	233	336	418	288
Co		16	3	17	15	0	23	22	31	41	16
Cu		0	0	nd							
Ni		11	29	17	9	12	17	35	29	11	14
Sc		9	1	1	4	0	3	10	3	3	4
V		19	12	12	11	5	16	19	15	10	10
Zn		1157	1372	934	1165	1010	1314	863	689	999	1085

Analysed by XRF at the Dept. of Earth and Planetary Sciences, McGill University, by T. Amedhali

F, Be, Li were analysed by ACME Lab. Ltd., Vancouver. Det. lim. 100 ppm F; <0.1 ppm Be, Li.

detection limits: 100 ppm for majors, 1 ppm for traces

**Table 2**

*Concentration of REE and selected trace elements in hand-samples from drill hole SL-18*

		SL-182									
		1	2	3	4	5	6	7	8	9	10
<b>La</b>	ppm	723	713	10	1080	1210	nd	nd	nd	nd	677
<b>Ce</b>		1169	1372	1469	2421	2308	1400	1601	813	727	1264
<b>Nd</b>		536	733	654	1220	921	nd	724	528	nd	705
<b>Sm</b>		nd	nd	nd	nd	nd	nd	nd	nd	nd	nd
<b>Gd</b>		nd	nd	nd	90	nd	nd	nd	nd	nd	nd
<b>Dy</b>		nd	nd	nd	nd	nd	nd	nd	nd	nd	nd
<b>Ho</b>		nd	nd	nd	nd	nd	nd	nd	nd	nd	nd
<b>Er</b>		nd	nd	nd	nd	nd	nd	nd	nd	294	nd
<b>Tm</b>		nd	nd	nd	nd	nd	nd	nd	nd	nd	nd
<b>Yb</b>		nd	nd	239	10	10	265	292	584	330	nd
<b>Lu</b>		nd	nd	nd	nd	nd	nd	nd	nd	nd	nd
<b>As</b>		23	21	10	93	16	53	56	36	86	32
<b>Hf</b>		289	216	318	195	200	634	510	536	425	374
<b>Mo</b>		3220	2360	3320	2130	2080	5770	4780	4980	4230	3600
<b>Sn</b>		nd	nd	nd	nd	nd	nd	nd	nd	nd	nd
<b>Ta</b>		nd	nd	nd	nd	nd	619	399	241	273	247
<b>W</b>		nd	nd	nd	nd	nd	nd	153	191	231	nd

Analysed by XRF at the Dept. of Earth and Planetary Sciences, McGill University,  
by T. Amedhali.

detection limits: 20 ppm

